Subcellular properties and embryo-scale dynamics driving morphogenesis

Alphy John

UNIVERSITÉ CÔTE D'AZUR

ÉCOLE DOCTORALE
SCIENCES DE LA VIE ET DE LA SANTÉ

THÈSE DE DOCTORAT

Propriétés subcellulaires et dynamique à l'échelle de l'embryon gouvernant la morphogenèse

Alphy JOHN

Institut de Biologie Valrose
Equipe «Morphogenèse et mécanique des tissus épithéliaux»

Présentée en vue de l'obtention du grade de docteur en SVS Interactions moléculaires et cellulaires **d'**Université Côte d'Azur

Dirigée par : Matteo RAUZI, Ph.D.

Devant le jury, composé de :
Eric WIESCHAUS, Prof., Princeton U., États-Unis
Natalie DYE, Ph.D., MPI-CBG, Dresden, Allemagne
Raymond KELLER, Prof., University of Virginia, États-Unis
Carl-Philipp HEISENBERG, Prof., IST Austria, Autriche
Florence BESSE, Ph.D., iBV, Nice, France

Soutenue le : 15/09/2021

RÉGION SUD PROVENCE ALPES CÔTE D'AZUR

LUXENDO A BRUKER COMPANY

HFSP International Human Frontier Science Program Organization

Propriétés subcellulaires et dynamique à l'échelle de l'embryon gouvernant la morphogenèse

Jury:

Président du jury*

Florence BESSE, Ph.D., iBV, Nice, France.

Rapporteurs

Eric WIESCHAUS, Prof., Princeton U., États-Unis

Natalie DYE, Ph.D., MPI-CBG, Dresden, Allemagne

Examinateurs

Raymond KELLER, Prof., University of Virginia, États-Unis

Carl-Philipp HEISENBERG, Prof., IST Austria, Autriche

Invités

Matteo RAUZI, Ph.D., iBV, Nice, France

Propriétés subcellulaires et dynamique à l'échelle de l'embryon gouvernant la morphogenèse

La morphogénèse est le processus de remodelage du zygote, la cellule œuf fécondée, qui permet d'obtenir la forme finale de l'animal. Chez l'embryon, les combinaisons de profils d'expression génique déterminent les axes de symétrie du corps et établissent les coordonnées spatiotemporelles de spécification des cellules. Ces profils affectent aussi l'organisation des composants du cytosquelette pour réguler la morphogénèse des tissus. Tandis qu'un travail important a été réalisé pour comprendre comment les motifs d'expression génique antéro-postérieur (AP) et dorso-ventral (DV) contrôlent indépendamment la morphogénèse, on en sait toujours peu sur l'impact du croisement de ces motifs. Nous utilisons l'embryon de drosophile comme modèle et nous concentrons sur le processus de repliement tissulaire, un processus vital pour l'animal. Des anomalies de repliement peuvent en effet altérer la neurulation chez les vertébrés et la gastrulation chez l'ensemble des animaux organisés en trois feuillets primordiaux. Les études passées ont montré qu'un réseau d'actomyosine, couvrant la surface médiale-apicale des futures cellules mésodermiques, et sous le contrôle du motif d'expression génique DV, joue un rôle clé dans l'invagination du mésoderme. Néanmoins, les preuves expérimentales et théoriques ont plaidé contre la constriction apicale comme seul mécanisme responsable de l'invagination. Dans cette étude, j'ai mis à jour un réseau jonctionnel sous contrôle des profils d'expression génique AP et DV. Ce réseau contractile génère une tension le long de l'axe apico-basal des cellules et dans le plan du tissu, initiant l'interacalation des cellules à 10-15 µm à l'intérieur de l'épithélium mésodermique. Les forces latérales dans les cellules mésodermiques semblent jouer un rôle à la fois dans l'extension du mésoderme et dans l'invagination. Pour conclure, à travers l'implémentation de microscopie à feuillet de lumière 4D, d'ablation infrarouge femtoseconde pour perturber le cytosquelette et d'optogénétique pour contrôler synthétiquement la morphologie tissulaire, ce travail montre sous un jour nouveau l'origine et les fonctions d'un mécanisme inédit responsable de l'élongation et du repliement coordonnés du tissu.

Mots clés : Gastrulation, Morphogenèse concomitante, Modélisation des gènes, Contractilité de l'actomyosine , Jonctions adhérentes

Subcellular properties and embryo-scale dynamics driving morphogenesis

Morphogenesis is the process of reshaping single-cell zygotes to the final form of a developed animal. Embryonic gene patterning systems determine the body axes and lay down the spatiotemporal specification coordinates for cells. Gene patterning systems also affect the organization of cytoskeletal components in order to drive tissue morphogenesis. While much work was done to understand how AP and DV patterning independently control morphogenesis, little is known on how cross-patterning functions. We use the *Drosophila* embryo as a model system and focus on the process of tissue folding, a process that is vital for the animal since folding defects can impair neurulation in vertebrates and gastrulation in all animals which are organized into the three germ layers. Past work has shown that an actomyosin meshwork spanning the apical-medial side of prospective mesoderm cells and under the control of the embryo DV patterning plays a key role in mesoderm invagination. Nevertheless, both experimental and theoretical pieces of evidence have argued against apical constriction being the sole mechanism driving invagination. In this study, I have uncovered a lateral cell junctional network under the control of both AP and DV patterning. This contractile network generates tension along the apical-basal axis and within the tissue plane, 10-15 µm inside the mesoderm epithelium initiating lateral cell intercalation. Lateral forces in mesoderm cells seem to play a multivalent role in both driving mesoderm extension and invagination. Finally, by implementing 4D multi-view light-sheet imaging, infra-red femtosecond ablation to perturb the cytoskeleton, and optogenetics to synthetically control tissue morphology, this work shines new light on the origin and functions of a novel mechanism responsible for coordinated tissue elongation and folding.

Keywords: Gastrulation, Concomitant morphogenesis, Gene patterning, Actomyosin contractility, Adherens junctions

Contents

Chapter II- Results

Chapter III- Discussion

Bibliography

Annex

Dedicated to my Amma and Koochi

Acknowledgments

A Ph.D. is a long adventurous journey and with boundless love and appreciation, I would like to extend my heartfelt gratitude and appreciation to all who helped me to bring this day to reality. Here is a small tribute to all those people.

To begin with, I would like to thank my thesis supervisor **Dr. Matteo Rauzi** for allowing me to carry out original research in his team. He was a friend more than a supervisor, and his doors were always open. He was always there to back me during all the troubleshooting, provided guidance and feedback throughout this project. He also supported me being an independent researcher, by giving ears to my ideas and providing the opportunity to train students. He taught me how to critically approach a research work and be self-critical of my research.

I am thankful to my fellow lab members, **Barth**, **Anna**, **Nico**, and **Abdul**, who were there always to cheer me up, for all the stimulating discussions, and for all the fun we have had in the last four years. Ph.D. in France was quite an adventure for me as I have not traveled so far before. Barth and Anna helped me a lot in the initial days to smoothen this big cultural jump. I also thank Dr. Arnaud Hubstenberger and his team members for being jovial neighbors.

Besides my advisor, I would like to express my deep and sincere gratitude to the members of my thesis committee: **Dr. Florence Besse**, **Dr. Yohanns Bellaiche**, **Dr. Robert Arkowitz**, and **Dr. Pascal Therond**, for their insightful comments and encouragement, but also for the constructive questioning which incented me to widen my research from various perspectives.

I would like to extend my gratitude to all the funding agencies, especially **UCA**, **Region-Sud**, and the socioeconomic partner, **Bruker Luxendo**, for all the financial supports during the course of research. I am also thankful to **ED85** for financially supporting my attendance at a one-month workshop at KITP, UCSB, USA.

I am highly indebted to the research community at iBV, especially the fly community, for their constant support, and for providing necessary scientific input for completing this endeavor. I also take this opportunity to express me to express my special gratitude towards the engineers at the **PRISM** imaging platform at iBV, specially **Magali**, **Simon**, **Baptiste**, and **Sameh**, for training me to use different microscopic techniques. I would also convey my deep regards to all administrative staff both at iBV and UCA, particularly Hanane, Sandy, Cendrine, and Karen. I am also grateful to **Konstanze** and all staff of the **UCA welcome center**, who made my transition to Nice smoother by helping with all documentation and paperwork.

I would like to thank all the supporting staff at the institute, especially, Soumita, Mouna, Shanthi, Anita, and Dominica for organizing all the reagents and fly media used for research, making our lives easier.

I would like to take this opportunity also to thank **Dr. Jishy Varghese** and members of my alma mater, **IISER Thiruvananthapuram**, for providing the first glance to the field of scientific research. It would have been impossible for me to thrive in my doctoral work without the support of my friends and family. Firstly, I would like to thank my parents for all the love they bestowed upon me. My special and heartily thanks to my friends, **Kavya**, **Vishnu**, **Ananya**, **Akshai**, **Dinil**, and **Naeem** for all the joyful moments we had together. Lockdown was a difficult period but my dear pets, **Soman** and **Kunjunni** were there to cheer me up. I also thank my dear **Manu** for all his support and encouragement.

Finally, to my caring, loving, and supportive **Kaavi**: my deepest gratitude. Your encouragement when the times got rough is much appreciated and duly noted. It was a great comfort and relief when I was around you. My heartfelt thanks.

During these difficult times, I cannot leave acknowledging our Corona warriors. Bravo doctors, nurses, teachers, researchers, sanitation workers, public servants, volunteers, and all other people supporting this fight against this pandemic. Thank you!

Finally, last but not the least, I thank my experimental model, the little masters, the fruit flies.

List of Figures

List of Abbreviations

AAJ . Apical adherens junctions

AJC . Apical junctional complex

AMG . Anterior midgut

BAJ . Basal adherens junctions

CE . Convergence extension

CF . Cephalic fold

DTF . Dorsal transverse fold

E-cad . Epithelial cadherin

ECM . Extracellular matrix

ECs . Extracellular cadherin

EL . Egg length

EMT . Epithelial to mesenchymal transition

FC . Furrow canals

GBE . Germ band extension

GBR . Germband retraction

GD . Gastrulation defective

IF . Intermediate filaments

JAM . Junctional adhesion molecules

MHP . Median hinge points

MiMIC . *Minos* Mediated Integration Cassette

NM II . Non-muscle myosin II (MyoII)

pAJs . Primordial adherens junctions

PMG . Posterior midgut

VE . Vascular epithelium

VFF . Ventral furrow formation

Chapter I

Introduction

1. Embryogenesis

Sexually reproducing metazoans start their life from a single cell, the zygote. The male and female gametes meet and their pronuclei fuse to form the zygote during fertilization. The zygotic cell undergoes a division cycle to form a two-celled embryo. The word embryo was coined from the Greek word "*embruon*", meaning the young one. The process of the early development of an organism called embryogenesis involves cell division, growth, cellular movement and rearrangements, cell specification, and formation of the final form of the organism. Embryogenesis includes various stages including cleavage, gastrulation, neurulation, and organogenesis (Barresi & Gilbert, 2019). Embryogenesis starts with a series of mitotic divisions of the large zygotic cell, a process known as cleavage. Each daughter cells produced by this cleavage cycle are known as blastomeres. The cleavage-stage begins with the zygote, progresses through the morula stage (16-to-64 cells), and terminates at the start of the blastula stage (O'Farrell, Stumpff, & Su, 2004). Gastrulation follows cleavage and is the process of defining the primary germ layers: ectoderm, mesoderm, and endoderm (Figure 1) (*Gastrulation: From Cells to Embryo*, 2004). These tissue layers are known as primary germ layers because cell groups belonging to different organs in a fully developed organism can be traced back to these germ layers. Neurulation follows gastrulation and is the process by which the ectoderm is transformed into the nervous tissue, following induction from the underlying notochord (Smith & Schoenwolf, 1997). The final step during embryonic development is organogenesis, a process by which cells from different germ layers cooperate to form specialized organs like the heart, limbs, etc. (Collins & Stainier, 2016).

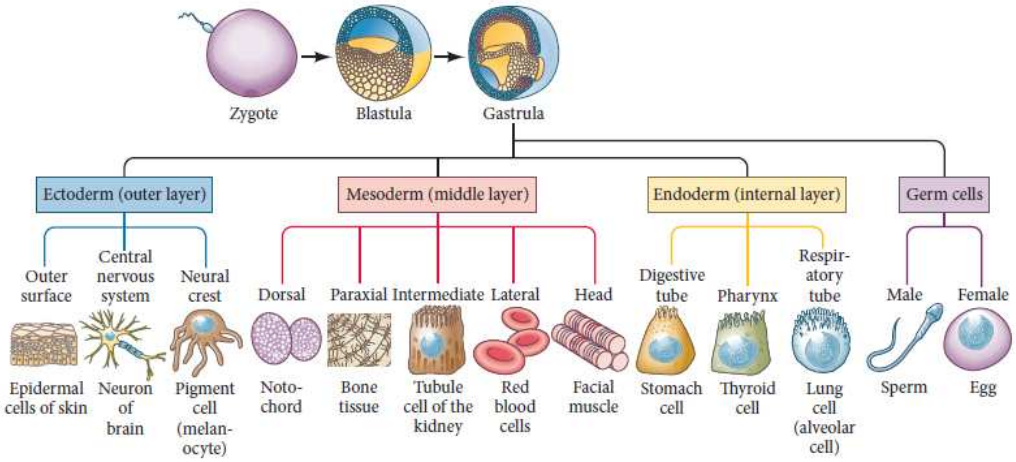

Figure 1. Gastrulation

Gastrulation is the process by which embryonic regions are specified into three germ layers: endoderm, mesoderm, and ectoderm. All cell types in an adult organism are derived from these primary tissues. Image adapted from (Barresi & Gilbert, 2019).

What makes the research to unravel the cellular and molecular mechanisms driving embryogenesis obligatory? Embryogenesis is a key step during the life of an organism as this step determines whether an organism develops an eye in the orbit and not ears. According to renowned developmental biologist Lewis Wolpert, "it is not birth, death, or marriage, but gastrulation which is truly the most time in your life". Embryogenesis follows a developmental program, with steps happening in an orderly fashion, and any problem with this developmental program can lead to developmental disorders like neurulation-defects (anencephaly, spina bifida, etc.), or can even lead to premature death, making it essential to study the processes during embryogenesis.

The study of embryonic development has always grabbed the attention of both scientists and philosophers equally, to date, as this could shed light on the origin of life. Greek philosopher, Aristotle (342-22 BCE) was among the pioneers to describe fertilization and embryogenesis in great detail. He has discussed the formation of an organism and its organs in *De generatione animalium* (on the generation of animals). Although Aristotle managed to create a systematic catalog of the processes of development based on his observations and anatomical studies, not all were without fault. One such example was his theory of spontaneous generation (*generatio spontanea*), which suggested that while some animals originated from fertilization, others like flies and eels are grown spontaneously from rotting meat. It was centuries later after cautious experiments by Louis Pasteur, this theory was negated. In continuous attempts to understand the processes driving embryogenesis, many animal models have emerged, due to ease of their availability, ease of handling, and experimental manipulations, like *C.elegans*, *Drosophila*, sea urchin, ascidians, zebrafish, *Xenopus*, and mouse. Despite the differences they exhibit during embryogenesis, some basic principles and processes seem to be present across different phyla like cell proliferation, cell differentiation (generation of functionally distinct cells), pattern formation (various cell types display species-specific spatial arrangements), cell movements, apoptosis (programmed cell death), and morphogenesis (shape formation). A

changing trend in the use of model systems was always present, reliant on the improvement of fluorescence microscopy techniques, interdisciplinary approaches, and accessibility to different genetic tools. These extensive studies using diverse model systems have made it increasingly clear that the key features of embryogenesis remained unaltered during the course of evolution. In this study, I have used developing *Drosophila* embryos to address the research question.

1.1 Why *Drosophila*?

The meticulous use of *Drosophila* for scientific research was kick-started by the unanticipated discovery of the *white* mutation by Thomas H. Morgan and the identification of its linkage to the X-chromosome (Morgan, 1910). There are numerous reasons for *Drosophila* to turn out to be such a popular research model to address questions related to development:

(i). they have a very short life cycle, with one day to complete the entire process of embryogenesis.

(ii). they are relatively cheap and easy to maintain in the lab.

(iii). they have a relatively smaller genome (four pairs of chromosomes) with low levels of redundancy, i.e., one protein class is often encoded by one or very few genes. This makes it easier to observe mutant phenotypes.

(iv). their genome is fully sequenced and currently (Adams et al., 2000; Celniker et al., 2002; Hoskins et al., 2007; Rubin, 1998), it is estimated that there are ~ 14,000 genes (Misra et al., 2002). These genes and gene products are well annotated and each of them has a dedicated page on a database platform called Flybase (https://flybase.org/).

(v). *Drosophila* exhibits high levels of genetic conservation. For example, approximately 75% of genes associated with human diseases have a conserved counterpart in flies (Reiter, Potocki, Chien, Gribskov, & Bier, 2001).

(vi). a variety of genetic tools are available for blocking or activating molecular pathways with high spatio-temporal resolution (Hales, Korey, Larracuente, & Roberts, 2015). Any gene of interest can be expressed in a tissue-specific manner using UAS/Gal4 system (Brand & Perrimon, 1993; Elliott & Brand, 2008). Tools for clonal analysis are available to study the function of deleterious mutations and cell lineage analysis (St Johnston, 2002). Gene and protein expression and their localization can be monitored

using available tools like the MiMIC system (Venken et al., 2011) to tag endogenous loci using fluorescent markers, tags, or Gal4.

(vii). efficient adaptation of the CRISPR/Cas system made it extremely easy to produced targeted mutations to study the functions of genes.

(viii). availability of different stocks from public repositories like BDSC, VDRC, KDGRC, etc. For instance, VDRC has RNAi lines (Carthew, 2001) to knock down ~88% of *Drosophila* genes (Dietzl et al., 2007).

(ix). *Drosophila* embryonic development is relatively faster and embryos are transparent enough to perform fluorescence microscopy. Genes and molecular pathways identified during embryonic development show significant conservation across phyla.

Thus, the above-mentioned reasons allow the use of *Drosophila* as an imperative model for research in developmental biology.

1.2 *Drosophila* early embryonic development

In contrast to other model systems, insect embryos undergo superficial cleavage, that is large centrally-placed yolk delimits the cell division to the periphery of embryos. After fertilization, the first thirteen cell divisions are incomplete. No cell membrane other than the egg itself, ensheath each cell during this time, leaving the embryo to be a syncytial blastoderm (Figure 2). These nuclei share a common cytoplasm, and molecules diffuse all over the embryo freely. For the duration of the initial three divisions, nuclei remain clustered at the anterior third of the embryo, and later during the fourth to sixth divisions, the nuclei are evenly distributed along the length of the embryo (Yamaguchi, Date, & Matsukage, 1991). The first eight nuclear divisions occur at the center of the embryo, averaging eight minutes each, producing 256 nuclei (Zalokar, 1976). Then they slowly migrate towards the periphery of the embryo, where the mitotic divisions continue (Foe & Alberts, 1983). During the ninth nuclear division cycle, about five nuclei at the posterior pole bud out and get enclosed by a membrane, to form pole cells that produce future gametes in the adult organism. By the tenth nuclear division cycle, most of the other nuclei reach the periphery of the embryo and undergo four more rounds of division (Foe & Alberts, 1983). The plasma membrane starts growing inward in a process called cellularization (Lecuit, 2004; Mazumdar & Mazumdar, 2002), separating each nucleus into individual cells (Figure 3), following the thirteenth cell cycle, producing a cellular blastoderm (Figard, Xu, Garcia, Golding, &

Sokac, 2013; Lecuit & Wieschaus, 2000; Loncar & Singer, 1995). Cellularization is a biphasic process: the first slow phase is characterized by invagination of the cell membrane and actomyosin cortex between nuclei to form the furrow canals (Figure 3B) and the second phase begins when the furrow canal traverses the nucleus, the invagination becomes faster and the actomyosin network constricts to separate cells from the yolk plasm (Figure 3C-E). Interestingly, cytoplasmic bridges still connect the cells to the yolk sac until gastrulation begins. These cytoplasmic connections are pinched off in a cytokinesis-like event only when the gastrulation and early germband elongation begins, i.e. this is the point when embryonic cells are completely individualized (Blankenship & Wieschaus, 2001). The cellular blastoderm has ~ 6,000 cells regularly arranged around the yolky core of the embryo and is formed within four hours post-fertilization (Turner & Mahowald, 1977).

Figure 2. Early development of *Drosophila* embryo

The first thirteen cell divisions after the fuson of the pronuclei are incomplete. These division cycles are partial, they are karyokinetic cycles and do not proceed to cytokinesis, leaving the embryo to be a syncytial blastoderm. For the duration of the initial three divisions, nuclei remain clustered at the anterior third of the embryo, and later during the fourth to sixth divisions, the nuclei are evenly distributed along the length of the embryo. The first eight nuclear divisions occur at the center of the embryo, averaging eight minutes each, producing 256 nuclei. Then they slowly migrate towards the periphery of the embryo, where the mitotic divisions continue. Image courtesy: (Barresi & Gilbert, 2019).

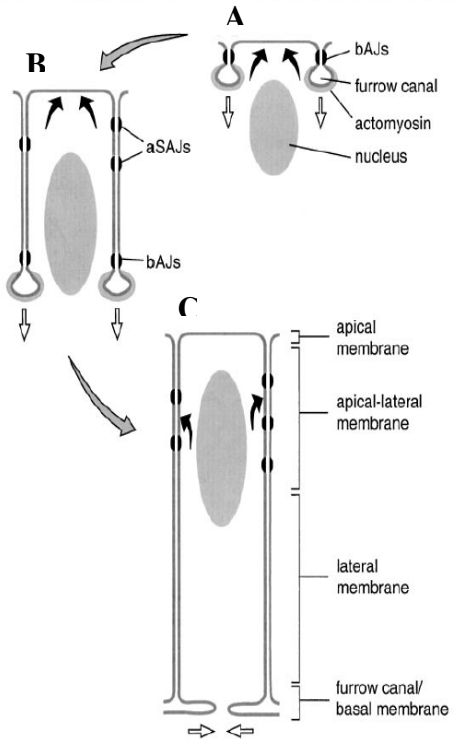

Figure 3. Stages of cellularization in *Drosophila* embryo

A) Cellularization commences (slow phase). Furrow canals form between each nuclei. Basal adherens junctions (bAJs) form just above the fourrow canals. B) End of slow phase and beginning of fast phase. Apical adherens junctions are assembled on the apical cortex. C) Cellularization ends when the actomyosin deposited in the furrow canal constricts, separating blastoderm cells from the yolk. Image adapted from (Tepass, Tanentzapf, Ward, & Fehon, 2001).

1.2.1 Midblastula transition

During the early cleavage cycle, the first thirteen nuclear divisions occur within three hours of fertilization. The nuclear division cycles toggle between M and S phases, with extremely short G1 and G2 phases, permitting division cycles to proceed swiftly, compared to the representative cell cycle duration of 24 hours. Cell cycles 1-10 occur in synchrony, which lasts around 8 minutes each. The last division cycle of the syncytial blastoderm, cycle 13, takes a bit longer, around 25 minutes. Cycle 14 which happens after cellularization, is asynchronous; some groups of cells take around 75 minutes, while others take 175 minutes (Foe, 1989). Processes before cellularization do not require zygotic gene products and they mainly count on maternally supplied transcripts and proteins (Merrill,

Sweeton, & Wieschaus, 1988). The transcription rate from zygotic nuclei (that starts around cycle 11) accelerates during cycle 14 (Merrill et al., 1988; Zusman & Wieschaus, 1985). This marks the commencement of the midblastula transition or maternal-to-zygotic transition step. Midblastula transition is observed during the development of other invertebrate and vertebrate embryos like *Xenopus* (Newport & Kirschner, 1982a, 1982b). Edgar and colleagues have shown using the haploid mutant embryos that the timing of midblastula transition in *Drosophila* embryos is regulated by the nuclear-to-cytoplasmic ratio (Edgar, Kiehle, & Schubiger, 1986; Edgar & Schubiger, 1986).

1.2.2 Gastrulation

By the end of cellularization, the *Drosophila* embryo is a prolate spheroid with ~6000 cells around the periphery. Gastrulation begins with the invagination of the prospective mesoderm inside the embryo. During this period, groups of precursor cells to three germ layers undergo dramatic changes resulting in the internalization of both mesoderm and endoderm (Gheisari et al., 2020) (Figure 4).

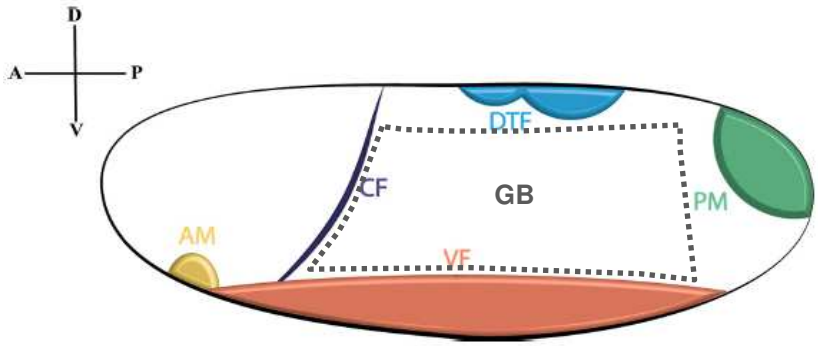

Figure 4. Map of morphogenetic movements in *Drosophila* embryo

Schematic representation of a blastoderm stage embryo with regions undergoing distinct morphogenetic movements depicted: anterior midgut (AM) invagination, cephalic furrow (CF) formation, ventral furrow (VF) formation, germband (GB) extension, dorsal transverse fold (DTF) formation, and posterior midgut (PM) invagination. Embrynic body axes are indicated in the inset: A-anterior, P-posterior, D-dorsal, and V-ventral. Image modified from (Gheisari et al., 2020).

1.2.2.1 Mesoderm invagination

Drosophila gastrulation begins during the midblastula transition when a band of around 1,000 cells (~10 to 12 cells wide and 80 cells long) at the ventral midline encompassing ~80% of the egg length and ~20% of the circumference, undergoes apical constriction, forming a furrow at the ventral side (ventral furrow), which eventually invaginates inside the embryo to form prospective mesoderm (Kam, Minden, Agard, Sedat, & Leptin, 1991; Leptin & Grunewald, 1990; Sweeton et al., 1991). The furrow eventually pinches off from the embryonic surface to form a transient ventral tube, which then flattens, cells dissociate and migrate beneath the ventral ectoderm, a process marking the epithelial-to-mesenchymal transition (EMT) (Leptin, 1999) (Figure 5).

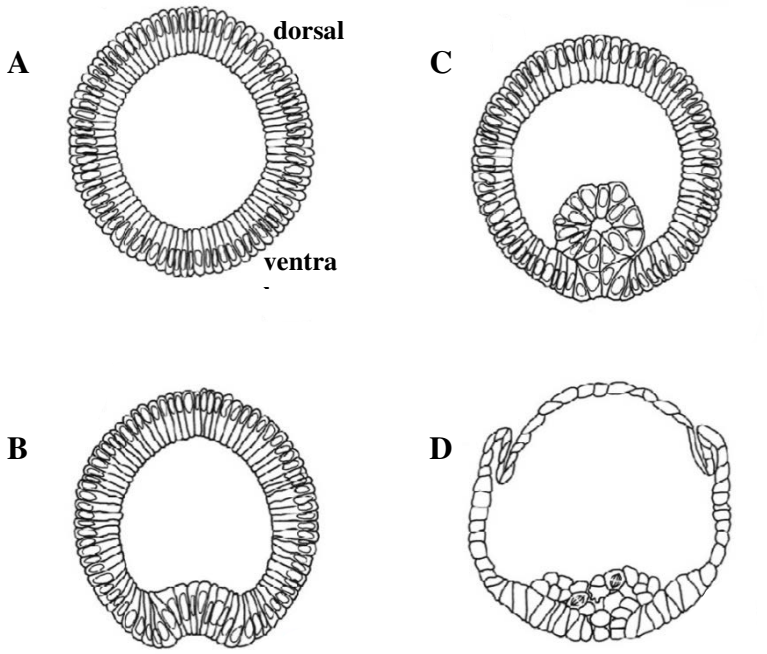

Figure 5. Steps during mesoderm invagination

Graphical representations of cross-sections from developing *Drosophila* embryo at different stages of mesoderm invagination: (A) blastoderm stage embryo at the end of cellularization, (B) 15 minutes later, a furrow is formed at the ventral side after the prospective mesoderm cells constrict their apical surface, (C) mesoderm is completely invaginated and forms a tube inside the embryo, and (D) approximately 45 minutes after the initiation of gastrulation, the mesoderm tube collapses, the mesoderm cells lose their epithelial characters, they initiate the EMT program, starts migrating over the underlying ectoderm. Image modified from (Leptin, 2005).

1.2.2.2 Posterior midgut invagination

The endoderm primordium in the *Drosophila* embryo lies at two different locations, anterior and posterior to the presumptive mesoderm anlage (Poulson, 1950). Another marked event during the first step of gastrulation is the posterior midgut (PMG) invagination, which happens few minutes after ventral furrow formation (Sweeton et al., 1991) (Figure 6A-C). Pole cells are internalized together with PMG during invagination (Sweeton et al., 1991).

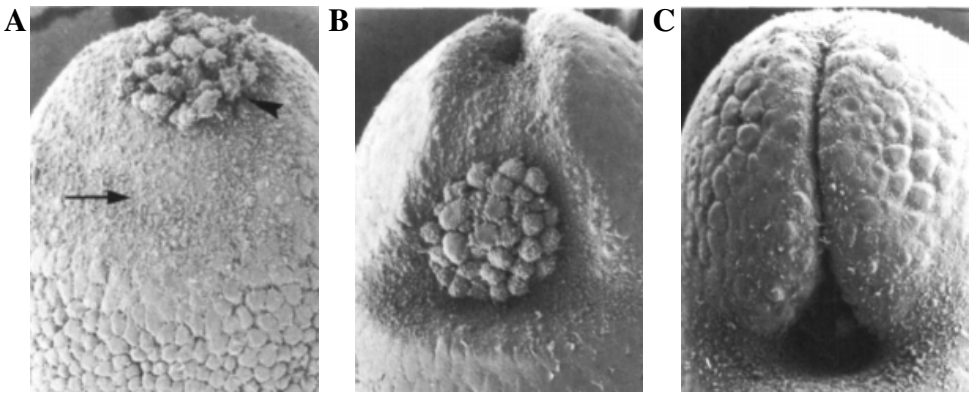

Figure 6. Steps during PMG invagination

Representative zoom in of SEM micrographs depicting different stages of PMG invagination: (A) a group of cells at the posterior pole which are precusors of posterior midgut, flattens their apical surface (arrow), with pole cells sitting on the PMG cells (arrowheads) (B) apical constriction of PMG cells create a disc-shaped furrow, and (C) lastly, as the germband extends, the PMG invaginates inside the embryo, taking in the pole cells with them(Sweeton et al., 1991).

1.2.2.3 Germband extension

Once the embryo has initiated PMG invagination, the ectodermal cells on the lateral surface undergo convergence and extension, a process known as germband extension (GBE) (Figure 7). The germband tissue extends posteriorly, and as the embryo is encased in a tough case, wraps around the dorsal side of the embryo. By the end of GBE, cells ordained to make the larval posterior structures will be placed next to the head region (Figure 7). Germband is comprised of ectoderm and mesoderm tissue, which gives rise to the segmented section of the larva. These cells are precursors to the dorsal epidermis, neurogenic ectoderm, mesectoderm, and mesoderm. Initially, the germband populates the posterior two-third of the embryonic dorsolateral surface, whose boundaries at anterior is demarcated by the transient cephalic fold and at posterior by the ventral furrow/PMG

boundary. GBE is a biphasic process (Hartenstein, 1985); during the initial fast phase, the germband extends ~60% egg length over 30 minutes, and during the later slow phase which spans for the next 70 minutes, the germband reaches its maximal extended condition (70% egg length from posterior to anterior). By the completion of GBE, the germband is twice long and half wide in comparison to the original proportions (Hartenstein, 1985; Turner & Mahowald, 1977).

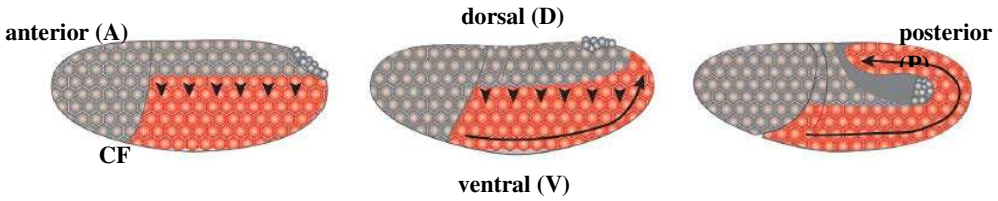

Figure 7. Germband extension (GBE)

During GBE, a band of cells on the lateral side of the embryo (marked in red) extends along the AP axis, while converging along the DV axis. Image modified from (Gheisari, Aakhte, & Muller, 2020).

1.2.2.4 Transient folds

Three transient folds are visible on the lateral side of the embryo during gastrulation and germband extension. A transient fold, called cephalic furrow (CF), is formed at a distance close to one-third from the anterior pole of the embryo. The CF appears as vertical indentations along both lateral sides with a slight delay of around 5 minutes to initiation of ventral furrow formation (Figure 8A). As the CF formation progresses, these folds take a tilted dorsoventral course, expanding along the dorsoventral axis, forming a ring-like cleft that is about 30µm deep (A. K. Spencer, Siddiqui, & Thomas, 2015). CF subdivides the anterior-posterior axis into two territories: the head and the metameric germband. CF is a transient, dynamic structure, different portions of the outer embryonic layer are temporarily taken inside the fold during the entire duration of GBE. Even though the exact role of CF is still unknown, it is thought that CF could help the anterior cells to keep their position during GBE, as evidenced in a study by *Costa et al.* in which mutant embryos lacking CF showed an anterior expansion of germband compared to wildtype (Costa, Sweeton, & Wieschaus, 1993).

Other folds observed on the dorsal side of the embryo, shortly after the onset of gastrulation, are called dorsal transverse folds (DTF). DTF comprises of two folds, anterior DTF and posterior DTF (Figure 8B) (Y. C. Wang et al., 2012). The posterior DTF appears slightly earlier than the anterior DTF. After the initiation of DTF, they spread laterally. The anterior DTF is shallower compared to the posterior DTF, as the number of cells recruited into the former is less. The DTFs are also transient structures like cephalic furrow, taking inside embryonic cells on the surface for a short period and by the end of GBE, these structures disappear (Turner & Mahowald, 1977).

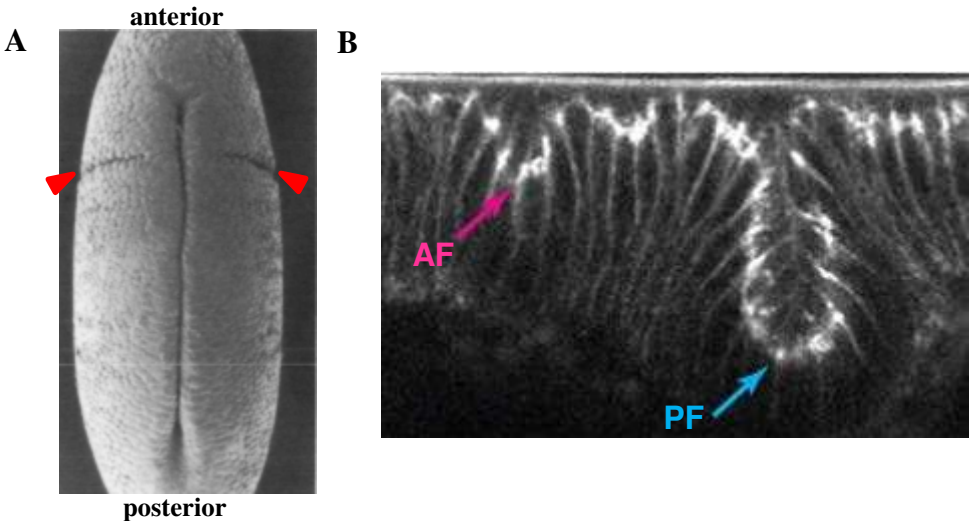

Figure 8. Transient folds

(A) SEM micrograph depicting cephalic fold (red arrowheads). Image modified from (Sweeton, Parks, Costa, & Wieschaus, 1991). (B) Fluorescent image showing two transient dorsal folds: AF, anterior fold and PF, posterior fold. Image adapted from (Y. C. Wang, Khan, Kaschube, & Wieschaus, 2012).

1.2.2.5 Anterior midgut invagination

The ventral furrow invagination extends about 50µm anterior to the cephalic fold, where it bifurcates to make two branches, creating a Y-shaped dent called anterior midgut (AMG) invagination (Hartenstein, 1985). AMG invagination is delayed by five minutes compared to ventral furrow formation but exhibits similar cell shape changes to the mesoderm precursors. It is difficult to tell apart AMG from invagination mesoderm during the invagination phase as they share continuous lumen. Later, a spurt of mitotic divisions in this region generates a large cluster of cells,

which gets completely disconnected from the mesoderm and becomes the endoderm (Costa et al., 1993; Poulson, 1950; Turner & Mahowald, 1977).

1.2.2.6 Germband retraction

Once the germband is fully extended, the germband starts retracting (Figure 9A). Germband retraction (GBR) or shortening restores the anatomical relationships of the larva; i.e. the caudal end of the hindgut is reinstated to the posterior end of the embryo (Schock & Perrimon, 2002a). It is during this step the anterior and posterior midgut anlagen fuse, tracheal tree forms due to the establishment of continuity among different segments, and the gonads form. After the germband starts retracting, the dorsal side of the embryo remains open, which is covered by a monolayer of squamous extraembryonic epithelium, known as amnioserosa.

1.2.2.7 Dorsal closure

As the germband retracts, the dorsal epidermal primordium on either side of the embryo starts extending towards the dorsal midline, resulting in the closure of the opening left by GBR at the dorsal side. This process is known as dorsal closure (DC) (Figure 9B) (Hayes & Solon, 2017). The amnioserosa tissue shrinks and is completely removed by the end of DC. The epidermal cells progressively fuse and result in connected, scarless tissue.

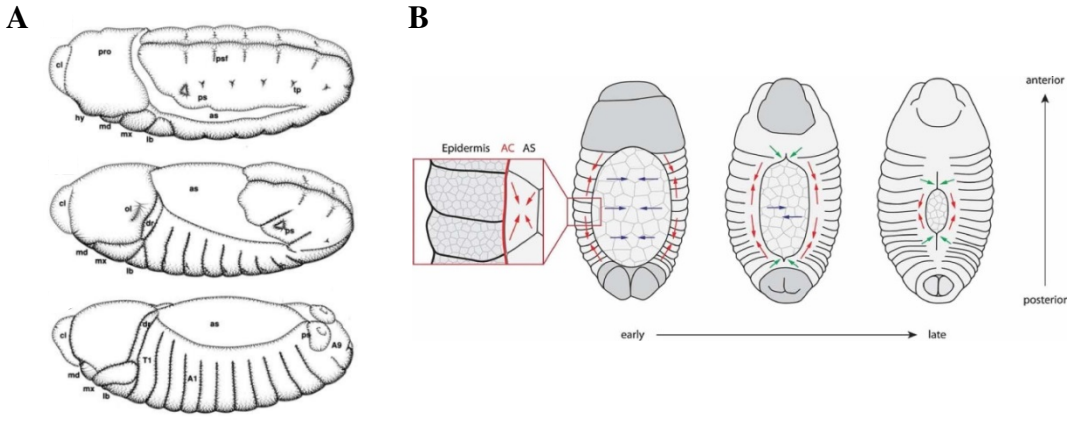

Figure 9. Germband retraction and dorsal closure

(A) Graphical representation of germband retraction. Image courtesy: Hartenstein, V. 1993. (B) Schematic drawings of the process of dorsal closure. Image adapted from (Heisenberg, 2009).

2. Gastrulation movements and cell shape changes

In nature, organisms exhibit a wide range of morphologies, pointing to a fundamental question: how does matter organize itself to produce distinct tissue structures, without an architect? The process of sculpting the final shape of organs and organisms is known as morphogenesis (Hogan, 1999). Cells, both individual and group, undergo discrete shape changes to produce the intricate design of a developing embryo during morphogenesis. As far as living matter is concerned, while a huge number of shapes can be modeled using combinations of cell shape changes (Huzita & Scimemi, 1989), the number of basic epithelia transformations that are shown to mold an embryo is seven (Rauzi, 2020). A piece of tissue can (i) grow, (ii) shrink, (iii) thicken, (iv) thin, (v) bend, (vi) converge and extend, and (vii) twist (Figure 10), to produce the final shape and body plan of a mature organism.

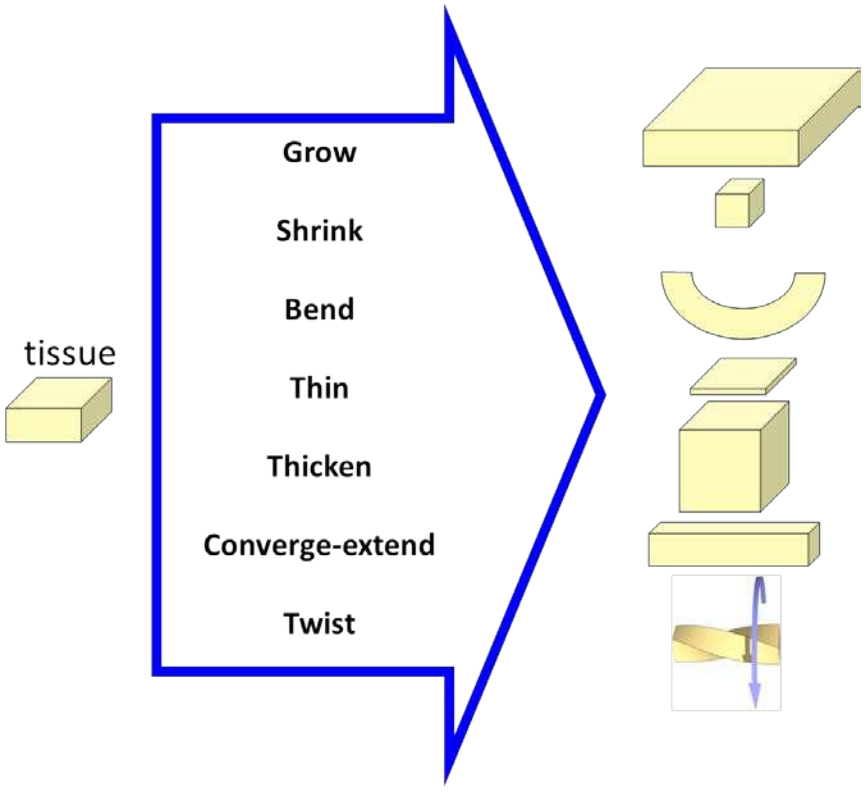

Figure 10. Basic epithelia transformations

Epithelial sheet display variety of form and shape but the basic set of shape transformations that occur during development are 7: a piece of tissue can grow, shrink, bend, thin, thicken, converge-extend, and twist.

2.1 Epithelial cells: basic units of development

Cells constituting the tissue undergoing morphogenetic processes can be either of epithelial or mesenchymal nature. Most of these events happen by deforming epithelial sheets (Heisenberg & Bellaiche, 2013; Quintin et al., 2008; St Johnston & Sanson, 2011). A remarkable feature of epithelial cells is that they are highly polarized along their apical-basal axis, whereas mesenchymal cells are not. Mesenchymal cells may display polarity, but the direction of their polarity axis is random.

Different types of epithelia are classified primarily based on their thickness, and cell morphology (Gibson & Gibson, 2009). Epithelial tissues are classified based on thickness into three: simple, stratified, and pseudostratified (Figure 11A-C). Simple epithelia are monolayer of epithelial cells, whereas, stratified epithelia are composed of two or more layers of cells. Pseudostratified epithelia are extraordinary in the way that they are monolayer epithelia, but since nuclei of constituent cells are arranged in different locations along the apical-basal axis, imparting a sense of multilayered epithelia. Each cell in a pseudostratified epithelium maintains both apical and basal connections, conferring them a spindle shape. Epithelia are also categorized based on their constituent cell shape into three: squamous, cuboidal, and columnar (Figure 11D-F). Squamous epithelium has cells that are wider than their height, making them flattened. Squamous epithelial cells may appear as flat, rounded, or scale-like polygonal plates. Cuboidal epithelia have cells that have equal height and width, making the vertical section made from these cells looks isometric. Columnar epithelia have cells that have a height-to-width ratio of more than one. They are polygonal when sectioned horizontally, similar to cuboidal cells.

Epithelial morphogenesis is a key process during development, organogenesis, and even pathogenesis, whether it is in the simplesvariety of organisms depends on epithelia and their derivatives for their development and tissue maintenance. Though these organisms have well diverged in the evolutionary tree, certain evolutionarily conserved structural features remain unaltered concerning epithelial architecture, including apical-basal polarization, creation of cell-cell contact junctions, and assembly of the paracellular diffusion barrier.

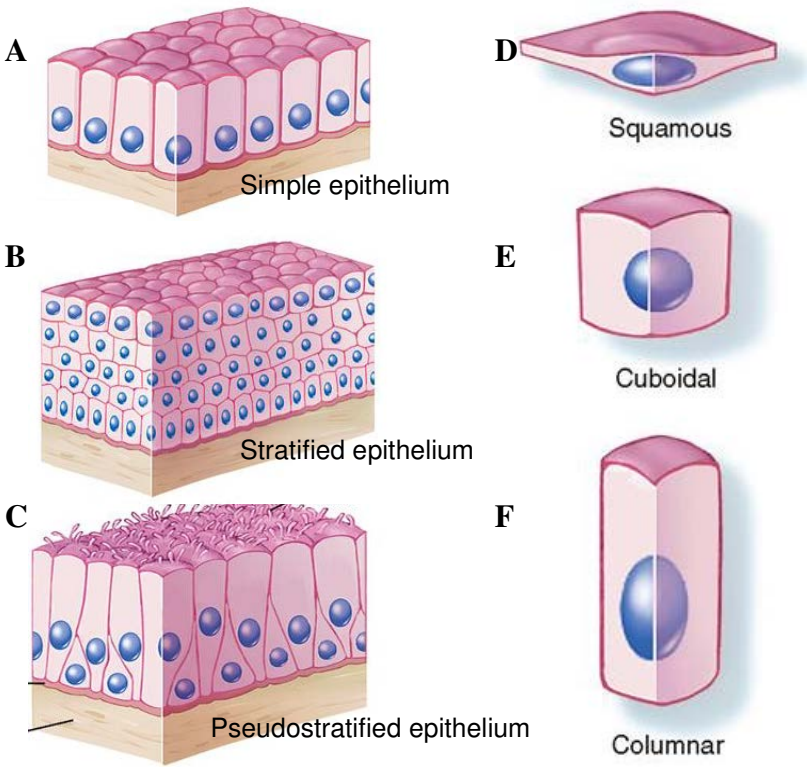

Figure 11. Classification of epithelia

Major classifications of epithelia are based on their thickness and cell shape. Epithelia are classified based on thickness (A-C) into simple (A), stratified (B), and (C) pseudostratified and based on cell shape (D-F) into squamous (D), cuboidal (E), and columnar (F). Image courtesy: basicmedicalkey.com

2.1.1 Epithelial cells are highly polarized

Epithelia function as both protective sheathing from the environment and to act as a barrier between different chemical milieu. They do so by forming a highly robust, tightly associated, coherent sheet of cells. In contrast to mesenchymal cells, epithelial cells are highly polarized with well-defined polarity axes and are laterally interconnected through junctions (Fristrom, 1988). Epithelial cells display two major types of polarity: apical-basal polarity and planar cell polarity (PCP) (H. Zallen & Zallen, 1976). Epithelial cells have distinct membrane domains along the apical-basal axis established by asymmetric segregation of membrane proteins and lipids, leading to the apical-basal polarity (Figure 12A) (Martin-Belmonte & Mostov, 2008). Apical-basal polarity is essential for maintaining the integrity of the epithelial sheets and will be discussed in detail in the following subsection. In addition to apical-basal polarity, epithelial cells

exhibit a second mode of polarity along the plane of the tissue, orthogonal to the apical-basal axis, namely planar cell polarity (PCP) (Figure 12B). PCP is essential during morphogenesis, especially when certain morphogenetic behavior are polarized in the plane of the epithelial sheet (reviewed in (M. T. Butler & Wallingford, 2017; J. A. Zallen, 2007)).

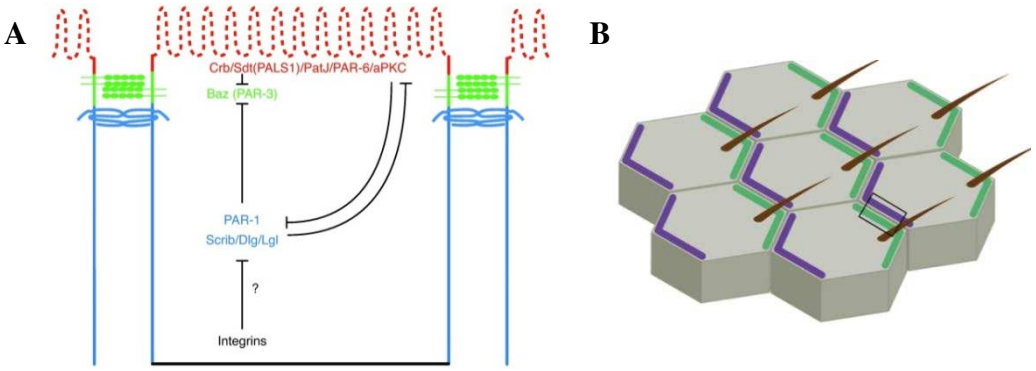

Figure 12. Epithelial cells are polarized

(A) Apical-basal polarity. Epithelial cells have distinct membrane domains along the apical-basal axis. Apical domain is depicted in red, junctional domain dividing apical and lateral domains in green, lateral domains in blue, and the basal domain in black. Mutually exclusive molecular interactions establish and stabilize apical-basal polarity. Image adapted from (St Johnston & Sanson, 2011). (B) Planar cell polarity (PCP). Protein components are asymmetrically localized along the plane of the tissue orthogonal to the apical-basal polarity. Image adapted from (M. T. Butler & Wallingford, 2017).

2.1.1.1 Apical-basal polarity in epithelial cells

The epithelial plasma membrane is subdivided into immiscible apical and basolateral domains (Tepass et al., 2001). Epithelial cells have atleast four distinct domains along the apical-basal axis: apical, junctional, lateral, and basal (St Johnston & Sanson, 2011). Generally, the apical surface of epithelial cells faces towards the exterior (in the case of epidermal epithelia) or the luminal spaces (in the case of internal organs like the gut). The apical domain is divided into the free apical domain and a region where neighboring cells make contact. This region is known as the marginal zone in *Drosophila* and is related to tight junctions in vertebrates (Tepass et al., 2001). The basolateral domain is divided into lateral involved in cell-cell adhesion and basal surfaces. The basal surface of the epithelial cells is usually connected to the extracellular basal lamina secreted by the cells (Fristrom, 1988). However, this is not true always, as epithelial cells engaged actively during development lack a well-defined

basal lamina. In particular cases, basal lamina existing *a priori* is either degraded or even detached from the epithelia, during morphogenetic movements (Svoboda & O'Shea, 1987).

2.1.1.2 Establishing apical-basal polarity in epithelial cells

The establishment of apical-basal polarity in epithelial cells is critical as it is required for them to perform their barrier function. The distribution of both surface and cytosolic components, including membrane lipids, transmembrane proteins, and associated cortical proteins, echoes the apical-basal polarity of epithelial cells, creating these distinct domains (Figure 12A) (Schock & Perrimon, 2002b; Wodarz, 2002). In epithelia, cell membranes form specific domains with the action of three evolutionarily conserved protein complexes (Roignot, Peng, & Mostov, 2013): the apical Par protein system, the Crumbs (Crb)/Pals1/PatJ complex, and the Scribble complex, originally identified in *Drosophila* and *C.elegans* (Assemat, Bazellieres, Pallesi-Pocachard, Le Bivic, & Massey-Harroche, 2008), are now identified as key components of polarity-generating signaling pathways across the animal kingdom (Nance & Zallen, 2011; St Johnston & Ahringer, 2010; B. J. Thompson, 2013; Wodarz, 2002). Major components of the apical/junctional Par system include Par3 (Bazooka, Baz in *Drosophila*), Par6, and atypical protein kinase (aPKC). The Crumbs complex comprises integral membrane protein Crumbs (Crb), Pals1 (Stardust in *Drosophila*), and the Pals1-associated tight junction homolog, PatJ. Both the apical Par and Crb complexes are vital for defining the apical domain of the epithelial cells (Macara, 2004; Margolis, 2018). The basolateral domain of epithelial cells is defined by the localization of the components belonging to the Scribble complex, including Scribble (Scrib), Discs Large (Dlg), and Lethal Giant Larvae (Lgl) (Elsum, Yates, Humbert, & Richardson, 2012), together with the Yurt (Yrt) group (Yrt, Cora, Na+/K+-ATPase, Neurexin IV (Nrx IV)) (Laprise et al., 2009), and Par1 (Benton & St Johnston, 2003).

Proteins belonging to these complexes depend primarily on modular protein-protein interactions in order to establish distinct signaling centers along the apical, lateral, and basal domains. Many polarity proteins, for instance, have numerous PSD95-Dlg-ZO1 (PDZ) domains, that enable them to interact and then become bound to cortical F-actin (Bilder, 2001, 2003; Bilder, Schober, & Perrimon, 2003; Roh & Margolis, 2003). Crb can directly interact with the PDZ domain of Pals1 through its C-terminal tail (Bachmann, Schneider, Theilenberg, Grawe, & Knust, 2001; Y. Hong,

Stronach, Perrimon, Jan, & Jan, 2001; Roh, Fan, Liu, & Margolis, 2003). Pals1 acts as a scaffold that hosts multiple protein-protein interaction sites that enable its interaction with Lin-7 through one of its L27 domain and PatJ through its second L27 domain (Roh et al., 2002). The key Par complex protein aPKC directly interacts with Par6 through PB1 domains (Macara, 2004). Similarly, Par complex components Par6 and Par3 are also PDZ domain scaffold proteins that take part in multiple modular protein-protein interactions (Macara, 2004).

2.1.1.3 How is polarity generated?

The principal cues that initiate polarization in epithelial cells are cell-cell and cell-extracellular matrix (ECM) contacts (Drubin & Nelson, 1996; Yeaman, Grindstaff, Hansen, & Nelson, 1999). Cell-cell adhesion is chiefly mediated by the molecules of the cadherin superfamily (see also the section on E Cad-mediated cell adhesion later) (Tepass, Truong, Godt, Ikura, & Peifer, 2000), and cell-ECM contact is largely facilitated by the transmembrane receptors of the integrin family (Giancotti & Ruoslahti, 1999). For long, the establishment of apical junctional complex (AJC), including the tight junctions (also dubbed as zonula occludens) and adherens junctions (also known as zonula adherens), is thought to precede epithelial polarization. Cell adhesion molecules play pivotal roles in the early steps of epithelial polarization. Before getting fully polarized, the epithelial plasma membrane has cadherin-containing cell contacts scattered throughout. During the early phase of cell-cell contact formation, cells assemble spot-like, primordial adherens junctions (pAJs) which contain E-Cadherin, nectins, or JAMs, but do not have polarity proteins like Par3, aPKC, or Lgl (Suzuki et al., 2002). At this phase, even the tight junction in the *zonula occludens* has not yet formed and several of its components are found together with the adherens junction components, along the lateral surface (Fleming, Ghassemifar, & Sheth, 2000; Rajasekaran, Hojo, Huima, & Rodriguez-Boulan, 1996; Sheth et al., 2000). In a later phase, adherens proteins coalesce into a belt-like adhesive complex called *zonula adherens* in the apical-lateral region of the plasma membrane. During this period the components of adherens and tight junctions get separated and sorted, resulting in the assembly of tight junctions (Fleming et al., 2000). Par3-aPKC-Par6 is recruited to pAJs only after their formation (Suzuki et al., 2002). During this process, various components of adhesion participate in the polarization of epithelial cells. Studies in mammalian cells have shown that Jam-A facilitates the correct localization of Par-aPKC complex and E-Cad and nectins activate the Rho family small GTPases Cdc42 and Rac1

(Fukuhara et al., 2004; Yamada & Nelson, 2007), which is a necessary step in activating the Par-aPKC complex (Yamanaka et al., 2001).

2.1.1.4 How is polarity stabilized?

When the epithelial cells are fully polarized, the Par-aPKC and Crb complexes localize to the apical domain and the Scribble-Lgl-Dlg complex remains localized to the basolateral domain. Once the final polarity is established, it is maintained by the mutually exclusive localization of these components facilitated by agonistic phosphorylations (Figure 12A) (Bilder et al., 2003; Morais-de-Sa, Mirouse, & St Johnston, 2010; Suzuki et al., 2004; Tanentzapf & Tepass, 2003). The Par1 kinase, shown to be localized to the lateral epithelial membrane (D. Cohen, Brennwald, Rodriguez-Boulan, & Musch, 2004; Doerflinger, Benton, Shulman, & St Johnston, 2003), regulates the localization of polarity proteins. Par1 can phosphorylate Par3, which in turn leads to 14-3-3 protein interaction with phosphorylated Par3 (Benton & St Johnston, 2003; Hurd et al., 2003). Par1 membrane targeting is blocked when phosphorylated by aPKC, hence it is excluded from the apical domain (Hurov, Watkins, & Piwnica-Worms, 2004; Suzuki et al., 2004). Another target of aPKC is a lateral protein, Lgl. Lgl forms a separate complex with aPKC and Par6, which excludes Par3 (Yamanaka et al., 2003). Lgl, when phosphorylated, is excluded from the apical domain and facilitates its targeting to the basolateral surface (Betschinger, Mechtler, & Knoblich, 2003; Plant et al., 2003). Similarly, it was shown that the Scribble-Lgl-Dlg pathway along the basolateral domain antagonizes the apical Crb and Par-aPKC complexes (Bilder et al., 2003; Tanentzapf & Tepass, 2003). Par1 inhibits basolateral localization of Par3, whereas Lgl blocks Par6 from localizing to basolateral domains (Doerflinger et al., 2010; Hutterer, Betschinger, Petronczki, & Knoblich, 2004). Studies in *Drosophila* have shown that blocking basolateral protein activity impedes the localization of apical domain proteins, leading to an expansion towards lateral surfaces (Bilder, 2004).

Tight or septate junctions also play a critical role in keeping apical and basolateral domains demixed. The tight junction occurs as the apical-most junctions in vertebrate epithelial cells, and they play a key role in stably separating apical and the basolateral membrane domains by establishing a diffusion barrier in the plane of the membrane, blocking free dispersal of biological macromolecules into interepithelial space (Figure 13A) (Cereijido, Valdes, Shoshani, & Contreras, 1998; Stevenson & Keon, 1998; Tsukita, Furuse, & Itoh, 2001; Zahraoui, Louvard, & Galli, 2000; Zihni,

Mills, Matter, & Balda, 2016). Claudins, Occludins, and junctional adhesion molecules (JAMs) are the well-characterized components of mammalian tight junctions (Rodriguez-Boulan & Macara, 2014). In contrast to vertebrates, invertebrate epithelial cells do not have tight junctions, instead, they develop septate junctions, that localize immediately basal to the adherens junction (Figure 13B). Septate junctions inhibit the paracellular diffusion of ions and biomolecules (Banerjee, Sousa, & Bhat, 2006; Daniel et al., 2018).

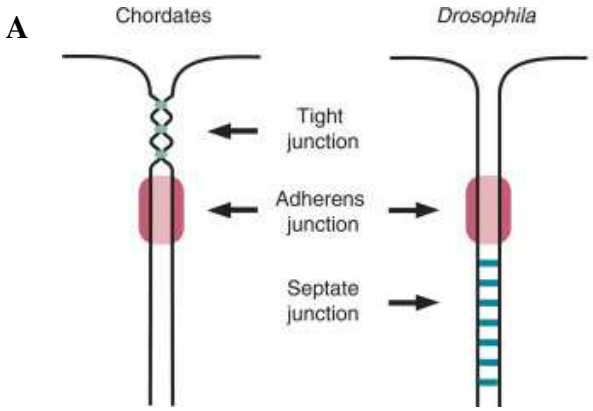

Figure 13. Tight and septate junctions

(A) Tight junctions are found in chordate epithelia, apical to the zonula adherens. (B) Septate junctions found in non chordates like *Drosophila* are present basal to zonula adherens. These epithelial cells lack tight junctions. Image adapted from (Hou, 2019).

As described before, the *Drosophila* embryo starts its life as a syncytium, and later, individual nuclei are ensheathed by plasma membrane during a process called cellularization, generating ~ 6000 cells around the periphery (Figure 14) (Mazumdar & Mazumdar, 2002). Cellularization is a fascinating process as it displays hybrid nature: it combines processes from both cytokinesis and epithelial polarization (Lecuit, 2004). The end product of cellularization is a contiguous epithelial monolayer around the yolk. Cellularization thus involves polarization of the ingressing lipid membrane and assembling apical adherens junctions that connect the epithelial cells. Studies have shown that evolutionarily conserved proteins necessary for junction-assembly like Dlg (O. K. Lee et al., 2003) and vesicular transport like Rab11 (Pelissier, Chauvin, & Lecuit, 2003; Riggs et al., 2003) are essential for cellularization. Initiation of cellularization is marked by the formation of dome-like plasma membrane structures called somatic buds above each nucleus. During the slow phase of cellularization, shallow

membrane invaginations separate neighboring somatic buds and these invaginations fold to from donut-shaped furrow canals (FCs) (Figure 3A). Basal adherens junctions (BAJs) are assembled just above the FCs, interrupting the continuous plasma membrane (Hunter, Sung, Schejter, & Wieschaus, 2002; Hunter & Wieschaus, 2000; Muller & Wieschaus, 1996). FC has analogous nature to the cytokinetic ring in composition, containing components like filamentous actin (F-actin), non-muscle myosin II (MyoII), Spectrins, Septins, etc. (Adam, Pringle, & Peifer, 2000; Lecuit, Samanta, & Wieschaus, 2002; Thomas & Williams, 1999; Warn & Robert-Nicoud, 1990), whereas the BAJs have molecules related to cell-cell adhesion like E-Cad and β-Catenin (β-Cat). The composition of FCs also includes junctional proteins such as PatJ (Bhat et al., 1999; Pielage, Stork, Bunse, & Klambt, 2003). The fast phase, which counts for more than half of the overall lateral membrane surface generated, is associated with the formation of apical adherens junctions (AAJs), where cells maintain their lateral contacts and are necessary for epithelial integrity. During this phase, E-Cad adhesion complexes occur in the subapical region as punctate structures called spotted-adherens junctions. By the end of cellularization, the E-Cad complexes form a continuous adhesive belt resulting in the maturation of AJs. At this stage, additional proteins required for the stabilization of E-Cad complexes and generating apical-basal polarity are recruited to the AAJs including aPKC (Wodarz, Ramrath, Grimm, & Knust, 2000), Par3 (Kuchinke, Grawe, & Knust, 1998), Par6 (Petronczki & Knoblich, 2001), and PatJ (Bhat et al., 1999). Interestingly, septate junctions are not present in the embryonic primary epithelium in *Drosophila* and form only after most morphogenetic movements have occurred (Tepass & Hartenstein, 1994).

Epithelial cells, highly polarized along the apical-basal axis, form a laterally coherent sheet, that can undergo specific shape changes, that provide the final form of organs and organisms. Major shape changes in epithelial tissues during development are discussed below.

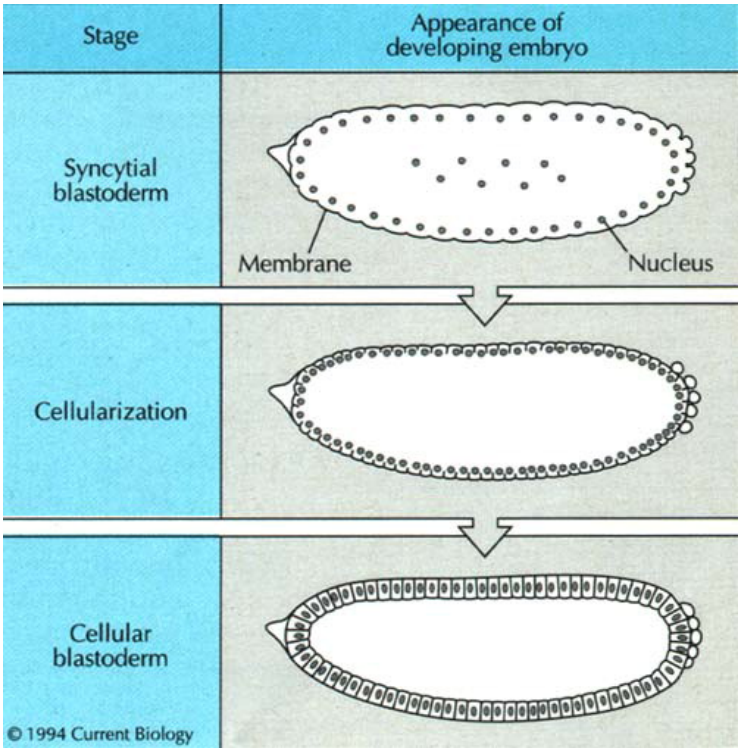

Figure 14. ***Drosophila*** **cellularization**

Sequential membrane invaginations around the syncytial blastoderm nuclei produces the ~ 6000 cells, arranged as a monolayer at the periphery. Image adapted from (Theurkauf, 1994).

2.2 Morphogenetic movements during gastrulation

Gastrulation is a process during embryogenesis that accompanies intense cellular movements and tissue-scale reorganizations. Four major modes of shape changes and cell movements have been observed during gastrulation: (i) apical constriction and tissue bending, (ii) convergence-extension, (iii) delamination, and (iv) cell migration (Gillard & Roper, 2020; Leptin, 2005).

2.2.1 Tissue bending

One of the earliest gastrulation-related morphogenetic movement in evolution is epithelial folding, that generates a two-layered structure from a monolayered epithelium (Figure 15A) (Lecuit et al., 2011). During epithelial folding, a large group of cells is translocated from the surface to inside the embryo (Denk-Lobnig & Martin, 2020). Epithelial folding or invagination occurs in sea urchin during archenteron formation (Kimberly & Hardin, 1998), it represents the first step in the case of *Drosophila* mesoderm invagination (Sweeton et al., 1991), and similar cell shape

changes that generate invagination is observed during initiation of involution in amphibians (bottle cells) (R. E. Keller, 1981). The bending of the epithelial sheet occurs in different steps (Figure 15B). First, the apical cortices of cells belonging to the bending epithelium undergo constriction, probably induced by actomyosin contractility. During this step, apically-constricted cells elongate along the apical-basal axis. Later, these cells shorten and expand their basal cortex, to become wedge-shaped or bottle-shaped (Pearl, Li, & Green, 2017; Sawyer et al., 2010). This results in the furrowing of a flat epithelial sheet to produce a concave furrow.

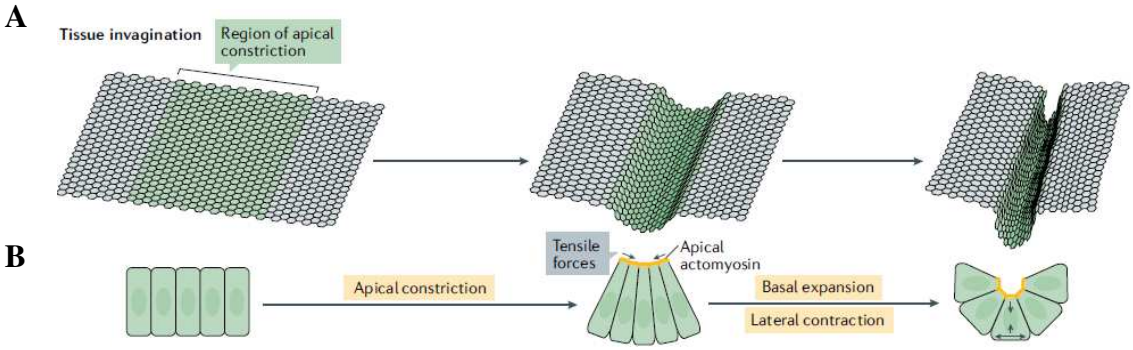

Figure 15. Tissue bending

(A) Tissue bending creates 3D shapes from 2D monolaye sheets. (B) Cell shape changes associated with apical constriction. Image adapted from {Collinet, 2021 #9909}.

Bending a sheet of epithelium can happen in the opposite direction, generating a convex furrow, when instead the basal surface constricts. Such a mechanism promotes the folding of the zebrafish mid-brain hind-brain (MBHB) boundary (Gutzman, Graeden, Lowery, Holley, & Sive, 2008) and optic cup (Nicolas-Perez et al., 2016). Interestingly, during some morphogenetic processes, both apical and basal surfaces constrict simultaneously. For instance, simultaneous apical and basal constrictions occur in neighboring regions of the developing mouse intestine, generating opposite curvature (Sumigray, Terwilliger, & Lechler, 2018). Simultaneous apical and basal constrictions can create complex 3D forms.

Folding an epithelial sheet does not always rely on polarized constriction of surfaces. It can also occur by relaxing either the basal or apical cortex of the cell. Such an event can be found in the folds of the *Drosophila* wing disc. Wing disc epithelium starts relatively as a flat sheet but forms three stereotypic folds later during development. A fold forms within the hinge

region (H/H fold) and a second one at the hinge/pouch region (H/P fold) (S. M. Cohen, 1993). Quantitative analysis of the apical surface of cells in the H/H fold showed that these surfaces do not change significantly during fold formation, despite that these cells become wedge-shaped. The basal surface in contrast increased in area and showed lower recoil velocity upon laser ablation, indicating that the mechanism driving this fold is basal relaxation rather than apical constriction (Sui et al., 2018). Altering mechanical properties along the lateral cortices also can play an important role in the process of folding (Kondo & Hayashi, 2015; Takeda, Sami, & Wang, 2018). Such a shortening along the apical-basal axis has been proposed to be a mechanism driving the dorsal transverse folds in developing *Drosophila* embryos (Y. C. Wang et al., 2012).

2.2.2 Cell rearrangement within the epithelial sheet

A piece of tissue can be also sculpted in the absence of overall cell shape changes or cell divisions. The dimensions of an epithelial sheet can be altered by rearranging the topology of cells, i.e. the connectivity among cells within the tissue (R. Keller, 2002; Kong et al., 2017). Cells exchange their neighbors to create new contacts with previously disjoint cells, in a process called cell intercalation, an analogous process to the "T1 topological transitions, or simply T1 transitions" in foams (Figure 16A) (Chae & Tabor, 1997; M. A. Spencer, Jabeen, & Lubensky, 2017). When intercalation occurs in a planar polarized manner, i.e., cell contacts lost are always oriented along one body axis and the new contacts are always formed in the orthogonal direction, such a transformation can lengthen the tissue along the axis of new contacts formed and reduce the width along the orthogonal direction (Rauzi, 2020; Siang, Fernandez-Gonzalez, & Feng, 2018).

Interestingly, cell interaction in dome-shaped invagination can transform it to long tubes, as observed in the case of archenteron formation in sea urchin (Hardin, 1989), or can create long narrow regions from short wide areas, as in the case of convergence-extension (CE) of epithelia during gastrulation and neurulation in vertebrates (R. Keller, Shih, & Sater, 1992; Shih & Keller, 1992a, 1992b; Wilson & Keller, 1991), CE of the dorsal ectoderm of *C.elegans* (Williams-Masson, Heid, Lavin, & Hardin, 1998), the notochord of ascidians (E. M. Munro & Odell, 2002), chick (Schoenwolf & Alvarez, 1989), and zebrafish (Glickman, Kimmel, Jones, & Adams, 2003), and GBE in *Drosophila* (Irvine & Wieschaus, 1994). Two modes of intercalary movements are described: during CE in early

vertebrate gastrulation, cell motility is associated with lamellipodia extensions (Wilson & Keller, 1991). During this step, cells that generate lamellipodia in random positions initially, start producing protrusions in a polarized manner along the mediolateral axis (Shih & Keller, 1992a). The second mode is described during *Drosophila* GBE, cell rearrangement is mediated by remodeling of contact surfaces of the neighboring cells apically (Bertet, Sulak, & Lecuit, 2004; Lecuit, 2004) or by resolving the basolateral protrusions (Sun et al., 2017). In this mode, cells change from a 6-neighbor configuration to a 4-neighbor configuration, by minimizing their contact surface with anterior and posterior neighbors to a point, and then going back to a 6-neighbor configuration in a different alignment with new contact surfaces between dorsal and ventral neighbors generated.

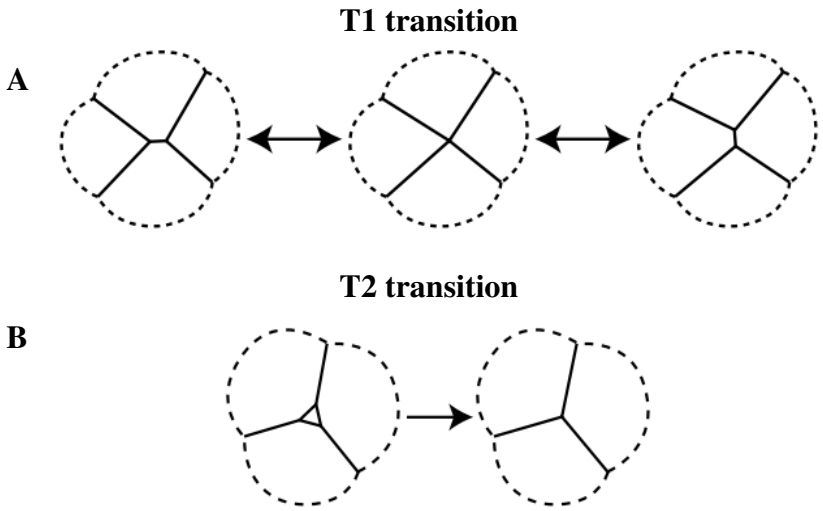

Figure 16. Topological transitions

(A) Schematic representation of T1 topological transition. (B) Schematic representation of T2 transition. Image adapted from (Staple et al., 2010).

2.2.3 Cell ingression or delamination

Cell ingression or delamination is a type of movement that enables a single cell or a group of cells to remove their contacts to their neighbors and move out of the epithelium (Leptin, 2005). It can be defined as an out-of-plane type of cell intercalation or also known as type 2 (T2) transition, similar to the process defined in the physics of foams (Figure 16B) (Chae & Tabor, 1997). Such movements are observed during epithelial-to-mesenchymal transition (EMT) during development (D. Shook & Keller, 2003) or metastasis (Plygawko, Kan, & Campbell, 2020). Epithelial cells adhere to

one another near their apical regions through septate or tight and adherens junctions. They often have also an extracellular matrix (ECM) as a support at the basal surface. These cell-cell contacts are disassembled in cells that undergo delamination, whereas the cells that are left behind reestablish contact junctions to seal the epithelium. Single cells lose their contacts during primary mesenchymal cell ingression in sea urchin embryos is a typical example of this process (S. Y. Wu, Ferkowicz, & McClay, 2007). Other examples include the ingression of endodermal precursors in *C.elegans* (J. Y. Lee & Goldstein, 2003), the ingression of mesodermal cells in the avian embryos (Eyal-Giladi & Kochav, 1976; Voiculescu, Bodenstein, Lau, & Stern, 2014) or amphibian embryos (D. R. Shook, Majer, & Keller, 2004), and delamination in adult epithelial cells to counterpoise growth to maintain tissue homeostasis (Eisenhoffer et al., 2012; Marinari et al., 2012).

2.2.4 Cell migration

Migration is a process in which the cells move on a substratum, which helps them to translocate from one position to another (Figure 17) (Horwitz & Webb, 2003). Migratory behavior commences with a cell reacting to an external cue that generates a polarity axis and the production of protrusions in the direction of the signal (Lecaudey & Gilmour, 2006; Montell, 2008; Rorth, 2007). Migrating cells form adhesive contacts on the substratum on which they migrate. These adhesion points function as both traction points and signaling centers that control adhesion dynamics and protrusion (Trepat, Chen, & Jacobson, 2012). Contraction results in the forward motion of the cell body and releasing contact points at the rear-end as the cell retracts, complete this motion cycle (Figure 17C, D). Examples of cell migration include spreading of the anterior mesoderm on the blastocoel roof of developing *Xenopus* embryo (Davidson, Hoffstrom, Keller, & DeSimone, 2002; Winklbauer & Selchow, 1992; Winklbauer, Selchow, Nagel, & Angres, 1992) and spreading of invaginated mesoderm on the ectoderm layer in *Drosophila* embryo (Leptin & Grunewald, 1990; McMahon, Reeves, Supatto, & Stathopoulos, 2010). Cell migration is not only restricted to development but can be seen in adults during both physiological and pathological contexts (Deisboeck & Couzin, 2009).

A common feature of cell shape changes described is that they are manifested by restructuring the cytoskeletal architecture of a cell with high spatiotemporal precision. The next section is dedicated to discussions on cytoskeleton and how cytoskeletal architecture is modulated by specific morphogenetic signals.

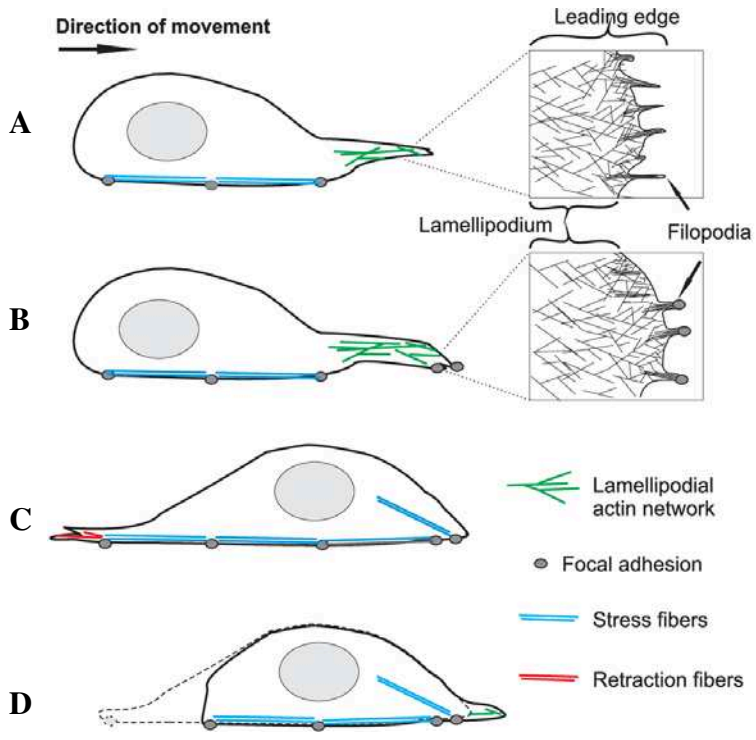

Figure 17. Cell migration

Graphical representation of cell migration on 2D matrix. (A) Cell migration is initiated by producing actin-rich protrusions at the leading edge, in response to the signal. (B) After protruding, new focal adhesions are formed at the leading front. (C) Actomyosin contractility provides traction force for the cell body and nuclus to translocate. (D) Finally, to move, the focal adhesion at rear end is disassembled. Image courtesy: Mattila, P., 2007.

3. Shape changes are orchestrated by cell cytoskeleton

D'Arcy Thompson was the pioneer to jot down in his 'On growth and form' that general principles governing morphogenetic movements obey in part the laws of physics (Briscoe & Kicheva, 2017; Heisenberg, 2017; D. W. Thompson, 1947). Advances made in the field of developmental biology linking disciplines of physics and mathematics, and the efforts to measure forces at tissue, cell, and subcellular scales have shown that the forces acting upon can be mapped to the final shape acquired by an organism. How are forces generated and transmitted during morphogenesis? The cytoskeleton acts as a support to maintain and stabilize cellular shapes and is made of various cytoplasmic polymer networks that are classified into three major classes: microtubules, intermediate filaments, and microfilaments. In the following section, various cytoskeletal components are presented, with subsections highlighting the roles of actin and MyoII.

3.1 Microtubules

Microtubules are hollow cylindrical structures, whose walls are made of polymers of tubulin, that form part of the cytoskeletal network, imparting structure and elongated shape to cells (Byers & Porter, 1964; Meiring & Akhmanova, 2020). Apart from their role as the cytoskeleton, they play vital roles in cytokinesis as they form spindle fibers to distribute the genetic material to daughter cells (McIntosh, 2016), nuclear positioning in migrating cells (Renkawitz et al., 2019), and cell motility as they form the axis of motility apparatuses like cilia and flagella (Viswanadha, Sale, & Porter, 2017). Microtubules also lay down the intracellular tracks for trafficking organelles, vesicles, and proteins (Barlan & Gelfand, 2017; Goodson & Jonasson, 2018). Motor proteins in Dyneins and Kinesins are known to bind to microtubule to facilitate the transport on microtubule tracks (Sweeney & Holzbaur, 2018).

α- and β-tubulin protein molecules are the individual building blocks of microtubules; heterodimers of α- and β-tubulin, also known as α β-tubulin, tubulin dimers, or simply tubulin (Figure 18A). Tubulin dimers polymerize linearly to form a protofilament. In most cases, microtubules are made by the 13 such protofilaments that are associated laterally and closed into a hollow polymer with a dimension of approximately 25 nm in width and a length scale ranging between <1 μm and >100 μm. Tubulin polymerizes

end-to-end with β-tubulin of one dimer binding the α-tubulin of the next in a GTP hydrolysis-dependent manner, thus the resultant tubulin polymer is polar with a fast-growing plus-end and a slow-growing minus-end with β-tubulin and α-tubulin exposed respectively (Figure 18B). Microtubules are rigid with a persistence length of ~5000 μm, owed by their larger diameter and tubular architecture (Gittes, Mickey, Nettleton, & Howard, 1993; Hawkins, Mirigian, Selcuk Yasar, & Ross, 2010).

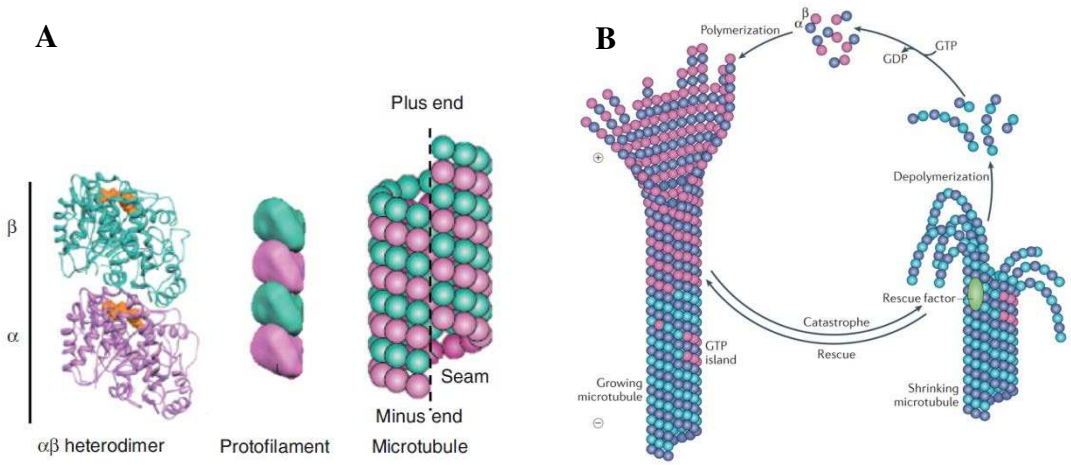

Figure 18. Microtubules

(A) The basic building blocks of microtubules are dimers of α- and β-tubulin. α/β dimers polymerize to form the protofilaments and 13 such protofilaments are conennected side-to-side to form a hollow cylindrical microtubule. Microtubules are polarized with two distinct ends, plus- and minus-ends. Image adapted from (Goodson & Jonasson, 2018). (B) Microtubule growth and disassembly s regulated by the hydrolysis of GTP bound to β-tubulin. Image adapted from (Akhmanova & Steinmetz, 2015).

3.2 Intermediate filaments

Intermediate filaments (IFs) are cytoskeletal elements of the cytosol that are intermediate in size in between microtubules and microfilaments, with a smaller diameter than microtubules (~10 μm) (Herrmann & Aebi, 1998, 2004). IFs were not shown directly involved in cell movement and shape changes, but play important role in maintaining shape, and provide tensile strength to the tissue (Stewart, 1990). The composition of IFs varies according to the cell type, for example, IFs are composed of Cytokeratins in epithelial cells, whereas IFs in mesenchyme cells are made of Vimentin (Steinert, Jones, & Goldman, 1984). IFs are not as stiff as microtubules or microfilaments and can buckle easily. Though less stiff, they have a high

tensile strength owing to their high resistance to external stress (Herrmann & Aebi, 2016).

3.3 Microfilaments

Microfilaments are also known as actin filaments as the major constituent of this cytoskeletal element are polymers of globular actin (G-actin) (Pollard, 2016). Microfilamentous network lines both the apical and basal surfaces of epithelial cells that exclude other organelles, representing the cell cortex (Chugh & Paluch, 2018). The most pronounced microfilamentous region in an epithelial cell is the circumferential ring that is associated with *zonula adherens* (Hirano, Nose, Hatta, Kawakami, & Takeichi, 1987). Apart from actin, several proteins bind these filaments that regulate polymerization dynamics and branching and mediate anchoring to the plasma membrane, like Cofilin, Profilin, α-actinin, Vinculin, etc (Pollard, 2016). Microfilaments are known to form stress fibers (bundle of fibers formed by a parallel array of F-actin filaments) near focal adhesion sites and mediate the protrusive activity of cells.

3.3.1 Actin

Actin, an abundant protein in cells, is known to be essential for cell division, cell motility, and cell homeostasis (Pollard, 2016). Individual actin molecules (globular actin, G-actin) polymerize to form filamentous-actin (F-actin) (Figure 19A) that can organize into rods, branched networks, or 3D gels, depending on the partner proteins they are bound to. G-actin is a globular protein whose primary polypeptide chain has 375 amino acids (Pollard, 2016). Individual F-actin filaments are two-stranded helical polymers (Figure 19B), 8 nm in diameter and the persistent length of these filaments can vary according to their binding protein partners: undecorated F-actin can be 9 μm in length, whereas F-actin bound by tropomyosin in muscle cells can be as long as 20 μm (Gittes et al., 1993). Actin filaments are malleable and fairly strong, resisting buckling upon applying multi-piconewton compressive forces and filament fracture when nanonewton tensile forces are applied. G-actin binding being polar, F-actin filaments exhibit two distinct ends: a fast-growing, ATP-bound monomer-rich end, known as the barbed or plus end, and a slow-growing end rich in ADP-bound monomers, known as the pointed end or minus end. Different cofactors and accessory proteins exist that can recognize specifically each of these ends, thereby alter the F-actin polymerization rates.

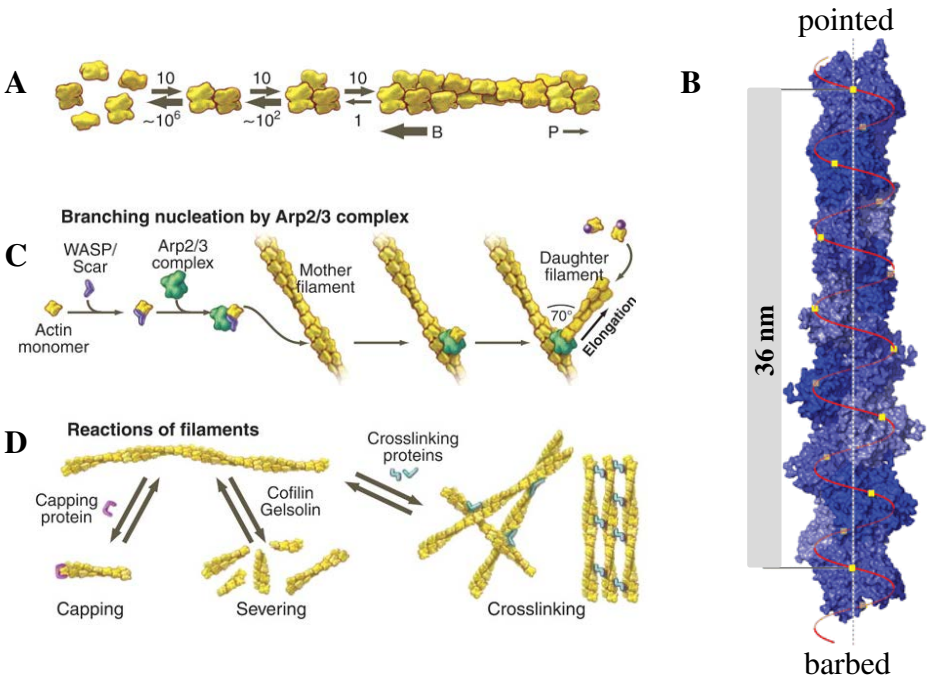

Figure 19. F-actin

(A) F-actin filaments are polymers of individual G-actin molecules. Once the rate limiting nucleation step is traversed, filaments grow rapidly by adding monomers at the barbed end (B) and slowly at the pointed end (P). Image adapted from (Pollard & Cooper, 2009). (B) Helical structure of F-actin filament reconstructed from cryo-EM images. F-actin filaments are two-stranded helical polymers, with 13 monomers arranged on a single helix repeating in almost exactly six left-handed turns. Image adapted from (Dominguez & Holmes, 2011). (C-D) F-actin filaments display distinct morphologies depending on the binding partners, for example Arp2/3 causes branching (C), whereas crosslinkers like Fimbrins can generate parallel bundles of Actin filaments (D). Images adapted from (Pollard & Cooper, 2009).

3.3.1.1 Factors affecting F-actin properties

A plethora of factors are known to affect F-actin properties including nucleotides bound to G-actin, protein molecules that bind either G-actin or F-actin and specific toxins (Figure 19C, D). Even though the energy currency ATP is not necessary for F-actin assembly *per se*, it can affect the rate of polymerization. When the system is depleted of ATP, the rate of polymerization is very slow and is not significantly different on both ends (Carlier, 1990; Korn, Carlier, & Pantaloni, 1987). Several protein partners are also known to affect the properties of actin filaments (Dominguez, 2009; Pollard & Cooper, 1986). For instance, Profilin and Cofilin are two proteins that accelerate polymerization or cause depolymerization respectively (Kanellos & Frame, 2016; Pring, Weber, & Bubb, 1992).

Proteins like Formins (Goode & Eck, 2007) and Arp2/3 (Carlsson, Wear, & Cooper, 2004; Pollard & Beltzner, 2002) can nucleate actin filaments, thereby affect branching, and Fimbrin acts as a crosslinker, producing parallel arrays of filaments (Volkmann, DeRosier, Matsudaira, & Hanein, 2001). Toxins secreted by groups of fungi had been shown to affect F-actin properties when injected into cells. For example, Cytochalasin is a molecule that binds to the plus end and blocks F-actin polymerization (Casella, Flanagan, & Lin, 1981). Other examples include Phalloidin, which binds the side of the filament, thereby stabilizing the polymer form (Dancker, Low, Hasselbach, & Wieland, 1975; Low, Dancker, & Wieland, 1975), and Latrunculin, which binds and sequesters G-actin, blocking polymerization (Spector, Shochet, Kashman, & Groweiss, 1983). F-actin is also bound by the myosin family of motor proteins like non-muscle myosin II (MyoII). Association of F-actin and MyoII forms active contractile machinery, which can generate tension upon MyoII activation (Houdusse & Sweeney, 2016).

3.4 The contractile machinery

Molecular motors associated with the cytoskeletal elements form the contractile machinery, generating movements and forces. It is thus fundamental to understand how motor proteins act as chemomechanical transducers in powering critical cellular processes including cytokinetic ring constriction, vesicle trafficking, exocytosis, organelle translocation, membrane deformation, and formation of protrusions (Bond, Brandstaetter, Sellers, Kendrick-Jones, & Buss, 2011; Hartman, Finan, Sivaramakrishnan, & Spudich, 2011; Ross, Ali, & Warshaw, 2008; Ross, Shuman, Holzbaur, & Goldman, 2008; Woolner & Bement, 2009). The cytoskeleton-bound molecular motors, myosins, kinesins, and dyneins, upon interacting with their respective cytoskeletal track, generate forces and movements (F-actin for myosins, and microtubule tracks for dyneins and kinesins) (Sweeney & Holzbaur, 2018). A general principle of cellular force generation is that, in all cases, force generation steps are driven by ATP hydrolysis and liberating hydrolysis products (ADP and inorganic phosphate), inducing conformational changes, altering track interactions (Tafoya & Bustamante, 2018). Among these identified molecular motors, myosin plays a central role in shaping cells and possibly has the well-investigated mechanisms of force production (Aguilar-Cuenca, Juanes-Garcia, & Vicente-Manzanares, 2014; Kasza & Zallen, 2011).

3.4.1 Myosin motors

Myosin belongs to a superfamily of motor proteins that power muscle contraction as well as force generation in eukaryotic cells, through its ATP-dependent cyclic interactions with F-actin. Members of this family of proteins are generally structured into two main parts: head and tail (Figure 20A). The head hosts the domains for actin binding and actin-activated ATPase activity. The head also has the lever arm, an extended helix containing variable numbers of calmodulin or calmodulin-like light chain binding sites. The head is followed by a coiled-coil region called a tail, which is required for self-association to form myosin minifilaments, in the case of some myosins, whereas in the case of others, tails bind and move cargoes. How do myosin motors generate contractile forces?

Seminal work performed on muscle cells in the 1950s led to the proposal of a widely accepted mechanism of actomyosin contractility, the 'sliding filament' theory (Figure 20B). The changes in the individual contractile unit of a muscle fiber called sarcomere when muscular tissue shortened were observed under high-resolution microscopes (A. F. Huxley & Niedergerke, 1954b; H. E. Huxley & Hanson, 1957). They found that the "A-band" rich in thick filaments of myosin, a zone in the repeating sarcomere, remains constant in length, whereas the "I band", which is abundant in thin actin filaments, reduced its length upon sarcomere contraction. This groundbreaking observation laid the founding stones of the sliding filament theory which states that the sliding of actin filaments across myosin generates contractile forces. Myosin activity in sarcomere shortening is a multistep process, appears as a molecular dance. The ATP-bound myosin head reaches forward, binds to F-actin, contracts, unbinds actin, and gets back in a new cycle to bind F-actin. This cycle is known as myosin-actin cycling (Houdusse & Sweeney, 2016; Sweeney & Houdusse, 2010). The main step that generates force during this cycle is the head contraction step known as the "power stroke", which is powered by the energy released from the hydrolysis of bound-ATP, which induces conformational changes in the head domain. Once the hydrolysis products, ADP and inorganic phosphate, are released, ATP swiftly rebinds the myosin head associated with actin filaments, releasing the association. Interestingly in sarcomeres, F-actin has a polar organization and the myosin motors also exhibit polar motion, with most of them being plus-end directed, except for class VI myosins (Wells et al., 1999), which are minus-end directed.

Such a polar organization of the actomyosin contractile units generates a net force. Advancement in the field of biophysics allowed researchers to measure the forces and properties of actomyosin contractile units. Fiber mechanics studies have shown that the myosin force is estimated to be between 6-10 pN (Piazzesi, Lucii, & Lombardi, 2002; Piazzesi et al., 2007; Piazzesi, Reconditi, et al., 2002). The myosin power stroke length is estimated to be around 7 nm (Knight, Veigel, Chambers, & Molloy, 2001; Tyska & Warshaw, 2002). The average stiffness of actomyosin was measured to be around 1.3 pN/nm, whereas that determined from muscle fibers generating isometric forces to be between 1-5 pN/nm (Barclay, 1998; A. F. Huxley & Tideswell, 1996; Piazzesi, Lucii, et al., 2002).

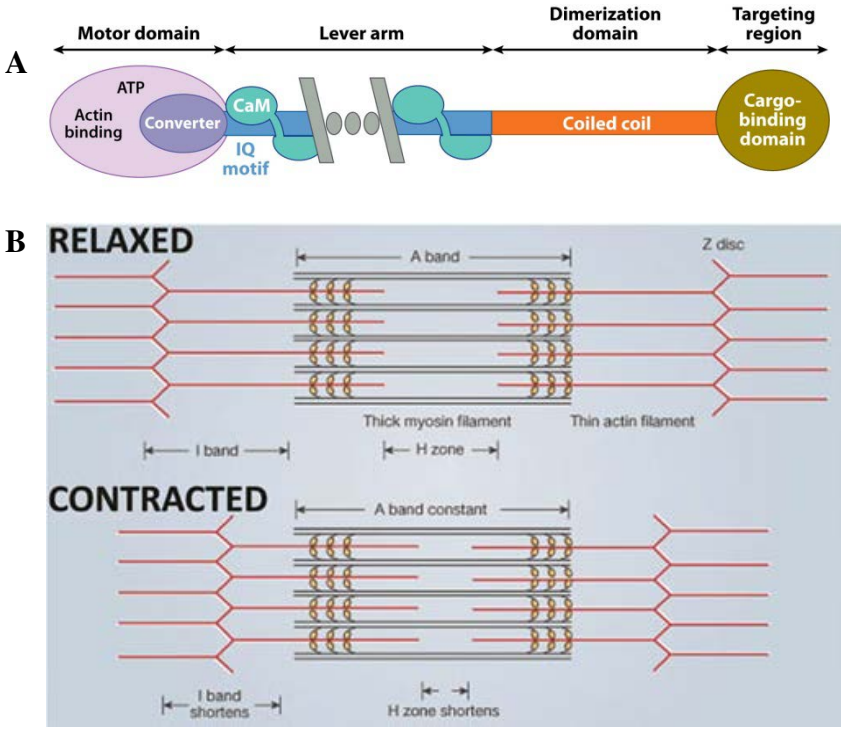

Figure 20. Myosin motor proteins

(A) Schematic representation of structure of motor proteins belonging to the myosin superfamily. The N-terminal head region forms the motor domain containing ATP- and actin-binding sites. The C-terminus of the head domain consists of motifs that can associate with reglators of motor activity. The C-terminal tail has coiled-coil sequences which is important for dimerization. The C-terminus also hosts cargo-binding domain depending on the myosin-type that is necessary for targeting the myosin to specific cargoes. Image adapted from (Sweeney & Houdusse, 2010). (B) Depiction of the sliding filament theory. Myosin in the central A-band slides over the actin filaments (red) generating a contractile force depending on ATP hydrolysis. Images adapted from (A. F. Huxley & Niedergerke, 1954a).

Fascinatingly, not all cells have a sarcomere-like organization of actomyosin present, for example, the cytokinetic ring (Carvalho, Desai, & Oegema, 2009). How cortical actomyosin networks constrict to generate a net force in the absence of polar organization F-actin and myosin. Studies using *in vitro* reconstituted systems have shown that, despite having randomly oriented actin filaments, contract on length scales that are reminiscent of the cell cortex, i.e. ~ 10µm (Bendix et al., 2008; Murrell & Gardel, 2012; Soares e Silva et al., 2011), indicating that an inherent actin polarity is dispensable for actomyosin polarity. These studies have led to the proposal that actomyosin network contraction is a result of F-actin behaving asymmetrically to tensile and compressive stress: actin filaments can accommodate high levels of tension and thus can be pulled, whereas actin filaments buckle upon compression (Murrell & Gardel, 2012; Soares e Silva et al., 2011), suggesting that the actomyosin network preferentially shrink rather than expand. Consistent with this idea, a correlation can be found between individual actin filament buckling and the extent of network contraction in reconstituted systems (Murrell & Gardel, 2012). Furthermore, multistage coarsening behavior of actomyosin is observed in solution, resulting in the self-organization of foci with myosin in the center, surrounded by actin filaments (Soares e Silva et al., 2011).

Non-muscle cells like epithelial cells also code for class II myosin, called non-muscle myosin II (NM II), that plays equivalent roles in force generation. Coarsening behavior of actomyosin networks with myosin foci surrounded by actin filaments *in vivo* in cell cortex, suggesting that either controlled assembly or self-organization of actomyosin networks could generate tensile forces (Luo et al., 2013; E. Munro, Nance, & Priess, 2004; Vavylonis, Wu, Hao, O'Shaughnessy, & Pollard, 2008).

3.4.1.1 Non-muscle myosin II (NM II)

NM II (MyoII) is a hexameric protein comprising of two heavy chains (coded by *zipper*, *zip* in *Drosophila*), two essential light chains, and two myosin regulatory light chains (MRLC) (coded by *spaghetti squash*, *sqh* in *Drosophila*) (Figure 21A) (Sellers, 2000). The N-terminus of the heavy chain forms the head domain that mediates ATP-dependent myosin-actin cycle. The heavy chain also has an intermediate neck domain where the light chains bind, and an extended C-terminal α-helical tail domain necessary for assembly of MyoII homodimers into bipolar minifilaments containing a few dozen heads through coiled-coil dimerization (Mahajan & Pardee, 1996; Niederman & Pollard, 1975; Vicente-Manzanares, Ma,

Adelstein, & Horwitz, 2009). These bipolar minifilaments act as fundamental units of force generation, by converting non-processive, unipolar hexamers into a highly processive motor (Verkhovsky, Svitkina, & Borisy, 1995). The essential light chains perform the function of stabilizing MyoII, whereas ATPase activity is gated by regulatory light chains.

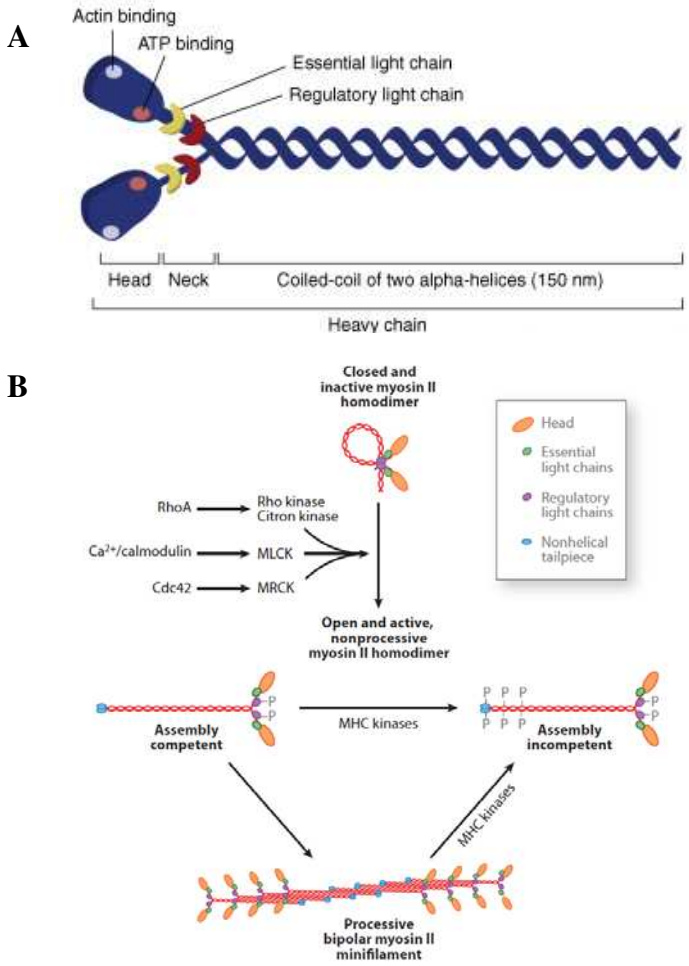

Figure 21. Non-muscle MyoII (MyoII) and its regulation by phosphorylation

(A) Schematic diagram of MyoII which is a hexamer consisting of two heavy chains (blue) with ATP- and actin-binding domains on their head, two essential light chains (yellow), and two regulatory light chains (red). Image adapted from (Quintin, Gally, & Labouesse, 2008). (B) Schematics of pathways controlling MyoII activation and assembly into bipolar minifilaments. MyoII hexamer is originally in a closed confirmation and is inactive. Phosphorylation of regulatory light chain by specific kinases converts MyoII hexamer to an open conformation, which represents the non-processive MyoII homodimer. Active MyoII assemble into processive bipolar minifilaments that can contract F-actin. Phoshorylation of the coiled-coil tail of myosin heavy chain by MHC kinases blocks assembly of minifilaments (Lecuit et al., 2011).

3.4.1.2 Regulation of NM II activity by phosphorylating MRLC

MyoII contractility is a tightly regulated process; specific molecular pathways exist at the level of minifilament assembly. Opposed to the regulation of myosin motor activity in muscles by specific protein partners, NM II activity is regulated by reversible phosphorylation of particular amino acid residues present on MRLCs and heavy chains (Vicente-Manzanares et al., 2009). The most important mode of regulation is by the phosphorylation of the MRLC on two highly conserved amino acid residues, for instance, Serine 19 and Threonine 18 in vertebrate MyoII (Hirata, Takahashi, & Yazawa, 2009). Structural studies on purified MyoII have shown that when unphosphorylated MRLC is present, MyoII homodimer adopts a folded conformation in which F-actin binding and ATPase activity are impaired by head-head associations and minifilament formation is blocked by head-tail association (Jung, Komatsu, Ikebe, & Craig, 2008). MRLC phosphorylations unfold this repressive conformation, causing myosin contraction (Figure 21B) (Craig, Smith, & Kendrick-Jones, 1983). Single phosphorylation on Ser 19 increases the ATPase activity in the presence of actin filaments (Somlyo & Somlyo, 2003; Wendt, Taylor, Trybus, & Taylor, 2001) and additional phosphorylation on Thr 18 is shown to further increase this activity (Hirata et al., 2009). More than a dozen kinases are shown to act upon these residues to regulate the spatiotemporal activity of MyoII including the myosin light chain kinase (MLCK, a kinase triggered by Ca^{2+}/calmodulin activity), Rho kinase (ROCK or Rok), and citron kinase (both of them are activated by RhoA, leucine zipper interacting kinase (ZIPK), and myotonia dystrophy-elated Cdc42-binding kinase (MRCK) which is activated by Cdc42 (Leung, Chen, Tan, Manser, & Lim, 1998; Matsumura, 2005; Somlyo & Somlyo, 2003; Tan, Yong, Dong, Lim, & Leung, 2008). Phosphorylation is reversible and dephosphorylation is mediated by enzymes called phosphatases. MRLC phosphorylation is reversed by myosin phosphatase, protein phosphatase 1 (PP1) (Ito, Nakano, Erdodi, & Hartshorne, 2004). Interestingly, PP1 activity is also regulated by ROCK-mediated phosphorylation of the regulatory subunit of PP1, MYPT1, blocking phosphatase activity (Matsumura & Hartshorne, 2008). The right amount of kinases and phosphatases enable cells to maintain the homeostasis of the actomyosin networks and contractility (Julian & Olson, 2014; Schofield & Bernard, 2013). Protein kinase C (PKC) performs a special function of inhibiting MRLC activation by phosphorylating Ser1, Ser2, and Thr9 residues on

MRLC, rendering it to be unsuitable as a substrate for MLCK (Nishikawa, Sellers, Adelstein, & Hidaka, 1984).

3.4.1.3 Regulation of NM II activity by phosphorylating heavy chain

The second means of regulating MyoII activity is by phosphorylating the heavy chain, which destabilizes minifilaments already present and/or blocks de novo generation (Figure 21B). Such a mechanism was first demonstrated in *Dictyostelium* (Egelhoff, Lee, & Spudich, 1993; Yumura et al., 2005). Later, numerous phosphorylation sites on the C-terminal rod and non-helical tailpiece were identified in vertebrate NM II heavy chain (Vicente-Manzanares et al., 2009), which are targets for PKC (Even-Faitelson & Ravid, 2006), casein kinase II (CKII) (Dulyaninova, Malashkevich, Almo, & Bresnick, 2005), and transient receptor potential melastatin 7 (TRPM7) (Clark et al., 2008). Phosphorylation of NM II heavy chain is an essential activity for maintaining the dynamics and redistribution of myosin between different activities; loss of this regulatory pathway result in overaccumulation or mislocalization of MyoII (Breckenridge, Dulyaninova, & Egelhoff, 2009; Clark et al., 2008; Even-Faitelson & Ravid, 2006).

3.4.1.4 Regulation of NM II activity by actin association

Mechanochemical feedbacks were also shown to affect MyoII accumulation as it was shown that MyoII gets activated in response to mechanical cues, like heightened cortical tension (Fernandez-Gonzalez, Simoes Sde, Roper, Eaton, & Zallen, 2009; Heissler & Sellers, 2016; Mitrossilis et al., 2017). One putative mechanism could be the mechanical feedback between actin filaments and myosin. *In vitro* studies have shown that feedback exists between actin association and myosin minifilament assembly. F-actin can promote minifilament formation directly and effectively, probably due to increased encounters between myosin homodimers (Mahajan & Pardee, 1996). Even though equatorially biased MyoII recruitment happens still in the absence of F-actin to a certain extent during cytokinesis; nevertheless F-actin is required in most cells for typical MyoII levels and persistence (Dean, Rogers, Stuurman, Vale, & Spudich, 2005; Foe & von Dassow, 2008; Kamijo et al., 2006; Zang & Spudich, 1998). A shred of direct evidence for the feedback between F-actin and MyoII recruitment came from the studies in *Dictyostelium* and *Drosophila*. Depolymerizing F-acting blocked the cortical recruitment of MyoII in response to a chemoattractant in *Dictyostelium* (Levi, Polyakov, & Egelhoff, 2002). A similar loss of cortical MyoII was observed upon F-

actin depolymerization in fly embryos (Bertet, Rauzi, & Lecuit, 2009), whereas an experimentally induced F-actin polymerization increased cortical MyoII accumulation (Bertet et al., 2009; Homem & Peifer, 2008). However, it remains to be addressed if the above-mentioned observations are due to a direct effect on MyoII recruitment or something indirect.

I have discussed in this section what are the components, mechanisms, and pathways responsible for force generation inside a cell. But when it comes to morphogenesis, the force generated individual cells seems to be coupled in order to achieve highly coordinated epithelial cell shape changes. A fundamental question exists: how is intracellularly generated tension coupled throughout the epithelial tissues?

3.5 Adherens junctions mechanically couple epithelial cells

In a seminal study, Townes and Holtfreter (1955) showed that cells collected from enzymatically dissociated embryos retain their ability to segregate when mixed *in vitro*, in a manner resonant of their original configuration (Townes & Holtfreter, 1955). Steinberg and others later in their 'differential adhesion hypothesis', proposed that the disparity in adhesion between cell types determined if, and how, cells underwent demixing in the above experiment (Steinberg, 1963, 1970). The developmental programs thus generate complex patterns of expression of distinct cadherin subtypes that drive cell sorting upon development (Takeichi, 1988).

3.5.1 Cadherin superfamily

As described in Section 2, epithelial cells are tightly bound laterally to each other through junctions; a major form being adherens junctions made of cadherin and associated proteins, to form a highly coherent sheet of cells (Halbleib & Nelson, 2006). Cadherin superfamily comprises classical cadherin, protocadherins, and atypical cadherins involved in planar cell polarity (Halbleib & Nelson, 2006). Studies in vertebrate embryos identified Cadherins originally as cell surface glycoproteins that arbitrate Ca^{2+}-dependent homophilic cell contacts (Gallin, Edelman, & Cunningham, 1983; Peyrieras, Hyafil, Louvard, Ploegh, & Jacob, 1983; Vestweber & Kemler, 1984; Yoshida & Takeichi, 1982). Cadherins are transmembrane proteins, highly conserved among metazoans, which play vital roles in tissue morphogenesis and homeostasis (Arboleda-Estudillo et al., 2010; Chihara & Nance, 2012; Hayashi & Carthew, 2004). Cadherins containing zonula adhesion that mediates intercellular adhesion can be seen as

electron-dense structures in electron microscopy micrographs (Figure 22A) (Farquhar & Palade, 1963). Cadherins are important in simple organisms too; family members of the same were identified also in the unicellular choanoflagellates (King, Hittinger, & Carroll, 2003), the Hydra (Hobmayer et al., 2000), and the sponge *Oscarella carrmela* (Nichols, Dirks, Pearse, & King, 2006). Since their discovery, epithelial Cadherin (E-Cad), and other classical cadherins such as N-, P-, and R-Cadherins, have become the keystone of intercellular adhesion complex that couples mechanically the actin filaments of neighboring cells, which was further supported by the observation that depletion of E-Cad cytoplasmic domain ended up in impairing cell-cell adhesion (Nagafuchi & Takeichi, 1988; Ozawa, Baribault, & Kemler, 1989).

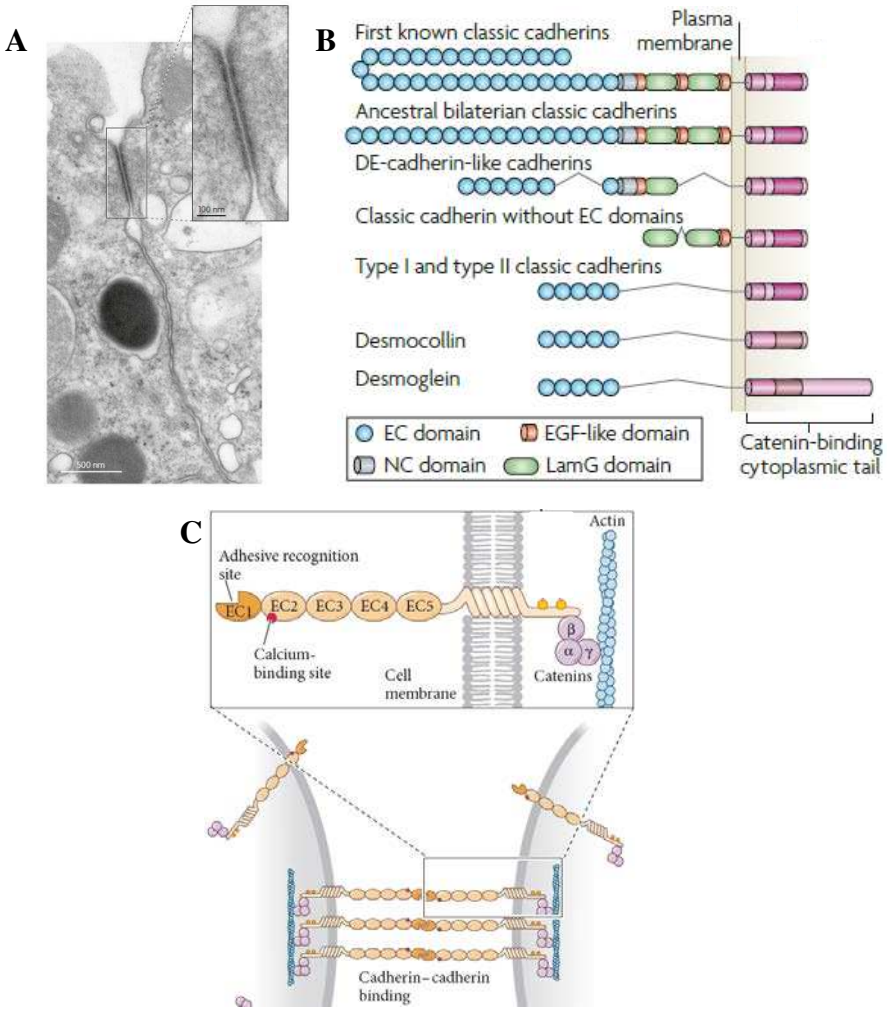

Figure 22. Cadherin family of proteins mediate intercellular adhesion

(A) EM micrograph showing electron-dense structures between cell membranes of two neighboring cells corresponding to adherens junctions. Image adapted from (Harris & Tepass, 2010). (B) Respresentation of domain organizations of cadherin family of proteins. The extracellular EC domains mediate homophilic interactions between Cadherin molecules. Adhesion sites are mechanically coupled to underlying actomyosin cortex through the intracellular Catenin-binding cytoplasmic tail of Cadherin molecules. Image adapted from (Harris & Tepass, 2010). (C) Schematic representation of Cadherin-mediated cell-cell adhesion. Homophilic binding of extracellular EC domains mediates cell-cell adhesion. Cells are mechanically coupled by linking actomyosin cortex to the adhesion sites through Cadherin/Catenin complex. Image courtesy: (Barresi & Gilbert, 2019).

More than 100 members of this family are identified with varied protein structures, but all having the characteristic extracellular cadherin repeats (ECs) (Figure 22B) (Nollet, Kools, & van Roy, 2000). Classical cadherins have five ECs in the extracellular domains and are subdivided into type I and type II cadherins. Type I cadherins such as E- and N-Cad mediate tough cell-cell adhesion and have a conserved HAV tripeptide motif in the most distal EC (EC1). Type II cadherins like vascular epithelium (VE) cadherin, on the contrary, lacks this motif. E-Cad homophilic interaction is mediated by the EC1domain that comprises conserved tryptophan residues that allow trans-cadherin binding (Chen, Posy, Ben-Shaul, Shapiro, & Honig, 2005; Nose, Nagafuchi, & Takeichi, 1988; Patel et al., 2006; Tamura, Shan, Hendrickson, Colman, & Shapiro, 1998). A prevalent model for cadherin-mediated cell adhesion is that cadherins are form cis-dimers with other cadherins on the same membrane initially and trans-dimers are then formed by interdigitating with cis-dimers on the opposing membrane (Figure 22C) (Fukata & Kaibuchi, 2001). Cadherins, in addition to their intercellular adhesion role, function as signaling modules for mediating cell fate specification (Lorthongpanich, Doris, Limviphuvadh, Knowles, & Solter, 2012; Sarpal et al., 2012), cell polarity (Bosveld et al., 2012; Y. Wang, Chang, & Nathans, 2010), and cell proliferation (C. M. Nelson & Chen, 2003; Schlegelmilch et al., 2011).

3.5.2 Molecular adaptors link actomyosin to cadherins

A widely accepted model proposed for coupling intercellular adhesion to force generation mechanisms is that β-Catenin (β-Cat) forms a complex with E-Cad and associates with α-Catenin (α-Cat), which in turn recruits F-actin (Figure 22C) (Niessen, Leckband, & Yap, 2011). This emanated from

the observations that cadherin intracellular domain is required for efficient cell aggregation in early experiments by Nagafuchi and Takeichi (Nagafuchi & Takeichi, 1988) and the identification of catenins (Ozawa et al., 1989) as binding partners of E-Cad cytoplasmic tails. While the extracellular E-Cad domain mediates intercellular adhesion, the intracellular tail forms complex with β-Cat and α-Cat. Since α-Cat was shown to associate directly with filamentous actin (Rimm, Koslov, Kebriaei, Cianci, & Morrow, 1995), it was thought that E-Cad/β-Cat/α-Cat complex link actomyosin cortex and adherens junctions. β-Cat acts as an adaptor linking cadherin intracellular domains to F-actin (Fukata & Kaibuchi, 2001; Gumbiner, 2000). Early struggles using purified proteins failed to reconstitute a minimal complex of cadherin cytoplasmic tail/β-Cat/α-Cat bound to F-actin (Drees, Pokutta, Yamada, Nelson, & Weis, 2005; W. J. Nelson, Drees, & Yamada, 2005; Yamada, Pokutta, Drees, Weis, & Nelson, 2005). It was later identified that the minimal cadherin-catenin complex binds stably to F-actin when force is applied, which led to the proposal of the catch-bond model (Buckley et al., 2014). Martin and colleagues have demonstrated the role of the E-Cad/catenin complex in coupling actomyosin to adherens junctions to generate stable shape changes and the coupling of mechanical forces across tissues. Knockdown of *e-cad* or *α-Cat* using RNA interference (RNAi) in the gastrulating *Drosophila* embryos produced tears in the apical actomyosin network in invaginating mesoderm (Martin, Gelbart, Fernandez-Gonzalez, Kaschube, & Wieschaus, 2010).

α-Cat interaction with F-actin can be also indirect, through the binding of proteins such as Vinculin (Choi et al., 2012; Rangarajan & Izard, 2012; Watabe-Uchida et al., 1998). Vinculin recruitment to junctions is predominantly mediated by binding to α-Cat which is also force-dependent (Huveneers et al., 2012; Leerberg et al., 2014; Yonemura, Wada, Watanabe, Nagafuchi, & Shibata, 2010). Force-dependent association of α-Cat and Vinculin was first suggested after the observation of force-dependent revealing of an epitope closer to the vinculin-binding domain of α-Cat *in vivo* (Yonemura et al., 2010). Recently using magnetic tweezers, it was shown that the vinculin-binding domain of α-Cat unfolds when isolated molecules are stretched using tweezers. Unfolding of the α-Cat domain induced Vinculin binding, which then stabilizes α-Cat in its open state (Yao et al., 2014).

In this section, I have provided an overview of the force generation machinery inside cells that produce the force for shaping cells, and how

contractile machinery is connected to the intercellular contact junctions in order to coordinate and couple cells mechanically at a tissue scale. Strict regulation of cell contractility and adhesion is essential for efficiently maneuvering the morphogenetic program. I will give an overview of the cell and molecular pathways that control cellular force generation and morphogenetic events during embryonic development in the following section.

4. From gene patterning to cell shape changes

A fundamental question that has attracted researchers is how the final form and shape of organs and organisms are coded in the genome. Identifying a one-to-one link between patterning and cell specification genes and morphogenetic machinery helps to seal the slit between phenotype and genotype. A remarkable example to understand the link between gene expression and morphogenesis is the cadherin subtype switching; such a process occurs during *Drosophila* development when the mesoderm cells expressing E-Cad switch to N-Cad. During this process, cells lose their epithelial characteristics and acquire fibroblastic features and migratory behavior (Oda, Tsukita, & Takeichi, 1998). Previously, morphogenesis was purely seen through a lens of tissue mechanics, without having concern about the roles of gene expression (R. Keller, 2012). However, these approaches failed to explain other fundamental processes like cell specification and patterning. The Heidelberg screen by Eric Wiechaus and Christiane Nusslein-Volhard was a breakthrough in this field; by cautious and stringent observation of mutagenic screen in developing *Drosophila* embryos, they identified molecular pathways that act as transducers of cell shapes (Nusslein-Volhard & Wieschaus, 1980; Wieschaus & Nusslein-Volhard, 2016).

The development of an embryo begins by dividing the embryonic body into discrete regions by the patterning genes. The patterning genes define the body axes of the embryo, which provides the coordinates for cells to take up unambiguous fates in a spatiotemporally regulated fashion. Interestingly, the genes involved in configuring embryonic tissues that mediate long-range patterning (Green & Sharpe, 2015; Lawrence, 2001) are not directly involved in shaping tissues, rather this task is carried out by the cellular cytoskeletal machinery present in cells, whose activity depends on the cell specification and fate. Thus the molecular components of the morphogenetic cascade can be classified into four main groups: (i) global strategists, (ii) local decision-makers, (iii) go-betweens, and (iv) movers

and shakers (Gilmour et al., 2017). Global strategists are generally the morphogens that are secreted molecules, that activate the downstream cascade of gene-regulatory networks that determine the cell fate in a concentration-dependent manner. The action of morphogens demarcates the region of cell specification, by activating downstream factors that are local decision-makers. Local decision-makers are generally transcription factors, which transduce the morphogen activity from the membrane to inside the nucleus causing transcriptional activation of the precise gene-regulatory network. These molecules owing to their nuclear localization, do not take part in shaping cells directly. These local decision-makers do not directly transcribe the genes coding cytoskeletal elements regulating cell shape change rather they cause the precise expression of intermediate proteins belonging to go-betweens. These molecular players enable cells to adjust the cellular morphogenetic toolkit with high spatiotemporal precision. The real players that bring on cell shape changes belong to the 'movers and shakers' group. They include components of actomyosin contractome, microtubule networks, adhesion molecules, and polarity proteins that define the position on a cell. Interestingly, many of these components are ubiquitously expressed in all cells, only their defined regulation by the morphogenetic program produces the required form and shape.

Vertebrate neurulation stands as an example of a morphogenetic process for which years of research have identified the genetic factors that have been linked to cell shape changes. Folding of the vertebrate neural plate involves the formation of dorsolateral and median hinge points (MHP). MHP forms when the cells along the midline of the neural plate undergo apical constriction and wedging (Schoenwolf, 1991). Genetic studies have shown that this process depends on ROCK activity, a downstream transducer of Rho pathway activity (Escuin et al., 2015; Riento & Ridley, 2003). Neuroepithelial cells maintain contact with one another through cadherin-based adherens junctions (E. Hong & Brewster, 2006) and a scaffold protein, Shroom3, localized to these cellular junctions, recruit ROCK to these apical junctions (Das et al., 2014; Hildebrand, 2005; Nishimura & Takeichi, 2008). ROCK phosphorylates the regulatory light chain of MyoII, causing actomyosin contractility, and apical constriction (Levayer & Lecuit, 2012; Matsumura, 2005). Several studies have now identified role for Shroom-family of proteins in morphogenesis (C. Lee, Le, & Wallingford, 2009), for example in case of apical constriction driving rosette formation in zebrafish lateral primordium (Ernst et al., 2012), during gut formation in *Xenopus* (Chung, Nascone-Yoder, Grover, Drysdale, &

Wallingford, 2010) and mouse lens placode morphogenesis (Lang, Herman, Reynolds, Hildebrand, & Plageman, 2014). Patterning genes involved in these cases for Shroom expression are also identified, for example, the transcription factor, Pitx in the case of *Xenopus* gut (Chung et al., 2010). FGF signaling was shown to mediate Shroom expression in zebrafish lateral line primordium (Ernst et al., 2012) and the transcription factor Pax6 in the case of mouse lens placode (Plageman et al., 2010).

I have used the mesoderm anlage of the developing *Drosophila* embryos as a research paradigm. In the first part of this section, I will describe the molecular pathways that specify the embryonic body axes in *Drosophila*. I study the processes of convergent extension and tissue folding of mesoderm during *Drosophila* gastrulation. Then in the coming sections, I will also provide an overview of what is known about the cellular and molecular pathways that regulate these processes in the fly embryos.

4.1 Axis specification in *Drosophila* embryo

Axis specification is essential for development as it provides the positional coordinates for cells to take up fates. Axis specification happens during oogenesis itself by regulating the localization of the mRNA of EGFR ligand, *gurken* (Figure 23) (Gavis, 1995). Gurken shows similarity to the transforming growth factor α (TGF α) family of growth factors (Neuman-Silberberg & Schupbach, 1996). The *Drosophila* oocyte begins its journey inside an egg chamber having a single oocyte and 15 sister nurse cells, all products of the divisions of a germline stem cell. These 16 germ cells are surrounded by a monolayered epithelium made of somatic follicle cells. The AP polarity is obvious earlier than the DV polarity as observed by the position of the oocyte to the posterior of the egg chamber. During the early stages of oogenesis, *gurken* mRNA is localized near the posterior end of the oocyte, beside the nucleus. This allows local translation of Gurken protein near the posterior end (Figure 23A). Gurken proteins bind and activate the EGF receptor Torpedo (Top) expressed by the follicle cells, initiating the mitogen-activated protein kinase (MAPK) cascade. It was shown that locally produced Gurken signal is sufficient to induce spatially restricted Top activation (Neuman-Silberberg & Schupbach, 1993, 1996). This results in posterior follicle cells taking up posterior fate, which eventually activates the Protein kinase A (PKA) pathway in the oocyte. PKA pathway activity orients the microtubule network in an AP polarized orientation, with plus ends towards the posterior. Such an orientation of the microtubule cytoskeleton helps to localize mRNAs of anterior determinants like *bicoid*

at the anterior pole and posterior determinants like *oskar* and *nanos* at the posterior pole of the oocyte (Gonzalez-Reyes, Elliott, & St Johnston, 1995). The oocyte nucleus takes a trip over this microtubule array towards the anterior end on Dynein motors. The nuclear localization is skewed during the anterior localization and hence the nucleus is placed at the anterior-dorsal position (Zhao, Graham, Raposo, & St Johnston, 2012). More precisely, whichever side nucleus ends up becomes the dorsal side, by the action of Gurken protein which is locally produced (Guichet, Peri, & Roth, 2001; Roth, Jordan, & Karess, 1999). Gurken binds Torpedo on the nearby follicle cells, making them take up a dorsal fate, blocking the default ventral fate (Figure 23B). This shows that the AP axis of the oocyte is the primary axis that defines the microtubule network orientation, which eventually directs DV axis formation (Gonzalez-Reyes et al., 1995). Mutations in components of the Gurken/Top pathway display defects in mRNA localization along the AP axis, apart from the initially described DV defects (Gonzalez-Reyes et al., 1995; Neuman-Silberberg & Schupbach, 1993; Roth, Neuman-Silberberg, Barcelo, & Schupbach, 1995). Hence before fertilization itself, the oocyte has predefined polarity axes that are used by the embryo to generate primary body axes. The *Drosophila* embryonic body is divided into two major body axes: anterior-posterior (AP) and dorsal-ventral (DV). Four systems of patterning genes are identified that are necessary for AP and DV axis determination in *Drosophila* embryos: the anterior, posterior, terminal, and dorsoventral systems (St Johnston & Nusslein-Volhard, 1992). Although these systems act through different biochemical pathways, they display some commonalities: (i) one gene product is restricted in a specific region of the oocyte and provide the spatial cue, (ii) an asymmetric distribution of a gene product that acts as a transcription factor as a result of the spatial cue, and (iii) concentration-dependent distribution of this transcription factor results in the expression of specific zygotic target genes.

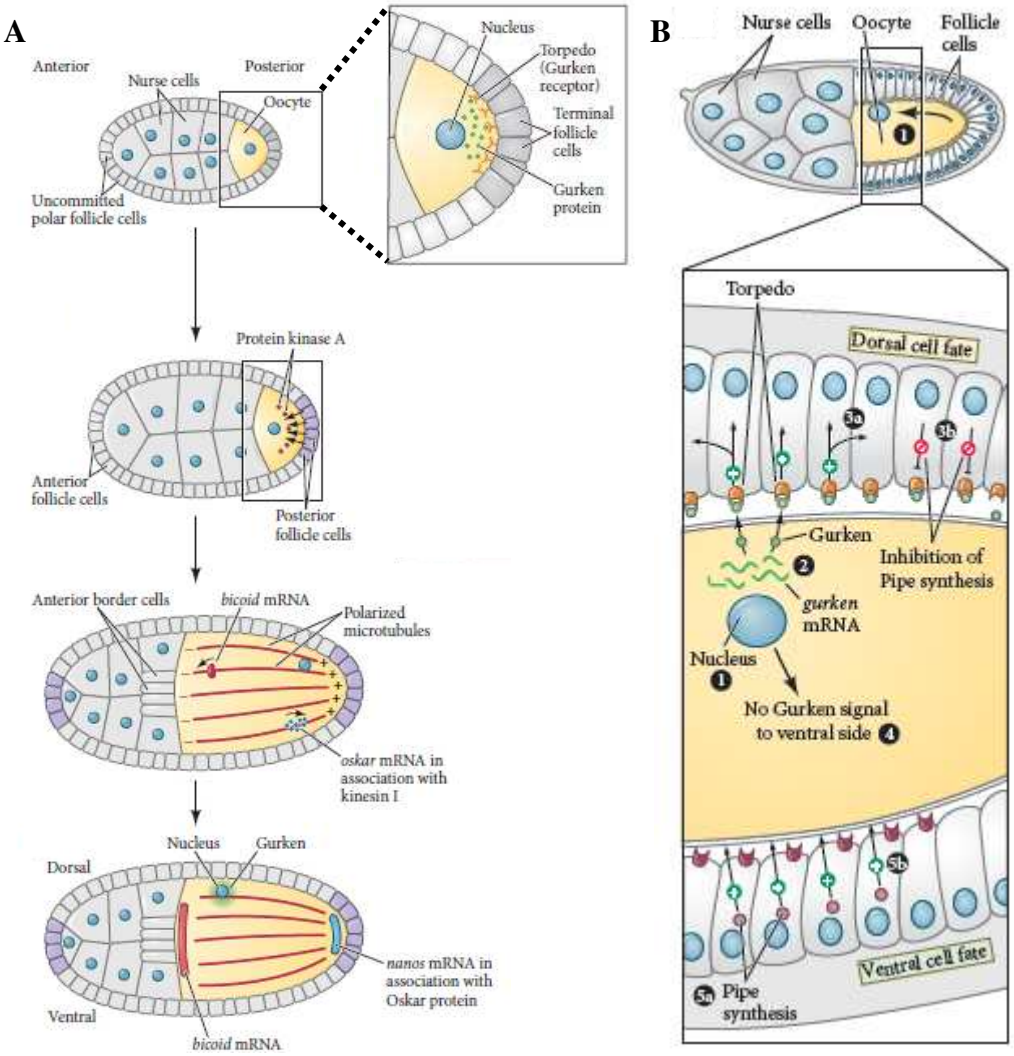

Figure 23. Pathways involved in AP and DV axes generation inside oocyte

(A) Schematic representation pathway generating AP axis inside oocyte by Gurken signalling. (B) Schematic diagram showing pathway generating DV axis inside oocyte by Gurken signalling. Images are taken from (Barresi & Gilbert, 2019).

4.1.1 *Drosophila* embryonic AP axis specification

The patterning along the AP axis is defined by three patterning systems acting largely independently: the anterior system, the posterior system, and the terminal system (Figure 24A). The anterior system provides the identity of the head and thorax, the posterior system act to define the segmented abdominal regions, and the terminal system is necessary for the formation

of the two poles, the non-segmented termini, the acron at the anterior and the telson at the posterior.

4.1.1.1 The anterior system

Bicoid (Bcd) is the key anterior morphogen identified in a pioneer screen by Nusslein-Volhard, Driever, and colleagues to identify maternal effectors of pattern formation (Driever & Nusslein-Volhard, 1988a, 1988b; Driever, Siegel, & Nusslein-Volhard, 1990). Bcd is thought to be the key anterior determination factor because: (i) Bcd protein has a graded distribution, with the peak concentration at the anterior region, (ii) Bcd is the only essential factor required to produce all anterior structures, while mutants of other genes have only partial effects (Frohnhofer, Lehmann, & Nusslein-Volhard, 1986; Nusslein-Volhard, Frohnhofer, & Lehmann, 1987; Schupbach & Wieschaus, 1986), (iii) injecting *bcd* mRNA to *bcd*-deficient embryos produced head structures at the injection site. Bcd is a homeobox protein (Berleth et al., 1988; Frigerio, Burri, Bopp, Baumgartner, & Noll, 1986) and acts as a transcriptional activator of zygotic genes (Driever & Nusslein-Volhard, 1989; Driever, Thoma, & Nusslein-Volhard, 1989; Struhl, Struhl, & Macdonald, 1989).

4.1.1.2 The posterior system

The posterior pole plasm, similar to the anterior cytoplasm, when transplanted, exhibits long-range pattern formation effects, and these effects are attributed to the posterior group of genes (Lehmann & Nusslein-Volhard, 1986, 1987, 1991; Sander & Lehmann, 1988). An important component of this system is Nanos (Nos) protein, whose mRNA is posteriorly localized (Ephrussi, Dickinson, & Lehmann, 1991; C. Wang & Lehmann, 1991). Mutant embryos derived from *nos* homozygous mothers do not form the abdomen (Lehmann & Nusslein-Volhard, 1986; Schupbach & Wieschaus, 1986).

bcd mRNA is tethered to the anterior pole and *nos* mRNA is localized to the posterior pole at the end of oogenesis and they remain translationally dormant until ovulation. Their protein products are produced after fertilization (Berleth et al., 1988; Frigerio et al., 1986; Gavis & Lehmann, 1992; Little, Tkacik, Kneeland, Wieschaus, & Gregor, 2011). When corresponding proteins are produced, they freely diffuse inside the syncytium forming the gradients. For instance, Bcd protein can be detected up until 80% egg length (EL), whereas 90% of *bcd* mRNA transcripts are localized to anterior 20% EL (Little et al., 2011). Two other maternally

deposited mRNAs are also involved in determining the body plan along the AP axis – *hunchback* (*hb*) and *caudal* (*cad*) as components of anterior and posterior systems respectively (Lehmann & Nusslein-Volhard, 1987; L. H. Wu & Lengyel, 1998). In contrast to *bcd* or *nos*, transcripts of *hb* and *cad* are ubiquitously present in the embryo but their translation is blocked by Bcd and Nos proteins at anterior and posterior poles respectively (Figure 24B, D). Thus, four maternal protein gradients are generated by these molecular interaction networks in the early embryos (Figure 24C); Bcd and Hb from anterior-to-posterior and Nos and Cad from posterior-to-anterior.

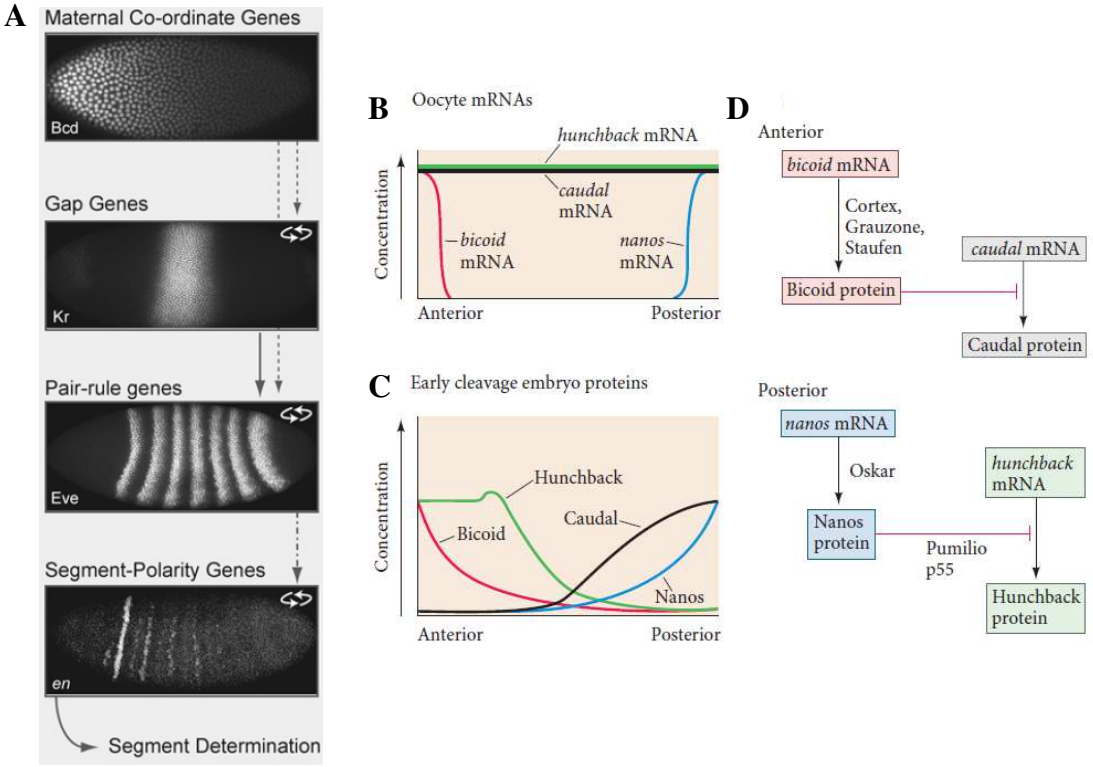

Figure 24. Pathways involved in AP axis determination inside embryo

(A) Cascade of maternal and zygotic pathways determining AP axis. Image taken from (Jaeger, 2011). (B-D) Plots showing the gradients of mRNA (B) and protein (C) of maternal effectors along the AP axis and the schematic diagram of protein-RNA interactions that generate these gradients. Image taken from (Barresi & Gilbert, 2019).

A cascade of molecular pathways is activated by these maternal effectors causing activation of particular zygotic genes that provide specific spatial identity along the AP axis (Figure 24A). The first zygotic genes to be expressed by the interactions between maternal effect genes are the gap genes coding transcription factors like Hb, Knirps, Giant, etc (Jaeger,

2011). They are termed so because mutants for these factors display gaps in the segmentation patterns and are expressed in broad, partly overlying fields. Combinations of different gap genes result in the expression of a class of genes called pair-rule genes like Even-skipped (Eve), Fushi-tarazu (Ftz), etc. Pair-rule genes code for transcription factors that divide the embryonic into periodic segments, resulting in a striped pattern of seven transverse bands (Akam, 1987). Pair-rule gene interaction networks activate the expression of segment polarity genes, whose protein products further subdivide the embryo into 14 parasegments (Akam, 1987). Permutations and combinations of the gap, pair-rule, and segment polarity gene interactions regulate another group of genes called the homeotic selector genes whose activity determines the developmental fate of each segment. However, patterning along the AP axis is not complete without the terminal system.

4.1.1.3 The terminal system

While the source of polarity in both anterior and posterior systems resides within the oocyte, the terminal system depends on the inductive activity of follicle cells. Mutations in genes belonging to this group result in deletion of the anterior- and posterior-most unsegmented regions of the embryo, the acron, and telson (Klingler, Erdelyi, Szabad, & Nusslein-Volhard, 1988; Nusslein-Volhard et al., 1987; Schupbach & Wieschaus, 1986). The maternally deposited Torso (a transmembrane receptor) protein in the oocyte is the main factor determining the terminal regions (Sprenger, Stevens, & Nusslein-Volhard, 1989). Torso is ubiquitously present. The ligand is encoded by *torsolike*, which is produced by follicle cells in the anterior and posterior tips, that activate the Torso pathway specifically at the terminals (Stevens, Frohnhofer, Klingler, & Nusslein-Volhard, 1990). Activation of the Torso pathway at the poles results in the expression of the zygotic target genes *huckebein* and *tailless* (Klingler et al., 1988; Weigel, Jurgens, Klingler, & Jackle, 1990).

4.1.2 *Drosophila* embryonic DV axis specification

Similar to the terminal system, embryonic DV axis specification also depends on the inductive activity of the follicle cells. This system is the most complex out of all four axes determination pathways. DV patterning also depends on the concentration gradient of a transcription factor but unlike the other systems, DV pattern is generated by the graded uptake of this morphogen into the nuclei of the syncytial blastoderm.

4.1.2.1 DV patterning in the oocyte

As described previously, the foundation for embryonic axes is laid during oogenesis itself by the Gurken-Torpedo signaling between oocyte and the follicle cells. Gurken-Torpedo signaling makes the follicle cells take dorsal fate (Figure 23B), which initiates the DV patterning signal (Figure 25A). Active Torpedo receptor in these follicle cells activates a transcription factor, Mirror, which inhibits the expression from *pipe* gene (Andreu et al., 2012; Fuchs, Cheung, Charbonnier, Shvartsman, & Pyrowolakis, 2012). Pipe protein modifies the vitelline membrane envelope by sulfating the proteins on it and is expressed only in the ventral follicle cells (Amiri & Stein, 2002; Sen, Goltz, Stevens, & Stein, 1998). The addition of sulfate group to proteins on ventral vitelline envelope allows the binding of Gastrulation-defective (GD) protein to this region. Other proteins are also recruited by GD to form a complex that cleaves Easter protease to its active form (Cho, Stevens, Sieverman, Nguyen, & Stein, 2012; Cho, Stevens, & Stein, 2010). Activated Easter cleaves the Spatzle protein to its active form; activated Spatzle binds and activates the Toll receptor (Chasan, Jin, & Anderson, 1992; C. C. Hong & Hashimoto, 1995; LeMosy, Tan, & Hashimoto, 2001). Toll receptor is maternally deposited and is ubiquitously distributed throughout the cell membranes of the embryo, but is activated only by cleaved Spatzle ligand present at the ventral region (Hashimoto, Gerttula, & Anderson, 1991; Hashimoto, Hudson, & Anderson, 1988).

4.1.2.2 DV patterning in the embryo

The Dorsal protein, a Rel transcription factor, is the key determinant of patterning the back and belly of the *Drosophila* embryo in a concentration-dependent manner (Figure 25B) (J. W. Hong, Hendrix, Papatsenko, & Levine, 2008; Jiang & Levine, 1993; Reeves et al., 2012). Dorsal activates the expression of genes that induce the ventral fate. The *dorsal* message is synthesized in the nurse cells and into the embryo and is not translated until about 90 minutes after fertilization. When the Dorsal protein is translated, it

is present throughout the embryo, without distinguishing between the dorsal or ventral side. How can a ubiquitously present factor act as a morphogen? Interestingly, Dorsal being a transcription factor is translocated only to the ventral cell nuclei, and the nuclear translocation depends on the Toll receptor activation (Roth, Stein, & Nusslein-Volhard, 1989; Rushlow, Han, Manley, & Levine, 1989; Steward, 1989). Translated Dorsal is initially bound by a protein partner called Cactus, throughout the embryo. Dorsal bound by the Cactus is blocked from entering the nucleus. Activation of the Toll receptor at the ventral side triggers a protein kinase, Pelle, which phosphorylates Cactus. Phosphorylated Cactus is degraded and Dorsal is freed, translocating it into the nucleus (Kidd, 1992; Reach et al., 1996; Shelton & Wasserman, 1993; Whalen & Steward, 1993). Since the Toll activity depends on the gradient of the ligand Spatzle (Rahimi et al., 2019), whose concentration is highest at the ventral side, Dorsal nuclear translocation also follows a similar gradient, with ventral-most cells having the highest concentration of Dorsal in the nucleus.

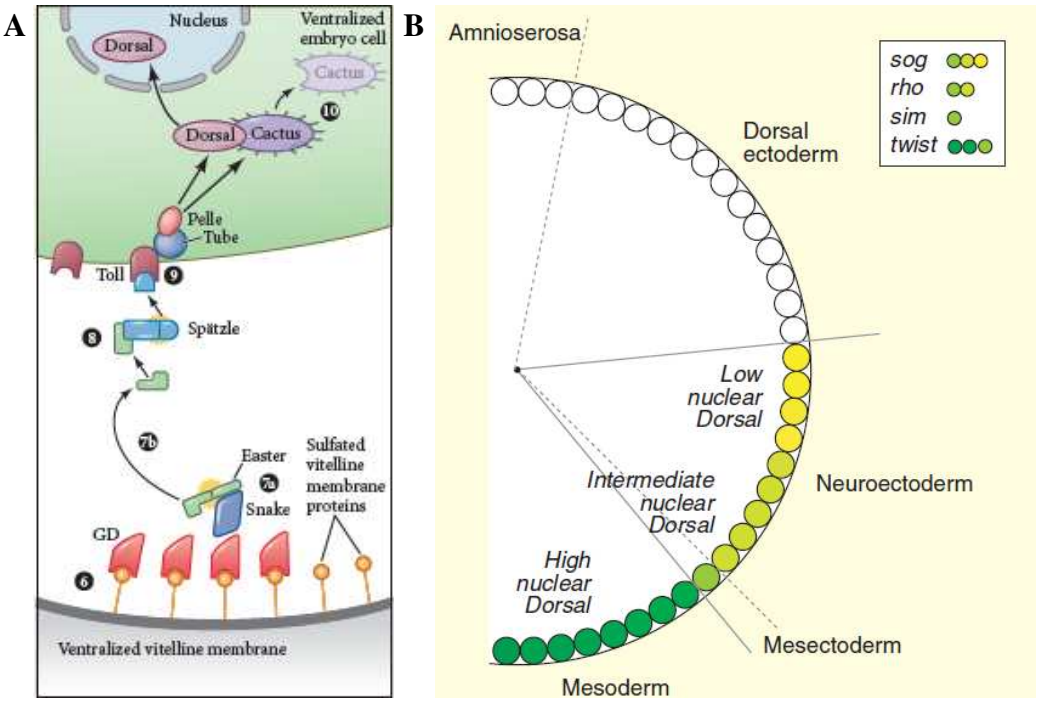

Figure 25. Pathways involved in DV axis determination inside embryo

(A) Cascade of molecular events that lead to nuclear translocation of Dorsal to the nucleus at ventral side. Image taken from (Barresi & Gilbert, 2019). (B) Schematic diagram representing different cell fates along the DV axis generated depending on gradient of nuclear Dorsal levels. Image adapted from (Moussian & Roth, 2005).

4.2 Gene expression to morphogenesis

I have given an overview of the gene patterning systems that define the major body axes of the *Drosophila* embryo above section. Interestingly, the components of gene patterning systems at this level are mostly transcription factors, that have a role inside the nucleus. Then, how is the message from these patterning signals relayed to the cytoskeletal elements during a morphogenetic event? I will give an overview of how gene patterning regulates two prominent morphogenetic processes in the gastrulating *Drosophila* embryo: the mesoderm invagination and germband extension.

4.2.1 Mesoderm invagination

Fly embryos undergo series of morphogenetic events during gastrulation, starting with a band of ~ 1000 cells at the ventral side with a mesodermal fate invaginate inside the embryo, a process known as ventral furrow formation (VFF) (Kam et al., 1991). Mesoderm cell fate is determined by two master transcription factors, Snail (Sna) and Twist (Twi), whose expression depends on Dorsal nuclear translocation in the ventral blastoderm cells (Ip, Park, Kosman, Yazdanbakhsh, & Levine, 1992). During VFF, the cells undergo a series of morphogenetic events, starting with apical constriction and elongation, followed by shortening and basal expansion (Leptin & Grunewald, 1990). It was shown that apical constriction is mediated by actomyosin contraction, which is downstream of the Rho pathway (Figure 26A) (Dawes-Hoang et al., 2005; Hacker & Perrimon, 1998; Martin, Kaschube, & Wieschaus, 2009). Rho is activated in these cells at the apical cortex by specific localization of RhoGEF2 (a guanine nucleotide exchange factor) which is regulated by T48 (a transmembrane protein shown to be an anchor for RhoGEF2) (Kolsch, Seher, Fernandez-Ballester, Serrano, & Leptin, 2007; Strutt & White, 1994) and Concertina (Cta, G-protein α subunit) (Barrett, Leptin, & Settleman, 1997). Cta is activated by the binding of the ventrally secreted ligand, Fog to the GPCR, Mist (Costa, Wilson, & Wieschaus, 1994; Dawes-Hoang et al., 2005; Manning, Peters, Peifer, & Rogers, 2013; Morize, Christiansen, Costa, Parks, & Wieschaus, 1998; Parks & Wieschaus, 1991). The expression of components regulating apical actomyosin contractility is under the control of Twi and Sna. Expression of Mist is under the control of DV patterning component Sna (Manning et al., 2013) and Fog and T48 expression are under the control Twi (Kolsch et al., 2007; Morize et al., 1998). Ventral cells in double mutant *twi*, *sna* embryos fail to constrict

apically and invaginate (Leptin, 1991). Expression of *twi* and *sna* is under the control of Dorsal protein (J. W. Hong et al., 2008).

4.2.2 Germband extension

Another prominent event during *Drosophila* gastrulation is the extension of tissue along the ventrolateral position towards the dorsal side, a process termed germband extension (GBE) (Irvine & Wieschaus, 1994). During GBE, the tissue undergoes convergent extension, resulting in reduced width along the DV axis and an almost two-fold increase in length along the AP axis. This process is facilitated by cells actively exchanging their neighbors, a process is known as cell intercalation or T1 transition (Irvine & Wieschaus, 1994). When the T1 transitions occur in a planar cell polarized (PCP) manner, a net elongation of tissue occurs (Rauzi, 2020; Rauzi, Verant, Lecuit, & Lenne, 2008; Tada & Heisenberg, 2012). During *Drosophila* GBE, cells specifically reduce their junctions along the DV axis and form new junctions along the orthogonal AP axis (Irvine & Wieschaus, 1994). This process is mediated by the PCP distribution of non-muscle MyoII along DV junctions (Bertet et al., 2004; Blankenship, Backovic, Sanny, Weitz, & Zallen, 2006; Rauzi, Lenne, & Lecuit, 2010). Interestingly, planar polarized MyoII recruitment and cell intercalation do not depend on the conventional PCP pathway (Wnt/Fz pathway) and are under the control of the AP patterning system (Figure 26B). Polarized T1 transitions and MyoII distribution was shown to be under the control of the AP patterning system as mutants of *eve* or *bicoid nanos torso-like* (*bnt-*) triple mutants that lack AP patterning shows a drastic reduction in intercalation and MyoII distribution polarity, translating it to reduced tissue extension during GBE (Irvine & Wieschaus, 1994; J. A. Zallen & Wieschaus, 2004). Recent studies have shown that the AP patterning system translates their action on actomyosin PCP distribution by regulating the expression of Toll2/6/8 receptors and Tartan/Ten-m (Pare et al., 2019; Pare et al., 2014). Furthermore, recent studies identified the pathways that transduce Toll pathways to PCP distribution of MyoII. Masako and colleagues identified Src kinase as a switch that induces interaction between Toll 2/6 receptors and phosphoinositide-3-kinase (PI3K), which translates Toll 2/6 signals to PCP distribution of MyoII (Tamada et al., 2021). In a second study, Jules and colleagues showed that Toll 8 signalling depends on the recruitment of adhesion GPCR, Circl, which signals via Rho pathway to generate PCP distribution of MyoII (Lavalou et al., 2021).

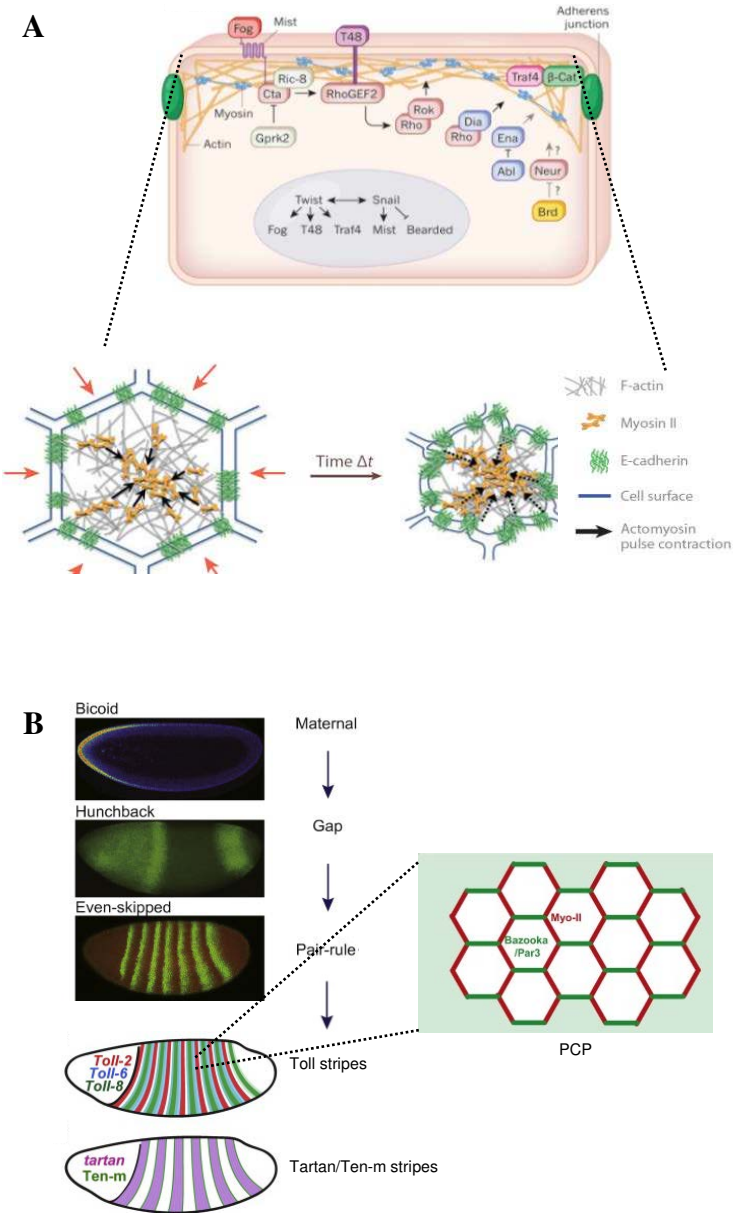

Figure 26. Morphogen to morphogenesis

(A) Schematic of gene expression regulation under the control of DV patterning leading to generation of apical contractile forces. Images adapted from (Gilmour, Rembold, & Leptin, 2017; Lecuit, Lenne, & Munro, 2011). (B) Schematic representation of the gene expression regulation that leads to planar polarized MyoII distribution in the lateral ectodermal cells during GBE, under the control of AP patterning system. Images adapted from (Kong et al., 2017; Pare et al., 2019).

5. Aim of the thesis

Control of morphogenetic pathways like folding and extension by specific gene patterning systems is well documented in the examples described in section 4. But for a long time, these morphogenetic programs were thought to be apparently uncoupled (simple morphogenesis). In reality, not all morphogenetic events occur in series. For example, during neurulation, the *Xenopus* neural plate undergoes extension along the AP axis simultaneously when it is getting folded along the orthogonal axis (Figure 27) (R. Keller et al., 1992). Cellular and molecular mechanisms driving such simultaneous events, hereby termed as '**concomitant morphogenesis**' (for more details refer to the book chapter attached as Annex I), have been left unexplored. Thus the main aim of my research is to identify cellular and molecular mechanisms driving concomitant morphogenesis and the contribution of synergy between orthogonal patterning signals in providing the cue for concomitant morphogenesis. To address this, I used mesoderm in gastrulating *Drosophila* embryo as a paradigm. Previous studies in *Drosophila* have shown that apical constriction regulates shape changes associated with ventral furrow formation. However, furrow formation accompanied by displacement of mesoderm tissue about 50-60 µm cannot be an outcome of apical constriction alone and mechanisms regulating this broad displacement remains elusive. Recent data from our lab showed that the seven transverse stripes of AP patterning component Eve are found to pass through the mesoderm anlage. However, mesoderm cells were not known to exchange their neighbors previously. Thus *Drosophila* mesoderm is a perfect example for studying the mechanisms that drive concomitant folding and extension, under the control of synergy between orthogonal patterning signals.

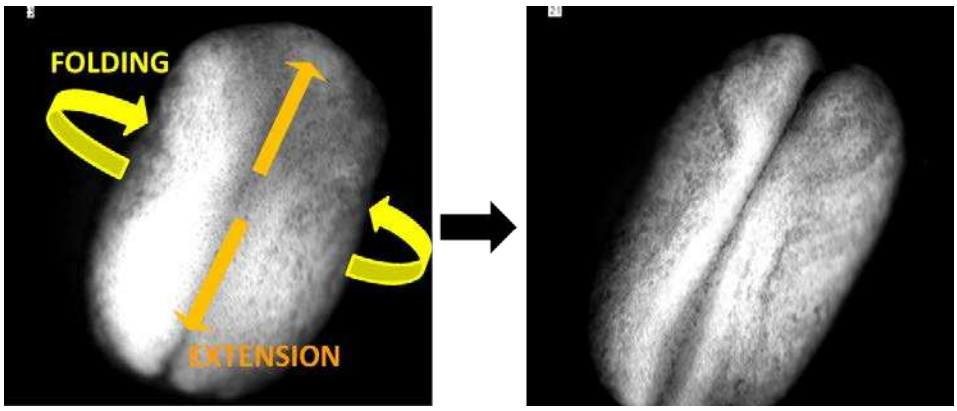

Figure 27. Concomitant morphogenesis during vertebrate neurulation

Xenopus neural plate undergoing concomitant folding and extension during neurulation. Images adapted from (Kong, Wolf, & Grosshans, 2017; Pare et

Chapter II

Results

6. Summary of research paper

The results of my research were recently published as a research article in the journal, Developmental Cell. A summary of the results is given below.

6.1. *Drosophila* mesoderm cells intercalate during invagination in a PCP fashion

A major challenge for studying the cellular processes driving mesoderm invagination is due to the movement of mesoderm cells inside the embryo, making it difficult to follow cell vertices over time. To tackle this issue, I used MultiView selective plane illumination microscopy (MuVi-SPIM) to image developing embryos *in toto* from two orthogonal views and used to generate digitally reconstructed 4D movies. Apical positions of mesoderm cells were followed in time and repositioned, allowing the cell vertices to be followed across time. This analysis showed that mesoderm cells intercalate simultaneously during invagination and ~60% of mesoderm cells intercalate during the first ten minutes of mesoderm invagination. Mesoderm cell intercalation is special as in the majority of the cells it is initiated at a lateral position ~10 µm from the apical site compared to the lateral ectoderm where intercalation is generally initiated apically. Cell intercalation in mesoderm is planar polarized, with the majority of the shrinking junctions oriented along the DV axis. Using optogenetic tools, I show that mesoderm cell intercalation is not a passive response to tissue folding.

6.2. MyosinII is recruited to the lateral cortex of mesoderm cells and mediates cell intercalation

To identify the molecular mechanism driving mesoderm cell intercalation, I followed the localization of fluorescently-labeled MyoII motor proteins

during mesoderm invagination. MyoII was found to be recruited to the lateral cortices ~5 minutes after apical recruitment of MyoII in mid-sagittal views. Furthermore, lateral MyoII colocalizes with membrane and F-actin, suggesting that it is cortical. MyoII was also found to colocalize with RhoGEF2 and Rho, indicating that the Rho pathway mediates lateral MyoII recruitment. In a surface view, lateral MyoII distribution was found to be planar polarized, localized preferentially to DV-oriented vertices. Using chemical and optogenetic tools, I showed that such a polarized distribution and activity of MyoII was necessary and sufficient to induce the shrinking of DV-oriented vertices.

6.3. AP-DV patterning synergy is necessary for the efficient convergence-extension of mesoderm

Since the mesoderm cell intercalation was planar polarized, I tested the role of the AP patterning pathway. Cell intercalation during GBE in AP patterning mutant embryos was abolished. Surprisingly, cell intercalation in mesoderm was not affected in *bnt* $^{-/-}$ embryos lacking AP patterning signals and had only a minor effect on polarity, whereas cell intercalation was drastically reduced in ventral cells of the *sna twi* $^{-/-}$ embryos. These results indicate that the gain of intercalation in mesoderm cells depends on ventral fate and not on the AP patterning. What role does mesoderm cell intercalation play. Intercalating germband was previously shown to extend but the extension of any sort in mesoderm tissue was not reported beforehand. To check if mesoderm tissue extends, I used the digitally reconstructed mid-sagittal sections from MuVI SPIM movies and observed that mesoderm tissue extends following apical constriction. Tissue extension was blocked in *sna twi* $^{-/-}$ embryos having fewer inetercalation events. Unexpectedly, tissue extension did not scale to the amount of cell intercalation in *bnt* $^{-/-}$ mutants embryos compared to wild-type, indicating that cell intercalation events in embryos were defective in extending the tissue. Mesoderm tube formed by the *bnt* $^{-/-}$ embryos was wider compared to wild-type embryos, indicating that intercalation is defective in

converging the tissue. A closer look at intercalating cells in *bnt* $^{-/-}$ embryos showed that these cells intercalate in a specific manner; intercalation begins with a regular lattice but ends with an irregular lattice, the two separating cells shrink their entire area while the cells creating new contact blow up (bow-tie intercalation). Interestingly, polarized lateral MyoII distribution in *bnt* $^{-/-}$ embryos was reduced. These results indicate that synergy between both AP and DV patterning is necessary for efficient folding and extension of mesoderm.

6.4. Mesoderm cells generate a second junctional tier laterally to mediate cell intercalation

A prerequisite for cells to intercalate is that they should be in contact. Lateral MyoII colocalized with junctional components like E-Cad, α-Cat, and β-Cat. Interestingly, lateral E-Cad foci are generated on the fly by MyoII coalescence and MyoII contractility is necessary for the assembly of the second junctional tier at the lateral cortex.

6.5. Formation of the second tier of MyoII at the lateral cortex depends on Snail and RhoGEF2

In toto analysis of the distribution of fluorescently labeled MyoII showed that lateral MyoII recruitment was restricted to mesoderm cells, and not in the dorsal or latera tissue, following the Snail expression domain. Using mutant and RNAi tools, I show that Snail-mediated signaling is both necessary and sufficient for lateral recruitment of MyoII. Excitingly, using the Dendra (fluorophore that emits in green wavelength, but can be converted to emit red wavelength by UV induction) labeled MyoII, I show that MyoII diffuses from the basal side by the end of cellularization, and this pool eventually gets accumulated sequentially at the apical and lateral cortices. How can then a cell regulate contractility at two different subcellular locations, which are separated in time when there is no directed transport of MyoII? I followed the localization of fluorescently labeled RhoGEF2 (upstream activator of Rho pathway and actomyosin

contractility) during mesoderm invagination and found that RhoGEF2 localization follows a temporal sequence; RhoGEF2 accumulates specifically to apical domain initially, and at around ~5 minutes, localizes to the lateral cortices. This observation illustrates that sequential activation of the Rho pathway at two distinct subcellular regions induces two-tier MyoII localization.

Article

Developmental Cell

A two-tier junctional mechanism drives simultaneous tissue folding and extension

Graphical abstract

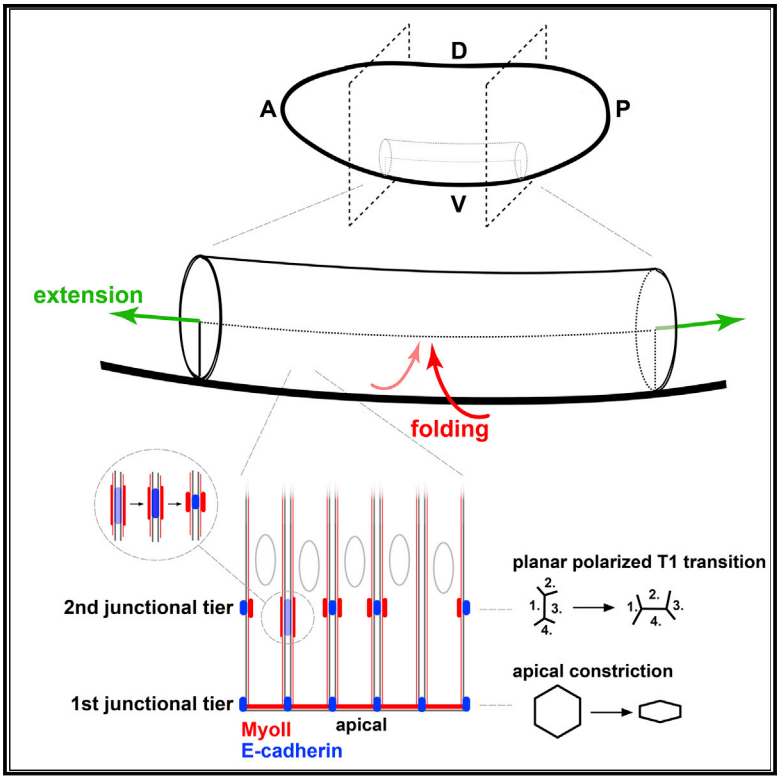

Authors

Alphy John, Matteo Rauzi

Correspondence

matteo.rauzi@univ-cotedazur.fr

In brief

John and Rauzi identify a combo-mechanism, based on two-tier adherens junctions, mediating simultaneous tissue folding and extension. While the first tier mediates cell apical constriction, the second mediates cell intercalation. The two-tier mechanism is under the control of anterior-posterior and dorsal-ventral gene patterning that act synergistically to drive composite morphogenesis.

Highlights

- The *Drosophila* prospective mesoderm undergoes simultaneous folding and extension
- Mesoderm cells form two-tier adherens junctions to drive composite morphogenesis
- Two-tier junctions mediate simultaneous apical constriction and intercalation
- Composite morphogenesis is controlled by AP and DV gene patterning synergy

John & Rauzi, 2021, Developmental Cell *56*, 1469–1483
May 17, 2021
https://doi.org/10.1016/j.devcel.2021.04.003

CellPress

Developmental Cell

CellPress

Article

A two-tier junctional mechanism drives simultaneous tissue folding and extension

Alphy John[1] and Matteo Rauzi[1,2,*]
[1]Université Côte d'Azur, CNRS, Inserm, iBV, Nice, France
[2]Lead contact
*Correspondence: matteo.rauzi@univ-cotedazur.fr
https://doi.org/10.1016/j.devcel.2021.04.003

SUMMARY

During embryo development, tissues often undergo multiple concomitant changes in shape. It is unclear which signaling pathways and cellular mechanisms are responsible for multiple simultaneous tissue shape transformations. We focus on the process of concomitant tissue folding and extension that is key during gastrulation and neurulation. We use the *Drosophila* embryo as model system and focus on the process of mesoderm invagination. Here, we show that the prospective mesoderm simultaneously folds and extends. We report that mesoderm cells, under the control of anterior-posterior and dorsal-ventral gene patterning synergy, establish two sets of adherens junctions at different apical-basal positions with specialized functions: while apical junctions drive apical constriction initiating tissue bending, lateral junctions concomitantly drive polarized cell intercalation, resulting in tissue convergence-extension. Thus, epithelial cells devise multiple specialized junctional sets that drive composite morphogenetic processes under the synergistic control of apparently orthogonal signaling sources.

INTRODUCTION

During embryo development, tissues remodel their shape to eventually provide form to the mature animal (Solnica-Krezel, 2005). Tissues can change shape in seven fundamental manners: they can grow, shrink, thicken, thin, twist, converge-extend, and buckle. In recent decades, researchers have been striving to identify and characterize the cellular mechanisms driving distinct morphogenetic processes. Remarkably, under the control of finely tuned signaling pathways, epithelial cells devise specialized strategies to specifically remodel their shape or topology (Basson, 2012; Gilmour et al., 2017; Jülicher and Eaton, 2017). For instance, during tissue folding, epithelial cells reduce their apical surface in a process referred to as apical constriction. During apical constriction, an actomyosin meshwork that is anchored to adherens junctions forms in the apical-medial cell region and subsequently contracts generating cortical tension driving cell surface reduction (Martin and Goldstein, 2014; Martin et al., 2009). Medial actomyosin networks are interconnected via junctions forming a supracellular contractile meshwork that is necessary for mesoderm internalization (Martin et al., 2010). Another example is planar-polarized cell intercalation during tissue convergence-extension (Keller et al., 2000; Rauzi, 2020; Walck-Shannon and Hardin, 2014). This process is based on junction remodeling and cell neighbor exchange: two neighboring cells shrink their contact junction and eventually a new junction is formed, which brings new cells into contact (Bertet et al., 2004; Blankenship et al., 2006). This process is referred to as cell intercalation or T1 transition. During tissue convergence-extension, intercalation is polarized resulting in cells coming together along one axis and moving apart one from each other along the orthogonal axis, leading to tissue narrowing and elongation, respectively (Irvine and Wieschaus, 1994). In the prospective ectoderm of the developing *Drosophila* embryo, this process is initiated by the interplay between the pulsatile medial-apical actomyosin meshwork and the junctional cortex that is enriched with MyoII in a polarized fashion (Rauzi et al., 2010). Polarized junctional contractions, generating cortical tension, initiate cell intercalation that eventually drives tissue convergence-extension (Fernandez-Gonzalez et al., 2009; Rauzi et al., 2008). This shows that epithelial cells fine-tune both junctions and the cytoskeleton to generate ad hoc cellular patterns of forces driving specific cell shape and topology changes.

During embryo development, epithelia can undergo different types of shape changes. While these changes can be sequential, and thus driven by specific sequential cellular mechanisms, this is not always the case. A single tissue can undergo multiple simultaneous shape transformations. For instance, in vertebrates, during neurulation, the dorsal tissue folds forming the neural tube while elongating along the anterior-posterior axis separating the future head from the anus (Keller, 2002). This raises an important question: how can a tissue undergo multiple simultaneous shape transformations if each transformation is per se driven by a functionally specific cellular mechanism? In addition, which signaling pathways are controlling composite morphogenetic processes? To address these questions, we focus on the processes of tissue folding and extension that

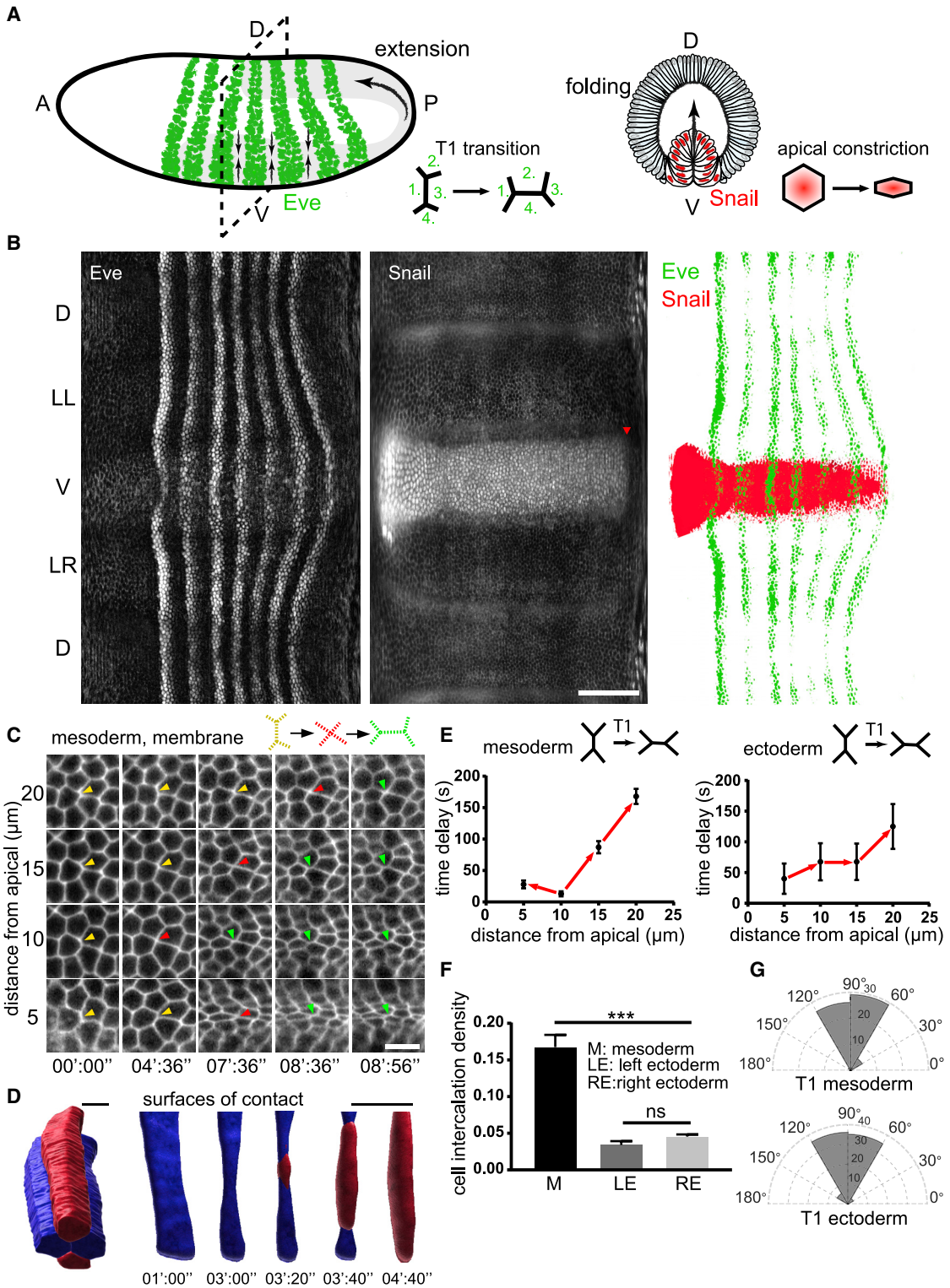

Figure 1. *Drosophila* embryonic mesoderm cells intercalate during invagination

(A) Eve is a component of the anterior-posterior patterning system during *Drosophila* embryo development and plays a key role in cell intercalation driving ectoderm convergence-extension. Snail is a component of the DV patterning system controlling cell apical constriction and mesoderm invagination.

(B) Eve and Snail protein expression at the onset of gastrulation. Dorsal (D), lateral left (LL), lateral right (LR), ventral (V). Red arrowhead marks the posterior boundary of *snail* expression. Scale bar, 50 μm.

(legend continued on next page)

play a key role during gastrulation and neurulation. As model system, we use the early developing *Drosophila* embryo and show that during gastrulation the prospective mesoderm undergoes simultaneous tissue folding and convergence-extension. By using confocal multiview light-sheet microscopy, laser manipulation, optogenetics, and quantitative big data image analysis, we seek to unravel the signaling pathways and the fundamental mechanisms driving composite morphogenetic processes.

RESULTS

Mesoderm cells intercalate in a planar-polarized fashion

During *Drosophila* early gastrulation, distinct parts of the germband epithelium undergo different shape transformations: while the prospective mesoderm folds on the ventral side moving cells to the interior of the embryo, the prospective ectoderm converges along the dorsal-ventral (DV) axis and extends along the anterior-posterior (AP) axis on both right and left lateral sides of the embryo in a symmetric fashion. Ventral folding is under the control of the Twist and Snail transcription factors (Leptin and Grunewald, 1990) (part of the DV gene patterning system) responsible for mesoderm cell apical constriction (Martin et al., 2009) (Figure 1A, right panel—Snail represented), a key cellular process in the initiation of tissue bending. Lateral convergence-extension is under the control of the pair-rule transcription factors (e.g., Even-skipped, part of the AP gene patterning system) that controls planar cell polarized cell intercalation (Irvine and Wieschaus, 1994), a key cellular process driving tissue convergence and extension (Figure 1A, left panel). Cell apical constriction does not take place and is not expected to take place on the embryo lateral sides since *twist* and *snail* are not expressed in these regions (Figure 1B, central panel—Snail shown). Cell intercalation has been reported to occur in the ectoderm but has never been observed in the mesoderm. Nevertheless, *eve* is expressed both in the lateral and ventral tissues (Figure 1B, left panel), giving rise to the hypothesis that cell intercalation could also occur in the mesoderm. To test this hypothesis, we monitored cell topology changes in the ventral tissue (supplemental information). Our data show that mesoderm cells intercalate during apical constriction and tissue folding (Figures 1C and 1D; Video S1, left, central-top, and right panels). While T1 transitions take place in both the ectoderm and mesoderm, cell intercalation initiation shows peculiar differences between the two tissues: while in the ectoderm, cell intercalation is initiated more apically and resolves toward the cell basal side (Figures 1E, right panel, and S1A), in the mesoderm, cell intercalation is initiated laterally (at ~10 μm from the cell apical side) and resolves concomitantly toward the cell apical and basal sides (Figures 1D and 1E left panel). We counted the number and orientation of T1s in the mesoderm halfway through tissue folding (Video S1, central-bottom panel). The density of mesoderm cell intercalation (number of cell intercalations/number of cells) is >0.15. Since an intercalation event involves at least 4 cells, this results in more than 60% of mesoderm cells engaged in cell intercalation during the first phase of mesoderm internalization. Using the same embryos in which we measured cell intercalation on the ventral side, we also measured cell intercalation on the right and left lateral sides during the same time period. While cell intercalation density in the left ectoderm was not significantly different from the right ectoderm, cell intercalation density in the mesoderm was >6-fold compared with the ectoderm over the same time period (Figure 1F). Much like the ectoderm, the process of cell intercalation in the mesoderm exhibits planar polarization (Figure 1G): neighboring anterior and posterior cells separate from each other while a dorsal and a ventral cell become new neighbors. Together, this demonstrates that planar-polarized cell intercalation is a major cellular process in the mesoderm tissue during ventral fold formation.

A PCP MyoII second tier initiates cell intercalation in mesoderm cells

How is planar-polarized cell intercalation driven in the mesoderm? Two hypotheses can be considered: cell intercalation could be the result (1) of the folding of the mesoderm tissue or (2) of an active cellular mechanism. Epithelial tissues, when folding and forming tubular structures, have a higher chance of forming scutoids (a topological configuration for which cells have different apical to basal neighbors; Gómez-Gálvez et al., 2018). To test this first hypothesis, we synthetically generated a furrow on the dorsal side of the embryo by inducing cell apical constriction using two-photon optogenetics to activate MyoII (Figure S1B and supplemental information) that showed similar cell shape changes and ingressed at a similar rate compared with the ventral furrow (2.41 ± 0.28 and 1.71 ± 0.11 μm/min, respectively) (Izquierdo et al., 2018).We then monitored cells over time to detect eventual intercalation events. No T1 transition occurred in ectopic furrows (Figure S1B). This result negates the hypothesis that mesoderm furrowing could drive cell intercalation per se. We thus explored the possibility of an active cellular mechanism that could initiate cell intercalation in the mesoderm (second hypothesis). To this end, we imaged mesoderm cells along sagittal sections. MyoII appears to be enriched at two different positions along the cell apical-basal axis: (1) at the apical side and (2) on the lateral side (Brodland et al., 2010) forming a two-tier distribution (Figure 2A; Video S2, left panel). The first tier has been extensively studied and corresponds to the apical-medial MyoII recruitment driving apical constriction (Martin et al., 2009), whereas the MyoII second tier is poorly studied.

(C) Mesoderm cell intercalation event shown at different distances from the apical cell side as function of time. Gap43mCherry is used for labeling membrane. Scale bar, 5 μm.
(D) Representative 3D reconstruction of a mesoderm cell-quartet (left). Scale bar, 5 μm. Time-lapse of surfaces of contact (reducing contact in blue and newly formed contact in red) during mesoderm cell intercalation (right). Scale bar, 10 μm.
(E) Time delay of cell neighbor exchange at different apical-basal positions in mesoderm (left) and ectoderm (right) tissues. Error bars represents mean error. 3 embryos, 30 cells.
(F) Cell intercalation density in mesoderm and ectoderm tissues during the first 10 min of mesoderm invagination. p value < 0.001 (***). Not significant (ns). 3 embryos. Error bars represent standard deviation.
(G) T1 orientation in mesoderm (top) and ectoderm (bottom) tissues. 90° represent a side shrinking along the DV axis and a new side forming along the AP axis. Mesoderm, n = 60 cells, 3 embryos. Ectoderm, n = 80 cells, 3 embryos.

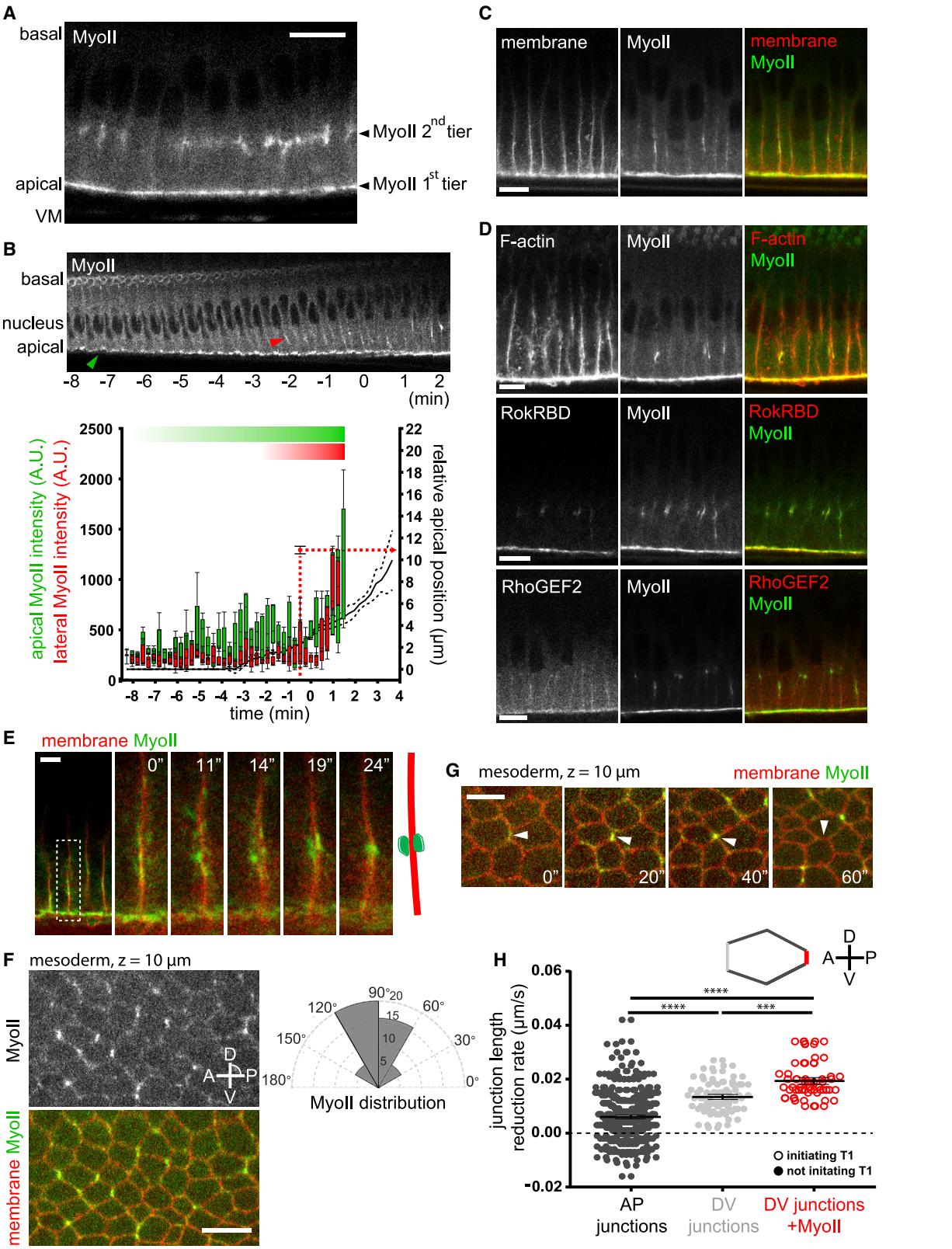

Figure 2. A MyoII second tier is established at the lateral cortex of mesoderm cells

(A) MyoII two-tiers form in mesoderm cells during invagination: the first tier is located at the cell apical side (bottom part of the panel) and the second tier laterally. Scale bar, 15 μm.

(legend continued on next page)

This tier forms ~10 μm from the apical cell surface with a 5-min delay after apical MyoII recruitment during nuclear displacement (Gelbart et al., 2012) (Figure 2B). MyoII is cortical since it colocalizes with cellular lateral membranes (Figure 2C). Both apical and lateral MyoII colocalize with F-actin, Rho, and RhoGEF2 enrichment (Figure 2C). This shows that the factors constituting the 'contracting hub' are present both apically and laterally in mesoderm cells. To better understand how the MyoII second tier forms, we implemented temporally resolved confocal imaging. Lateral MyoII clusters originate from the coalescence of MyoII speckles that flow forming a MyoII focus (Figure 2E). Lateral MyoII coalescence is reminiscent of MyoII pulses forming at the cell apical side (Martin et al., 2009; Rauzi et al., 2010). Nevertheless, and despite their similarities, lateral and apical pulses show a striking difference: while each apical pulse is formed within one cell, lateral flow and coalescence of MyoII speckles, which eventually result in a lateral MyoII focus, occur concomitantly at the interface between two adjacent cells (Figures 2E and S1C; Video S2, right panel). This phenomenon may emerge from underlying biochemical or mechanical lateral coupling between cells. To further characterize the distribution of MyoII, we monitored mesoderm cells over time along a coronal section 10 μm from the cell apical surface. At this location MyoII is distributed in a planar-polarized fashion with cell sides parallel to the DV axis highly enriched in MyoII (Figure 2F), reminiscent of MyoII junctional distribution in ectoderm cells (Bertet et al., 2004; Zallen and Wieschaus, 2004). We then monitored mesoderm cells over time: sides enriched in MyoII shorten initiating cell intercalation (Figure 2G). During furrow formation, all cell sides reduce in length since cells undergo constriction. Constriction takes place in an anisotropic fashion with cells reducing their sizes more along the DV than the AP axis (Martin et al., 2010) (Figure 1A, right panel). To test if MyoII could have a functional role in driving side shortening initiating cell intercalation, we measured the length reduction rate of cell sides. Because of the anisotropic constriction, sides parallel to the DV axis shorten at a higher rate compared with sides parallel to the AP axis. DV sides enriched in MyoII shorten with the highest rate and only these sides led to cell intercalation (Figure 2H). To directly test the role of MyoII in mesoderm cell intercalation, we inhibited MyoII activation by injecting a ROCK inhibitor, Y-27632. The treated embryos did not exhibit lateral MyoII recruitment and T1 transitions (Figure S1D; Video S3). We then tested the role of RhoGEF2 (an upstream activator of the Rho pathway) in mesoderm cell intercalation by using *rhogef2* RNAi embryos. In a RhoGEF2 knockdown background, cell intercalation in the mesoderm is impaired (Figure S1E). This demonstrates that MyoII activity is necessary for mesoderm cell intercalation.

Cell intercalation takes place in two steps: (1) a junction shrinks, and then, eventually, (2) a new junction extends bringing two new cells into contact. Both junction shrinkage and extension in the ectoderm cells result from the interplay between the two cortical networks: the medial-apical and junctional actomyosin networks (Collinet et al., 2015; Rauzi et al., 2010). Cell intercalation in the mesoderm is initiated 10 μm from the apical side (Figures 1C–1E) in the absence of a medial actomyosin network. We thus tested whether MyoII activation at the cortex is sufficient to drive side shrinkage per se. We activated MyoII cortically along one side, 10 μm from the apical surface, using two-photon optogenetics (Izquierdo et al., 2018). The activated side reduced its length within a few tens of seconds (Figure S1F). This shows that cortical-lateral MyoII is sufficient to initiate cell intercalation. How is side extension driven in absence of medial actomyosin network? Tissue-scale forces can facilitate cell intercalation (Rauzi, 2020). During ventral fold formation, tissue-scale forces along the AP axis are more than two times greater than along the DV axis (Martin et al., 2010). In order to test if tissue-scale forces contribute to cell intercalation in the mesoderm, we reduced AP tension in the mesoderm by laser dissecting the actomyosin network along two segments orthogonal to the AP axis (Figures S2A and S2B) and monitored cell intercalation. While the density of polarized side shrinkage was not significantly different compared with the control case, the density of new side extension was significantly reduced after laser dissection (Figures S2C and S2D). This shows that, while side shrinkage is driven by an active cellular mechanism, side extension is facilitated by tissue-scale forces. In conclusion, a two-tier MyoII system is established in mesoderm cells: while the first tier (apical tier) mediates cell apical constriction, the second tier (lateral tier) simultaneously mediates planar-polarized cell intercalation.

AP-DV patterning synergy drives simultaneous mesoderm folding and extension

In the prospective ectoderm, planar cell polarized intercalation is under the control of the AP patterning (Irvine and Wieschaus, 1994). In the prospective mesoderm genes known to control cell intercalation (AP patterning genes) and cell apical constriction (DV patterning genes) are expressed (Figure 1B). Previous work suggested that there might be no or little interaction between the DV and the AP pattern-forming systems (Roth, 1993). While it is known that the DV patterning genes control apical constriction

(B) Kymograph (top) and plot (average of 5 embryos, bottom) showing the temporal sequence of MyoII two-tier establishment. t = 0 min represents the time point when the furrow passes 5-μm depth. Green and red arrowheads in the kymograph mark apical and lateral MyoII accumulation onset respectively. The red dot on the plot represents the average position of the lateral MyoII foci. n = 15 cells, 3 embryos.
(C and D) Lateral MyoII colocalizes with membrane (GFP fusion to Gilgamesh) (C), F-actin (D, top), Rho-sensor (D, middle) and RhoGEF2 (D, bottom). Scale bar, 10 μm.
(E) Temporal sequence of cell-cell coordinated lateral MyoII coalescence. Scale bar, 5 μm.
(F) Distribution of lateral MyoII 10 μm from the apical cortex of mesoderm cells (left). Angular distribution of lateral MyoII (right). Scale bar, 10 μm. n = 30 cells, 3 embryos.
(G) Temporal sequence of an intercalation event in the mesoderm (10 μm from the cell apical side) showing MyoII enriching along a shrinking side during T1 transition. Scale bar, 5 μm.
(H) Junction reduction rate of AP, DV, and MyoII enriched DV sides (red). All and only sides enriched in MyoII initiate cell intercalation (empty circles). n = 30 intercalations, 3 embryos. p value < 0.0001 (****), p value < 0.001 (***).
See also Figures S1 and S2.

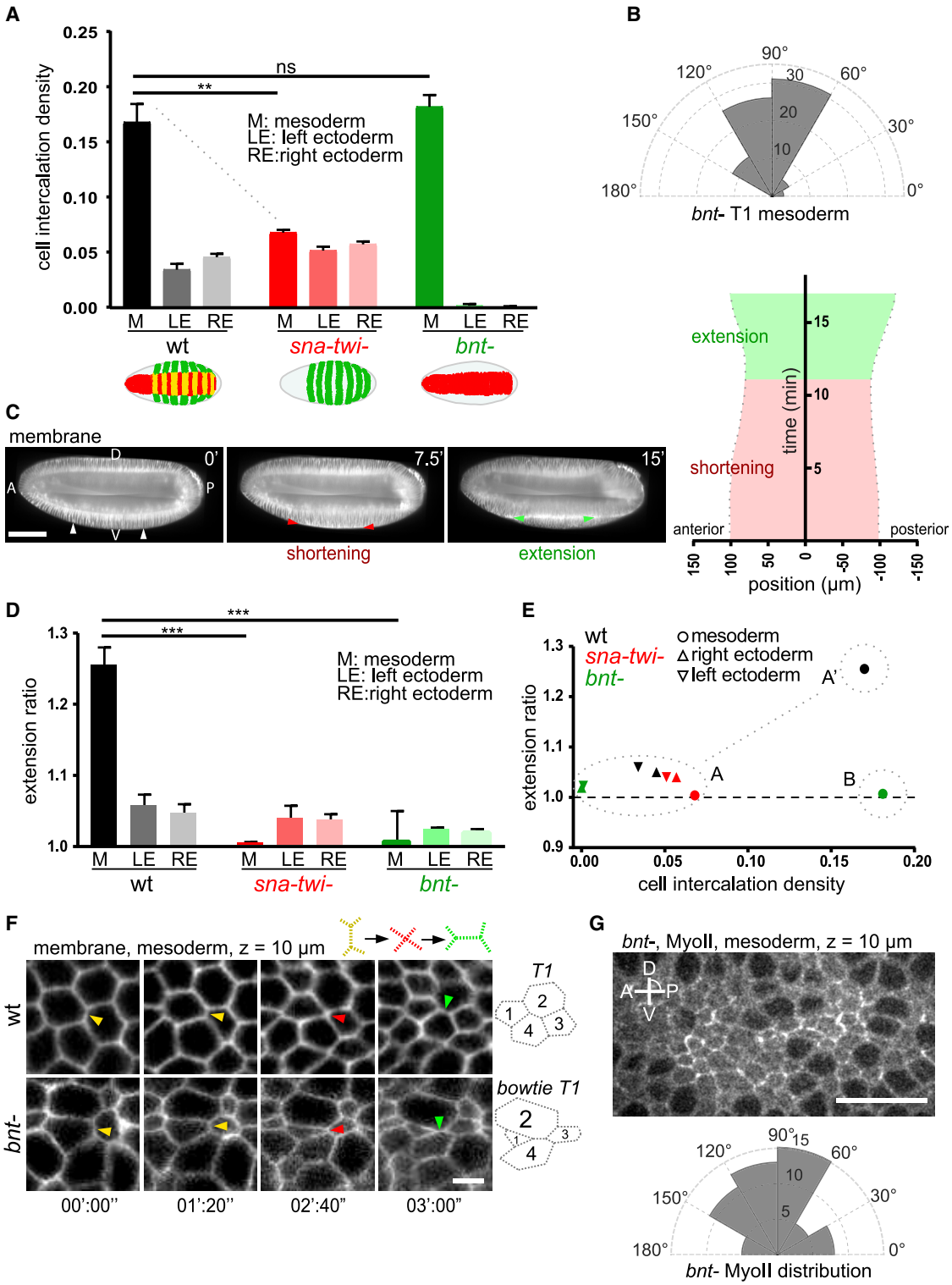

Figure 3. AP-DV patterning synergy is necessary for effective mesoderm convergence-extension

(A) Cell intercalation density in mesoderm and ectoderm tissues for wild type (WT), *sna−twi−* double mutant and *bicoid nanos toso-like* (*bnt−*) triple mutant embryos. n = 3 embryos. Drawings at the bottom of the graph show simplistic schematics of gene pattern expression. p value < 0.01 (**). Not significant (ns). Error bars represent standard deviation.

(B) T1 orientation distribution in *bnt−* mesoderms. n = 75 intercalations, 3 embryos.

(legend continued on next page)

(Leptin and Grunewald, 1990), how is cell intercalation controlled in the mesoderm? To uncover this, we measured cell intercalation in either AP or DV patterning mutants as, for instance, embryos deficient for either the three genes *bicoid*, *nanos*, and *torso-like* (Nüsslein-Volhard et al., 1987) (*bnt*−; Zallen and Wieschaus, 2004) or *snail* and *twist* (Leptin and Grunewald, 1990) (*sna*−*twi*−), respectively. In *sna*−*twi*− embryos cell intercalation density is strongly reduced in the ventral tissue but not in the lateral tissue, which does not express *snail* or *twist* (Figure 3A). In *bnt*− embryos cell intercalation density is strongly reduced in the ectoderm (Figure 3A) as shown in previous studies (Irvine and Wieschaus, 1994). Remarkably, intercalation density in the mesoderm of *bnt*− and wild-type embryos is not significantly different. This shows that cell intercalation density in the mesoderm is under the control of the DV patterning but not the AP patterning. Cell intercalation in both the ectoderm and the mesoderm is AP planar polarized. We expected that, in *bnt*− embryos, cell intercalation would not be planar polarized since the modulation of an instructive signal along the AP axis is in principle necessary to establish AP planar cell polarity (PCP). Nevertheless, our analysis shows that intercalation polarity in *bnt*− mutants, while slightly reduced compared with wild type and *sna*−*twi*− embryos (Figure S3A), is preserved (Figures 3B and S3B). This shows that AP patterning is not necessary for planar-polarized cell intercalation in the mesoderm tissue. Polarized cell intercalation drives lateral tissue convergence-extension in the prospective ectoderm (Irvine and Wieschaus, 1994). The mesoderm instead folds on the ventral side of the embryo. While the mesoderm is known to eventually extend after internalization as a consequence of collective cell migration (McMahon et al., 2008), mesoderm extension during tissue folding was not reported. Since mesoderm cells intercalate in a planar-polarized fashion, does the mesoderm tissue concomitantly extend while folding? To measure tissue extension we imaged the embryo using confocal multiview light-sheet microscopy (de Medeiros et al., 2015; Krzic et al., 2012), numerically reconstructed the embryo in 4D with isotropic spatial resolution and digitally sectioned the embryo along its mid-sagittal view (Figure 3C, see supplemental information). Our analysis shows that the mesoderm tissue, after reducing in length because of apical constriction, elongates along the AP axis (Figure 3C; Video S4). We then compared tissue extension in wild type and in either AP or DV mutated conditions by measuring the extension of the anterior mesoderm half that is devoid of any contribution from the posterior midgut movement (Figures S3C–S3G and supplemental information). Tissue extension scaled with cell intercalation for both ectoderm and mesoderm in all genetic backgrounds with the remarkable exception of the mesoderm in *bnt*− embryos (Figures 3A, 3D, and 3E). *bnt*− embryos present a paradoxical phenotype: the mesoderm tissue does not extend despite highly polarized cell intercalation density. To better understand why the mesoderm in *bnt*− embryos fails to extend, we monitored mesoderm cell intercalation in *bnt*− embryos over time. Wild-type mesoderm cells are organized in a regular lattice after a T1 transition, whereas in *bnt*− embryos these cells intercalate by swapping position in an aberrant fashion: opposing cells present small and large surface areas along the AP and DV axes, respectively, resulting in a quartet of cells in a bowtie-like conformation (bowtie-T1, Figures 3F and S3J). Stochastic cell surface areas in *bnt*− mesoderm cells are mirrored by a more scattered distribution of MyoII which is no longer strongly planar polarized (Figure 3G to compare with Figure 2F). In wild-type embryos, AP polarized tension contributes to cell intercalation in the mesoderm (Figure S2D). In order to test the role of AP tension in bowtie-T1, we performed laser dissections (as previously shown in Figure S2B) in *bnt*− embryos. After downregulating AP tension in a *bnt*− background, the number of cell intercalation strongly drops. One key feature additionally emerges from our laser ablation experiments and analysis: while in wild-type embryos the first phase of intercalation is preserved (i.e., side shortening, Figure S2C) and not the second (i.e., side extension, Figure S2D), in *bnt*− embryos both side shortening and extension are impaired (Figure S3I). This shows that AP tension plays a key role (1) in side extension but not side shortening during T1 and (2) in both side shortening and extension during bowtie-T1. Overall, this shows that the T1 and the bowtie-T1 processes are fundamentally different.

Remarkably, in *bnt*− embryos not only tissue extension is abolished but also convergence is affected as shown by a wider tube size formed by the folded mesoderm as previously reported (Figure S3H) (Brodland et al., 2010). While DV patterning controls cell intercalation density, AP patterning ensures planar cell polarized distribution of MyoII and regular T1 transitions. Finally, the synergy between AP and DV patterning controls simultaneous folding and convergence-extension.

Two-tier adherens junctions are established in mesoderm cells

Intercalation in a simple epithelium is a cell topological transformation that relies on the process of junction remodeling. A necessary pre-requisite for cells to undergo intercalation is thus to adhere to one another (i.e., to establish contact junctions) (Rauzi, 2020). In the *Drosophila* blastoderm epithelium, adherens junctions are established at a subapical cell zone (a few microns from the surface) (Harris and Peifer, 2004). In the mesoderm tissue, junctions are eventually relocated from a subapical region to the very apical cellular region during furrow formation (Kölsch et al., 2007). Nevertheless, cell intercalation in mesoderm cells is not initiated apically but laterally ~10 μm from the apical side (Figures 1C–1E) where no junctions have previously been reported.

(C) Temporal sequence of mesoderm contraction (red arrowheads) and extension (green arrowheads). Scale bar, 50 μm. Representative plot showing mesoderm extension during gastrulation (right).
(D) Tissue extension ratio of mesoderm and ectoderm tissues for wild type (WT), *sna*−*twi*− double mutant and *bicoid nanos toso-like* (*bnt*–) triple mutant embryos. n = 3 embryos for wt and *sna-twi*– and 5 embryos for *bnt*– mutants. p value < 0.001 (***). Error bars represent standard deviation.
(E) Cell intercalation density and tissue extension ratio correlation analysis. Groups A and A′ have tissue extension ratio scaling to cell intercalation density. Group B indicate an outlier with non-correlating cell intercalation density and tissue extension ratio.
(F) Temporal sequence of a cell intercalation event in wild type and *bnt*− mesoderm. *bnt*− mesoderm cells show bowtie-like intercalations. Scale bar, 5 μm.
(G) Lateral MyoII distribution at 10 μm from the apical cortex in *bnt*− mesoderm cells. Scale bar, 30 μm. Angular distribution of MyoII in *bnt*− mesoderm cells (bottom). n = 50 intercalations, 3 embryos.
See also Figure S3.

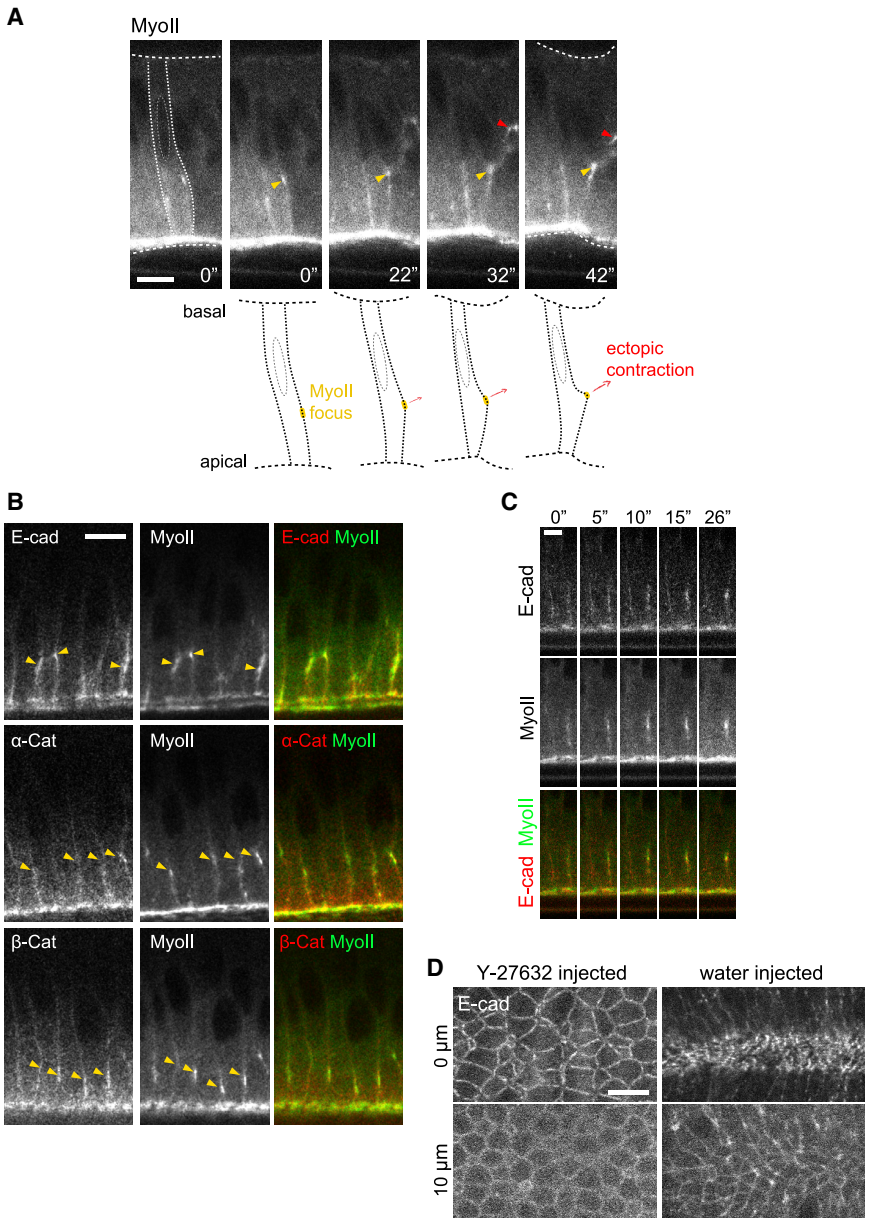

Figure 4. Mesoderm cells establish a second junctional tier at the lateral cortex during invagination

(A) Ectopic MyoII contraction (red arrowhead) bends the mesoderm cell lateral side by pulling on the MyoII focus (yellow arrowhead). Ectopic MyoII contraction also drives apical and basal bending (white-dotted line). A schematic representation is shown in the bottom panel.

(B) Lateral MyoII colocalizes with E-cad (top), α-Cat (middle), and β-Cat (bottom). Scale bar, 10 μm.

(C) Temporal sequence of MyoII and E-cad coalescence in mesoderm cells. Scale bar, 5 μm.

(D) E-cad distribution in mesoderm cells at 0 and 10 μm from the apical surface in Y-27632 and water-injected embryos. Scale bar, 15 μm.

This raises another paradox: how can intercalation take place in the absence of cell-cell contacts? To test the hypothesis that MyoII foci localize at cell-cell adhesion sites, we induced a local ectopic actomyosin contraction (by performing a micro-cavitation bubble using infrared femtosecond-pulsed laser; supplemental information) in a region neighboring a cell MyoII focus. Remarkably, the ectopic contraction bends the lateral cell side specifically at the MyoII focus (Figure 4A). This demonstrates that MyoII foci are localized at cell-cell lateral contacts. To test the possibility that these new contacts are adherens junctions, we imaged embryos expressing endogenous E-cadherin (E-cad), α-catenin, and β-catenin. Remarkably, MyoII foci colocalize with all these key adherens junction factors (Figure 4B). We then monitored MyoII and E-cad jointly over time: concomitantly to MyoII speckles coalescence, E-cad puncta condense eventually forming adhesion spots (Figure 4C). This phenomenon is similar to what has been reported in a previous study supporting the idea that actomyosin contraction drives focusing of E-cad forming spot adheres junctions at the apical region of mesoderm cells (Weng and Wieschaus, 2016). To test if actomyosin coalescence drive E-cad puncta formation, we injected the ROCK inhibitor Y-27632 to downregulate MyoII phosphorylation. In Y-27632-treated embryos, E-cad clusterizes apically but no E-cad puncta form 10 μm inside the tissue whereas, in water-injected control embryos, E-cad planar-polarized puncta form 10 μm inside the tissue (Figure 4D). Finally, two-tier cell adherens junctions (apically and laterally located) are established in the mesoderm tissue during simultaneous folding and extension.

Cell apical-basal tension facilitates mesoderm folding and not cell delamination

MyoII is strongly enriched ~10 μm from the cell apex where it eventually coalesces and forms MyoII foci (Figures 2A and 2E). Nevertheless, when imaging mesoderm cells by integrating the fluorescence signal for longer time periods (i.e., increasing S/N), MyoII appears also at lower levels decorating extensively the lateral cortex (Figure 5A). MyoII along the lateral side of cells was predicted to drive tension facilitating tissue bending during mesoderm folding (Brodland et al., 2010). In a recent study, scientists have tried to probe lateral tension in mesoderm cells during ventral folding by implementing green nanosecond pulsed laser ablation (Gracia et al., 2019), a technique that lacks spatial specificity (given the high energy of ns green pulses compared with infrared femtosecond pulses, for instance) and that is thus inappropriate for selective dissection inside the tissue (Rauzi and Lenne, 2011). To test lateral tension in mesoderm cells, we implemented infrared femtosecond (IR fs) pulsed laser ablation

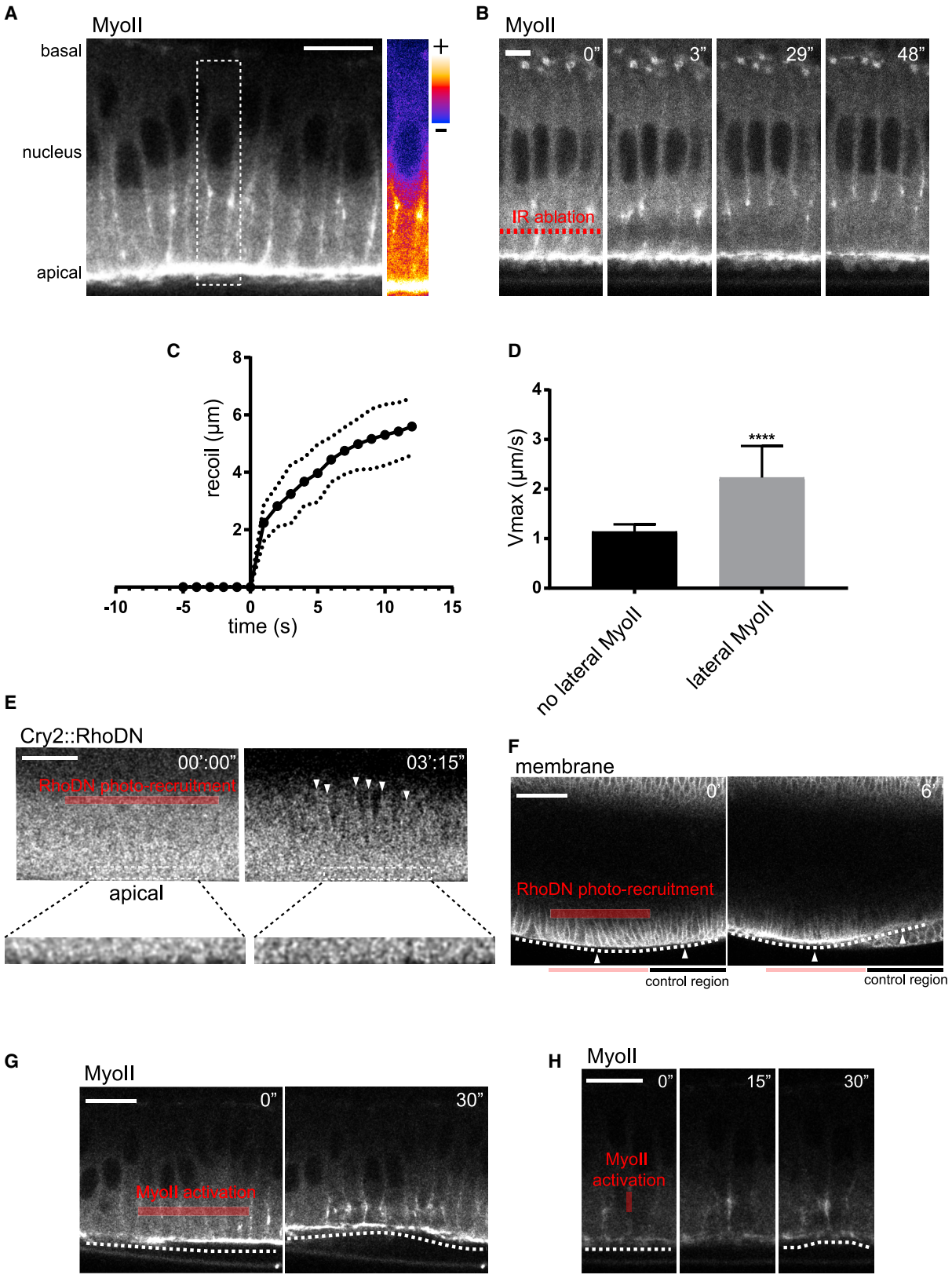

(legend on next page)

(which enables actomyosin dissection by preserving the cell membrane [Rauzi and Lenne, 2015] and is thus suitable for selective in-deep tissue surgery) to dissect the lateral cortex. After ablation, the lateral actomyosin cortex recoils away from the ablated region revealing local lateral tension (Figure 5B). We compared lateral tension before and during lateral MyoII recruitment by measuring the initial maximal recoil velocity of the actomyosin network (Figure 5C). Tension increased by a factor of two during MyoII lateral recruitment (Figure 5D). We wondered if lateral tension, driven by the lateral actomyosin cortex, could facilitate tissue bending as predicted for mesoderm folding by theoretical models (Brodland et al., 2010) and for other epithelia (Sui et al., 2018). To test this, laser dissection is an inappropriate technique since it can be spatially and temporally specific (if correctly implemented) but not protein specific. We therefore implemented two-photon IR fs optogenetics, which allows for protein distribution to be controlled in a spatial, temporal and protein specific fashion (Guglielmi and De Renzis, 2017). To downregulate lateral MyoII contractility we implemented RhoDN optogenetics and performed photo-activation in a region away from the apical zone (Figure 5E and supplemental information). The activated portion of the mesoderm failed to properly internalize compared with the control portion (Figure 5F). To further test the role of lateral tension, we implemented two-photon optogenetics this time to upregulate MyoII contractility along the lateral side (supplemental information) (Izquierdo et al., 2018). After activation, tension is increased bending the tissue locally (Figures 5G and 5H; Video S5). This demonstrates that MyoII-driven lateral tension facilitates mesoderm tissue bending.

Mesoderm morphogenesis during early *Drosophila* embryo gastrulation is a process that has been intensively studied over the last 30 years. Specialists in the field have shown that the mesoderm cells undergo two consecutive phases: (1) a first phase when cells change shape from columnar to wedged while maintaining cell-cell apical contacts and bending the tissue that becomes tube shaped and (2) a second phase when cells undergo epithelial to mesenchymal transition (EMT) resulting in the collapse of the tubular structure (Leptin, 2005). While Snail is known to play a key role in dismantling junctions to favor EMT (second phase) (Barrallo-Gimeno and Nieto, 2005), during tissue folding, junctions are rescued by apical actomyosin contractility, thus maintaining the integrity of the simple epithelium (first phase) (Weng and Wieschaus, 2016). Nevertheless, a recent study has speculated that mesoderm cells undergo delamination during the folding phase (Gracia et al., 2019) (first phase). To test delamination during folding, we imaged *klar-sicht*-deficient embryos (*klar*−) that do not show gastrulation defects and show enhanced transparency (because of lipid droplet clearance from the cytoplasmic region; Welte et al., 1998). *klar*− embryos are thus suited for in-deep tissue imaging. We imaged *klar*− embryos using confocal MuViSPIM light-sheet microscopy (providing *in toto* imaging of the embryo with a 200-nm resolution) and analyzed, in 3D, the apical position of mesoderm cells forming the doming region of the fold. All cells extended their apical side, reaching the furrow in a flower-like configuration (Figure S4A). This evidence rules out the possibility that cells undergo extrusion during folding and confirms the already well documented notion that cells maintain mesoderm tissue integrity during the first phase. In the *Drosophila* leg disc, cytoplasmic actomyosin cables, traveling apical to basal, have been proposed to induce apical-basal tension to drive cell extrusion (Monier et al., 2015). One major difference between the leg disc tissue and the prospective mesoderm is that mesoderm cells accumulate large amounts of apical MyoII throughout the tissue, which focuses and eventually reinforces apical adherens junctions (Weng and Wieschaus, 2016). Lateral tension in mesoderm cells during apical MyoII accumulation drives tissue bending (Figure 5H). We wondered if lateral tension would bend the tissue also in absence of apical MyoII. To test this, we implemented two-photon optogenetics to upregulate MyoII contractility along the lateral side of mesoderm cells prior to apical MyoII recruitment. Remarkably, the tissue did not bend and the activated cell initiated delamination (Figure S4B). This shows that lateral and apical tension work in tandem to drive tissue bending and not cell delamination.

Two-tier junction formation is under the control of Snail and sequential RhoGEF2 localization

What are the upstream factors controlling two-tier junction formation? Two-tier MyoII is established at the embryo ventral region (where the prospective mesodermal tissue is located) and not on the lateral and dorsal sides (Figure 6A). In addition, two-tier MyoII arrests posteriorly in a region where mesoderm and the posterior endoderm meet (Figure 6B). The two-tier MyoII distribution is thus restricted to a zone where Snail is known to be also restricted to (Figure 1B, red arrowhead) (Leptin, 1991). To test the possibility that two-tier MyoII is under the control of Snail, we imaged MyoII distribution in mutated embryos lacking the *snail* gene (*sna*−). In *sna*− embryos MyoII was no longer organized in two-tiers but exhibited the typical subapical distribution that is commonly reported in epithelial tissues (Figure 6C). To test if Snail is sufficient to control two-tier MyoII formation we imaged embryos in which Snail is ectopically produced also in the lateral ectoderm (i.e., where *snail* is normally repressed by Serpin (Ligoxygakis et al., 2003)) and monitored MyoII distribution. Under these conditions, MyoII two-tier distribution now

Figure 5. Cortical-lateral MyoII induces apical-basal tension facilitating mesoderm folding

(A) MyoII localization: MyoII accumulates forming foci (yellow, see fire LUT inset) at ~10 μm from the apical side and decorates at lower levels (orange, see fire LUT inset) the lateral cortex. Scale bar, 15 μm.

(B) IR fs laser ablation (red dashed line) of the lateral actomyosin cortex. Scale bar, 5 μm.

(C) MyoII recoil after laser dissection (time resolution 1 s). n = 10 cells, 10 embryos.

(D) Initial maximum recoil velocity before and after lateral MyoII recruitment. n = 10 cells, 10 embryos. p value < 0.0001 (****). Error bars represent error mean.

(E) Rho dominant negative (RhoDN) targeted photo-recruitment shows apical-basal spatial specificity. Red bar denotes the photo-activated region. RhoDN is only and specifically recruited to the region of activation (white arrowheads).

(F) RhoDN lateral photo-recruitment impairs mesoderm internalization along the photo-activated region. Scale bar, 50 μm.

(G and H) MyoII lateral activation causes apico-basal tissue bending. Red bar denotes the photo-activated region. Scale bar, 10 μm.

See also Figure S4.

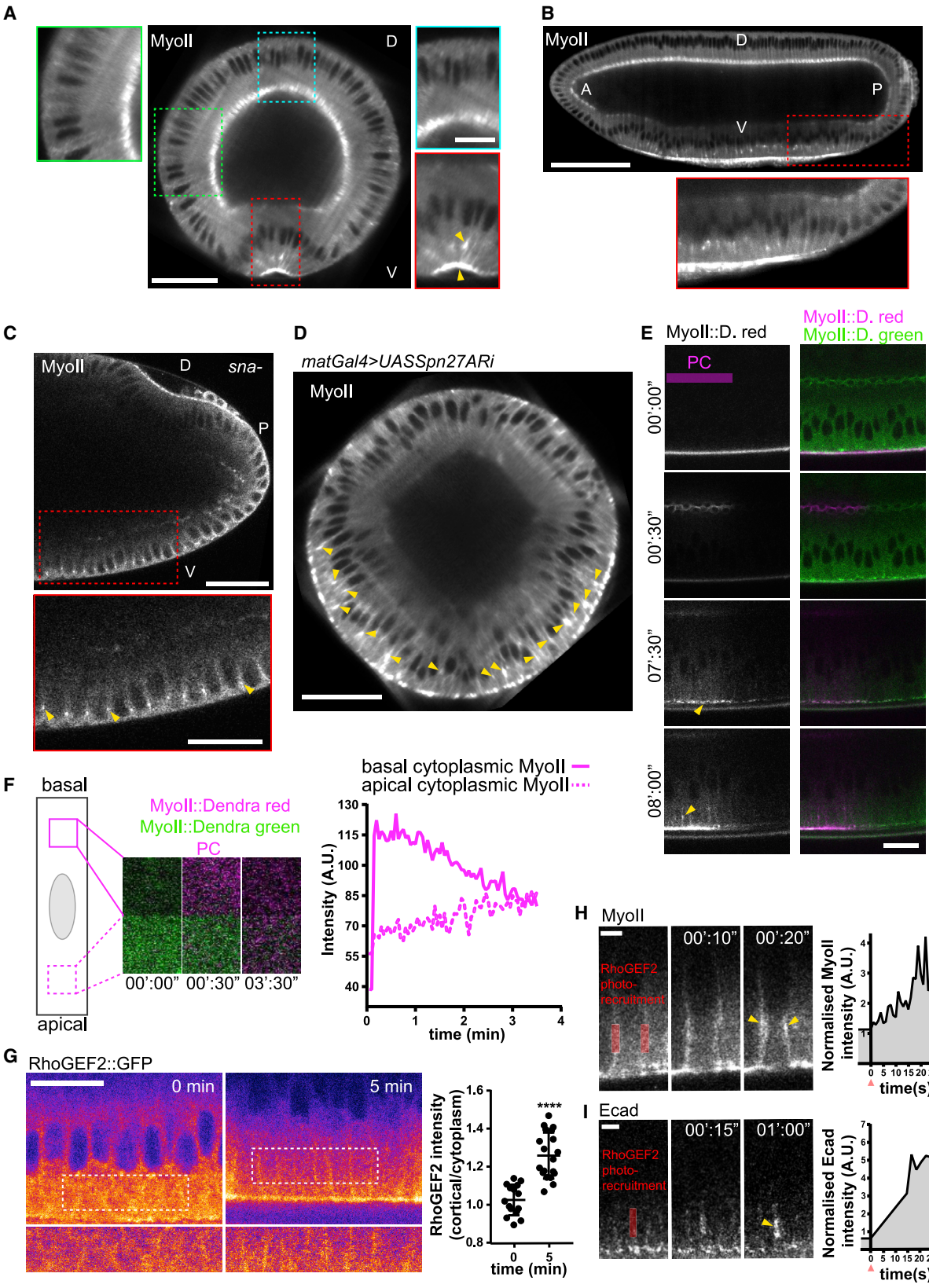

(legend on next page)

extends over the ectoderm beyond the mesodermal region (Figure 6D). This shows that Snail is necessary and sufficient to control two-tier MyoII formation.

Where does the lateral MyoII accumulation originate from? A previous study hypothesized that apical MyoII accumulation originates from the basal MyoII pool formed during cellularization (Dawes-Hoang et al., 2005). One possibility is that both apical and lateral MyoII accumulations may originate from the same basal MyoII pool. To test this hypothesis, we used a photo-convertible MyoII construct (MyoII Dendra, shifting the emission wavelength from green to red upon UV-induced photo-activation; Baker et al., 2010; Pinheiro et al., 2017) and photo-converted the basal MyoII pool at the onset of mesoderm folding. After several minutes, the basal photo-converted MyoII appears first at the apical side and eventually at the lateral side of mesoderm cells (Figure 6E). This demonstrates that the basal MyoII pool acts as a reservoir for apical and lateral MyoII accumulation. How is MyoII redistributed apically and laterally from the basal side? A process invoking targeted delivery of MyoII from the basal side prior to the apical and then to the lateral side could potentially take place. By monitoring cytoplasmic MyoII during the basal to apical MyoII shift, we could observe MyoII diffusing from basal to apical ultimately filling the entire cell (Figure 6F; Video S6). This evidence speaks against a MyoII targeting mechanism while favors the possibility that, thanks to MyoII-free diffusion, MyoII is available everywhere in the cell at the onset of mesoderm folding. Nevertheless, MyoII release from the cell basal side and free diffusion still do not explain the temporal succession of events where MyoII accumulates before apically and then laterally with a time delay of ~5 min (Figure 2B). If MyoII-free diffusion was the sole mechanism responsible for the temporal sequence of events, MyoII would accumulate before laterally and then apically since the lateral region is closer to the basal diffusion source. MyoII can bind to and accumulate at the cell actin cortex only if the regulatory light chain is phosphorylated. Since MyoII location inside the cell per se cannot explain the sequence of MyoII accumulation events, we further explored the possibility that MyoII is phosphorylated first apically and then laterally. RhoGEF2, downstream of the Snail pathway, is a key guanine nucleotide exchange factor that activates RhoA activity in mesoderm cells during fold formation (Kölsch et al., 2007). RhoGEF2 downregulation hampers apical MyoII activation, apical constriction and mesoderm invagination (Barrett et al., 1997; Dawes-Hoang et al., 2005; Fox and Peifer, 2007; Häcker and Perrimon, 1998; Padash Barmchi et al., 2005). We thus monitored with high spatial and temporal specificity the distribution of RhoGEF2 during two-tier junction formation. RhoGEF2 first accumulates at the apical cortex and eventually to the lateral cortex of mesoderm cells (Figure 6G). The necessity of RhoGEF2 in activating MyoII in mesoderm cells has been shown in previous work (Dawes-Hoang et al., 2005), nevertheless we wondered if RhoGEF2 is sufficient to form lateral MyoII foci and consequently E-cad spots that would eventually lead to the formation of ad hoc spot adherens junctions. To test this hypothesis, we used an optogenetic construct that allows to recruit RhoGEF2 at any region of a cell with spatial and temporal specificity by using IR fs pulsed laser (Izquierdo et al., 2018). After lateral targeted photo-activation, both MyoII and E-cad accumulate at the lateral region (Figures 6H and 6I). This shows that RhoGEF2 controls the formation of ad hoc adherens junctions. Thus, under the control of the Snail pathway, two-tier adherens junctions are formed by the sequential cortical recruitment of RhoGEF2.

DISCUSSION

While much work has been undertaken to uncover the mechanisms driving specific tissue morphogenetic changes, how composite morphogenetic processes, resulting from multiple simultaneous transformations, are controlled and driven remains elusive. In this study, we focus on the process of simultaneous tissue folding and extension that plays a pivotal role during embryo gastrulation and neurulation (Keller, 2002; Nielsen et al., 2020; Nishimura et al., 2012). We report that during early *Drosophila* gastrulation, the prospective mesoderm tissue converges and extends while folding. This composite process is driven by epithelial cells establishing two distinct sets of adherens junctions along the cell apical-basal axis. While the constituents of the two sets of junctions are the same, the function, the configuration, and the origin differ between the two. While the first junctional tier (located apically) mediates apical constriction initiating tissue bending, the second tier (located laterally at ~10 μm from the apical side) simultaneously mediates cell intercalation in a planar-polarized fashion driving tissue convergence-extension. The share of labor between the two sets of junctions results in the formation of a tubular epithelium extending along the AP axis while narrowing along its cross-section. Apical junctions in mesoderm cells are established during

Figure 6. Two-tier MyoII is under the control of Snail and of RhoGEF2 spatial-temporal localization

(A) Distribution of MyoII along the embryo cross-section during gastrulation onset. Scale bar, 50 μm. Close-up view of the mesoderm (red inset with apical and lateral MyoII tiers marked by arrowheads), of the lateral ectoderm (green inset) and the dorsal tissue (blue inset). Scale bar, 20 μm.

(B) Distribution of MyoII along the embryo mid-sagittal section during gastrulation onset. Scale bar, 50 μm. Close-up view of the posterior mesoderm (inset).

(C) Distribution of MyoII along the posterior mid-sagittal section of a *sna*– embryo during gastrulation onset. Scale bar, 50 μm. Close-up view showing MyoII organized in a single subapical tier (yellow arrowheads). Scale bar, 30 μm.

(D) MyoII distribution in an embryo expressing *spn27A* RNAi resulting in *snail* ectopic expression in the lateral tissues. MyoII second tier is marked by arrowheads. Scale bar, 50 μm.

(E) Temporal sequence showing photo-conversion (PC, magenta) of the basal Dendra-labeled MyoII. Dendra-labeled MyoII localizes before apically and eventually laterally (arrowheads). Scale bar, 20 μm.

(F) Photo-converted MyoII diffusion from the cell basal to the apical region.

(G) RhoGEF2 distribution at the onset of apical constriction and after a 5-min time period. Ratio between cortical-lateral RhoGEF2 versus cytoplasmic RhoGEF2 is plotted on y axis. Scale bar, 20 μm. n = 15 cells, 3 embryos. p value < 0.0001 (****).

(H and I) Temporal sequence showing MyoII (H) and E-cad (I) enrichment after targeted photo-recruitment of optoRhoGEF2. Red bars and red arrowheads denote the region and the time of photo-activation, respectively. Scale bar, 5 μm.

cellularization under the control of Par3 (a central component of the cell apical-basal polarity; Harris and Peifer, 2004). At the onset of tissue folding, these junctions eventually focus and translocate from a cell subapical to an apical position (Kölsch et al., 2007; Weng and Wieschaus, 2016). Apical junctions mediate medial-apical actomyosin anchorage, resulting in mesoderm cell apical constriction (Martin et al., 2009) and forming a supracellular actomyosin network that generates polarized tissue-scale forces (Martin et al., 2010). Lateral junctions are instead established during mesoderm folding (a morphogenetic phase in which Par3 is downregulated; Weng and Wieschaus, 2017). Not relying on apical-basal polarity, lateral junctions are formed 'on the fly' by the local coordinated coalescence of the lateral actomyosin network at the interface between two neighboring cells. Cortical cytoskeleton coalescence drives clustering of E-cadherin proteins and eventual formation of ad hoc lateral adherens junctions. We show that MyoII two-tier distribution is under the control of Snail. In addition, we show that lateral actomyosin enrichment and junction planar cell polarized formation is under the control of the AP patterning, setting the stage for mesoderm convergence-extension.

Intercalation in the mesoderm and in the ectoderm, while seemingly similar, show striking differences when compared with each other. In both ectoderm and mesoderm, the cortical distribution of MyoII is planar polarized under the control of the AP patterning (Bertet et al., 2004; Zallen and Wieschaus, 2004). Nevertheless, in the ectoderm the actomyosin cortex generates contractile forces remodeling pre-existing adherens junctions (Harris and Peifer, 2004), whereas in the mesoderm lateral actomyosin contractions cluster E-cadherin concomitantly forming and remodeling *de novo* adherens junctions. In the ectoderm, cell intercalation results from the interplay between the junctional and the medial-apical actomyosin networks for both vertical (parallel to the DV axis) junction shrinking (Rauzi et al., 2010) and new (parallel to the AP axis) junction extension (Collinet et al., 2015). In the mesoderm, in absence of a medial network, cortical actomyosin seems to suffice to initiate junction shrinkage. This could be explained by the fact that (1) in the mesoderm adherens junctions are laterally established along shrinking sides and not along the other cell sides that elongate (Vanderleest et al., 2018) opposing less resistance or (2) cells in the mesoderm reduce their apical size, therefore the junctional length to be remodeled eventually becomes shorter which requires less mechanical energy. While new junction extension results from medial actomyosin pulses pulling on a 4-way vertex (Collinet et al., 2015; Yu and Fernandez-Gonzalez, 2016), in the mesoderm polarized tissue-scale forces play a key role to resolve cell intercalation. Intercalation is under the control of the AP patterning in the ectoderm, while in the mesoderm it is under a nested control: the AP patterning insures regular and polarized topological transitions, while the DV patterning imposes a dual control by (1) boosting T1 transitions and (2) providing the mechanical boundary conditions to insure planar cell polarized intercalations in a timely fashion. Intercalation boosting in the mesoderm may be driven by high variance of lateral-cortical MyoII (Curran et al., 2017) while intercalation is polarized by anisotropic mechanical tension at the tissue scale, facilitating new junction extension. Mechanical polarity at the tissue scale could provide a redundant mechanism to insure intercalation polarity even in the absence of the AP genetic control. In the absence of AP patterning, cells undergo bowtie intercalation without driving tissue elongation. This corroborates the notion that aberrant polarized cell intercalation can occur without tissue extension (Collinet et al., 2015; Yin et al., 2008). Regular planar cell polarized intercalation (resulting in the mesoderm from the synergy between AP and DV patterning) ensures efficient tissue extension during mesoderm folding.

Dp114RhoGEF is a key guanine exchange factor that activates the Rho1 pathway for planar cell intercalation in the ectoderm (Garcia De Las Bayonas et al., 2019), in contrast to the mesoderm where RhoGEF2 is the key signaling GEF for both apical constriction (Barrett et al., 1997; Dawes-Hoang et al., 2005; Fox and Peifer, 2007; Häcker and Perrimon, 1998; Padash Barmchi et al., 2005) and cell intercalation. RhoGEF2 localization is sequential: it is recruited apically and then laterally, sequentially activating apical and lateral MyoII during nuclear apical-basal displacement. Microtubule networks play a key role during mesoderm invagination and are capable of transporting RhoGEF2 via the EB1 protein (Garcia De Las Bayonas et al., 2019; Ko et al., 2019; Rogers et al., 2004). In the future it will be important to further investigate the role of nuclear displacement and MT networks in the formation of two-tier adherens junctions.

What are the upstream signals responsible for planar cell polarized MyoII? Previous studies in the ectoderm have ruled out canonical signaling factors (e.g., Frizzled; Zallen and Wieschaus, 2004) and unveiled new signaling components expressed in stripes responsible for MyoII PCP (e.g., Toll and Tartan Ten-m receptors Paré et al., 2019, 2014). Remarkably in *twi*− embryos, Snail also forms an AP stripy pattern (Ip et al., 1994; Stathopoulos and Levine, 2002; Stathopoulos et al., 2002). Future work is now necessary to uncover the signaling pathway controlling MyoII PCP in the mesoderm.

While AP and DV gene patterning have been studied and interpreted as sources of orthogonal signals (Huang et al., 1997; Irvine and Wieschaus, 1994; Leptin, 1991; Roth, 1993) eventually controlling separated features of a system, this study shows for the first time how these signaling sources can cross-talk and act synergistically to control morphogenesis during embryo development. Future work is now necessary to further explore the interplay between these fundamental signaling sources.

STAR★METHODS

Detailed methods are provided in the online version of this paper and include the following:

- KEY RESOURCES TABLE
- RESOURCE AVAILABILITY
  - Lead contact
  - Materials availability
  - Data and code availability
- EXPERIMENTAL MODEL AND SUBJECT DETAILS
  - Mutants and fly stocks
- METHOD DETAILS
  - Time-lapse imaging
  - *In toto* 4-D imaging, digital reconstruction and data processing
  - Drug injections

- Dendra photoconversion
- Cry2 optorecruitment
- Actomyosin laser ablation
- Ectopic contraction
- Recoil velocity measurement

- QUANTIFICATION AND STATISTICAL ANALYSIS
  - 4D cell and surface contact segmentation and rendering
  - Cell intercalation density measurement
  - Cell intercalation propagation along apical-basal axis
  - Mesoderm extension measurement
  - Invaginated mesoderm width measurement
  - Mesoderm cell extrusion analysis
  - Intensity measurements
  - Statistics
  - Limitations of the study

SUPPLEMENTAL INFORMATION

Supplemental information can be found online at https://doi.org/10.1016/j.devcel.2021.04.003.

ACKNOWLEDGMENTS

We thank S. De Renzis, E. Wieschaus, S. Streichen, T. Lecuit, and Y. Bellaiche for providing fly stocks; F. Besse, Y. Bellaiche, and all members of the Rauzi lab for critical reading of the manuscript; B. Delorme for developing ImageJ tools for image analysis and for helping with 3D cell segmentation; A. Popkova for helping with the optogenetic lines; F. Besse, P. Therond, R. Arkowitz, Y. Bellaiche, S. Roth, V. Saraswathy, K. Pushpalatha and all members of the Rauzi lab for the fruitful discussions; the PRISM imaging facility for technical support. A.J. is supported by the scholarship Région SUD PACA–Enterprise (Bruker Luxendo)-UCA. This work was supported by the French Government through the UCAJEDI Investments for the Future project managed by the National Research Agency (ANR-15-IDEX-01), the Investments for the Future Labex SIGNALIFE (ANR-11-LABX-0028-01), the Tramplin-ERC program of the National Research Agency (ANR-16-TERC-0018-01), the ATIP-Avenir program of the CNRS and the Human Frontier Science Program (CDA00027/2017-C).

AUTHOR CONTRIBUTIONS

A.J. and M.R. planned the experiments. A.J. performed the experiments. M.R. performed initial preliminary experiments. A.J. performed data processing and quantifications. A.J. and M.R. analyzed the data. M.R. and A.J. wrote the manuscript.

DECLARATION OF INTERESTS

The authors declare no competing interests.

Received: November 13, 2020
Revised: February 18, 2021
Accepted: March 31, 2021
Published: April 22, 2021

REFERENCES

Baker, S.M., Buckheit, R.W., 3rd, and Falk, M.M. (2010). Green-to-red photoconvertible fluorescent proteins: tracking cell and protein dynamics on standard wide-field mercury arc-based microscopes. BMC Cell Biol *11*, 15.

Barrallo-Gimeno, A., and Nieto, M.A. (2005). The Snail genes as inducers of cell movement and survival: implications in development and cancer. Development *132*, 3151–3161.

Barrett, K., Leptin, M., and Settleman, J. (1997). The Rho GTPase and a putative RhoGEF mediate a signaling pathway for the cell shape changes in Drosophila gastrulation. Cell *91*, 905–915.

Basson, M.A. (2012). Signaling in cell differentiation and morphogenesis. Cold Spring Harb. Perspect. Biol. *4*, a008151.

Bertet, C., Sulak, L., and Lecuit, T. (2004). Myosin-dependent junction remodelling controls planar cell intercalation and axis elongation. Nature *429*, 667–671.

Blankenship, J.T., Backovic, S.T., Sanny, J.S., Weitz, O., and Zallen, J.A. (2006). Multicellular rosette formation links planar cell polarity to tissue morphogenesis. Dev. Cell *11*, 459–470.

Brodland, G.W., Conte, V., Cranston, P.G., Veldhuis, J., Narasimhan, S., Hutson, M.S., Jacinto, A., Ulrich, F., Baum, B., and Miodownik, M. (2010). Video force microscopy reveals the mechanics of ventral furrow invagination in Drosophila. Proc. Natl. Acad. Sci. USA *107*, 22111–22116.

Collinet, C., Rauzi, M., Lenne, P.F., and Lecuit, T. (2015). Local and tissue-scale forces drive oriented junction growth during tissue extension. Nat. Cell Biol. *17*, 1247–1258.

Curran, S., Strandkvist, C., Bathmann, J., de Gennes, M., Kabla, A., Salbreux, G., and Baum, B. (2017). Myosin II controls junction fluctuations to guide epithelial tissue ordering. Dev. Cell *43*, 480–492.e6.

Dawes-Hoang, R.E., Parmar, K.M., Christiansen, A.E., Phelps, C.B., Brand, A.H., and Wieschaus, E.F. (2005). folded gastrulation, cell shape change and the control of myosin localization. Development *132*, 4165–4178.

de Medeiros, G., Norlin, N., Gunther, S., Albert, M., Panavaite, L., Fiuza, U.M., Peri, F., Hiiragi, T., Krzic, U., and Hufnagel, L. (2015). Confocal multiview light-sheet microscopy. Nat. Commun. *6*, 8881.

Fernandez-Gonzalez, R., Simoes, Sde M., Röper, J.C., Eaton, S., and Zallen, J.A. (2009). Myosin II dynamics are regulated by tension in intercalating cells. Dev. Cell *17*, 736–743.

Fox, D.T., and Peifer, M. (2007). Abelson kinase (Abl) and RhoGEF2 regulate actin organization during cell constriction in Drosophila. Development *134*, 567–578.

Garcia De Las Bayonas, A., Philippe, J.M., Lellouch, A.C., and Lecuit, T. (2019). Distinct RhoGEFs activate apical and junctional contractility under control of G proteins during epithelial morphogenesis. Curr. Biol. *29*, 3370–3385.e7.

Gelbart, M.A., He, B., Martin, A.C., Thiberge, S.Y., Wieschaus, E.F., and Kaschube, M. (2012). Volume conservation principle involved in cell lengthening and nucleus movement during tissue morphogenesis. Proc. Natl. Acad. Sci. USA *109*, 19298–19303.

Gilmour, D., Rembold, M., and Leptin, M. (2017). From morphogen to morphogenesis and back. Nature *541*, 311–320.

Gómez-Gálvez, P., Vicente-Munuera, P., Tagua, A., Forja, C., Castro, A.M., Letrán, M., Valencia-Expósito, A., Grima, C., Bermúdez-Gallardo, M., Serrano-Pérez-Higueras, Ó., et al. (2018). Scutoids are a geometrical solution to three-dimensional packing of epithelia. Nat. Commun. *9*, 2960.

Gracia, M., Theis, S., Proag, A., Gay, G., Benassayag, C., and Suzanne, M. (2019). Mechanical impact of epithelial-mesenchymal transition on epithelial morphogenesis in Drosophila. Nat. Commun. *10*, 2951.

Guglielmi, G., and De Renzis, S. (2017). Optogenetic inhibition of apical constriction during Drosophila embryonic development. Methods Cell Biol *139*, 167–186.

Guignard, L., Fiúza, U.M., Leggio, B., Laussu, J., Faure, E., Michelin, G., Biasuz, K., Hufnagel, L., Malandain, G., Godin, C., and Lemaire, P. (2020). Contact area-dependent cell communication and the morphological invariance of ascidian embryogenesis. Science *369*, eaar5663.

Häcker, U., and Perrimon, N. (1998). DRhoGEF2 encodes a member of the Dbl family of oncogenes and controls cell shape changes during gastrulation in Drosophila. Genes Dev *12*, 274–284.

Harris, T.J., and Peifer, M. (2004). Adherens junction-dependent and -independent steps in the establishment of epithelial cell polarity in Drosophila. J. Cell Biol. *167*, 135–147.

Huang, A.M., Rusch, J., and Levine, M. (1997). An anteroposterior dorsal gradient in the Drosophila embryo. Genes Dev *11*, 1963–1973.

Ip, Y.T., Maggert, K., and Levine, M. (1994). Uncoupling gastrulation and mesoderm differentiation in the Drosophila embryo. EMBO J *13*, 5826–5834.

Irvine, K.D., and Wieschaus, E. (1994). Cell intercalation during Drosophila germband extension and its regulation by pair-rule segmentation genes. Development *120*, 827–841.

Izquierdo, E., Quinkler, T., and De Renzis, S. (2018). Guided morphogenesis through optogenetic activation of Rho signalling during early Drosophila embryogenesis. Nat. Commun. *9*, 2366.

Jülicher, F., and Eaton, S. (2017). Emergence of tissue shape changes from collective cell behaviours. Semin. Cell Dev. Biol. *67*, 103–112.

Keller, R. (2002). Shaping the vertebrate body plan by polarized embryonic cell movements. Science *298*, 1950–1954.

Keller, R., Davidson, L., Edlund, A., Elul, T., Ezin, M., Shook, D., and Skoglund, P. (2000). Mechanisms of convergence and extension by cell intercalation. Philos. Trans. R. Soc. Lond. B Biol. Sci. *355*, 897–922.

Ko, C.S., Tserunyan, V., and Martin, A.C. (2019). Microtubules promote intercellular contractile force transmission during tissue folding. J. Cell Biol. *218*, 2726–2742.

Kölsch, V., Seher, T., Fernandez-Ballester, G.J., Serrano, L., and Leptin, M. (2007). Control of Drosophila gastrulation by apical localization of adherens junctions and RhoGEF2. Science *315*, 384–386.

Krzic, U., Gunther, S., Saunders, T.E., Streichan, S.J., and Hufnagel, L. (2012). Multiview light-sheet microscope for rapid in toto imaging. Nat. Methods *9*, 730–733.

Leptin, M. (1991). Twist and snail as positive and negative regulators during Drosophila mesoderm development. Genes Dev *5*, 1568–1576.

Leptin, M. (2005). Gastrulation movements: the logic and the nuts and bolts. Dev. Cell *8*, 305–320.

Leptin, M., and Grunewald, B. (1990). Cell shape changes during gastrulation in Drosophila. Development *110*, 73–84.

Ligoxygakis, P., Roth, S., and Reichhart, J.M. (2003). A serpin regulates dorsal-ventral axis formation in the Drosophila embryo. Curr. Biol. *13*, 2097–2102.

Martin, A.C., Gelbart, M., Fernandez-Gonzalez, R., Kaschube, M., and Wieschaus, E.F. (2010). Integration of contractile forces during tissue invagination. J. Cell Biol. *188*, 735–749.

Martin, A.C., and Goldstein, B. (2014). Apical constriction: themes and variations on a cellular mechanism driving morphogenesis. Development *141*, 1987–1998.

Martin, A.C., Kaschube, M., and Wieschaus, E.F. (2009). Pulsed contractions of an actin-myosin network drive apical constriction. Nature *457*, 495–499.

McMahon, A., Supatto, W., Fraser, S.E., and Stathopoulos, A. (2008). Dynamic analyses of Drosophila gastrulation provide insights into collective cell migration. Science *322*, 1546–1550.

Monier, B., Gettings, M., Gay, G., Mangeat, T., Schott, S., Guarner, A., and Suzanne, M. (2015). Apico-basal forces exerted by apoptotic cells drive epithelium folding. Nature *518*, 245–248.

Nielsen, B.F., Nissen, S.B., Sneppen, K., Mathiesen, J., and Trusina, A. (2020). Model to link cell shape and polarity with organogenesis. iScience *23*, 100830.

Nishimura, T., Honda, H., and Takeichi, M. (2012). Planar cell polarity links axes of spatial dynamics in neural-tube closure. Cell *149*, 1084–1097.

Nüsslein-Volhard, C., Frohnhöfer, H.G., and Lehmann, R. (1987). Determination of anteroposterior polarity in Drosophila. Science *238*, 1675–1681.

Padash Barmchi, M., Rogers, S., and Häcker, U. (2005). DRhoGEF2 regulates actin organization and contractility in the Drosophila blastoderm embryo. J. Cell Biol. *168*, 575–585.

Paré, A.C., Naik, P., Shi, J., Mirman, Z., Palmquist, K.H., and Zallen, J.A. (2019). An LRR receptor-teneurin system directs planar polarity at compartment boundaries. Dev. Cell *51*, 208–221.e6.

Paré, A.C., Vichas, A., Fincher, C.T., Mirman, Z., Farrell, D.L., Mainieri, A., and Zallen, J.A. (2014). A positional Toll receptor code directs convergent extension in Drosophila. Nature *515*, 523–527.

Pinheiro, D., Hannezo, E., Herszterg, S., Bosveld, F., Gaugue, I., Balakireva, M., Wang, Z., Cristo, I., Rigaud, S.U., Markova, O., and Bellaïche, Y. (2017). Transmission of cytokinesis forces via E-cadherin dilution and actomyosin flows. Nature *545*, 103–107.

Rauzi, M. (2020). Cell intercalation in a simple epithelium. Philos. Trans. R. Soc. Lond. B Biol. Sci. *375*, 20190552.

Rauzi, M., and Lenne, P.F. (2011). Cortical forces in cell shape changes and tissue morphogenesis. Curr. Top. Dev. Biol. *95*, 93–144.

Rauzi, M., and Lenne, P.F. (2015). Probing cell mechanics with subcellular laser dissection of actomyosin networks in the early developing Drosophila embryo. Methods Mol. Biol. *1189*, 209–218.

Rauzi, M., Lenne, P.F., and Lecuit, T. (2010). Planar polarized actomyosin contractile flows control epithelial junction remodelling. Nature *468*, 1110–1114.

Rauzi, M., Verant, P., Lecuit, T., and Lenne, P.F. (2008). Nature and anisotropy of cortical forces orienting Drosophila tissue morphogenesis. Nat. Cell Biol. *10*, 1401–1410.

Rogers, S.L., Wiedemann, U., Häcker, U., Turck, C., and Vale, R.D. (2004). Drosophila RhoGEF2 associates with microtubule plus ends in an EB1-dependent manner. Curr. Biol. *14*, 1827–1833.

Roth, S. (1993). Mechanisms of dorsal-ventral axis determination in Drosophila embryos revealed by cytoplasmic transplantations. Development *117*, 1385–1396.

Solnica-Krezel, L. (2005). Conserved patterns of cell movements during vertebrate gastrulation. Curr. Biol. *15*, R213–R228.

Stathopoulos, A., and Levine, M. (2002). Linear signaling in the Toll-Dorsal pathway of Drosophila: activated Pelle kinase specifies all threshold outputs of gene expression while the bHLH protein twist specifies a subset. Development *129*, 3411–3419.

Stathopoulos, A., Van Drenth, M., Erives, A., Markstein, M., and Levine, M. (2002). Whole-genome analysis of dorsal-ventral patterning in the Drosophila embryo. Cell *111*, 687–701.

Sui, L., Alt, S., Weigert, M., Dye, N., Eaton, S., Jug, F., Myers, E.W., Jülicher, F., Salbreux, G., and Dahmann, C. (2018). Differential lateral and basal tension drive folding of Drosophila wing discs through two distinct mechanisms. Nat. Commun. *9*, 4620.

Vanderleest, T.E., Smits, C.M., Xie, Y., Jewett, C.E., Blankenship, J.T., and Loerke, D. (2018). Vertex sliding drives intercalation by radial coupling of adhesion and actomyosin networks during Drosophila germband extension. eLife *7*, e34586.

Walck-Shannon, E., and Hardin, J. (2014). Cell intercalation from top to bottom. Nat. Rev. Mol. Cell Biol. *15*, 34–48.

Welte, M.A., Gross, S.P., Postner, M., Block, S.M., and Wieschaus, E.F. (1998). Developmental regulation of vesicle transport in Drosophila embryos: forces and kinetics. Cell *92*, 547–557.

Weng, M., and Wieschaus, E. (2016). Myosin-dependent remodeling of adherens junctions protects junctions from Snail-dependent disassembly. J. Cell Biol. *212*, 219–229.

Weng, M., and Wieschaus, E. (2017). Polarity protein Par3/Bazooka follows myosin-dependent junction repositioning. Dev. Biol. *422*, 125–134.

Yin, C., Kiskowski, M., Pouille, P.A., Farge, E., and Solnica-Krezel, L. (2008). Cooperation of polarized cell intercalations drives convergence and extension of presomitic mesoderm during zebrafish gastrulation. J. Cell Biol. *180*, 221–232.

Yu, J.C., and Fernandez-Gonzalez, R. (2016). Local mechanical forces promote polarized junctional assembly and axis elongation in Drosophila. eLife *5*, e10757.

Zallen, J.A., and Wieschaus, E. (2004). Patterned gene expression directs bipolar planar polarity in Drosophila. Dev. Cell *6*, 343–355.

STAR★METHODS

KEY RESOURCES TABLE

REAGENT or RESOURCE	SOURCE	IDENTIFIER
Chemicals, peptides, and recombinant proteins		
ROCK inhibitor: Y-27632 dihydrochloride	TOCRIS, UK	Cat.# 1254
Experimental models: organisms/strains		
Drosophila: Eve::YFP	gift from S. Streichen, UCSB	N/A
Drosophila: Sna::Sgfp	VDRC	318449
Drosophila: UbiGap43 mCherry;;TM6/MKRS	gift from S. de Renzis, EMBL Heidelberg	N/A
Drosophila: Resille GFP	M. Rauzi	Rauzi and Lenne, 2015
Drosophila: w[*]; P{w[+mC]=PTT-GB}gish [Spider]	Bloomington	59025
Drosophila: Sqh::mCherry/CyO; SpiderGFP/TM6	this study	N/A
Drosophila: Spaghetti squash (Sqh)::mCherry (II)	M. Rauzi	Rauzi and Lenne, 2015
Drosophila: Utrophin GFP	M. Rauzi	Rauzi and Lenne, 2015
Drosophila: GFP::ROK[K116A]	gift from T. Lecuit, IBDM	N/A
Drosophila: *w[*]; P{w[+mC]=sqh-sfGFP-RhoGEF2}30*	Bloomington	76260
Drosophila: *Δhalo sna-twi-*/CyO	gift from M. Leptin, EMBL Heidelberg	N/A
Drosophila: *Δhalosna-twi-/CyO, Sqh::GFP*; Gap43mCherry/TM6	this study	N/A
Drosophila: *bnt*/TM3	gift from E. Wieschaus, Princeton	N/A
Drosophila: Resille::GFP, Sqh::mCherry/CyO	M. Rauzi	N/A
Drosophila: Resille::GFP, Sqh::mCherry/ CyO; *bnt*/TM6	this study	N/A
Drosophila: E-Cad::GFP(3x)/CyO	gift from Y. Bellaiche, Institut Curie	N/A
Drosophila: E-Cad::GFP(3x), Sqh::mCherry/CyO	gift from X. Wang, Centre de Biologie Intégrative (CBI)	N/A
Drosophila: y[1] w[*] Mi{PT-GFSTF.1}arm [MI08675-GFSTF.1]	Bloomington	60561
Drosophila: βCat GFP; Sqh::mCherry/CyO	this study	N/A
Drosophila: y[1] w[*]; Mi{PT-GFSTF.0} alpha-Cat[MI02577-GFSTF.0]	Bloomington	59405
Drosophila: Sqh::mCherry/CyO; α-Cat::GFP/TM6	this study	N/A
Drosophila: UbiGap43 mCherry;; *klar-*	this study	N/A
Drosophila: *Δhalo sna-*/CyO, Sqh::GFP	gift from E. Wieschaus, Princeton U.	N/A
Drosophila: *UAS spn27A RNAi*	VDRC	330188
Drosophila: Sqh::mCherry; tub^{mat15} Gal4	this study	N/A
Drosophila: w[*]; M{w[+mC]=UAS-RhoGEF2.shRNA}ZH-86Fb	Bloomington	76255
Drosophila: Sqh::Dendra2/TM6	gift from Y. Bellaiche, Institut Curie	N/A
Drosophila: UASp Cry2::RhoGEF2/CyO; UASp CIBN::pmGFP/ TM3	gift from S. de Renzis, EMBL Heidelberg	N/A

(*Continued on next page*)

Continued

REAGENT or RESOURCE	SOURCE	IDENTIFIER
Drosophila: *pubi*: Gap43::mCherry;; *posk*: Gal4/TM6	gift from S. de Renzis, EMBL Heidelberg	N/A
Drosophila: psqh: Sqh::mCherry; *posk*: Gal4/TM6	gift from S. de Renzis, EMBL Heidelberg	N/A
Drosophila: E-Cad::mKate2 (3X)	gift from Y. Bellaiche, Institut Curie	N/A
Drosophila: E-Cad::mKate2 (3X); *posk*: Gal4/TM6	this study	N/A
Drosophila: UASp CIBN::pmGFP; UASp Cry2::mCherry::Rho1[N19Y189]/TM3, Sb	gift from E. Wieschaus, Princeton U.	N/A
Drosophila: UbiGap43 mCherry; tub^{mat67} Gal4; tub^{mat15} Gal4	this study	N/A
Drosophila: $klar^{-/-}$	gift from E. Wieschaus, Princeton U.	N/A
Software and algorithms		
GraphPad Prism 7	GraphPad	https://www.graphpad.com/
ImageJ		https://imagej.nih.gov/ij/
Matlab	MathWorks	https://www.mathworks.com/products/matlab.html
Imaris	Bitplane	https://imaris.oxinst.com/
ASTEC	Open access	https://github.com/astec-segmentation

RESOURCE AVAILABILITY

Lead contact

Further information and requests for resources should be directed to and will be fulfilled by the Lead Contact, Matteo Rauzi (matteo.rauzi@univ-cotedazur.fr)

Materials availability

Upon request.

Data and code availability

The 4D image analysis code ASTEC (Guignard et al., 2020), used for 4D side contact segmentation and analysis, is open source and available at https://github.com/astec-segmentation.

EXPERIMENTAL MODEL AND SUBJECT DETAILS

Mutants and fly stocks

All stocks and crosses were maintained at room temperature. Even-skipped (Eve) protein expression was monitored using the fly stock Eve::YFP (gift from S. Streichen). For monitoring Snail (Sna) protein expression, fly stock expressing Sna GFP fusion was obtained from VDRC (ID 318449). Fly stocks expressing mCherry fusion to Gap43 (Figures 1C, 3C, 3F, S1, and S3C) or GFP fusion to resille (Figure S3A) or Gilgamesh (Spider) (Figures 2, S2, and S4) were used for labelling membrane. MyoII localization was observed using the fly stock expressing mCherry fusion to *Drosophila* Myosin regulatory light chain (MRLC), Spaghetti squash (Sqh) under the control of *sqh* promoter. F-actin localization was monitored using the fly stock expressing GFP fusion of the F-actin binding protein Utrophin (Utr) under the control of *sqh* promoter. Fly stock expressing GFP fusion of Rok with mutated kinase activity was used as a sensor of Rho activity (gift from T. Lecuit). For RhoGEF2 localization, fly stock expressing GFP fusion of RhoGEF2 under *sqh* promoter was obtained from Bloomington (# 76260). *sna-twi-* zygotic double mutant embryos were obtained from *Δhalo sna-twi-*/CyO mothers. Homozygous *sna-twi-* mutant embryos were selected by looking for the halo mutation, that shows an observable phenotype during yolk clearance. Maternal and zygotic (M/Z) triple mutant embryos for the genes *bicoid*, *nanos* and *torso-like* (*bnt-*) were collected from resille::GFP, Sqh::mCherry/CyO; *bnt-* homozygous mothers (gift from E. Wieschaus). For monitoring the localization of adherence complex proteins, flies expressing GFP fusion to E-Cadherin (E-Cad::GFP(3x)/CyO, gift from Y. Bellaiche), to α-Catenin (Bloomington #59405) and to β-Catenin (Bloomington #60561) were used. For assessing MyoII localization in *sna-* mutant embryos, homozygous embryos labelled by halo mutation were collected from *Δhalo sna-*/CyO, Sqh::GFP (gift from E. Wieschaus) stock. Sna ectopic expression to lateral sides of the embryo is achieved by downregulating *sna* repressor Serpin

Spn27A using shRNA-mediated silencing. *UAS spn27A RNAi* flies were obtained from VDRC (#330188). To achieve ectopic Sna expression, embryos were collected from Sqh::mCherry/*UAS spn27A RNAi*; *tub*^{mat} Gal4/+ mothers.

For photoconversion experiments, fly stock expressing Sqh fused to Dendra2 was used (gift from Y. Bellaiche). For ectopic fold formation and induced junction shrinkage, embryos from $_{p}$*ubi*: Gap43::mCherry/+; *UASp* Cry2::RhoGEF2/+; *UASp* CIBN::pmGFP/$_{p}$*osk* Gal4 mothers. For photoactivation of MyoII localization, embryos were collected from Sqh::mCherry/ *UASp* Cry2::RhoGEF2; *UASp* CIBN::pmGFP/$_{p}$*osk* Gal4 mothers. For photoactivation of E-Cad localization, embryos were collected from endo E-Cad::mKate2 (3X)/*UASp* Cry2::RhoGEF2; *UASp* CIBN::pmGFP/$_{p}$*osk* Gal4 mothers. E-cad::mKate2(3X) was a gift from Y.Bellaiche. For photorecruitment of RhoDN experiments, embryos were collected from $_{p}$*ubi*: Gap43::mCherry/+; *UASp* Cry2::RhoDN::mCherry/ *tub*^{mat} Gal4; *UASp* CIBN::pmGFP/ *tub*^{mat} Gal4 mothers. Control experiment for RhoDN localization was performed on embryos collected from *UASp* Cry2::RhoDN::mCherry/ *tub*^{mat} Gal4; *UASp* CIBN::pmGFP/ *tub*^{mat} Gal4 mothers. Optogenetic fly stocks are a gift from S. De Renzis. To monitor cell extrusion during mesoderm invagination, embryos from *klarsicht (klar-)* homozygous mothers expressing Gap43::mCherry was used. *klar-* fly stock was gifted by E. Wieschaus.

METHOD DETAILS

Time-lapse imaging

Embryos were mounted on glass-bottom plate in water after dechorionation and imaged on Zeiss 780 LSM confocal with 40x 1.1 NA objective using 488 nm and 561 nm lasers. Imaging data was obtained using the Zeiss zen software. For observing polarity of MyoII in mesoderm cells and for injections, embryos were imaged on Nikon spinning disc microscope with 60x 1.2 NA objective with 1.5x optovar, using 488 nm and 561 nm lasers. Data was acquired using Metamorph software.

In toto 4-D imaging, digital reconstruction and data processing

Embryos were dechorionated in bleach before mounting and selected for appropriate stage. Embryos were mounted in a glass capillary filled with 0.5% gelrite, with their long axis parallel to the capillary. A small portion of the gelrite cylinder containing the embryo was pushed out to image on Luxendo MuVi SPIM with an Olympus 20x 1.0 NA objective, using 488 nm and 594 nm lasers. Z-stacks were acquired with a step-size of 1 μm and during each acquisition; embryos were imaged in two opposing orthogonal views (0°-dorsal-ventral view, 90°-lateral view). Thus, for every single time point, four 3-D stacks of embryo were recorded. Stacks were fused (Rauzi and Lenne, 2015) to obtain a final isotropic pixel resolution of 0.29 μm. Once the stacks were aligned and fused, the unrolled views of Sna::GFP and Eve::YFP embryos were made following the MATLAB protocol described in Rauzi and Lenne (2015).

Drug injections

A stock solution of Rok kinase inhibitor, Y-27632 (from TOCRIS), was prepared at a concentration of 100 mM in water. From the stock, 50 mM Y-27632 was injected into embryos at the end of cellularization to inhibit MyoII activity. As a control experiment, water injected embryos were used. Before injection, stage-selected, dechorionated embryos were dried in a box with silica beads for 9 minutes. Dried embryos were mounted in halocarbon oil before injection.

Dendra photoconversion

Dendra photoconversion was carried out on the Zeiss 780 LSM confocal with a 40x 1.2 NA objective, using bleach mode with a 405 Argon laser, 110 μW at the focal point. Dendra before photoconversion was imaged using 488 nm laser. Photoconverted Dendra fluorescence was acquired using 561 nm laser and TRITC filter cube.

Cry2 optorecruitment

Cry2 optogenetic experiments were carried out on Zeiss 780 LSM confocal microscope with a 40x 1.2 NA objective, using bleach mode on Zeiss Zen software, with 2-P MaiTai tunable laser. Photorecruitment of RhoGEF2 was achieved by line activation on cortex using 950nm, 18 mW laser power at the focal point, 100 iterations, 6.5 μs pixel dwell. Photorecruitment of RhoGEF2 for producing ectopic fold was done over a z-stack by rectangular activation on apical side of dorsal cells using 950nm, 18 mW laser power at the focal point, 30 iterations, 2.4 μs pixel dwell. Photorecruitment of RhoDN was achieved on mid-sagittal sections by line activation on cortex using 950nm, 32 mW laser power at the focal point, 100 iterations, 6.5 μs pixel dwell, at 35 μm from apical side of mesoderm cells.

Actomyosin laser ablation

Actomyosin network ablation was performed using a tunable femtosecond-pulsed infrared laser (IR fs, MaiTai) coupled into a Zeiss 780 LSM confocal microscope, tuned at 950 nm. Ablation was achieved using the bleaching mode on Zeiss Zen software with a laser power of 140 mW at the focal point, single iteration and 1 μs pixel dwell, with a frame rate of 1s. This experiment was performed using 40x 1.2 NA objective.

Ectopic contraction

Ectopic contraction of MyoII was achieved by inducing a cavitation bubble using targeted IR fs (MaiTai), tuned at 950 nm, near lateral cortex of mesoderm cells (140 mW at the focal point, 5 iterations, 1 μs pixel dwell). Embryos were imaged on Zeiss 780 LSM confocal microscope using 40x 1.2 NA objective. Images were acquired using Zeiss Zen software.

Recoil velocity measurement

Recoil was measured using the point-picker plugin developed for Fiji by following the cut end of the actin fiber. Distance moved by actin fiber after ablation was plotted against time and measured the first derivative to deduce the maximum recoil velocity. DV ablation of actomyosin to have isotropic apical tension was also performed using the above settings.

QUANTIFICATION AND STATISTICAL ANALYSIS

4D cell and surface contact segmentation and rendering

ASTEC (Guignard et al., 2020) was used for 4D side contact segmentation. Imaris was used for 4D cell segmentation and for 3D rendering.

Cell intercalation density measurement

For the cell intercalation analysis, time points were restacked for keeping each plane of invaginating furrow constant throughout time. To do so, furrow invagination was followed over time. Black planes were added to the front and back of the stacks accordingly, corresponding to the distance invaginated by the furrow tip. Cell intercalation was monitored on the middle portion of the mesoderm, which was flat enough. To compare between different embryos, both wild type and mutants, t=0 was set to the time point of initiation of apical constriction in case of wild type and *bnt*- mutant embryos and t=0 was set as initiation of cephalic fold in case of *sna-twi*- mutant embryos. Cell intercalation was monitored for first 10 minutes after initiation of apical constriction in case of wild type and *bnt*- mutant embryos and for first 7 minutes after initiation of cephalic fold in case of *sna-twi*- mutant embryos. Cell intercalation density was measured at 10 μm from apical side, which is the ratio of number of cell intercalations to total number of cells.

Cell intercalation propagation along apical-basal axis

For apical-basal propagation of cell intercalation, planes were selected up to 20 μm with a step-size of 5 microns. Individual intercalation event was monitored and t=0 was assigned to the plane that reach a four-way vertex first. Then the time delay for reaching four-way vertex and eventually junction lengthening was measured for other planes. Angles of intercalation and junctions enriched with MyoII, with respect to AP and DV axes, were measured using Fiji macro and the graphs were plotted using polar histogram function in Matlab. To measure the junction length reduction rates, length of individual vertex was monitored over time using a Fiji macro. From the length vs time plot, slope gave the junction length reduction rates.

Mesoderm extension measurement

Cross and mid-sagittal sections were obtained using Fiji by selecting out a single plane from the 3-D fused stack. Cross-sections are taken at half embryo length. Mesoderm extension was measured using the mid-sagittal sections. The cell on half-length of mid-sagittal section was marked as an identity point. Cells that were 100 μm, both anterior and posterior, from this identity point was marked. Their distance from the identity point was followed over time. The initial mesoderm length was set as distance between anterior cell to identity point at the end of mesoderm constriction phase. The final mesoderm length was set as distance between these points after 15 minutes of initiation of apical constriction in case of wildtype or *bnt*- mutant embryos or 12 minutes of initiation of cephalic furrow in case of *sna-twi*- mutant embryos. We had to limit ourselves to these time frames because after this point mesoderm invaginates too deep to be analyzed.

Invaginated mesoderm width measurement

End-to-end width of invaginated mesoderm was measured on the cross-section of wildtype and *bnt*- mutant embryos. Widths were normalized to the average diameter of the embryo to make embryo-to-embryo data comparable.

Mesoderm cell extrusion analysis

Homozygous *klar* mutant embryos expressing Gap43::mCherry were imaged on MuVi SPIM and the data was fused. Both apical and basal side of each mesoderm cell was manually tracked and apical positions were plotted against furrow tip position, after the mesoderm has invaginated and the two limbs have closed.

Intensity measurements

MyoII intensity (Figures 1B and 5H), E-Cad intensity (Figure 5I) and Dendra intensity (Figure 5F) were measured using the point-picker plugin developed for Fiji, which measures average intensity from a 3 x 3 ROI. RhoGEF2 intensity (Figure 5G) in cytoplasm and at cortex was measured using Fiji and the ratio between cortical to cytoplasmic RhoGEF2 was calculated.

Statistics

All data with more than ten values are represented as mean±SEM and with less than ten values as mean±SD. For comparison between multiple groups, one-way ANOVA test was used and for comparison between two groups, Mann-Whitney test was used (Graphpad Prism software). A p-value<0.05 was considered as significant.

Limitations of the study

Live imaging of RhoGEF2 in a *sna−* embryo was not possible since the three-time constructed *Δhalo sna/CyO; psqh:GFP::RhoGEF2* strain always resulted in an unhealthy fly line.

Developmental Cell, Volume *56*

Supplemental information

A two-tier junctional mechanism drives simultaneous tissue folding and extension

Alphy John and Matteo Rauzi

SUPPLEMENTARY FIGURES

Figure S1: A MyoII second-tier is established at the lateral cortex of mesoderm cells. Related to Figure 2.

(A) Time lapse of surfaces of contact (reducing contact in blue and newly formed contact in red) during ectoderm cell intercalation (right). Scale bar 10 µm.

(B) Induced fold of 15 µm depth at the dorsal side of the embryo by MyoII activation. Red ROI marks the photo-activated region. Cross-section shown along the dashed line. Scale bar 50 µm. Quantification of cell intercalation in a wild type and an induced fold shown in the plot on right. n=3 embryos. **p value < 0.01.

(C) Lateral MyoII speckles along the facing cortices of two neighbouring mesoderm cells. MyoII and membrane intensities are measured over the AB line: the membrane intensity peak (red arrowhead) is interposed between the two MyoII intensity peaks (green arrowheads).

(D) Left panel: MyoII distribution in mesoderm cells (left panel) 10 µm from apical surface in Y-27632 (50 mM Rok kinase inhibitor) injected embryos. Scale bar 30 µm. Right panel: cell intercalation density in water-injected control and Y-27632-injected embryos. n=3 embryos for control injection and 5 embryos for Y-2632 injection. **p value < 0.01.

(E) Cell intercalation density in mesoderm after RNAi-mediated knockdown of *rhogef2*. n=3 embryos for wildtype and 5 embryos for *rhogef2 RNAi*. **p value < 0.01.

(F) Left panel: temporal sequence showing junction shrinkage upon targeted MyoII activation. Red line denotes the region of photo-activation. Scale bar 5 µm. Right panel: side shrinkage rate after local MyoII activation.

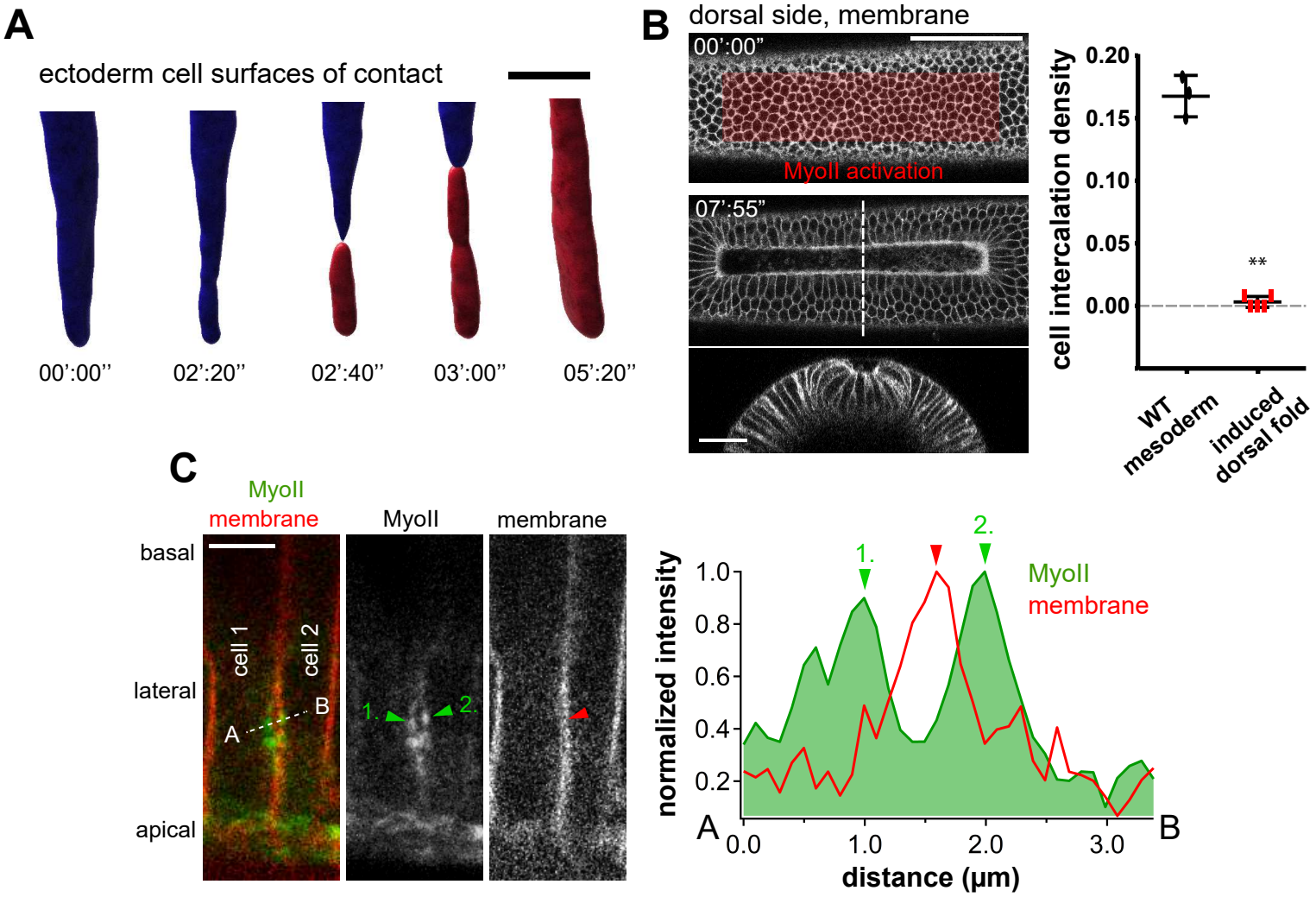
A
ectoderm cell surfaces of contact
00':00''
02':20''
02':40''
03':00''
05':20''
B
dorsal side, membrane
00':00"
MyoII activation
07':55"
cell intercalation density
0.20
0.15
0.10
0.05
0.00
**
WT mesoderm
induced dorsal fold
C
MyoII
membrane
MyoII
membrane
basal
lateral
apical
cell 1
cell 2
A
B
1.
2.
normalized intensity
1.0
0.8
0.6
0.4
0.2
A
0.0
1.0
2.0
3.0
B
distance (µm)
MyoII
membrane
D
Y-27632 injected
mesoderm, z = 10 µm
MyoII
MyoII
membrane
cell intercalation density
0.20
0.15
0.10
0.05
0.00
**
water injected
Y-27632 injected
E
cell intercalation density
0.25
0.20
0.15
0.10
0.05
0.00
**
WT
rhogef2 RNAi
F
mesoderm, membrane, z = 10 µm
MyoII activation
0"
0"
22"
34"
junction length reduction rate (µm/s)
0.08
0.06
0.04
0.02
0.00

Figure S1

Figure S2: Anterior-posterior supracellular tension is not responsible for side shrinkage but for new side extension. Related to Figure 2.

(A) Anterior and posterior DV dissections of the supracellular actomyosin network spanning the mesoderm tissue reduces AP cortical tension.

(B) Representative image sequence showing supracellular actomyosin network dissection. Red dotted lines denote the region of laser dissection. Scale bar 50 µm.

(C and D) side shrinking (C) and new side extension (D) densities after laser dissection of the supracellular actomyosin network. n=5 embryos. Ns, not significant. **p value < 0.01.

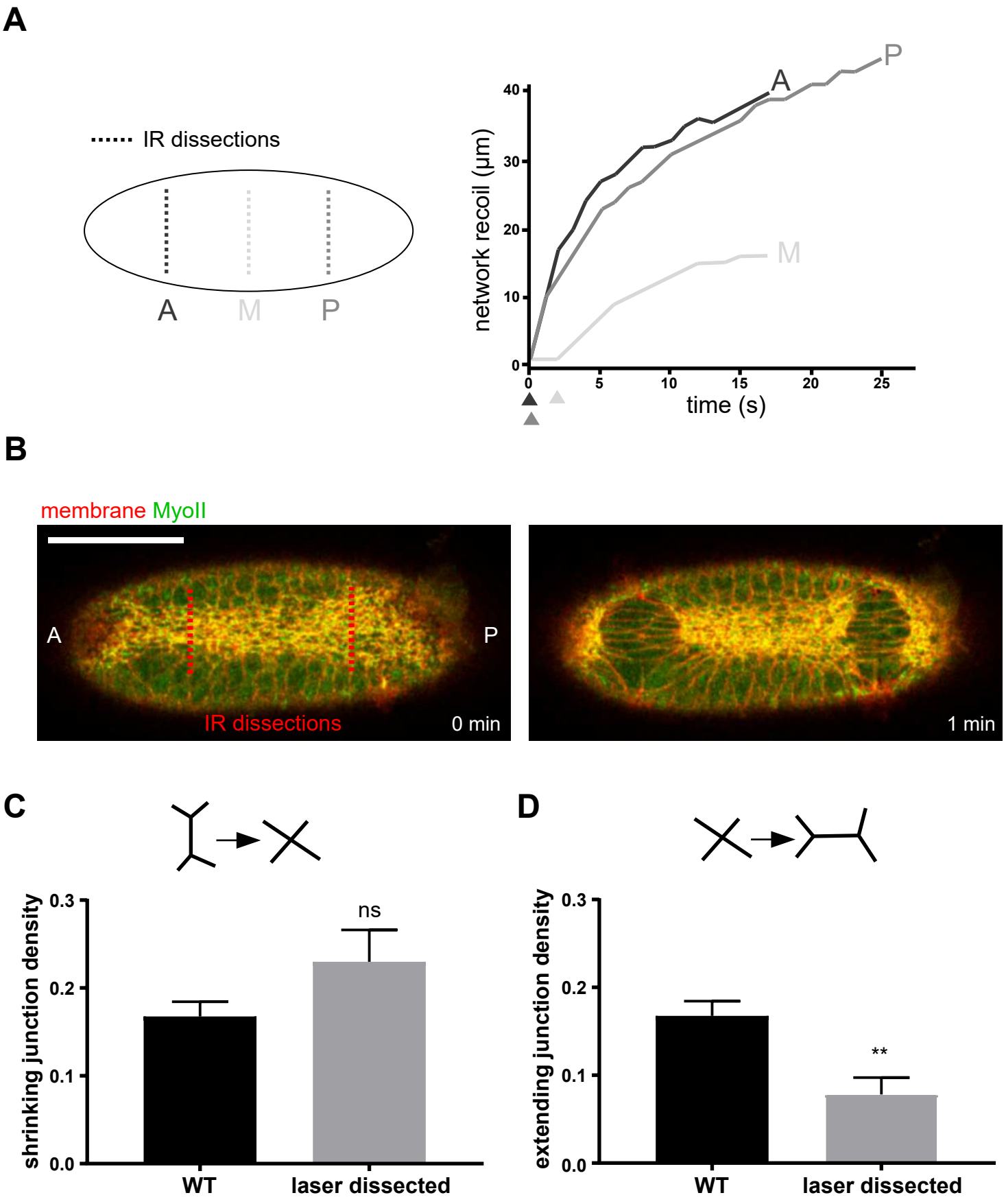
A
IR dissections
A
M
P
network recoil (µm)
40
30
20
10
0
0
5
10
15
20
25
time (s)
A
P
M
B
membrane MyoII
A
P
IR dissections
0 min
1 min
C
shrinking junction density
0.3
0.2
0.1
0.0
ns
WT
laser dissected
D
extending junction density
0.3
0.2
0.1
0.0
**
WT
laser dissected

Figure S2

Figure S3: AP-DV patterning synergy is necessary for effective mesoderm convergence-extension. Related to Figure 3.

(A) T1 angle standard deviation in function of the average in wild-type and mutant embryos. The standard deviation of a homogenous distribution of angles is indicated by the blue arrow (B).

(C and D) Correlation plot between average cell intercalation density and average tissue extension ratio of both anterior and posterior halves of wild type and mutant embryos.

(E-G) Individual data points of wild-type (E), *sna-twi-* (F), and *bnt-* (G) embryos on a correlation plot between cell intercalation density and tissue extension ratio of both anterior (filled symbol) and posterior (open symbols) halves.

(H) Left: cross-section of wild-type (left, top) and *bnt-* (left, bottom) embryos during mesoderm invagination (furrow depth 30 µm). Black bars indicate the width of the tubular folded tissue. Scale bar 50 µm. Right: normalized width of the tubular mesoderm epithelium in wild type and *bnt-* conditions. n=5 embryos. Width of mesoderm is normalized to the average diameter of embryos. ****p value < 0.0001.

(I) side shrinking and new side extension densities after laser dissection of the supracellular actomyosin network in *bnt-* embryos. n=5 embryos. ***p value < 0.001.

(J) 3D reconstruction of cell quartet undergoing bowtie T1-transition in *bnt-* embryos. Scale bar 5 µm.

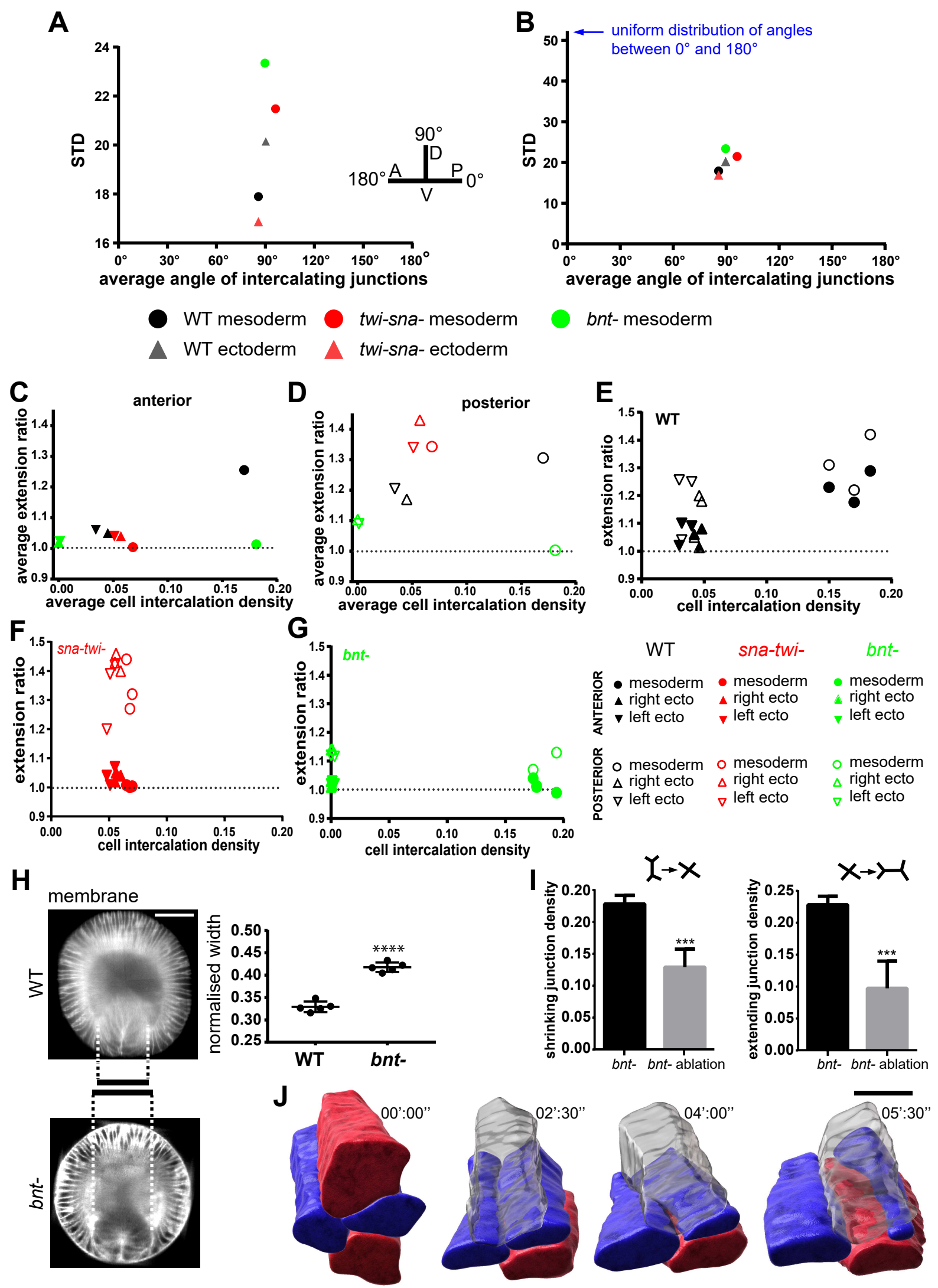
A
STD
average angle of intercalating junctions
90°
D
180° A P 0°
V
B
uniform distribution of angles
between 0° and 180°
STD
average angle of intercalating junctions
WT mesoderm
twi-sna- mesoderm
bnt- mesoderm
WT ectoderm
twi-sna- ectoderm
C
anterior
average extension ratio
average cell intercalation density
D
posterior
average extension ratio
average cell intercalation density
E
WT
extension ratio
cell intercalation density
F
sna-twi-
extension ratio
cell intercalation density
G
bnt-
extension ratio
cell intercalation density
WT
sna-twi-
bnt-
ANTERIOR
POSTERIOR
mesoderm
right ecto
left ecto
H
membrane
WT
bnt-
normalised width
****
WT
bnt-
I
shrinking junction density
***
bnt-
bnt- ablation
extending junction density
***
bnt-
bnt- ablation
J
00':00''
02':30''
04':00''
05':30''

Figure S3

Figure S4: Mesoderm cells do not extrude during tissue invagination and lateral MyoII contractility, in the absence of apical constriction, induces cell extrusion. Related to Figure 5.

(A) 3D embryo trunk rendering (top left) and cross-section (top, right) showing a close-up view of mesoderm cells during tissue folding in a membrane labelled *klar*- embryo increasing epithelia transparency for deep tissue imaging. Scale bar 25 µm. Bottom panel: position of the apical side of mesoderm cells with respect to the furrow position (0 µm). n=276 cells, 3 embryos.

(B) Representative time lapse showing cell extrusion initiation (yellow arrowhead) upon lateral MyoII activation at a stage when MyoII is still not apically recruited. Red bar indicates the photo-activated region. Scale bar 15 µm.

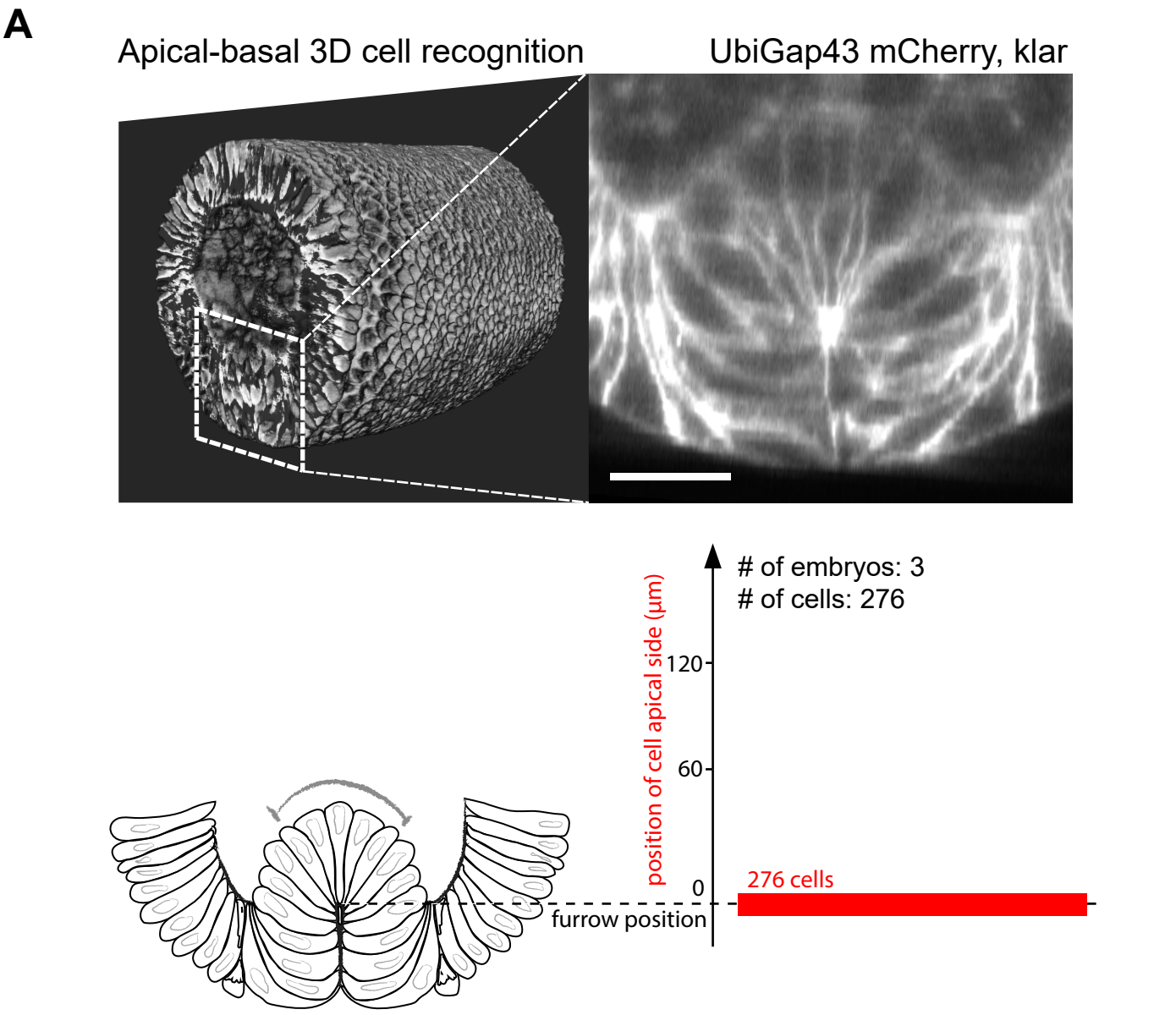
A
Apical-basal 3D cell recognition
UbiGap43 mCherry, klar
# of embryos: 3
# of cells: 276
position of cell apical side (µm)
120
60
0
276 cells
furrow position
B
MyoII
00':00"
00':24"
00':48"
01':06"
MyoII activation

Figure S4

Chapter III

Discussions

Remarkably, invaginating *Drosophila* mesoderm tissue concomitantly undergoes extension (Figure 28A). I have shown that mesoderm cells undergo neighbor exchange, but in a specific mode; intercalation is initiated at 10µm from the apical side and is resolved more apically and laterally. Mesoderm cells assemble a two-tiered junctional complex during this process (Figure 28B): while the first tier at the apical side was shown to tether actomyosin at the apical side to generate a tissue-spanning network, the second tier at the lateral side mediates mesoderm cell intercalation. Myosin (MyoII) is recruited to the lateral cortex in a PCP fashion which facilitates contraction of junctions oriented in the DV axis. Lateral MyoII recruitment *per se* is under the control of DV patterning, whereas its PCP recruitment is regulated by the AP patterning system. While DV junction reduction is mediated by PCP MyoII, new junction extension depends on anisotropic tension along the AP axis. In the absence of AP polarity, intercalation still occurs in the mesoderm, however, this type of cell rearrangement is not the same as wildtype intercalation but is defective in extending the tissue. This mode is termed bow-tie intercalation. I further show that both junction reduction and extension in AP patterning mutants are reduced upon laser ablation of the apical network indicating the role of anisotropic apical tension in inducing cell neighbor exchange. Taken together, I propose a model in which synergy between the AP and DV patterning signals drive concomitant folding and extension of the invaginating mesoderm in *Drosophila* embryo.

Said so, in this study, I have unveiled a novel morphogenetic mechanism that drives concomitant tissue extension and folding that is mediated by orthogonal patterning signals during *Drosophila* gastrulation. There are still significant questions to be addressed which will be discussed below.

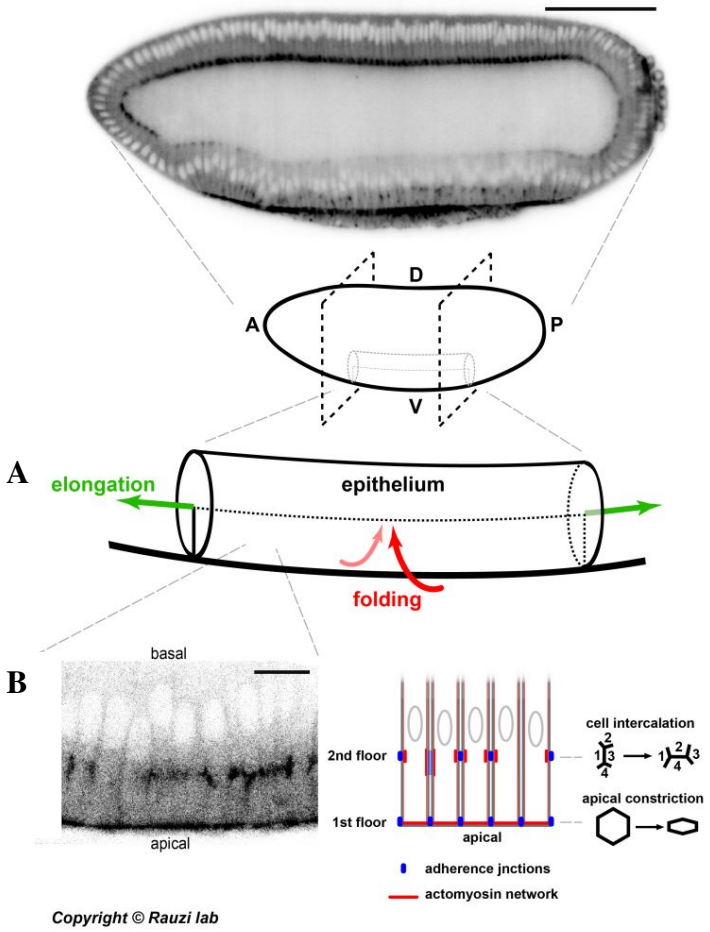

Figure 28. Model for concomitant morphogenesis of mesoderm

(A) Invaginating *Drosophila* mesoderm tissue concomitantly undergoes extension. (B) Mesoderm cells undergo neighbor exchange, but in a specific mode; intercalation is initiated at 10µm from the apical side and is resolved more apically and laterally. Mesoderm cells assemble a two-tiered junctional complex during this process: while the first tier at the apical side was shown to tether actomyosin at the apical side to generate a tissue-spanning network, the second tier at the lateral side mediates mesoderm cell intercalation. Lateral MyoII recruitment per se is under the control of DV patterning, whereas its PCP recruitment is regulated by the AP patterning system.

8.1. How AP patterning synergize with DV patterning signals at the cellular and molecular level?

Even-skipped (Eve) bands are found to intersect the Snail (Sna)/Twist (Twi) expressing domain. However, it is not known whether any of the DV patterning components exhibit AP polarity. It was shown previously that Twi expression is graded along the DV axis, which depends on the Dorsal (Dl) gradient whereas Sna expression is homogeneous, which is under the control of feedback regulation by Twi and Dl (Ip et al., 1992; Leptin, 1991). Unexpectedly, in the absence of the *twi* gene, *sna* mRNA expression becomes stripy along the AP axis (Figure 29) (Ip, Maggert, & Levine, 1994; Stathopoulos & Levine, 2002; Stathopoulos, Van Drenth, Erives, Markstein, & Levine, 2002). It could be that this stripy pattern along the AP axis is masked by the feedback regulation of Sna expression by Twi and Dl in wild-type embryos. Strikingly, graded expression of these upstream regulators was shown to play critical roles during morphogenesis. For instance, graded Twi expression along the DV axis is necessary to generate a graded activity of MyoII activity, with the highest activity at ventral midline, an essential feature for tissue folding (Heer et al., 2017). Nevertheless, the role of this stripy expression pattern of Snail is not known yet. It would be interesting to test whether stripy Snail expression is disrupted in AP-mutants and whether such pattern mediates the PCP distribution of lateral MyoII.

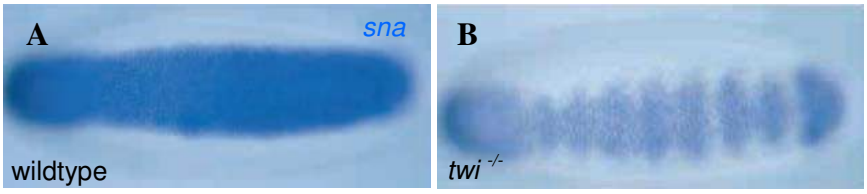

Figure 29. Stripy *sna* expression

sna mRNA expression in wildtype (A) and *twi* $^{-/-}$ embryos (B). Notice that sna expression becomes stripy in *twi* $^{-/-}$ embryos. Image adapted from (Stathopoulos & Levine, 2002).

8.2. How is the PCP pattern of MyoII generated in the mesoderm?

The role of AP patterning in polarizing MyoII localization was first demonstrated during GBE. Planar polarized intercalation during GBE is not under the control of the Wnt PCP pathway, rather depends on the specification of the AP axis by the patterning genes (Irvine & Wieschaus, 1994; J. A. Zallen & Wieschaus, 2004). It was unclear until recently how the patterning genes, which are generally transcription factors localized to the nucleus, talk to cytoskeletal regulators in order to regulate MyoII in a PCP fashion. Research from Zallen's group identified a mechanism in which differential expression of Toll receptors in stripes along the AP axis restricts MyoII activity to DV vertices, which is disrupted in mutants for AP patterning components like *eve* or *runt* (Pare et al., 2014). Some cells still maintain MyoII polarity even in the absence of Toll receptors, indicating that additional pathways are necessary for PCP distribution of MyoII. Pare and colleagues have identified an additional pathway involving Tartan (leucine-rich-repeat, LRR receptor) and Tenurin system, is necessary for the PCP MyoII distribution and organization of compartment boundary cells (Pare et al., 2019). How is Toll receptors convey this planar polarizing message to the underlying actomyosin contractile unit? Recently, Zallen's group has further deciphered that Toll receptors mediate MyoII planar localization by targeting Src- and PI3-kinase (PI3K) activity to specific membrane domains (Tamada et al., 2021). None of these components were previously shown to be expressed or active in the mesoderm during invagination. It would be thus interesting to test if PCP MyoII localization in mesoderm during folding and extension is under the control of these molecular pathways.

An additional putative mechanism for activating MyoII in a PCP fashion could be by polarized localization of the upstream factor RhoGEF2. I have shown that lateral MyoII recruitment is under the control of the RhoGEF2/Rho pathway. Interestingly, optogenetic localization of

RhoGEF2 was sufficient to induce MyoII activity. I did not test whether RhoGEF2 is recruited in a PCP fashion similar to MyoII in the wild-type embryo. Preliminary results point to a PCP distribution of RhoGEF2 at the lateral position. It would be necessary to prove this aspect and identify the molecular mechanisms that lead to RhoGEF2 PCP localization. How can a cytosolic small biomolecule like RhoGEF2 be distributed in a PCP manner? It was shown that the transmembrane anchor, T48 is necessary for local recruitment of RhoGEF2 to activate the Rho pathway during apical constriction of the mesoderm cells (Kolsch et al., 2007). However, it is not known if T48 is present at the lateral cortices and if T48 has a planar polarized distribution. Another potential mechanism could be a polarized delivery of RhoGEF2 to lateral DV cortices. It was previously shown in both S2 cells and embryos that RhoGEF2 binds to microtubule plus-end binding protein, EB1, and is released at specific locations by the activity of Concertina (Cta), the α-subunit of G-protein (Garcia De Las Bayonas, Philippe, Lellouch, & Lecuit, 2019; Rogers, Wiedemann, Hacker, Turck, & Vale, 2004). An interesting experiment would be to analyze the distribution of EB1 and Cta and test if either of these proteins exhibits a PCP distribution. If these components show PCP distribution at the lateral cortex, creating optogenetic tools to block their functions in a spatiotemporally specific manner will be useful to address the functional role of such localization.

Microtubules themselves could be distributed in a polarized manner and could participate in the polarized distribution of RhoGEF2. Microtubules have been shown to play a pivotal role in generating and stabilizing PCP in epithelial cells. For example, Yuko and colleagues tested the role of microtubules in generating PCP in the wing epithelium of *Drosophila* by disrupting the microtubule network using colchicine or paclitaxel treatment (Shimada, Yonemura, Ohkura, Strutt, & Uemura, 2006). Microtubules showed polarized distribution in these cells and facilitate transport and proper distribution of PCP regulators. In another example, Andrew and colleagues tested the role of microtubules in the stabilization of polarity in

the floorplate cells of zebrafish embryos (Mathewson, Berman, & Moens, 2019). The microtubule organizing center (MTOC) displays polarized distribution, near the basal body of the primary cilia. Disrupting microtubules using nocodazole induced rapid loss of polarized distribution of PCP pathway components. Remarkably, the polarized distribution of the microtubule network in these examples facilitates the directed transport of PCP pathway components to their respective membrane compartments. It would be thus logical to test the role of microtubules in planar cell polarized distribution of MyoII at lateral cortices in invaginating mesoderm.

8.3. Contribution of T1 transitions to the tissue convergent-extension process

An intriguing observation was that despite having an equivalent amount of cell rearrangements in the mesoderm of AP patterning mutants (even though they were bow-tie intercalations) as that of the wild-type embryos, the former tissue fails to extend. An open question is regarding the exact active contribution of T1 transitions to the tissue elongation process. A well-studied model for T1 transitions is GBE during *Drosophila* gastrulation. Although T1 transitions correspond to a major event during GBE (Irvine & Wieschaus, 1994), blocking cell intercalation alone had only a subtle effect on total tissue extension; *eve* mutants with almost null cell intercalations did not show a significant reduction in extension, whereas mutants for posterior midgut (PMG) invagination had a drastic reduction of total tissue extension (L. C. Butler et al., 2009; Lye et al., 2015). Then, what purpose does cell intercalation serve? Importantly, three different roles can be foreseen for cell intercalation in an active tissue (Figure 30). First, if a single cell starts exchanging its neighbor contacts continuously, this could allow the translocation of that cell to a different location along the plane of the tissue. Secondly, planar polarized cell intercalation can drive the extension of the tissue along one axis and contraction along the opposite axis. The third function of cell intercalation

is to accommodate the tissue strain to avoid cell stretching when an external force is applied. Interestingly, epithelial cells at the ventral side of *sna twi* double mutants which lack both apical constriction and lateral cell intercalation stretched during PMG invagination, indicating a role for intercalation in accommodating tissue strain. Thus pinpointing the net impact of cell intercalation events on total tissue elongation is a critical subject to be addressed. For this, tissue elongation as a result of cell intercalation should be measured in the absence of any external forces. Matteo and colleagues depicted that gastrulation movements in different parts of the *Drosophila* embryo are coupled (Rauzi et al., 2015_ENREF_308). To address the aforementioned question, *Drosophila* germband is one of the suited model systems and the correlation between cell intercalation and tissue extension should be measured in mutant embryos with normal cell intercalations but lacking both mesoderm folding and PMG invagination (two major external factors that were shown to affect cell shape changes and intercalation in germband.

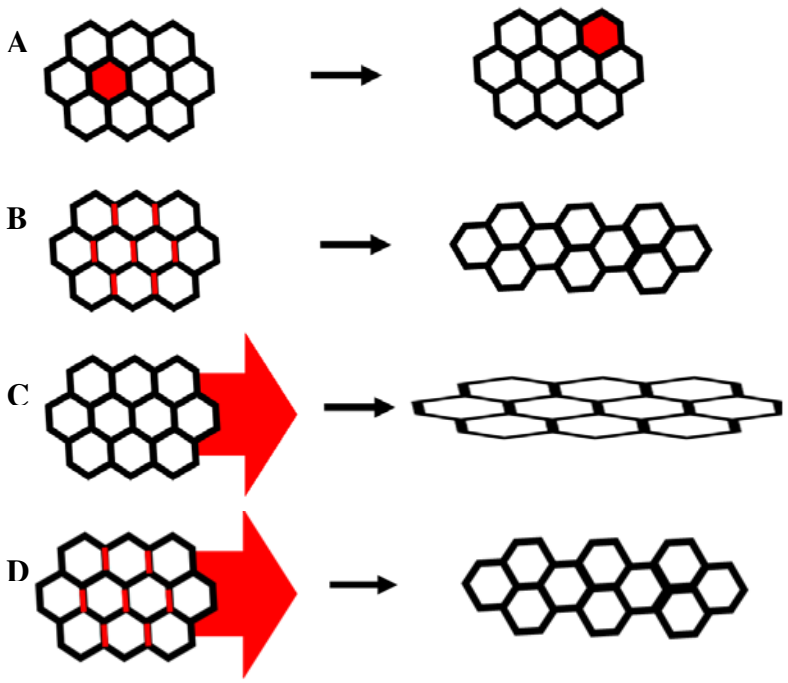

Figure 30. Functional roles of cell intercalation

(A) Cell translocation. When a single cell exchanges its neighbors multiple time, this allows it to translocate from one position to another. (B) Tissue elongation. Planar polarized cell intercalation extends the tissue along one axis and simultaneously reduces its width along the orthogonal axis. (C-D) Accomodation of stretching strain. A sheet of tissue stretches in the presence of an external force (red arrow)in the absence of cell intercalation (C), whereas the strain due to stretch is accommodated when the cells intercalate (D).

8.4. Role of mechanosensing in mesoderm cell intercalation

I have performed laser dissection experiments to test the role of anisotropic tension along the AP axis in new junction formation. Interestingly, when two cuts were made along the DV axis, the cells in between the cuts were hyperconstricted and they had an enhanced PCP distribution of MyoII at the lateral cortex (data not shown). This is indicative of a mechanosensitive mechanism at play. Mechanical signals are converted into the biochemical signals inside cells by the mechanotransductive pathways. Research by Philippe-Alexandre and colleagues has shown that Fog-dependent apical recruitment of MyoII is a mechanosensitive pathway in a wild-type embryo. In this study, they showed that indenting mesoderm rescued apical MyoII recruitment and constriction in *sna* mutant embryos; apical MyoII is absent in unindented *sna* mutant embryos (Pouille, Ahmadi, Brunet, & Farge, 2009). From these observations, they put forward the model that Sna-mediated initial random apical constriction provides the mechanical signal for Fog-mediated apical MyoII recruitment in wild-type embryos. In addition, adherens junction components like E Cad, α-Cat, and Vinculins are shown to be tension-sensitive proteins (Borghi et al., 2012; Buckley et al., 2014; le Duc et al., 2010; Yao et al., 2014), demonstrating the significance of mechanotransductive pathways during mesoderm invagination. It would be thus essential to recognize the mechanosensitive pathway, if any, that causes the recruitment of lateral MyoII.

8.5. Is patterning synergy at the level of tissue morphogenesis evolutionarily conserved?

This present study uncovered a novel morphogenetic mechanism during development driving concomitant morphogenesis. Remarkably, the concomitant morphogenesis observed is not because of the simple addition of morphogenetic pathways under the control of two orthogonal axes patterning systems. Tissue folding and extension in series do not necessarily require cell intercalation to happen at the lateral cortices. Also, a new contact junction is created at the lateral cortices of mesoderm cells 'on the fly' by actomyosin coalescence, during folding and extension. Thus, a novel cellular mechanism emerges from the synergy between these axes patterning signals, to drive concomitant morphogenesis. Similar concomitant morphogenetic processes are described in other model systems during embryonic development (reviewed in John and Rauzi, 2021, see Annex I). For example, during vertebrate neurulation (Figure 27), the neural plate tissue converges and extends along the AP axis, while folding along the orthogonal axis (Elul, Koehl, & Keller, 1997; R. Keller et al., 1992). Folding is the result of apical constriction, whereas tissue extension is mediated by planar polarized cell intercalation (Elul, Koehl, & Keller, 1998; Moore, Stanisstreet, & Evans, 1987; Schroeder, 1970). A closer look at the causative mechanism of this morphogenetic event was given by Nishimura and colleagues in their study on chick neurulation. They proposed a model in which anisotropic actomyosin contractility drives both cell intercalation and promotes tissue bending (Nishimura, Honda, & Takeichi, 2012). However, a detailed analysis has to be performed to identify the molecular, subcellular, and cellular mechanisms that drive concomitant tissue folding and extension during vertebrate neurulation. It is still unclear whether a synergy between axes patterning systems exists during the aforesaid process.

9. Conclusions

Gene patterning signals provide essential road maps for the embryonic cells to take up precise fates and undergo predefined morphogenetic movements. A fundamental question addressed over these years is how these patterns talk to the cytoskeletal elements to mediate distinct morphogenetic programs. Individual morphogenetic pathways and their link to corresponding patterning signals have gained a major share of attention, meanwhile, concomitant morphogenetic events like folding and extension, generated by the synergy between gene patterning signals stayed unexplored. In this work, I unravel novel cellular and molecular mechanisms that emerge from the synergy between orthogonal body axes patterning signals, that mediate simultaneous folding and extension of the *Drosophila* mesoderm during gastrulation. Several questions remain open. What are the downstream effectors of Sna-pathway that mediate MyoII recruitment to the lateral cortex? What determines the position of lateral MyoII foci to be at around 10 µm from the apical cortex, whether it is because these cells have constricted apical cortices? Why is bow-tie intercalation defective in extending the tissue? Given the conservation of such concomitant events throughout the evolutionary tree, it is thus necessary to identify and characterize such mechanisms during morphogenesis in other metazoan models.

Bibliography

Adam, J. C., Pringle, J. R., & Peifer, M. (2000). Evidence for functional differentiation among Drosophila septins in cytokinesis and cellularization. *Mol Biol Cell, 11*(9), 3123-3135. doi: 10.1091/mbc.11.9.3123

Adams, M. D., Celniker, S. E., Holt, R. A., Evans, C. A., Gocayne, J. D., Amanatides, P. G., . . . Venter, J. C. (2000). The genome sequence of Drosophila melanogaster. *Science, 287*(5461), 2185-2195. doi: 10.1126/science.287.5461.2185

Aguilar-Cuenca, R., Juanes-Garcia, A., & Vicente-Manzanares, M. (2014). Myosin II in mechanotransduction: master and commander of cell migration, morphogenesis, and cancer. *Cell Mol Life Sci, 71*(3), 479-492. doi: 10.1007/s00018-013-1439-5

Akam, M. (1987). The molecular basis for metameric pattern in the Drosophila embryo. *Development, 101*(1), 1-22.

Akhmanova, A., & Steinmetz, M. O. (2015). Control of microtubule organization and dynamics: two ends in the limelight. *Nat Rev Mol Cell Biol, 16*(12), 711-726. doi: 10.1038/nrm4084

Amiri, A., & Stein, D. (2002). Dorsoventral patterning: a direct route from ovary to embryo. *Curr Biol, 12*(15), R532-534. doi: 10.1016/s0960-9822(02)01031-x

Andreu, M. J., Gonzalez-Perez, E., Ajuria, L., Samper, N., Gonzalez-Crespo, S., Campuzano, S., & Jimenez, G. (2012). Mirror represses pipe expression in follicle cells to initiate dorsoventral axis formation in Drosophila. *Development, 139*(6), 1110-1114. doi: 10.1242/dev.076562

Arboleda-Estudillo, Y., Krieg, M., Stuhmer, J., Licata, N. A., Muller, D. J., & Heisenberg, C. P. (2010). Movement directionality in collective migration of germ layer progenitors. *Curr Biol, 20*(2), 161-169. doi: 10.1016/j.cub.2009.11.036

Assemat, E., Bazellieres, E., Pallesi-Pocachard, E., Le Bivic, A., & Massey-Harroche, D. (2008). Polarity complex proteins. *Biochim Biophys Acta, 1778*(3), 614-630. doi: 10.1016/j.bbamem.2007.08.029

Bachmann, A., Schneider, M., Theilenberg, E., Grawe, F., & Knust, E. (2001). Drosophila Stardust is a partner of Crumbs in the control of epithelial cell polarity. *Nature, 414*(6864), 638-643. doi: 10.1038/414638a

Banerjee, S., Sousa, A. D., & Bhat, M. A. (2006). Organization and function of septate junctions: an evolutionary perspective. *Cell Biochem Biophys, 46*(1), 65-77. doi: 10.1385/CBB:46:1:65

Barclay, C. J. (1998). Estimation of cross-bridge stiffness from maximum thermodynamic efficiency. *J Muscle Res Cell Motil, 19*(8), 855-864. doi: 10.1023/a:1005409708838

Barlan, K., & Gelfand, V. I. (2017). Microtubule-Based Transport and the Distribution, Tethering, and Organization of Organelles. *Cold Spring Harb Perspect Biol, 9*(5). doi: 10.1101/cshperspect.a025817

Barresi, M. J. F., & Gilbert, S. F. (2019). *Developmental Biology* (12 ed.).

Barrett, K., Leptin, M., & Settleman, J. (1997). The Rho GTPase and a putative RhoGEF mediate a signaling pathway for the cell shape changes in Drosophila gastrulation. *Cell, 91*(7), 905-915. doi: 10.1016/s0092-8674(00)80482-1

Bendix, P. M., Koenderink, G. H., Cuvelier, D., Dogic, Z., Koeleman, B. N., Brieher, W. M., . . . Weitz, D. A. (2008). A quantitative analysis of contractility in active cytoskeletal protein networks. *Biophys J, 94*(8), 3126-3136. doi: 10.1529/biophysj.107.117960

Benton, R., & St Johnston, D. (2003). Drosophila PAR-1 and 14-3-3 inhibit Bazooka/PAR-3 to establish complementary cortical domains in polarized cells. *Cell, 115*(6), 691-704. doi: 10.1016/s0092-8674(03)00938-3

Berleth, T., Burri, M., Thoma, G., Bopp, D., Richstein, S., Frigerio, G., . . . Nusslein-Volhard, C. (1988). The role of localization of bicoid RNA in organizing the anterior pattern of the Drosophila embryo. *EMBO J, 7*(6), 1749-1756.

Bertet, C., Rauzi, M., & Lecuit, T. (2009). Repression of Wasp by JAK/STAT signalling inhibits medial actomyosin network assembly and apical cell constriction in

intercalating epithelial cells. *Development, 136*(24), 4199-4212. doi: 10.1242/dev.040402
Bertet, C., Sulak, L., & Lecuit, T. (2004). Myosin-dependent junction remodelling controls planar cell intercalation and axis elongation. *Nature, 429*(6992), 667-671. doi: 10.1038/nature02590
Betschinger, J., Mechtler, K., & Knoblich, J. A. (2003). The Par complex directs asymmetric cell division by phosphorylating the cytoskeletal protein Lgl. *Nature, 422*(6929), 326-330. doi: 10.1038/nature01486
Bhat, M. A., Izaddoost, S., Lu, Y., Cho, K. O., Choi, K. W., & Bellen, H. J. (1999). Discs Lost, a novel multi-PDZ domain protein, establishes and maintains epithelial polarity. *Cell, 96*(6), 833-845. doi: 10.1016/s0092-8674(00)80593-0
Bilder, D. (2001). PDZ proteins and polarity: functions from the fly. *Trends Genet, 17*(9), 511-519. doi: 10.1016/s0168-9525(01)02407-6
Bilder, D. (2003). PDZ domain polarity complexes. *Curr Biol, 13*(17), R661-662. doi: 10.1016/s0960-9822(03)00599-2
Bilder, D. (2004). Epithelial polarity and proliferation control: links from the Drosophila neoplastic tumor suppressors. *Genes Dev, 18*(16), 1909-1925. doi: 10.1101/gad.1211604
Bilder, D., Schober, M., & Perrimon, N. (2003). Integrated activity of PDZ protein complexes regulates epithelial polarity. *Nat Cell Biol, 5*(1), 53-58. doi: 10.1038/ncb897
Blankenship, J. T., Backovic, S. T., Sanny, J. S., Weitz, O., & Zallen, J. A. (2006). Multicellular rosette formation links planar cell polarity to tissue morphogenesis. *Dev Cell, 11*(4), 459-470. doi: 10.1016/j.devcel.2006.09.007
Blankenship, J. T., & Wieschaus, E. (2001). Two new roles for the Drosophila AP patterning system in early morphogenesis. *Development, 128*(24), 5129-5138.
Bond, L. M., Brandstaetter, H., Sellers, J. R., Kendrick-Jones, J., & Buss, F. (2011). Myosin motor proteins are involved in the final stages of the secretory pathways. *Biochem Soc Trans, 39*(5), 1115-1119. doi: 10.1042/BST0391115
Borghi, N., Sorokina, M., Shcherbakova, O. G., Weis, W. I., Pruitt, B. L., Nelson, W. J., & Dunn, A. R. (2012). E-cadherin is under constitutive actomyosin-generated tension that is increased at cell-cell contacts upon externally applied stretch. *Proc Natl Acad Sci U S A, 109*(31), 12568-12573. doi: 10.1073/pnas.1204390109
Bosveld, F., Bonnet, I., Guirao, B., Tlili, S., Wang, Z., Petitalot, A., . . . Bellaiche, Y. (2012). Mechanical control of morphogenesis by Fat/Dachsous/Four-jointed planar cell polarity pathway. *Science, 336*(6082), 724-727. doi: 10.1126/science.1221071
Brand, A. H., & Perrimon, N. (1993). Targeted gene expression as a means of altering cell fates and generating dominant phenotypes. *Development, 118*(2), 401-415.
Breckenridge, M. T., Dulyaninova, N. G., & Egelhoff, T. T. (2009). Multiple regulatory steps control mammalian nonmuscle myosin II assembly in live cells. *Mol Biol Cell, 20*(1), 338-347. doi: 10.1091/mbc.E08-04-0372
Briscoe, J., & Kicheva, A. (2017). The physics of development 100years after D'Arcy Thompson's "On Growth and Form". *Mech Dev, 145*, 26-31. doi: 10.1016/j.mod.2017.03.005
Buckley, C. D., Tan, J., Anderson, K. L., Hanein, D., Volkmann, N., Weis, W. I., . . . Dunn, A. R. (2014). Cell adhesion. The minimal cadherin-catenin complex binds to actin filaments under force. *Science, 346*(6209), 1254211. doi: 10.1126/science.1254211
Butler, L. C., Blanchard, G. B., Kabla, A. J., Lawrence, N. J., Welchman, D. P., Mahadevan, L., . . . Sanson, B. (2009). Cell shape changes indicate a role for extrinsic tensile forces in Drosophila germ-band extension. *Nat Cell Biol, 11*(7), 859-864. doi: 10.1038/ncb1894
Butler, M. T., & Wallingford, J. B. (2017). Planar cell polarity in development and disease. *Nat Rev Mol Cell Biol, 18*(6), 375-388. doi: 10.1038/nrm.2017.11
Byers, B., & Porter, K. R. (1964). Oriented Microtubules in Elongating Cells of the Developing Lens Rudiment after Induction. *Proc Natl Acad Sci U S A, 52*, 1091-1099. doi: 10.1073/pnas.52.4.1091

Carlier, M. F. (1990). Actin polymerization and ATP hydrolysis. *Adv Biophys, 26*, 51-73. doi: 10.1016/0065-227x(90)90007-g
Carlsson, A. E., Wear, M. A., & Cooper, J. A. (2004). End versus side branching by Arp2/3 complex. *Biophys J, 86*(2), 1074-1081. doi: 10.1016/S0006-3495(04)74182-X
Carthew, R. W. (2001). Gene silencing by double-stranded RNA. *Curr Opin Cell Biol, 13*(2), 244-248. doi: 10.1016/s0955-0674(00)00204-0
Carvalho, A., Desai, A., & Oegema, K. (2009). Structural memory in the contractile ring makes the duration of cytokinesis independent of cell size. *Cell, 137*(5), 926-937. doi: 10.1016/j.cell.2009.03.021
Casella, J. F., Flanagan, M. D., & Lin, S. (1981). Cytochalasin D inhibits actin polymerization and induces depolymerization of actin filaments formed during platelet shape change. *Nature, 293*(5830), 302-305. doi: 10.1038/293302a0
Celniker, S. E., Wheeler, D. A., Kronmiller, B., Carlson, J. W., Halpern, A., Patel, S., . . . Rubin, G. M. (2002). Finishing a whole-genome shotgun: release 3 of the Drosophila melanogaster euchromatic genome sequence. *Genome Biol, 3*(12), RESEARCH0079. doi: 10.1186/gb-2002-3-12-research0079
Cereijido, M., Valdes, J., Shoshani, L., & Contreras, R. G. (1998). Role of tight junctions in establishing and maintaining cell polarity. *Annu Rev Physiol, 60*, 161-177. doi: 10.1146/annurev.physiol.60.1.161
Chae, J. J., & Tabor, M. (1997). Dynamics of foams with and without wall rupture. *Physical Review E, 55*, 598-610.
Chasan, R., Jin, Y., & Anderson, K. V. (1992). Activation of the easter zymogen is regulated by five other genes to define dorsal-ventral polarity in the Drosophila embryo. *Development, 115*(2), 607-616.
Chen, C. P., Posy, S., Ben-Shaul, A., Shapiro, L., & Honig, B. H. (2005). Specificity of cell-cell adhesion by classical cadherins: Critical role for low-affinity dimerization through beta-strand swapping. *Proc Natl Acad Sci U S A, 102*(24), 8531-8536. doi: 10.1073/pnas.0503319102
Chihara, D., & Nance, J. (2012). An E-cadherin-mediated hitchhiking mechanism for C. elegans germ cell internalization during gastrulation. *Development, 139*(14), 2547-2556. doi: 10.1242/dev.079863
Cho, Y. S., Stevens, L. M., Sieverman, K. J., Nguyen, J., & Stein, D. (2012). A ventrally localized protease in the Drosophila egg controls embryo dorsoventral polarity. *Curr Biol, 22*(11), 1013-1018. doi: 10.1016/j.cub.2012.03.065
Cho, Y. S., Stevens, L. M., & Stein, D. (2010). Pipe-dependent ventral processing of Easter by Snake is the defining step in Drosophila embryo DV axis formation. *Curr Biol, 20*(12), 1133-1137. doi: 10.1016/j.cub.2010.04.056
Choi, H. J., Pokutta, S., Cadwell, G. W., Bobkov, A. A., Bankston, L. A., Liddington, R. C., & Weis, W. I. (2012). alphaE-catenin is an autoinhibited molecule that coactivates vinculin. *Proc Natl Acad Sci U S A, 109*(22), 8576-8581. doi: 10.1073/pnas.1203906109
Chugh, P., & Paluch, E. K. (2018). The actin cortex at a glance. *J Cell Sci, 131*(14). doi: 10.1242/jcs.186254
Chung, M. I., Nascone-Yoder, N. M., Grover, S. A., Drysdale, T. A., & Wallingford, J. B. (2010). Direct activation of Shroom3 transcription by Pitx proteins drives epithelial morphogenesis in the developing gut. *Development, 137*(8), 1339-1349. doi: 10.1242/dev.044610
Clark, K., Middelbeek, J., Lasonder, E., Dulyaninova, N. G., Morrice, N. A., Ryazanov, A. G., . . . van Leeuwen, F. N. (2008). TRPM7 regulates myosin IIA filament stability and protein localization by heavy chain phosphorylation. *J Mol Biol, 378*(4), 790-803. doi: 10.1016/j.jmb.2008.02.057
Cohen, D., Brennwald, P. J., Rodriguez-Boulan, E., & Musch, A. (2004). Mammalian PAR-1 determines epithelial lumen polarity by organizing the microtubule cytoskeleton. *J Cell Biol, 164*(5), 717-727. doi: 10.1083/jcb.200308104
Cohen, S. M. (1993). *Imaginal disc development* (M. Bate & A. Martinez Arias Eds. Vol. 2): Cold Spring Harbor Laboratory Press.

Collinet, C., & Lecuit, T. (2021). Programmed and self-organized flow of information during morphogenesis. *Nat Rev Mol Cell Biol, 22*(4), 245-265. doi: 10.1038/s41580-020-00318-6

Collins, M. M., & Stainier, D. Y. (2016). Organ Function as a Modulator of Organ Formation: Lessons from Zebrafish. *Curr Top Dev Biol, 117*, 417-433. doi: 10.1016/bs.ctdb.2015.10.017

Costa, M., Sweeton, D., & Wieschaus, E. (1993). Gastrulation in Drosophila: Cellular Mechanisms of Morphogenetic Movements, the Development of Drosophila melanogaster. *Cold Spring Harbor Laboratory Press*, 425-466.

Costa, M., Wilson, E. T., & Wieschaus, E. (1994). A putative cell signal encoded by the folded gastrulation gene coordinates cell shape changes during Drosophila gastrulation. *Cell, 76*(6), 1075-1089. doi: 10.1016/0092-8674(94)90384-0

Craig, R., Smith, R., & Kendrick-Jones, J. (1983). Light-chain phosphorylation controls the conformation of vertebrate non-muscle and smooth muscle myosin molecules. *Nature, 302*(5907), 436-439. doi: 10.1038/302436a0

Dancker, P., Low, I., Hasselbach, W., & Wieland, T. (1975). Interaction of actin with phalloidin: polymerization and stabilization of F-actin. *Biochim Biophys Acta, 400*(2), 407-414. doi: 10.1016/0005-2795(75)90196-8

Daniel, E., Daude, M., Kolotuev, I., Charish, K., Auld, V., & Le Borgne, R. (2018). Coordination of Septate Junctions Assembly and Completion of Cytokinesis in Proliferative Epithelial Tissues. *Curr Biol, 28*(9), 1380-1391 e1384. doi: 10.1016/j.cub.2018.03.034

Das, D., Zalewski, J. K., Mohan, S., Plageman, T. F., VanDemark, A. P., & Hildebrand, J. D. (2014). The interaction between Shroom3 and Rho-kinase is required for neural tube morphogenesis in mice. *Biol Open, 3*(9), 850-860. doi: 10.1242/bio.20147450

Davidson, L. A., Hoffstrom, B. G., Keller, R., & DeSimone, D. W. (2002). Mesendoderm extension and mantle closure in Xenopus laevis gastrulation: combined roles for integrin alpha(5)beta(1), fibronectin, and tissue geometry. *Dev Biol, 242*(2), 109-129. doi: 10.1006/dbio.2002.0537

Dawes-Hoang, R. E., Parmar, K. M., Christiansen, A. E., Phelps, C. B., Brand, A. H., & Wieschaus, E. F. (2005). folded gastrulation, cell shape change and the control of myosin localization. *Development, 132*(18), 4165-4178. doi: 10.1242/dev.01938

Dean, S. O., Rogers, S. L., Stuurman, N., Vale, R. D., & Spudich, J. A. (2005). Distinct pathways control recruitment and maintenance of myosin II at the cleavage furrow during cytokinesis. *Proc Natl Acad Sci U S A, 102*(38), 13473-13478. doi: 10.1073/pnas.0506810102

Deisboeck, T. S., & Couzin, I. D. (2009). Collective behavior in cancer cell populations. *Bioessays, 31*(2), 190-197. doi: 10.1002/bies.200800084

Denk-Lobnig, M., & Martin, A. C. (2020). Divergent and combinatorial mechanical strategies that promote epithelial folding during morphogenesis. *Curr Opin Genet Dev, 63*, 24-29. doi: 10.1016/j.gde.2020.02.014

Dietzl, G., Chen, D., Schnorrer, F., Su, K. C., Barinova, Y., Fellner, M., . . . Dickson, B. J. (2007). A genome-wide transgenic RNAi library for conditional gene inactivation in Drosophila. *Nature, 448*(7150), 151-156. doi: 10.1038/nature05954

Doerflinger, H., Benton, R., Shulman, J. M., & St Johnston, D. (2003). The role of PAR-1 in regulating the polarised microtubule cytoskeleton in the Drosophila follicular epithelium. *Development, 130*(17), 3965-3975. doi: 10.1242/dev.00616

Doerflinger, H., Vogt, N., Torres, I. L., Mirouse, V., Koch, I., Nusslein-Volhard, C., & St Johnston, D. (2010). Bazooka is required for polarisation of the Drosophila anterior-posterior axis. *Development, 137*(10), 1765-1773. doi: 10.1242/dev.045807

Dominguez, R. (2009). Actin filament nucleation and elongation factors--structure-function relationships. *Crit Rev Biochem Mol Biol, 44*(6), 351-366. doi: 10.3109/10409230903277340

Dominguez, R., & Holmes, K. C. (2011). Actin structure and function. *Annu Rev Biophys, 40*, 169-186. doi: 10.1146/annurev-biophys-042910-155359

Drees, F., Pokutta, S., Yamada, S., Nelson, W. J., & Weis, W. I. (2005). Alpha-catenin is a molecular switch that binds E-cadherin-beta-catenin and regulates actin-filament assembly. *Cell, 123*(5), 903-915. doi: 10.1016/j.cell.2005.09.021

Driever, W., & Nusslein-Volhard, C. (1988a). The bicoid protein determines position in the Drosophila embryo in a concentration-dependent manner. *Cell, 54*(1), 95-104. doi: 10.1016/0092-8674(88)90183-3

Driever, W., & Nusslein-Volhard, C. (1988b). A gradient of bicoid protein in Drosophila embryos. *Cell, 54*(1), 83-93. doi: 10.1016/0092-8674(88)90182-1

Driever, W., & Nusslein-Volhard, C. (1989). The bicoid protein is a positive regulator of hunchback transcription in the early Drosophila embryo. *Nature, 337*(6203), 138-143. doi: 10.1038/337138a0

Driever, W., Siegel, V., & Nusslein-Volhard, C. (1990). Autonomous determination of anterior structures in the early Drosophila embryo by the bicoid morphogen. *Development, 109*(4), 811-820.

Driever, W., Thoma, G., & Nusslein-Volhard, C. (1989). Determination of spatial domains of zygotic gene expression in the Drosophila embryo by the affinity of binding sites for the bicoid morphogen. *Nature, 340*(6232), 363-367. doi: 10.1038/340363a0

Drubin, D. G., & Nelson, W. J. (1996). Origins of cell polarity. *Cell, 84*(3), 335-344. doi: 10.1016/s0092-8674(00)81278-7

Dulyaninova, N. G., Malashkevich, V. N., Almo, S. C., & Bresnick, A. R. (2005). Regulation of myosin-IIA assembly and Mts1 binding by heavy chain phosphorylation. *Biochemistry, 44*(18), 6867-6876. doi: 10.1021/bi0500776

Edgar, B. A., Kiehle, C. P., & Schubiger, G. (1986). Cell cycle control by the nucleo-cytoplasmic ratio in early Drosophila development. *Cell, 44*(2), 365-372. doi: 10.1016/0092-8674(86)90771-3

Edgar, B. A., & Schubiger, G. (1986). Parameters controlling transcriptional activation during early Drosophila development. *Cell, 44*(6), 871-877. doi: 10.1016/0092-8674(86)90009-7

Egelhoff, T. T., Lee, R. J., & Spudich, J. A. (1993). Dictyostelium myosin heavy chain phosphorylation sites regulate myosin filament assembly and localization in vivo. *Cell, 75*(2), 363-371. doi: 10.1016/0092-8674(93)80077-r

Eisenhoffer, G. T., Loftus, P. D., Yoshigi, M., Otsuna, H., Chien, C. B., Morcos, P. A., & Rosenblatt, J. (2012). Crowding induces live cell extrusion to maintain homeostatic cell numbers in epithelia. *Nature, 484*(7395), 546-549. doi: 10.1038/nature10999

Elliott, D. A., & Brand, A. H. (2008). The GAL4 system : a versatile system for the expression of genes. *Methods Mol Biol, 420*, 79-95. doi: 10.1007/978-1-59745-583-1_5

Elsum, I., Yates, L., Humbert, P. O., & Richardson, H. E. (2012). The Scribble-Dlg-Lgl polarity module in development and cancer: from flies to man. *Essays Biochem, 53*, 141-168. doi: 10.1042/bse0530141

Elul, T., Koehl, M. A., & Keller, R. (1997). Cellular mechanism underlying neural convergent extension in Xenopus laevis embryos. *Dev Biol, 191*(2), 243-258. doi: 10.1006/dbio.1997.8711

Elul, T., Koehl, M. A., & Keller, R. E. (1998). Patterning of morphogenetic cell behaviors in neural ectoderm of Xenopus laevis. *Ann N Y Acad Sci, 857*, 248-251. doi: 10.1111/j.1749-6632.1998.tb10124.x

Ephrussi, A., Dickinson, L. K., & Lehmann, R. (1991). Oskar organizes the germ plasm and directs localization of the posterior determinant nanos. *Cell, 66*(1), 37-50. doi: 10.1016/0092-8674(91)90137-n

Ernst, S., Liu, K., Agarwala, S., Moratscheck, N., Avci, M. E., Dalle Nogare, D., . . . Lecaudey, V. (2012). Shroom3 is required downstream of FGF signalling to mediate proneuromast assembly in zebrafish. *Development, 139*(24), 4571-4581. doi: 10.1242/dev.083253

Escuin, S., Vernay, B., Savery, D., Gurniak, C. B., Witke, W., Greene, N. D., & Copp, A. J. (2015). Rho-kinase-dependent actin turnover and actomyosin disassembly are

necessary for mouse spinal neural tube closure. *J Cell Sci, 128*(14), 2468-2481. doi: 10.1242/jcs.164574
Even-Faitelson, L., & Ravid, S. (2006). PAK1 and aPKCzeta regulate myosin II-B phosphorylation: a novel signaling pathway regulating filament assembly. *Mol Biol Cell, 17*(7), 2869-2881. doi: 10.1091/mbc.e05-11-1001
Eyal-Giladi, H., & Kochav, S. (1976). From cleavage to primitive streak formation: a complementary normal table and a new look at the first stages of the development of the chick. I. General morphology. *Dev Biol, 49*(2), 321-337. doi: 10.1016/0012-1606(76)90178-0
Farquhar, M. G., & Palade, G. E. (1963). Junctional complexes in various epithelia. *J Cell Biol, 17*, 375-412. doi: 10.1083/jcb.17.2.375
Fernandez-Gonzalez, R., Simoes Sde, M., Roper, J. C., Eaton, S., & Zallen, J. A. (2009). Myosin II dynamics are regulated by tension in intercalating cells. *Dev Cell, 17*(5), 736-743. doi: 10.1016/j.devcel.2009.09.003
Figard, L., Xu, H., Garcia, H. G., Golding, I., & Sokac, A. M. (2013). The plasma membrane flattens out to fuel cell-surface growth during Drosophila cellularization. *Dev Cell, 27*(6), 648-655. doi: 10.1016/j.devcel.2013.11.006
Fleming, T. P., Ghassemifar, M. R., & Sheth, B. (2000). Junctional complexes in the early mammalian embryo. *Semin Reprod Med, 18*(2), 185-193. doi: 10.1055/s-2000-12557
Foe, V. E. (1989). Mitotic domains reveal early commitment of cells in Drosophila embryos. *Development, 107*(1), 1-22.
Foe, V. E., & Alberts, B. M. (1983). Studies of nuclear and cytoplasmic behaviour during the five mitotic cycles that precede gastrulation in Drosophila embryogenesis. *J Cell Sci, 61*, 31-70.
Foe, V. E., & von Dassow, G. (2008). Stable and dynamic microtubules coordinately shape the myosin activation zone during cytokinetic furrow formation. *J Cell Biol, 183*(3), 457-470. doi: 10.1083/jcb.200807128
Frigerio, G., Burri, M., Bopp, D., Baumgartner, S., & Noll, M. (1986). Structure of the segmentation gene paired and the Drosophila PRD gene set as part of a gene network. *Cell, 47*(5), 735-746. doi: 10.1016/0092-8674(86)90516-7
Fristrom, D. (1988). The cellular basis of epithelial morphogenesis. A review. *Tissue Cell, 20*(5), 645-690. doi: 10.1016/0040-8166(88)90015-8
Frohnhofer, H. G., Lehmann, R., & Nusslein-Volhard, C. (1986). Manipulating the anteroposterior pattern of the Drosophila embryo. *J Embryol Exp Morphol, 97 Suppl*, 169-179.
Fuchs, A., Cheung, L. S., Charbonnier, E., Shvartsman, S. Y., & Pyrowolakis, G. (2012). Transcriptional interpretation of the EGF receptor signaling gradient. *Proc Natl Acad Sci U S A, 109*(5), 1572-1577. doi: 10.1073/pnas.1115190109
Fukata, M., & Kaibuchi, K. (2001). Rho-family GTPases in cadherin-mediated cell-cell adhesion. *Nat Rev Mol Cell Biol, 2*(12), 887-897. doi: 10.1038/35103068
Fukuhara, T., Shimizu, K., Kawakatsu, T., Fukuyama, T., Minami, Y., Honda, T., . . . Takai, Y. (2004). Activation of Cdc42 by trans interactions of the cell adhesion molecules nectins through c-Src and Cdc42-GEF FRG. *J Cell Biol, 166*(3), 393-405. doi: 10.1083/jcb.200401093
Gallin, W. J., Edelman, G. M., & Cunningham, B. A. (1983). Characterization of L-CAM, a major cell adhesion molecule from embryonic liver cells. *Proc Natl Acad Sci U S A, 80*(4), 1038-1042. doi: 10.1073/pnas.80.4.1038
Garcia De Las Bayonas, A., Philippe, J. M., Lellouch, A. C., & Lecuit, T. (2019). Distinct RhoGEFs Activate Apical and Junctional Contractility under Control of G Proteins during Epithelial Morphogenesis. *Curr Biol, 29*(20), 3370-3385 e3377. doi: 10.1016/j.cub.2019.08.017
Gastrulation: From Cells to Embryo. (2004). Cold Spring Harbor Laboratory Press.
Gavis, E. R. (1995). Pattern formation. Gurken meets torpedo for the first time. *Curr Biol, 5*(11), 1252-1254. doi: 10.1016/s0960-9822(95)00250-8
Gavis, E. R., & Lehmann, R. (1992). Localization of nanos RNA controls embryonic polarity. *Cell, 71*(2), 301-313. doi: 10.1016/0092-8674(92)90358-j

Gheisari, E., Aakhte, M., & Muller, H. J. (2020). Gastrulation in Drosophila melanogaster: Genetic control, cellular basis and biomechanics. *Mech Dev, 163*, 103629. doi: 10.1016/j.mod.2020.103629

Giancotti, F. G., & Ruoslahti, E. (1999). Integrin signaling. *Science, 285*(5430), 1028-1032. doi: 10.1126/science.285.5430.1028

Gibson, W. T., & Gibson, M. C. (2009). Cell topology, geometry, and morphogenesis in proliferating epithelia. *Curr Top Dev Biol, 89*, 87-114. doi: 10.1016/S0070-2153(09)89004-2

Gillard, G., & Roper, K. (2020). Control of cell shape during epithelial morphogenesis: recent advances. *Curr Opin Genet Dev, 63*, 1-8. doi: 10.1016/j.gde.2020.01.003

Gilmour, D., Rembold, M., & Leptin, M. (2017). From morphogen to morphogenesis and back. *Nature, 541*(7637), 311-320. doi: 10.1038/nature21348

Gittes, F., Mickey, B., Nettleton, J., & Howard, J. (1993). Flexural rigidity of microtubules and actin filaments measured from thermal fluctuations in shape. *J Cell Biol, 120*(4), 923-934. doi: 10.1083/jcb.120.4.923

Glickman, N. S., Kimmel, C. B., Jones, M. A., & Adams, R. J. (2003). Shaping the zebrafish notochord. *Development, 130*(5), 873-887. doi: 10.1242/dev.00314

Gonzalez-Reyes, A., Elliott, H., & St Johnston, D. (1995). Polarization of both major body axes in Drosophila by gurken-torpedo signalling. *Nature, 375*(6533), 654-658. doi: 10.1038/375654a0

Goode, B. L., & Eck, M. J. (2007). Mechanism and function of formins in the control of actin assembly. *Annu Rev Biochem, 76*, 593-627. doi: 10.1146/annurev.biochem.75.103004.142647

Goodson, H. V., & Jonasson, E. M. (2018). Microtubules and Microtubule-Associated Proteins. *Cold Spring Harb Perspect Biol, 10*(6). doi: 10.1101/cshperspect.a022608

Green, J. B., & Sharpe, J. (2015). Positional information and reaction-diffusion: two big ideas in developmental biology combine. *Development, 142*(7), 1203-1211. doi: 10.1242/dev.114991

Guichet, A., Peri, F., & Roth, S. (2001). Stable anterior anchoring of the oocyte nucleus is required to establish dorsoventral polarity of the Drosophila egg. *Dev Biol, 237*(1), 93-106. doi: 10.1006/dbio.2001.0354

Gumbiner, B. M. (2000). Regulation of cadherin adhesive activity. *J Cell Biol, 148*(3), 399-404. doi: 10.1083/jcb.148.3.399

Gutzman, J. H., Graeden, E. G., Lowery, L. A., Holley, H. S., & Sive, H. (2008). Formation of the zebrafish midbrain-hindbrain boundary constriction requires laminin-dependent basal constriction. *Mech Dev, 125*(11-12), 974-983. doi: 10.1016/j.mod.2008.07.004

Hacker, U., & Perrimon, N. (1998). DRhoGEF2 encodes a member of the Dbl family of oncogenes and controls cell shape changes during gastrulation in Drosophila. *Genes Dev, 12*(2), 274-284. doi: 10.1101/gad.12.2.274

Halbleib, J. M., & Nelson, W. J. (2006). Cadherins in development: cell adhesion, sorting, and tissue morphogenesis. *Genes Dev, 20*(23), 3199-3214. doi: 10.1101/gad.1486806

Hales, K. G., Korey, C. A., Larracuente, A. M., & Roberts, D. M. (2015). Genetics on the Fly: A Primer on the Drosophila Model System. *Genetics, 201*(3), 815-842. doi: 10.1534/genetics.115.183392

Hardin, J. (1989). Local shifts in position and polarized motility drive cell rearrangement during sea urchin gastrulation. *Dev Biol, 136*(2), 430-445. doi: 10.1016/0012-1606(89)90268-6

Harris, T. J., & Tepass, U. (2010). Adherens junctions: from molecules to morphogenesis. *Nat Rev Mol Cell Biol, 11*(7), 502-514. doi: 10.1038/nrm2927

Hartenstein, V. C.-O., J. A. (1985). Fate-mapping in wild-type Drosophila melanogaster. *Roux's Arch Dev Biol*(194), 181-195.

Hartman, M. A., Finan, D., Sivaramakrishnan, S., & Spudich, J. A. (2011). Principles of unconventional myosin function and targeting. *Annu Rev Cell Dev Biol, 27*, 133-155. doi: 10.1146/annurev-cellbio-100809-151502

Hashimoto, C., Gerttula, S., & Anderson, K. V. (1991). Plasma membrane localization of the Toll protein in the syncytial Drosophila embryo: importance of transmembrane signaling for dorsal-ventral pattern formation. *Development, 111*(4), 1021-1028.

Hashimoto, C., Hudson, K. L., & Anderson, K. V. (1988). The Toll gene of Drosophila, required for dorsal-ventral embryonic polarity, appears to encode a transmembrane protein. *Cell, 52*(2), 269-279. doi: 10.1016/0092-8674(88)90516-8

Hawkins, T., Mirigian, M., Selcuk Yasar, M., & Ross, J. L. (2010). Mechanics of microtubules. *J Biomech, 43*(1), 23-30. doi: 10.1016/j.jbiomech.2009.09.005

Hayashi, T., & Carthew, R. W. (2004). Surface mechanics mediate pattern formation in the developing retina. *Nature, 431*(7009), 647-652. doi: 10.1038/nature02952

Hayes, P., & Solon, J. (2017). Drosophila dorsal closure: An orchestra of forces to zip shut the embryo. *Mech Dev, 144*(Pt A), 2-10. doi: 10.1016/j.mod.2016.12.005

Heer, N. C., Miller, P. W., Chanet, S., Stoop, N., Dunkel, J., & Martin, A. C. (2017). Actomyosin-based tissue folding requires a multicellular myosin gradient. *Development, 144*(10), 1876-1886. doi: 10.1242/dev.146761

Heisenberg, C. P. (2009). Dorsal closure in Drosophila: cells cannot get out of the tight spot. *Bioessays, 31*(12), 1284-1287. doi: 10.1002/bies.200900109

Heisenberg, C. P. (2017). D'Arcy Thompson's 'on Growth and form': From soap bubbles to tissue self-organization. *Mech Dev, 145*, 32-37. doi: 10.1016/j.mod.2017.03.006

Heisenberg, C. P., & Bellaiche, Y. (2013). Forces in tissue morphogenesis and patterning. *Cell, 153*(5), 948-962. doi: 10.1016/j.cell.2013.05.008

Heissler, S. M., & Sellers, J. R. (2016). Various Themes of Myosin Regulation. *J Mol Biol, 428*(9 Pt B), 1927-1946. doi: 10.1016/j.jmb.2016.01.022

Herrmann, H., & Aebi, U. (1998). Structure, assembly, and dynamics of intermediate filaments. *Subcell Biochem, 31*, 319-362.

Herrmann, H., & Aebi, U. (2004). Intermediate filaments: molecular structure, assembly mechanism, and integration into functionally distinct intracellular Scaffolds. *Annu Rev Biochem, 73*, 749-789. doi: 10.1146/annurev.biochem.73.011303.073823

Herrmann, H., & Aebi, U. (2016). Intermediate Filaments: Structure and Assembly. *Cold Spring Harb Perspect Biol, 8*(11). doi: 10.1101/cshperspect.a018242

Hildebrand, J. D. (2005). Shroom regulates epithelial cell shape via the apical positioning of an actomyosin network. *J Cell Sci, 118*(Pt 22), 5191-5203. doi: 10.1242/jcs.02626

Hirano, S., Nose, A., Hatta, K., Kawakami, A., & Takeichi, M. (1987). Calcium-dependent cell-cell adhesion molecules (cadherins): subclass specificities and possible involvement of actin bundles. *J Cell Biol, 105*(6 Pt 1), 2501-2510. doi: 10.1083/jcb.105.6.2501

Hirata, N., Takahashi, M., & Yazawa, M. (2009). Diphosphorylation of regulatory light chain of myosin IIA is responsible for proper cell spreading. *Biochem Biophys Res Commun, 381*(4), 682-687. doi: 10.1016/j.bbrc.2009.02.121

Hobmayer, B., Rentzsch, F., Kuhn, K., Happel, C. M., von Laue, C. C., Snyder, P., . . . Holstein, T. W. (2000). WNT signalling molecules act in axis formation in the diploblastic metazoan Hydra. *Nature, 407*(6801), 186-189. doi: 10.1038/35025063

Hogan, B. L. (1999). Morphogenesis. *Cell, 96*(2), 225-233. doi: 10.1016/s0092-8674(00)80562-0

Homem, C. C., & Peifer, M. (2008). Diaphanous regulates myosin and adherens junctions to control cell contractility and protrusive behavior during morphogenesis. *Development, 135*(6), 1005-1018. doi: 10.1242/dev.016337

Hong, C. C., & Hashimoto, C. (1995). An unusual mosaic protein with a protease domain, encoded by the nudel gene, is involved in defining embryonic dorsoventral polarity in Drosophila. *Cell, 82*(5), 785-794. doi: 10.1016/0092-8674(95)90475-1

Hong, E., & Brewster, R. (2006). N-cadherin is required for the polarized cell behaviors that drive neurulation in the zebrafish. *Development, 133*(19), 3895-3905. doi: 10.1242/dev.02560

Hong, J. W., Hendrix, D. A., Papatsenko, D., & Levine, M. S. (2008). How the Dorsal gradient works: insights from postgenome technologies. *Proc Natl Acad Sci U S A, 105*(51), 20072-20076. doi: 10.1073/pnas.0806476105

Hong, Y., Stronach, B., Perrimon, N., Jan, L. Y., & Jan, Y. N. (2001). Drosophila Stardust interacts with Crumbs to control polarity of epithelia but not neuroblasts. *Nature, 414*(6864), 634-638. doi: 10.1038/414634a

Horwitz, R., & Webb, D. (2003). Cell migration. *Curr Biol, 13*(19), R756-759. doi: 10.1016/j.cub.2003.09.014

Hoskins, R. A., Carlson, J. W., Kennedy, C., Acevedo, D., Evans-Holm, M., Frise, E., . . . Celniker, S. E. (2007). Sequence finishing and mapping of Drosophila melanogaster heterochromatin. *Science, 316*(5831), 1625-1628. doi: 10.1126/science.1139816

Hou, J. (2019). *Paracellular Channel Evolution*: Academic Press.

Houdusse, A., & Sweeney, H. L. (2016). How Myosin Generates Force on Actin Filaments. *Trends Biochem Sci, 41*(12), 989-997. doi: 10.1016/j.tibs.2016.09.006

Hunter, C., Sung, P., Schejter, E. D., & Wieschaus, E. (2002). Conserved domains of the Nullo protein required for cell-surface localization and formation of adherens junctions. *Mol Biol Cell, 13*(1), 146-157. doi: 10.1091/mbc.01-08-0418

Hunter, C., & Wieschaus, E. (2000). Regulated expression of nullo is required for the formation of distinct apical and basal adherens junctions in the Drosophila blastoderm. *J Cell Biol, 150*(2), 391-401. doi: 10.1083/jcb.150.2.391

Hurd, T. W., Fan, S., Liu, C. J., Kweon, H. K., Hakansson, K., & Margolis, B. (2003). Phosphorylation-dependent binding of 14-3-3 to the polarity protein Par3 regulates cell polarity in mammalian epithelia. *Curr Biol, 13*(23), 2082-2090. doi: 10.1016/j.cub.2003.11.020

Hurov, J. B., Watkins, J. L., & Piwnica-Worms, H. (2004). Atypical PKC phosphorylates PAR-1 kinases to regulate localization and activity. *Curr Biol, 14*(8), 736-741. doi: 10.1016/j.cub.2004.04.007

Hutterer, A., Betschinger, J., Petronczki, M., & Knoblich, J. A. (2004). Sequential roles of Cdc42, Par-6, aPKC, and Lgl in the establishment of epithelial polarity during Drosophila embryogenesis. *Dev Cell, 6*(6), 845-854. doi: 10.1016/j.devcel.2004.05.003

Huveneers, S., Oldenburg, J., Spanjaard, E., van der Krogt, G., Grigoriev, I., Akhmanova, A., . . . de Rooij, J. (2012). Vinculin associates with endothelial VE-cadherin junctions to control force-dependent remodeling. *J Cell Biol, 196*(5), 641-652. doi: 10.1083/jcb.201108120

Huxley, A. F., & Niedergerke, R. (1954a). Measurement of muscle striations in stretch and contraction. *J Physiol, 124*(2), 46-47P.

Huxley, A. F., & Niedergerke, R. (1954b). Structural changes in muscle during contraction; interference microscopy of living muscle fibres. *Nature, 173*(4412), 971-973. doi: 10.1038/173971a0

Huxley, A. F., & Tideswell, S. (1996). Filament compliance and tension transients in muscle. *J Muscle Res Cell Motil, 17*(4), 507-511. doi: 10.1007/BF00123366

Huxley, H. E., & Hanson, J. (1957). Quantitative studies on the structure of cross-striated myofibrils. I. Investigations by interference microscopy. *Biochim Biophys Acta, 23*(2), 229-249. doi: 10.1016/0006-3002(57)90325-6

Huzita, H., & Scimemi, B. (1989). The Algebra of Paper-folding (Origami). *Proceedings of the First International Meeting of Origami Science and Technology*, 205–222.

Ip, Y. T., Maggert, K., & Levine, M. (1994). Uncoupling gastrulation and mesoderm differentiation in the Drosophila embryo. *EMBO J, 13*(24), 5826-5834.

Ip, Y. T., Park, R. E., Kosman, D., Yazdanbakhsh, K., & Levine, M. (1992). dorsal-twist interactions establish snail expression in the presumptive mesoderm of the Drosophila embryo. *Genes Dev, 6*(8), 1518-1530. doi: 10.1101/gad.6.8.1518

Irvine, K. D., & Wieschaus, E. (1994). Cell intercalation during Drosophila germband extension and its regulation by pair-rule segmentation genes. *Development, 120*(4), 827-841.

Ito, M., Nakano, T., Erdodi, F., & Hartshorne, D. J. (2004). Myosin phosphatase: structure, regulation and function. *Mol Cell Biochem, 259*(1-2), 197-209. doi: 10.1023/b:mcbi.0000021373.14288.00
Jaeger, J. (2011). The gap gene network. *Cell Mol Life Sci, 68*(2), 243-274. doi: 10.1007/s00018-010-0536-y
Jiang, J., & Levine, M. (1993). Binding affinities and cooperative interactions with bHLH activators delimit threshold responses to the dorsal gradient morphogen. *Cell, 72*(5), 741-752. doi: 10.1016/0092-8674(93)90402-c
Julian, L., & Olson, M. F. (2014). Rho-associated coiled-coil containing kinases (ROCK): structure, regulation, and functions. *Small GTPases, 5*, e29846. doi: 10.4161/sgtp.29846
Jung, H. S., Komatsu, S., Ikebe, M., & Craig, R. (2008). Head-head and head-tail interaction: a general mechanism for switching off myosin II activity in cells. *Mol Biol Cell, 19*(8), 3234-3242. doi: 10.1091/mbc.E08-02-0206
Kam, Z., Minden, J. S., Agard, D. A., Sedat, J. W., & Leptin, M. (1991). Drosophila gastrulation: analysis of cell shape changes in living embryos by three-dimensional fluorescence microscopy. *Development, 112*(2), 365-370.
Kamijo, K., Ohara, N., Abe, M., Uchimura, T., Hosoya, H., Lee, J. S., & Miki, T. (2006). Dissecting the role of Rho-mediated signaling in contractile ring formation. *Mol Biol Cell, 17*(1), 43-55. doi: 10.1091/mbc.e05-06-0569
Kanellos, G., & Frame, M. C. (2016). Cellular functions of the ADF/cofilin family at a glance. *J Cell Sci, 129*(17), 3211-3218. doi: 10.1242/jcs.187849
Kasza, K. E., & Zallen, J. A. (2011). Dynamics and regulation of contractile actin-myosin networks in morphogenesis. *Curr Opin Cell Biol, 23*(1), 30-38. doi: 10.1016/j.ceb.2010.10.014
Keller, R. (2002). Shaping the vertebrate body plan by polarized embryonic cell movements. *Science, 298*(5600), 1950-1954. doi: 10.1126/science.1079478
Keller, R. (2012). Developmental biology. Physical biology returns to morphogenesis. *Science, 338*(6104), 201-203. doi: 10.1126/science.1230718
Keller, R., Shih, J., & Sater, A. (1992). The cellular basis of the convergence and extension of the Xenopus neural plate. *Dev Dyn, 193*(3), 199-217. doi: 10.1002/aja.1001930302
Keller, R. E. (1981). An experimental analysis of the role of bottle cells and the deep marginal zone in gastrulation of Xenopus laevis. *J Exp Zool, 216*(1), 81-101. doi: 10.1002/jez.1402160109
Kidd, S. (1992). Characterization of the Drosophila cactus locus and analysis of interactions between cactus and dorsal proteins. *Cell, 71*(4), 623-635. doi: 10.1016/0092-8674(92)90596-5
Kimberly, E. L., & Hardin, J. (1998). Bottle cells are required for the initiation of primary invagination in the sea urchin embryo. *Dev Biol, 204*(1), 235-250. doi: 10.1006/dbio.1998.9075
King, N., Hittinger, C. T., & Carroll, S. B. (2003). Evolution of key cell signaling and adhesion protein families predates animal origins. *Science, 301*(5631), 361-363. doi: 10.1126/science.1083853
Klingler, M., Erdelyi, M., Szabad, J., & Nusslein-Volhard, C. (1988). Function of torso in determining the terminal anlagen of the Drosophila embryo. *Nature, 335*(6187), 275-277. doi: 10.1038/335275a0
Knight, A. E., Veigel, C., Chambers, C., & Molloy, J. E. (2001). Analysis of single-molecule mechanical recordings: application to acto-myosin interactions. *Prog Biophys Mol Biol, 77*(1), 45-72. doi: 10.1016/s0079-6107(01)00010-4
Kolsch, V., Seher, T., Fernandez-Ballester, G. J., Serrano, L., & Leptin, M. (2007). Control of Drosophila gastrulation by apical localization of adherens junctions and RhoGEF2. *Science, 315*(5810), 384-386. doi: 10.1126/science.1134833
Kondo, T., & Hayashi, S. (2015). Mechanisms of cell height changes that mediate epithelial invagination. *Dev Growth Differ, 57*(4), 313-323. doi: 10.1111/dgd.12224

Kong, D., Wolf, F., & Grosshans, J. (2017). Forces directing germ-band extension in Drosophila embryos. *Mech Dev, 144*(Pt A), 11-22. doi: 10.1016/j.mod.2016.12.001

Korn, E. D., Carlier, M. F., & Pantaloni, D. (1987). Actin polymerization and ATP hydrolysis. *Science, 238*(4827), 638-644. doi: 10.1126/science.3672117

Kuchinke, U., Grawe, F., & Knust, E. (1998). Control of spindle orientation in Drosophila by the Par-3-related PDZ-domain protein Bazooka. *Curr Biol, 8*(25), 1357-1365. doi: 10.1016/s0960-9822(98)00016-5

Lang, R. A., Herman, K., Reynolds, A. B., Hildebrand, J. D., & Plageman, T. F., Jr. (2014). p120-catenin-dependent junctional recruitment of Shroom3 is required for apical constriction during lens pit morphogenesis. *Development, 141*(16), 3177-3187. doi: 10.1242/dev.107433

Laprise, P., Lau, K. M., Harris, K. P., Silva-Gagliardi, N. F., Paul, S. M., Beronja, S., . . . Tepass, U. (2009). Yurt, Coracle, Neurexin IV and the Na(+),K(+)-ATPase form a novel group of epithelial polarity proteins. *Nature, 459*(7250), 1141-1145. doi: 10.1038/nature08067

Lavalou, J., Mao, Q., Harmansa, S., Kerridge, S., Lellouch, A. C., Philippe, J. M., . . . Lecuit, T. (2021). Formation of polarized contractile interfaces by self-organized Toll-8/Cirl GPCR asymmetry. *Dev Cell, 56*(11), 1574-1588 e1577. doi: 10.1016/j.devcel.2021.03.030

Lawrence, P. A. (2001). Morphogens: how big is the big picture? *Nat Cell Biol, 3*(7), E151-154. doi: 10.1038/35083096

le Duc, Q., Shi, Q., Blonk, I., Sonnenberg, A., Wang, N., Leckband, D., & de Rooij, J. (2010). Vinculin potentiates E-cadherin mechanosensing and is recruited to actin-anchored sites within adherens junctions in a myosin II-dependent manner. *J Cell Biol, 189*(7), 1107-1115. doi: 10.1083/jcb.201001149

Lecaudey, V., & Gilmour, D. (2006). Organizing moving groups during morphogenesis. *Curr Opin Cell Biol, 18*(1), 102-107. doi: 10.1016/j.ceb.2005.12.001

Lecuit, T. (2004). Junctions and vesicular trafficking during Drosophila cellularization. *J Cell Sci, 117*(Pt 16), 3427-3433. doi: 10.1242/jcs.01312

Lecuit, T., Lenne, P. F., & Munro, E. (2011). Force generation, transmission, and integration during cell and tissue morphogenesis. *Annu Rev Cell Dev Biol, 27*, 157-184. doi: 10.1146/annurev-cellbio-100109-104027

Lecuit, T., Samanta, R., & Wieschaus, E. (2002). slam encodes a developmental regulator of polarized membrane growth during cleavage of the Drosophila embryo. *Dev Cell, 2*(4), 425-436. doi: 10.1016/s1534-5807(02)00141-7

Lecuit, T., & Wieschaus, E. (2000). Polarized insertion of new membrane from a cytoplasmic reservoir during cleavage of the Drosophila embryo. *J Cell Biol, 150*(4), 849-860. doi: 10.1083/jcb.150.4.849

Lee, C., Le, M. P., & Wallingford, J. B. (2009). The shroom family proteins play broad roles in the morphogenesis of thickened epithelial sheets. *Dev Dyn, 238*(6), 1480-1491. doi: 10.1002/dvdy.21942

Lee, J. Y., & Goldstein, B. (2003). Mechanisms of cell positioning during C. elegans gastrulation. *Development, 130*(2), 307-320. doi: 10.1242/dev.00211

Lee, O. K., Frese, K. K., James, J. S., Chadda, D., Chen, Z. H., Javier, R. T., & Cho, K. O. (2003). Discs-Large and Strabismus are functionally linked to plasma membrane formation. *Nat Cell Biol, 5*(11), 987-993. doi: 10.1038/ncb1055

Leerberg, J. M., Gomez, G. A., Verma, S., Moussa, E. J., Wu, S. K., Priya, R., . . . Yap, A. S. (2014). Tension-sensitive actin assembly supports contractility at the epithelial zonula adherens. *Curr Biol, 24*(15), 1689-1699. doi: 10.1016/j.cub.2014.06.028

Lehmann, R., & Nusslein-Volhard, C. (1986). Abdominal segmentation, pole cell formation, and embryonic polarity require the localized activity of oskar, a maternal gene in Drosophila. *Cell, 47*(1), 141-152. doi: 10.1016/0092-8674(86)90375-2

Lehmann, R., & Nusslein-Volhard, C. (1987). hunchback, a gene required for segmentation of an anterior and posterior region of the Drosophila embryo. *Dev Biol, 119*(2), 402-417. doi: 10.1016/0012-1606(87)90045-5

Lehmann, R., & Nusslein-Volhard, C. (1991). The maternal gene nanos has a central role in posterior pattern formation of the Drosophila embryo. *Development, 112*(3), 679-691.
LeMosy, E. K., Tan, Y. Q., & Hashimoto, C. (2001). Activation of a protease cascade involved in patterning the Drosophila embryo. *Proc Natl Acad Sci U S A, 98*(9), 5055-5060. doi: 10.1073/pnas.081026598
Leptin, M. (1991). twist and snail as positive and negative regulators during Drosophila mesoderm development. *Genes Dev, 5*(9), 1568-1576. doi: 10.1101/gad.5.9.1568
Leptin, M. (1999). Gastrulation in Drosophila: the logic and the cellular mechanisms. *EMBO J, 18*(12), 3187-3192. doi: 10.1093/emboj/18.12.3187
Leptin, M. (2005). Gastrulation movements: the logic and the nuts and bolts. *Dev Cell, 8*(3), 305-320. doi: 10.1016/j.devcel.2005.02.007
Leptin, M., & Grunewald, B. (1990). Cell shape changes during gastrulation in Drosophila. *Development, 110*(1), 73-84.
Leung, T., Chen, X. Q., Tan, I., Manser, E., & Lim, L. (1998). Myotonic dystrophy kinase-related Cdc42-binding kinase acts as a Cdc42 effector in promoting cytoskeletal reorganization. *Mol Cell Biol, 18*(1), 130-140. doi: 10.1128/MCB.18.1.130
Levayer, R., & Lecuit, T. (2012). Biomechanical regulation of contractility: spatial control and dynamics. *Trends Cell Biol, 22*(2), 61-81. doi: 10.1016/j.tcb.2011.10.001
Levi, S., Polyakov, M. V., & Egelhoff, T. T. (2002). Myosin II dynamics in Dictyostelium: determinants for filament assembly and translocation to the cell cortex during chemoattractant responses. *Cell Motil Cytoskeleton, 53*(3), 177-188. doi: 10.1002/cm.10068
Little, S. C., Tkacik, G., Kneeland, T. B., Wieschaus, E. F., & Gregor, T. (2011). The formation of the Bicoid morphogen gradient requires protein movement from anteriorly localized mRNA. *PLoS Biol, 9*(3), e1000596. doi: 10.1371/journal.pbio.1000596
Loncar, D., & Singer, S. J. (1995). Cell membrane formation during the cellularization of the syncytial blastoderm of Drosophila. *Proc Natl Acad Sci U S A, 92*(6), 2199-2203. doi: 10.1073/pnas.92.6.2199
Lorthongpanich, C., Doris, T. P., Limviphuvadh, V., Knowles, B. B., & Solter, D. (2012). Developmental fate and lineage commitment of singled mouse blastomeres. *Development, 139*(20), 3722-3731. doi: 10.1242/dev.086454
Low, I., Dancker, P., & Wieland, T. (1975). Stabilization of F-actin by phalloidin. Reversal of the destabilizing effect of cytochalasin B. *FEBS Lett, 54*(2), 263-265. doi: 10.1016/0014-5793(75)80088-3
Luo, W., Yu, C. H., Lieu, Z. Z., Allard, J., Mogilner, A., Sheetz, M. P., & Bershadsky, A. D. (2013). Analysis of the local organization and dynamics of cellular actin networks. *J Cell Biol, 202*(7), 1057-1073. doi: 10.1083/jcb.201210123
Lye, C. M., Blanchard, G. B., Naylor, H. W., Muresan, L., Huisken, J., Adams, R. J., & Sanson, B. (2015). Mechanical Coupling between Endoderm Invagination and Axis Extension in Drosophila. *PLoS Biol, 13*(11), e1002292. doi: 10.1371/journal.pbio.1002292
Macara, I. G. (2004). Parsing the polarity code. *Nat Rev Mol Cell Biol, 5*(3), 220-231. doi: 10.1038/nrm1332
Mahajan, R. K., & Pardee, J. D. (1996). Assembly mechanism of Dictyostelium myosin II: regulation by K+, Mg2+, and actin filaments. *Biochemistry, 35*(48), 15504-15514. doi: 10.1021/bi9618981
Manning, A. J., Peters, K. A., Peifer, M., & Rogers, S. L. (2013). Regulation of epithelial morphogenesis by the G protein-coupled receptor mist and its ligand fog. *Sci Signal, 6*(301), ra98. doi: 10.1126/scisignal.2004427
Margolis, B. (2018). The Crumbs3 Polarity Protein. *Cold Spring Harb Perspect Biol, 10*(3). doi: 10.1101/cshperspect.a027961
Marinari, E., Mehonic, A., Curran, S., Gale, J., Duke, T., & Baum, B. (2012). Live-cell delamination counterbalances epithelial growth to limit tissue overcrowding. *Nature, 484*(7395), 542-545. doi: 10.1038/nature10984

Martin-Belmonte, F., & Mostov, K. (2008). Regulation of cell polarity during epithelial morphogenesis. *Curr Opin Cell Biol, 20*(2), 227-234. doi: 10.1016/j.ceb.2008.01.001

Martin, A. C., Gelbart, M., Fernandez-Gonzalez, R., Kaschube, M., & Wieschaus, E. F. (2010). Integration of contractile forces during tissue invagination. *J Cell Biol, 188*(5), 735-749. doi: 10.1083/jcb.200910099

Martin, A. C., Kaschube, M., & Wieschaus, E. F. (2009). Pulsed contractions of an actin-myosin network drive apical constriction. *Nature, 457*(7228), 495-499. doi: 10.1038/nature07522

Mathewson, A. W., Berman, D. G., & Moens, C. B. (2019). Microtubules are required for the maintenance of planar cell polarity in monociliated floorplate cells. *Dev Biol, 452*(1), 21-33. doi: 10.1016/j.ydbio.2019.04.007

Matsumura, F. (2005). Regulation of myosin II during cytokinesis in higher eukaryotes. *Trends Cell Biol, 15*(7), 371-377. doi: 10.1016/j.tcb.2005.05.004

Matsumura, F., & Hartshorne, D. J. (2008). Myosin phosphatase target subunit: Many roles in cell function. *Biochem Biophys Res Commun, 369*(1), 149-156. doi: 10.1016/j.bbrc.2007.12.090

Mazumdar, A., & Mazumdar, M. (2002). How one becomes many: blastoderm cellularization in Drosophila melanogaster. *Bioessays, 24*(11), 1012-1022. doi: 10.1002/bies.10184

McIntosh, J. R. (2016). Mitosis. *Cold Spring Harb Perspect Biol, 8*(9). doi: 10.1101/cshperspect.a023218

McMahon, A., Reeves, G. T., Supatto, W., & Stathopoulos, A. (2010). Mesoderm migration in Drosophila is a multi-step process requiring FGF signaling and integrin activity. *Development, 137*(13), 2167-2175. doi: 10.1242/dev.051573

Meiring, J. C. M., & Akhmanova, A. (2020). Microtubules keep large cells in shape. *J Cell Biol, 219*(6). doi: 10.1083/jcb.202004031

Merrill, P. T., Sweeton, D., & Wieschaus, E. (1988). Requirements for autosomal gene activity during precellular stages of Drosophila melanogaster. *Development, 104*(3), 495-509.

Misra, S., Crosby, M. A., Mungall, C. J., Matthews, B. B., Campbell, K. S., Hradecky, P., . . . Lewis, S. E. (2002). Annotation of the Drosophila melanogaster euchromatic genome: a systematic review. *Genome Biol, 3*(12), RESEARCH0083. doi: 10.1186/gb-2002-3-12-research0083

Mitrossilis, D., Roper, J. C., Le Roy, D., Driquez, B., Michel, A., Menager, C., . . . Farge, E. (2017). Mechanotransductive cascade of Myo-II-dependent mesoderm and endoderm invaginations in embryo gastrulation. *Nat Commun, 8*, 13883. doi: 10.1038/ncomms13883

Montell, D. J. (2008). Morphogenetic cell movements: diversity from modular mechanical properties. *Science, 322*(5907), 1502-1505. doi: 10.1126/science.1164073

Moore, D. C., Stanisstreet, M., & Evans, G. E. (1987). Morphometric analyses of changes in cell shape in the neuroepithelium of mammalian embryos. *J Anat, 155*, 87-99.

Morais-de-Sa, E., Mirouse, V., & St Johnston, D. (2010). aPKC phosphorylation of Bazooka defines the apical/lateral border in Drosophila epithelial cells. *Cell, 141*(3), 509-523. doi: 10.1016/j.cell.2010.02.040

Morgan, T. H. (1910). Sex Limited Inheritance in Drosophila. *Science, 32*(812), 120-122. doi: 10.1126/science.32.812.120

Morize, P., Christiansen, A. E., Costa, M., Parks, S., & Wieschaus, E. (1998). Hyperactivation of the folded gastrulation pathway induces specific cell shape changes. *Development, 125*(4), 589-597.

Moussian, B., & Roth, S. (2005). Dorsoventral axis formation in the Drosophila embryo--shaping and transducing a morphogen gradient. *Curr Biol, 15*(21), R887-899. doi: 10.1016/j.cub.2005.10.026

Muller, H. A., & Wieschaus, E. (1996). armadillo, bazooka, and stardust are critical for early stages in formation of the zonula adherens and maintenance of the polarized blastoderm epithelium in Drosophila. *J Cell Biol, 134*(1), 149-163. doi: 10.1083/jcb.134.1.149

Munro, E., Nance, J., & Priess, J. R. (2004). Cortical flows powered by asymmetrical contraction transport PAR proteins to establish and maintain anterior-posterior polarity in the early C. elegans embryo. *Dev Cell, 7*(3), 413-424. doi: 10.1016/j.devcel.2004.08.001

Munro, E. M., & Odell, G. M. (2002). Polarized basolateral cell motility underlies invagination and convergent extension of the ascidian notochord. *Development, 129*(1), 13-24.

Murrell, M. P., & Gardel, M. L. (2012). F-actin buckling coordinates contractility and severing in a biomimetic actomyosin cortex. *Proc Natl Acad Sci U S A, 109*(51), 20820-20825. doi: 10.1073/pnas.1214753109

Nagafuchi, A., & Takeichi, M. (1988). Cell binding function of E-cadherin is regulated by the cytoplasmic domain. *EMBO J, 7*(12), 3679-3684.

Nance, J., & Zallen, J. A. (2011). Elaborating polarity: PAR proteins and the cytoskeleton. *Development, 138*(5), 799-809. doi: 10.1242/dev.053538

Nelson, C. M., & Chen, C. S. (2003). VE-cadherin simultaneously stimulates and inhibits cell proliferation by altering cytoskeletal structure and tension. *J Cell Sci, 116*(Pt 17), 3571-3581. doi: 10.1242/jcs.00680

Nelson, W. J., Drees, F., & Yamada, S. (2005). Interaction of cadherin with the actin cytoskeleton. *Novartis Found Symp, 269*, 159-168; discussion 168-177, 223-130.

Neuman-Silberberg, F. S., & Schupbach, T. (1993). The Drosophila dorsoventral patterning gene gurken produces a dorsally localized RNA and encodes a TGF alpha-like protein. *Cell, 75*(1), 165-174.

Neuman-Silberberg, F. S., & Schupbach, T. (1996). The Drosophila TGF-alpha-like protein Gurken: expression and cellular localization during Drosophila oogenesis. *Mech Dev, 59*(2), 105-113. doi: 10.1016/0925-4773(96)00567-9

Newport, J., & Kirschner, M. (1982a). A major developmental transition in early Xenopus embryos: I. characterization and timing of cellular changes at the midblastula stage. *Cell, 30*(3), 675-686. doi: 10.1016/0092-8674(82)90272-0

Newport, J., & Kirschner, M. (1982b). A major developmental transition in early Xenopus embryos: II. Control of the onset of transcription. *Cell, 30*(3), 687-696. doi: 10.1016/0092-8674(82)90273-2

Nichols, S. A., Dirks, W., Pearse, J. S., & King, N. (2006). Early evolution of animal cell signaling and adhesion genes. *Proc Natl Acad Sci U S A, 103*(33), 12451-12456. doi: 10.1073/pnas.0604065103

Nicolas-Perez, M., Kuchling, F., Letelier, J., Polvillo, R., Wittbrodt, J., & Martinez-Morales, J. R. (2016). Analysis of cellular behavior and cytoskeletal dynamics reveal a constriction mechanism driving optic cup morphogenesis. *Elife, 5*. doi: 10.7554/eLife.15797

Niederman, R., & Pollard, T. D. (1975). Human platelet myosin. II. In vitro assembly and structure of myosin filaments. *J Cell Biol, 67*(1), 72-92. doi: 10.1083/jcb.67.1.72

Niessen, C. M., Leckband, D., & Yap, A. S. (2011). Tissue organization by cadherin adhesion molecules: dynamic molecular and cellular mechanisms of morphogenetic regulation. *Physiol Rev, 91*(2), 691-731. doi: 10.1152/physrev.00004.2010

Nishikawa, M., Sellers, J. R., Adelstein, R. S., & Hidaka, H. (1984). Protein kinase C modulates in vitro phosphorylation of the smooth muscle heavy meromyosin by myosin light chain kinase. *J Biol Chem, 259*(14), 8808-8814.

Nishimura, T., Honda, H., & Takeichi, M. (2012). Planar cell polarity links axes of spatial dynamics in neural-tube closure. *Cell, 149*(5), 1084-1097. doi: 10.1016/j.cell.2012.04.021

Nishimura, T., & Takeichi, M. (2008). Shroom3-mediated recruitment of Rho kinases to the apical cell junctions regulates epithelial and neuroepithelial planar remodeling. *Development, 135*(8), 1493-1502. doi: 10.1242/dev.019646

Nollet, F., Kools, P., & van Roy, F. (2000). Phylogenetic analysis of the cadherin superfamily allows identification of six major subfamilies besides several solitary members. *J Mol Biol, 299*(3), 551-572. doi: 10.1006/jmbi.2000.3777

Nose, A., Nagafuchi, A., & Takeichi, M. (1988). Expressed recombinant cadherins mediate cell sorting in model systems. *Cell, 54*(7), 993-1001. doi: 10.1016/0092-8674(88)90114-6

Nusslein-Volhard, C., Frohnhofer, H. G., & Lehmann, R. (1987). Determination of anteroposterior polarity in Drosophila. *Science, 238*(4834), 1675-1681. doi: 10.1126/science.3686007

Nusslein-Volhard, C., & Wieschaus, E. (1980). Mutations affecting segment number and polarity in Drosophila. *Nature, 287*(5785), 795-801. doi: 10.1038/287795a0

O'Farrell, P. H., Stumpff, J., & Su, T. T. (2004). Embryonic cleavage cycles: how is a mouse like a fly? *Curr Biol, 14*(1), R35-45. doi: 10.1016/j.cub.2003.12.022

Oda, H., Tsukita, S., & Takeichi, M. (1998). Dynamic behavior of the cadherin-based cell-cell adhesion system during Drosophila gastrulation. *Dev Biol, 203*(2), 435-450. doi: 10.1006/dbio.1998.9047

Ozawa, M., Baribault, H., & Kemler, R. (1989). The cytoplasmic domain of the cell adhesion molecule uvomorulin associates with three independent proteins structurally related in different species. *EMBO J, 8*(6), 1711-1717.

Pare, A. C., Naik, P., Shi, J., Mirman, Z., Palmquist, K. H., & Zallen, J. A. (2019). An LRR Receptor-Teneurin System Directs Planar Polarity at Compartment Boundaries. *Dev Cell, 51*(2), 208-221 e206. doi: 10.1016/j.devcel.2019.08.003

Pare, A. C., Vichas, A., Fincher, C. T., Mirman, Z., Farrell, D. L., Mainieri, A., & Zallen, J. A. (2014). A positional Toll receptor code directs convergent extension in Drosophila. *Nature, 515*(7528), 523-527. doi: 10.1038/nature13953

Parks, S., & Wieschaus, E. (1991). The Drosophila gastrulation gene concertina encodes a G alpha-like protein. *Cell, 64*(2), 447-458. doi: 10.1016/0092-8674(91)90652-f

Patel, S. D., Ciatto, C., Chen, C. P., Bahna, F., Rajebhosale, M., Arkus, N., . . . Shapiro, L. (2006). Type II cadherin ectodomain structures: implications for classical cadherin specificity. *Cell, 124*(6), 1255-1268. doi: 10.1016/j.cell.2005.12.046

Pearl, E. J., Li, J., & Green, J. B. (2017). Cellular systems for epithelial invagination. *Philos Trans R Soc Lond B Biol Sci, 372*(1720). doi: 10.1098/rstb.2015.0526

Pelissier, A., Chauvin, J. P., & Lecuit, T. (2003). Trafficking through Rab11 endosomes is required for cellularization during Drosophila embryogenesis. *Curr Biol, 13*(21), 1848-1857. doi: 10.1016/j.cub.2003.10.023

Petronczki, M., & Knoblich, J. A. (2001). DmPAR-6 directs epithelial polarity and asymmetric cell division of neuroblasts in Drosophila. *Nat Cell Biol, 3*(1), 43-49. doi: 10.1038/35050550

Peyrieras, N., Hyafil, F., Louvard, D., Ploegh, H. L., & Jacob, F. (1983). Uvomorulin: a nonintegral membrane protein of early mouse embryo. *Proc Natl Acad Sci U S A, 80*(20), 6274-6277. doi: 10.1073/pnas.80.20.6274

Piazzesi, G., Lucii, L., & Lombardi, V. (2002). The size and the speed of the working stroke of muscle myosin and its dependence on the force. *J Physiol, 545*(1), 145-151. doi: 10.1113/jphysiol.2002.028969

Piazzesi, G., Reconditi, M., Linari, M., Lucii, L., Bianco, P., Brunello, E., . . . Lombardi, V. (2007). Skeletal muscle performance determined by modulation of number of myosin motors rather than motor force or stroke size. *Cell, 131*(4), 784-795. doi: 10.1016/j.cell.2007.09.045

Piazzesi, G., Reconditi, M., Linari, M., Lucii, L., Sun, Y. B., Narayanan, T., . . . Irving, M. (2002). Mechanism of force generation by myosin heads in skeletal muscle. *Nature, 415*(6872), 659-662. doi: 10.1038/415659a

Pielage, J., Stork, T., Bunse, I., & Klambt, C. (2003). The Drosophila cell survival gene discs lost encodes a cytoplasmic Codanin-1-like protein, not a homolog of tight junction PDZ protein Patj. *Dev Cell, 5*(6), 841-851. doi: 10.1016/s1534-5807(03)00358-7

Plageman, T. F., Jr., Chung, M. I., Lou, M., Smith, A. N., Hildebrand, J. D., Wallingford, J. B., & Lang, R. A. (2010). Pax6-dependent Shroom3 expression regulates apical constriction during lens placode invagination. *Development, 137*(3), 405-415. doi: 10.1242/dev.045369

Plant, P. J., Fawcett, J. P., Lin, D. C., Holdorf, A. D., Binns, K., Kulkarni, S., & Pawson, T. (2003). A polarity complex of mPar-6 and atypical PKC binds, phosphorylates and regulates mammalian Lgl. *Nat Cell Biol, 5*(4), 301-308. doi: 10.1038/ncb948

Plygawko, A. T., Kan, S., & Campbell, K. (2020). Epithelial-mesenchymal plasticity: emerging parallels between tissue morphogenesis and cancer metastasis. *Philos Trans R Soc Lond B Biol Sci, 375*(1809), 20200087. doi: 10.1098/rstb.2020.0087

Pollard, T. D. (2016). Actin and Actin-Binding Proteins. *Cold Spring Harb Perspect Biol, 8*(8). doi: 10.1101/cshperspect.a018226

Pollard, T. D., & Beltzner, C. C. (2002). Structure and function of the Arp2/3 complex. *Curr Opin Struct Biol, 12*(6), 768-774. doi: 10.1016/s0959-440x(02)00396-2

Pollard, T. D., & Cooper, J. A. (1986). Actin and actin-binding proteins. A critical evaluation of mechanisms and functions. *Annu Rev Biochem, 55*, 987-1035. doi: 10.1146/annurev.bi.55.070186.005011

Pollard, T. D., & Cooper, J. A. (2009). Actin, a central player in cell shape and movement. *Science, 326*(5957), 1208-1212. doi: 10.1126/science.1175862

Pouille, P. A., Ahmadi, P., Brunet, A. C., & Farge, E. (2009). Mechanical signals trigger Myosin II redistribution and mesoderm invagination in Drosophila embryos. *Sci Signal, 2*(66), ra16. doi: 10.1126/scisignal.2000098

Poulson, D. F. (1950). Histogenesis, Organogenesis, and Differentiation in the Embryo of Drosophila melanogaster, Biology of Drosophila. *Cold Spring Harbour Laboratory Press, 168-274*.

Pring, M., Weber, A., & Bubb, M. R. (1992). Profilin-actin complexes directly elongate actin filaments at the barbed end. *Biochemistry, 31*(6), 1827-1836. doi: 10.1021/bi00121a035

Quintin, S., Gally, C., & Labouesse, M. (2008). Epithelial morphogenesis in embryos: asymmetries, motors and brakes. *Trends Genet, 24*(5), 221-230. doi: 10.1016/j.tig.2008.02.005

Rahimi, N., Averbukh, I., Carmon, S., Schejter, E. D., Barkai, N., & Shilo, B. Z. (2019). Dynamics of Spaetzle morphogen shuttling in the Drosophila embryo shapes gastrulation patterning. *Development, 146*(21). doi: 10.1242/dev.181487

Rajasekaran, A. K., Hojo, M., Huima, T., & Rodriguez-Boulan, E. (1996). Catenins and zonula occludens-1 form a complex during early stages in the assembly of tight junctions. *J Cell Biol, 132*(3), 451-463. doi: 10.1083/jcb.132.3.451

Rangarajan, E. S., & Izard, T. (2012). The cytoskeletal protein alpha-catenin unfurls upon binding to vinculin. *J Biol Chem, 287*(22), 18492-18499. doi: 10.1074/jbc.M112.351023

Rauzi, M. (2020). Cell intercalation in a simple epithelium. *Philos Trans R Soc Lond B Biol Sci, 375*(1809), 20190552. doi: 10.1098/rstb.2019.0552

Rauzi, M., Krzic, U., Saunders, T. E., Krajnc, M., Ziherl, P., Hufnagel, L., & Leptin, M. (2015). Embryo-scale tissue mechanics during Drosophila gastrulation movements. *Nat Commun, 6*, 8677. doi: 10.1038/ncomms9677

Rauzi, M., Lenne, P. F., & Lecuit, T. (2010). Planar polarized actomyosin contractile flows control epithelial junction remodelling. *Nature, 468*(7327), 1110-1114. doi: 10.1038/nature09566

Rauzi, M., Verant, P., Lecuit, T., & Lenne, P. F. (2008). Nature and anisotropy of cortical forces orienting Drosophila tissue morphogenesis. *Nat Cell Biol, 10*(12), 1401-1410. doi: 10.1038/ncb1798

Reach, M., Galindo, R. L., Towb, P., Allen, J. L., Karin, M., & Wasserman, S. A. (1996). A gradient of cactus protein degradation establishes dorsoventral polarity in the Drosophila embryo. *Dev Biol, 180*(1), 353-364. doi: 10.1006/dbio.1996.0308

Reeves, G. T., Trisnadi, N., Truong, T. V., Nahmad, M., Katz, S., & Stathopoulos, A. (2012). Dorsal-ventral gene expression in the Drosophila embryo reflects the dynamics and precision of the dorsal nuclear gradient. *Dev Cell, 22*(3), 544-557. doi: 10.1016/j.devcel.2011.12.007

Reiter, L. T., Potocki, L., Chien, S., Gribskov, M., & Bier, E. (2001). A systematic analysis of human disease-associated gene sequences in Drosophila melanogaster. *Genome Res, 11*(6), 1114-1125. doi: 10.1101/gr.169101

Renkawitz, J., Kopf, A., Stopp, J., de Vries, I., Driscoll, M. K., Merrin, J., . . . Sixt, M. (2019). Nuclear positioning facilitates amoeboid migration along the path of least resistance. *Nature, 568*(7753), 546-550. doi: 10.1038/s41586-019-1087-5

Riento, K., & Ridley, A. J. (2003). Rocks: multifunctional kinases in cell behaviour. *Nat Rev Mol Cell Biol, 4*(6), 446-456. doi: 10.1038/nrm1128

Riggs, B., Rothwell, W., Mische, S., Hickson, G. R., Matheson, J., Hays, T. S., . . . Sullivan, W. (2003). Actin cytoskeleton remodeling during early Drosophila furrow formation requires recycling endosomal components Nuclear-fallout and Rab11. *J Cell Biol, 163*(1), 143-154. doi: 10.1083/jcb.200305115

Rimm, D. L., Koslov, E. R., Kebriaei, P., Cianci, C. D., & Morrow, J. S. (1995). Alpha 1(E)-catenin is an actin-binding and -bundling protein mediating the attachment of F-actin to the membrane adhesion complex. *Proc Natl Acad Sci U S A, 92*(19), 8813-8817. doi: 10.1073/pnas.92.19.8813

Rodriguez-Boulan, E., & Macara, I. G. (2014). Organization and execution of the epithelial polarity programme. *Nat Rev Mol Cell Biol, 15*(4), 225-242. doi: 10.1038/nrm3775

Rogers, S. L., Wiedemann, U., Hacker, U., Turck, C., & Vale, R. D. (2004). Drosophila RhoGEF2 associates with microtubule plus ends in an EB1-dependent manner. *Curr Biol, 14*(20), 1827-1833. doi: 10.1016/j.cub.2004.09.078

Roh, M. H., Fan, S., Liu, C. J., & Margolis, B. (2003). The Crumbs3-Pals1 complex participates in the establishment of polarity in mammalian epithelial cells. *J Cell Sci, 116*(Pt 14), 2895-2906. doi: 10.1242/jcs.00500

Roh, M. H., Makarova, O., Liu, C. J., Shin, K., Lee, S., Laurinec, S., . . . Margolis, B. (2002). The Maguk protein, Pals1, functions as an adapter, linking mammalian homologues of Crumbs and Discs Lost. *J Cell Biol, 157*(1), 161-172. doi: 10.1083/jcb.200109010

Roh, M. H., & Margolis, B. (2003). Composition and function of PDZ protein complexes during cell polarization. *Am J Physiol Renal Physiol, 285*(3), F377-387. doi: 10.1152/ajprenal.00086.2003

Roignot, J., Peng, X., & Mostov, K. (2013). Polarity in mammalian epithelial morphogenesis. *Cold Spring Harb Perspect Biol, 5*(2). doi: 10.1101/cshperspect.a013789

Rorth, P. (2007). Collective guidance of collective cell migration. *Trends Cell Biol, 17*(12), 575-579. doi: 10.1016/j.tcb.2007.09.007

Ross, J. L., Ali, M. Y., & Warshaw, D. M. (2008). Cargo transport: molecular motors navigate a complex cytoskeleton. *Curr Opin Cell Biol, 20*(1), 41-47. doi: 10.1016/j.ceb.2007.11.006

Ross, J. L., Shuman, H., Holzbaur, E. L., & Goldman, Y. E. (2008). Kinesin and dynein-dynactin at intersecting microtubules: motor density affects dynein function. *Biophys J, 94*(8), 3115-3125. doi: 10.1529/biophysj.107.120014

Roth, S., Jordan, P., & Karess, R. (1999). Binuclear Drosophila oocytes: consequences and implications for dorsal-ventral patterning in oogenesis and embryogenesis. *Development, 126*(5), 927-934.

Roth, S., Neuman-Silberberg, F. S., Barcelo, G., & Schupbach, T. (1995). cornichon and the EGF receptor signaling process are necessary for both anterior-posterior and dorsal-ventral pattern formation in Drosophila. *Cell, 81*(6), 967-978. doi: 10.1016/0092-8674(95)90016-0

Roth, S., Stein, D., & Nusslein-Volhard, C. (1989). A gradient of nuclear localization of the dorsal protein determines dorsoventral pattern in the Drosophila embryo. *Cell, 59*(6), 1189-1202. doi: 10.1016/0092-8674(89)90774-5

Rubin, G. M. (1998). The Drosophila genome project: a progress report. *Trends Genet, 14*(9), 340-343. doi: 10.1016/s0168-9525(98)01568-6

Rushlow, C. A., Han, K., Manley, J. L., & Levine, M. (1989). The graded distribution of the dorsal morphogen is initiated by selective nuclear transport in Drosophila. *Cell, 59*(6), 1165-1177. doi: 10.1016/0092-8674(89)90772-1

Sander, K., & Lehmann, R. (1988). Drosophila nurse cells produce a posterior signal required for embryonic segmentation and polarity. *Nature, 335*(6185), 68-70. doi: 10.1038/335068a0

Sarpal, R., Pellikka, M., Patel, R. R., Hui, F. Y., Godt, D., & Tepass, U. (2012). Mutational analysis supports a core role for Drosophila alpha-catenin in adherens junction function. *J Cell Sci, 125*(Pt 1), 233-245. doi: 10.1242/jcs.096644
Sawyer, J. M., Harrell, J. R., Shemer, G., Sullivan-Brown, J., Roh-Johnson, M., & Goldstein, B. (2010). Apical constriction: a cell shape change that can drive morphogenesis. *Dev Biol, 341*(1), 5-19. doi: 10.1016/j.ydbio.2009.09.009
Schlegelmilch, K., Mohseni, M., Kirak, O., Pruszak, J., Rodriguez, J. R., Zhou, D., . . . Camargo, F. D. (2011). Yap1 acts downstream of alpha-catenin to control epidermal proliferation. *Cell, 144*(5), 782-795. doi: 10.1016/j.cell.2011.02.031
Schock, F., & Perrimon, N. (2002a). Cellular processes associated with germ band retraction in Drosophila. *Dev Biol, 248*(1), 29-39. doi: 10.1006/dbio.2002.0698
Schock, F., & Perrimon, N. (2002b). Molecular mechanisms of epithelial morphogenesis. *Annu Rev Cell Dev Biol, 18*, 463-493. doi: 10.1146/annurev.cellbio.18.022602.131838
Schoenwolf, G. C. (1991). Cell movements driving neurulation in avian embryos. *Dev Suppl, Suppl 2*, 157-168.
Schoenwolf, G. C., & Alvarez, I. S. (1989). Roles of neuroepithelial cell rearrangement and division in shaping of the avian neural plate. *Development, 106*(3), 427-439.
Schofield, A. V., & Bernard, O. (2013). Rho-associated coiled-coil kinase (ROCK) signaling and disease. *Crit Rev Biochem Mol Biol, 48*(4), 301-316. doi: 10.3109/10409238.2013.786671
Schroeder, T. E. (1970). Neurulation in Xenopus laevis. An analysis and model based upon light and electron microscopy. *J Embryol Exp Morphol, 23*(2), 427-462.
Schupbach, T., & Wieschaus, E. (1986). Germline autonomy of maternal-effect mutations altering the embryonic body pattern of Drosophila. *Dev Biol, 113*(2), 443-448. doi: 10.1016/0012-1606(86)90179-x
Sellers, J. R. (2000). Myosins: a diverse superfamily. *Biochim Biophys Acta, 1496*(1), 3-22. doi: 10.1016/s0167-4889(00)00005-7
Sen, J., Goltz, J. S., Stevens, L., & Stein, D. (1998). Spatially restricted expression of pipe in the Drosophila egg chamber defines embryonic dorsal-ventral polarity. *Cell, 95*(4), 471-481. doi: 10.1016/s0092-8674(00)81615-3
Shelton, C. A., & Wasserman, S. A. (1993). pelle encodes a protein kinase required to establish dorsoventral polarity in the Drosophila embryo. *Cell, 72*(4), 515-525. doi: 10.1016/0092-8674(93)90071-w
Sheth, B., Fontaine, J. J., Ponza, E., McCallum, A., Page, A., Citi, S., . . . Fleming, T. P. (2000). Differentiation of the epithelial apical junctional complex during mouse preimplantation development: a role for rab13 in the early maturation of the tight junction. *Mech Dev, 97*(1-2), 93-104. doi: 10.1016/s0925-4773(00)00416-0
Shih, J., & Keller, R. (1992a). Cell motility driving mediolateral intercalation in explants of Xenopus laevis. *Development, 116*(4), 901-914.
Shih, J., & Keller, R. (1992b). Patterns of cell motility in the organizer and dorsal mesoderm of Xenopus laevis. *Development, 116*(4), 915-930.
Shimada, Y., Yonemura, S., Ohkura, H., Strutt, D., & Uemura, T. (2006). Polarized transport of Frizzled along the planar microtubule arrays in Drosophila wing epithelium. *Dev Cell, 10*(2), 209-222. doi: 10.1016/j.devcel.2005.11.016
Shook, D., & Keller, R. (2003). Mechanisms, mechanics and function of epithelial-mesenchymal transitions in early development. *Mech Dev, 120*(11), 1351-1383. doi: 10.1016/j.mod.2003.06.005
Shook, D. R., Majer, C., & Keller, R. (2004). Pattern and morphogenesis of presumptive superficial mesoderm in two closely related species, Xenopus laevis and Xenopus tropicalis. *Dev Biol, 270*(1), 163-185. doi: 10.1016/j.ydbio.2004.02.021
Siang, L. C., Fernandez-Gonzalez, R., & Feng, J. J. (2018). Modeling cell intercalation during Drosophila germband extension. *Phys Biol, 15*(6), 066008. doi: 10.1088/1478-3975/aad865
Smith, J. L., & Schoenwolf, G. C. (1997). Neurulation: coming to closure. *Trends Neurosci, 20*(11), 510-517. doi: 10.1016/s0166-2236(97)01121-1
Soares e Silva, M., Depken, M., Stuhrmann, B., Korsten, M., MacKintosh, F. C., & Koenderink, G. H. (2011). Active multistage coarsening of actin networks driven

by myosin motors. *Proc Natl Acad Sci U S A, 108*(23), 9408-9413. doi: 10.1073/pnas.1016616108
Somlyo, A. P., & Somlyo, A. V. (2003). Ca2+ sensitivity of smooth muscle and nonmuscle myosin II: modulated by G proteins, kinases, and myosin phosphatase. *Physiol Rev, 83*(4), 1325-1358. doi: 10.1152/physrev.00023.2003
Spector, I., Shochet, N. R., Kashman, Y., & Groweiss, A. (1983). Latrunculins: novel marine toxins that disrupt microfilament organization in cultured cells. *Science, 219*(4584), 493-495. doi: 10.1126/science.6681676
Spencer, A. K., Siddiqui, B. A., & Thomas, J. H. (2015). Cell shape change and invagination of the cephalic furrow involves reorganization of F-actin. *Dev Biol, 402*(2), 192-207. doi: 10.1016/j.ydbio.2015.03.022
Spencer, M. A., Jabeen, Z., & Lubensky, D. K. (2017). Vertex stability and topological transitions in vertex models of foams and epithelia. *Eur Phys J E Soft Matter, 40*(1), 2. doi: 10.1140/epje/i2017-11489-4
Sprenger, F., Stevens, L. M., & Nusslein-Volhard, C. (1989). The Drosophila gene torso encodes a putative receptor tyrosine kinase. *Nature, 338*(6215), 478-483. doi: 10.1038/338478a0
St Johnston, D. (2002). The art and design of genetic screens: Drosophila melanogaster. *Nat Rev Genet, 3*(3), 176-188. doi: 10.1038/nrg751
St Johnston, D., & Ahringer, J. (2010). Cell polarity in eggs and epithelia: parallels and diversity. *Cell, 141*(5), 757-774. doi: 10.1016/j.cell.2010.05.011
St Johnston, D., & Nusslein-Volhard, C. (1992). The origin of pattern and polarity in the Drosophila embryo. *Cell, 68*(2), 201-219. doi: 10.1016/0092-8674(92)90466-p
St Johnston, D., & Sanson, B. (2011). Epithelial polarity and morphogenesis. *Curr Opin Cell Biol, 23*(5), 540-546. doi: 10.1016/j.ceb.2011.07.005
Staple, D. B., Farhadifar, R., Roper, J. C., Aigouy, B., Eaton, S., & Julicher, F. (2010). Mechanics and remodelling of cell packings in epithelia. *Eur Phys J E Soft Matter, 33*(2), 117-127. doi: 10.1140/epje/i2010-10677-0
Stathopoulos, A., & Levine, M. (2002). Linear signaling in the Toll-Dorsal pathway of Drosophila: activated Pelle kinase specifies all threshold outputs of gene expression while the bHLH protein Twist specifies a subset. *Development, 129*(14), 3411-3419.
Stathopoulos, A., Van Drenth, M., Erives, A., Markstein, M., & Levine, M. (2002). Whole-genome analysis of dorsal-ventral patterning in the Drosophila embryo. *Cell, 111*(5), 687-701. doi: 10.1016/s0092-8674(02)01087-5
Steinberg, M. S. (1963). Reconstruction of tissues by dissociated cells. Some morphogenetic tissue movements and the sorting out of embryonic cells may have a common explanation. *Science, 141*(3579), 401-408. doi: 10.1126/science.141.3579.401
Steinberg, M. S. (1970). Does differential adhesion govern self-assembly processes in histogenesis? Equilibrium configurations and the emergence of a hierarchy among populations of embryonic cells. *J Exp Zool, 173*(4), 395-433. doi: 10.1002/jez.1401730406
Steinert, P. M., Jones, J. C., & Goldman, R. D. (1984). Intermediate filaments. *J Cell Biol, 99*(1 Pt 2), 22s-27s. doi: 10.1083/jcb.99.1.22s
Stevens, L. M., Frohnhofer, H. G., Klingler, M., & Nusslein-Volhard, C. (1990). Localized requirement for torso-like expression in follicle cells for development of terminal anlagen of the Drosophila embryo. *Nature, 346*(6285), 660-663. doi: 10.1038/346660a0
Stevenson, B. R., & Keon, B. H. (1998). The tight junction: morphology to molecules. *Annu Rev Cell Dev Biol, 14*, 89-109. doi: 10.1146/annurev.cellbio.14.1.89
Steward, R. (1989). Relocalization of the dorsal protein from the cytoplasm to the nucleus correlates with its function. *Cell, 59*(6), 1179-1188. doi: 10.1016/0092-8674(89)90773-3
Stewart, M. (1990). Intermediate filaments: structure, assembly and molecular interactions. *Curr Opin Cell Biol, 2*(1), 91-100. doi: 10.1016/s0955-0674(05)80037-7

Struhl, G., Struhl, K., & Macdonald, P. M. (1989). The gradient morphogen bicoid is a concentration-dependent transcriptional activator. *Cell, 57*(7), 1259-1273. doi: 10.1016/0092-8674(89)90062-7

Strutt, D. I., & White, R. A. (1994). Characterisation of T48, a target of homeotic gene regulation in Drosophila embryogenesis. *Mech Dev, 46*(1), 27-39. doi: 10.1016/0925-4773(94)90035-3

Sui, L., Alt, S., Weigert, M., Dye, N., Eaton, S., Jug, F., . . . Dahmann, C. (2018). Differential lateral and basal tension drive folding of Drosophila wing discs through two distinct mechanisms. *Nat Commun, 9*(1), 4620. doi: 10.1038/s41467-018-06497-3

Sumigray, K. D., Terwilliger, M., & Lechler, T. (2018). Morphogenesis and Compartmentalization of the Intestinal Crypt. *Dev Cell, 45*(2), 183-197 e185. doi: 10.1016/j.devcel.2018.03.024

Sun, Z., Amourda, C., Shagirov, M., Hara, Y., Saunders, T. E., & Toyama, Y. (2017). Basolateral protrusion and apical contraction cooperatively drive Drosophila germ-band extension. *Nat Cell Biol, 19*(4), 375-383. doi: 10.1038/ncb3497

Suzuki, A., Hirata, M., Kamimura, K., Maniwa, R., Yamanaka, T., Mizuno, K., . . . Ohno, S. (2004). aPKC acts upstream of PAR-1b in both the establishment and maintenance of mammalian epithelial polarity. *Curr Biol, 14*(16), 1425-1435. doi: 10.1016/j.cub.2004.08.021

Suzuki, A., Ishiyama, C., Hashiba, K., Shimizu, M., Ebnet, K., & Ohno, S. (2002). aPKC kinase activity is required for the asymmetric differentiation of the premature junctional complex during epithelial cell polarization. *J Cell Sci, 115*(Pt 18), 3565-3573. doi: 10.1242/jcs.00032

Svoboda, K. K., & O'Shea, K. S. (1987). An analysis of cell shape and the neuroepithelial basal lamina during optic vesicle formation in the mouse embryo. *Development, 100*(2), 185-200.

Sweeney, H. L., & Holzbaur, E. L. F. (2018). Motor Proteins. *Cold Spring Harb Perspect Biol, 10*(5). doi: 10.1101/cshperspect.a021931

Sweeney, H. L., & Houdusse, A. (2010). Structural and functional insights into the Myosin motor mechanism. *Annu Rev Biophys, 39*, 539-557. doi: 10.1146/annurev.biophys.050708.133751

Sweeton, D., Parks, S., Costa, M., & Wieschaus, E. (1991). Gastrulation in Drosophila: the formation of the ventral furrow and posterior midgut invaginations. *Development, 112*(3), 775-789.

Tada, M., & Heisenberg, C. P. (2012). Convergent extension: using collective cell migration and cell intercalation to shape embryos. *Development, 139*(21), 3897-3904. doi: 10.1242/dev.073007

Tafoya, S., & Bustamante, C. (2018). Molecular switch-like regulation in motor proteins. *Philos Trans R Soc Lond B Biol Sci, 373*(1749). doi: 10.1098/rstb.2017.0181

Takeda, M., Sami, M. M., & Wang, Y. C. (2018). A homeostatic apical microtubule network shortens cells for epithelial folding via a basal polarity shift. *Nat Cell Biol, 20*(1), 36-45. doi: 10.1038/s41556-017-0001-3

Takeichi, M. (1988). Cadherins: key molecules for selective cell-cell adhesion. *IARC Sci Publ*(92), 76-79.

Tamada, M., Shi, J., Bourdot, K. S., Supriyatno, S., Palmquist, K. H., Gutierrez-Ruiz, O. L., & Zallen, J. A. (2021). Toll receptors remodel epithelia by directing planar-polarized Src and PI3K activity. *Dev Cell, 56*(11), 1589-1602 e1589. doi: 10.1016/j.devcel.2021.04.012

Tamura, K., Shan, W. S., Hendrickson, W. A., Colman, D. R., & Shapiro, L. (1998). Structure-function analysis of cell adhesion by neural (N-) cadherin. *Neuron, 20*(6), 1153-1163. doi: 10.1016/s0896-6273(00)80496-1

Tan, I., Yong, J., Dong, J. M., Lim, L., & Leung, T. (2008). A tripartite complex containing MRCK modulates lamellar actomyosin retrograde flow. *Cell, 135*(1), 123-136. doi: 10.1016/j.cell.2008.09.018

Tanentzapf, G., & Tepass, U. (2003). Interactions between the crumbs, lethal giant larvae and bazooka pathways in epithelial polarization. *Nat Cell Biol, 5*(1), 46-52. doi: 10.1038/ncb896

Tepass, U., & Hartenstein, V. (1994). The development of cellular junctions in the Drosophila embryo. *Dev Biol, 161*(2), 563-596. doi: 10.1006/dbio.1994.1054
Tepass, U., Tanentzapf, G., Ward, R., & Fehon, R. (2001). Epithelial cell polarity and cell junctions in Drosophila. *Annu Rev Genet, 35*, 747-784. doi: 10.1146/annurev.genet.35.102401.091415
Tepass, U., Truong, K., Godt, D., Ikura, M., & Peifer, M. (2000). Cadherins in embryonic and neural morphogenesis. *Nat Rev Mol Cell Biol, 1*(2), 91-100. doi: 10.1038/35040042
Theurkauf, W. E. (1994). Actin cytoskeleton. Through the bottleneck. *Curr Biol, 4*(1), 76-78. doi: 10.1016/s0960-9822(00)00019-1
Thomas, G. H., & Williams, J. A. (1999). Dynamic rearrangement of the spectrin membrane skeleton during the generation of epithelial polarity in Drosophila. *J Cell Sci, 112 (Pt 17)*, 2843-2852.
Thompson, B. J. (2013). Cell polarity: models and mechanisms from yeast, worms and flies. *Development, 140*(1), 13-21. doi: 10.1242/dev.083634
Thompson, D. W. (1947). *On growth and form*: Cambridge Univ. Press.
Townes, P. L., & Holtfreter, J. (1955). Directed movements and selective adhesion of embryonic amphibian cells. *Journal of Experimental Zoology*.
Trepat, X., Chen, Z., & Jacobson, K. (2012). Cell migration. *Compr Physiol, 2*(4), 2369-2392. doi: 10.1002/cphy.c110012
Tsukita, S., Furuse, M., & Itoh, M. (2001). Multifunctional strands in tight junctions. *Nat Rev Mol Cell Biol, 2*(4), 285-293. doi: 10.1038/35067088
Turner, F. R., & Mahowald, A. P. (1977). Scanning electron microscopy of Drosophila melanogaster embryogenesis. II. Gastrulation and segmentation. *Dev Biol, 57*(2), 403-416. doi: 10.1016/0012-1606(77)90225-1
Tyska, M. J., & Warshaw, D. M. (2002). The myosin power stroke. *Cell Motil Cytoskeleton, 51*(1), 1-15. doi: 10.1002/cm.10014
Vavylonis, D., Wu, J. Q., Hao, S., O'Shaughnessy, B., & Pollard, T. D. (2008). Assembly mechanism of the contractile ring for cytokinesis by fission yeast. *Science, 319*(5859), 97-100. doi: 10.1126/science.1151086
Venken, K. J., Schulze, K. L., Haelterman, N. A., Pan, H., He, Y., Evans-Holm, M., . . . Bellen, H. J. (2011). MiMIC: a highly versatile transposon insertion resource for engineering Drosophila melanogaster genes. *Nat Methods, 8*(9), 737-743. doi: 10.1038/nmeth.1662
Verkhovsky, A. B., Svitkina, T. M., & Borisy, G. G. (1995). Myosin II filament assemblies in the active lamella of fibroblasts: their morphogenesis and role in the formation of actin filament bundles. *J Cell Biol, 131*(4), 989-1002. doi: 10.1083/jcb.131.4.989
Vestweber, D., & Kemler, R. (1984). Some structural and functional aspects of the cell adhesion molecule uvomorulin. *Cell Differ, 15*(2-4), 269-273. doi: 10.1016/0045-6039(84)90084-8
Vicente-Manzanares, M., Ma, X., Adelstein, R. S., & Horwitz, A. R. (2009). Non-muscle myosin II takes centre stage in cell adhesion and migration. *Nat Rev Mol Cell Biol, 10*(11), 778-790. doi: 10.1038/nrm2786
Viswanadha, R., Sale, W. S., & Porter, M. E. (2017). Ciliary Motility: Regulation of Axonemal Dynein Motors. *Cold Spring Harb Perspect Biol, 9*(8). doi: 10.1101/cshperspect.a018325
Voiculescu, O., Bodenstein, L., Lau, I. J., & Stern, C. D. (2014). Local cell interactions and self-amplifying individual cell ingression drive amniote gastrulation. *Elife, 3*, e01817. doi: 10.7554/eLife.01817
Volkmann, N., DeRosier, D., Matsudaira, P., & Hanein, D. (2001). An atomic model of actin filaments cross-linked by fimbrin and its implications for bundle assembly and function. *J Cell Biol, 153*(5), 947-956. doi: 10.1083/jcb.153.5.947
Wang, C., & Lehmann, R. (1991). Nanos is the localized posterior determinant in Drosophila. *Cell, 66*(4), 637-647. doi: 10.1016/0092-8674(91)90110-k
Wang, Y., Chang, H., & Nathans, J. (2010). When whorls collide: the development of hair patterns in frizzled 6 mutant mice. *Development, 137*(23), 4091-4099. doi: 10.1242/dev.057455

Wang, Y. C., Khan, Z., Kaschube, M., & Wieschaus, E. F. (2012). Differential positioning of adherens junctions is associated with initiation of epithelial folding. *Nature, 484*(7394), 390-393. doi: 10.1038/nature10938

Warn, R. M., & Robert-Nicoud, M. (1990). F-actin organization during the cellularization of the Drosophila embryo as revealed with a confocal laser scanning microscope. *J Cell Sci, 96 (Pt 1)*, 35-42.

Watabe-Uchida, M., Uchida, N., Imamura, Y., Nagafuchi, A., Fujimoto, K., Uemura, T., . . . Takeichi, M. (1998). alpha-Catenin-vinculin interaction functions to organize the apical junctional complex in epithelial cells. *J Cell Biol, 142*(3), 847-857. doi: 10.1083/jcb.142.3.847

Weigel, D., Jurgens, G., Klingler, M., & Jackle, H. (1990). Two gap genes mediate maternal terminal pattern information in Drosophila. *Science, 248*(4954), 495-498. doi: 10.1126/science.2158673

Wells, A. L., Lin, A. W., Chen, L. Q., Safer, D., Cain, S. M., Hasson, T., . . . Sweeney, H. L. (1999). Myosin VI is an actin-based motor that moves backwards. *Nature, 401*(6752), 505-508. doi: 10.1038/46835

Wendt, T., Taylor, D., Trybus, K. M., & Taylor, K. (2001). Three-dimensional image reconstruction of dephosphorylated smooth muscle heavy meromyosin reveals asymmetry in the interaction between myosin heads and placement of subfragment 2. *Proc Natl Acad Sci U S A, 98*(8), 4361-4366. doi: 10.1073/pnas.071051098

Whalen, A. M., & Steward, R. (1993). Dissociation of the dorsal-cactus complex and phosphorylation of the dorsal protein correlate with the nuclear localization of dorsal. *J Cell Biol, 123*(3), 523-534. doi: 10.1083/jcb.123.3.523

Wieschaus, E., & Nusslein-Volhard, C. (2016). The Heidelberg Screen for Pattern Mutants of Drosophila: A Personal Account. *Annu Rev Cell Dev Biol, 32*, 1-46. doi: 10.1146/annurev-cellbio-113015-023138

Williams-Masson, E. M., Heid, P. J., Lavin, C. A., & Hardin, J. (1998). The cellular mechanism of epithelial rearrangement during morphogenesis of the Caenorhabditis elegans dorsal hypodermis. *Dev Biol, 204*(1), 263-276. doi: 10.1006/dbio.1998.9048

Wilson, P., & Keller, R. (1991). Cell rearrangement during gastrulation of Xenopus: direct observation of cultured explants. *Development, 112*(1), 289-300.

Winklbauer, R., & Selchow, A. (1992). Motile behavior and protrusive activity of migratory mesoderm cells from the Xenopus gastrula. *Dev Biol, 150*(2), 335-351. doi: 10.1016/0012-1606(92)90246-d

Winklbauer, R., Selchow, A., Nagel, M., & Angres, B. (1992). Cell interaction and its role in mesoderm cell migration during Xenopus gastrulation. *Dev Dyn, 195*(4), 290-302. doi: 10.1002/aja.1001950407

Wodarz, A. (2002). Establishing cell polarity in development. *Nat Cell Biol, 4*(2), E39-44. doi: 10.1038/ncb0202-e39

Wodarz, A., Ramrath, A., Grimm, A., & Knust, E. (2000). Drosophila atypical protein kinase C associates with Bazooka and controls polarity of epithelia and neuroblasts. *J Cell Biol, 150*(6), 1361-1374. doi: 10.1083/jcb.150.6.1361

Woolner, S., & Bement, W. M. (2009). Unconventional myosins acting unconventionally. *Trends Cell Biol, 19*(6), 245-252. doi: 10.1016/j.tcb.2009.03.003

Wu, L. H., & Lengyel, J. A. (1998). Role of caudal in hindgut specification and gastrulation suggests homology between Drosophila amnioproctodeal invagination and vertebrate blastopore. *Development, 125*(13), 2433-2442.

Wu, S. Y., Ferkowicz, M., & McClay, D. R. (2007). Ingression of primary mesenchyme cells of the sea urchin embryo: a precisely timed epithelial mesenchymal transition. *Birth Defects Res C Embryo Today, 81*(4), 241-252. doi: 10.1002/bdrc.20113

Yamada, S., & Nelson, W. J. (2007). Localized zones of Rho and Rac activities drive initiation and expansion of epithelial cell-cell adhesion. *J Cell Biol, 178*(3), 517-527. doi: 10.1083/jcb.200701058

Yamada, S., Pokutta, S., Drees, F., Weis, W. I., & Nelson, W. J. (2005). Deconstructing the cadherin-catenin-actin complex. *Cell, 123*(5), 889-901. doi: 10.1016/j.cell.2005.09.020

Yamaguchi, M., Date, T., & Matsukage, A. (1991). Distribution of PCNA in Drosophila embryo during nuclear division cycles. *J Cell Sci, 100 (Pt 4)*, 729-733.

Yamanaka, T., Horikoshi, Y., Sugiyama, Y., Ishiyama, C., Suzuki, A., Hirose, T., . . . Ohno, S. (2003). Mammalian Lgl forms a protein complex with PAR-6 and aPKC independently of PAR-3 to regulate epithelial cell polarity. *Curr Biol, 13*(9), 734-743. doi: 10.1016/s0960-9822(03)00244-6

Yamanaka, T., Horikoshi, Y., Suzuki, A., Sugiyama, Y., Kitamura, K., Maniwa, R., . . . Ohno, S. (2001). PAR-6 regulates aPKC activity in a novel way and mediates cell-cell contact-induced formation of the epithelial junctional complex. *Genes Cells, 6*(8), 721-731. doi: 10.1046/j.1365-2443.2001.00453.x

Yao, M., Qiu, W., Liu, R., Efremov, A. K., Cong, P., Seddiki, R., . . . Yan, J. (2014). Force-dependent conformational switch of alpha-catenin controls vinculin binding. *Nat Commun, 5*, 4525. doi: 10.1038/ncomms5525

Yeaman, C., Grindstaff, K. K., Hansen, M. D., & Nelson, W. J. (1999). Cell polarity: Versatile scaffolds keep things in place. *Curr Biol, 9*(14), R515-517. doi: 10.1016/s0960-9822(99)80324-8

Yonemura, S., Wada, Y., Watanabe, T., Nagafuchi, A., & Shibata, M. (2010). alpha-Catenin as a tension transducer that induces adherens junction development. *Nat Cell Biol, 12*(6), 533-542. doi: 10.1038/ncb2055

Yoshida, C., & Takeichi, M. (1982). Teratocarcinoma cell adhesion: identification of a cell-surface protein involved in calcium-dependent cell aggregation. *Cell, 28*(2), 217-224. doi: 10.1016/0092-8674(82)90339-7

Yumura, S., Yoshida, M., Betapudi, V., Licate, L. S., Iwadate, Y., Nagasaki, A., . . . Egelhoff, T. T. (2005). Multiple myosin II heavy chain kinases: roles in filament assembly control and proper cytokinesis in Dictyostelium. *Mol Biol Cell, 16*(9), 4256-4266. doi: 10.1091/mbc.e05-03-0219

Zahraoui, A., Louvard, D., & Galli, T. (2000). Tight junction, a platform for trafficking and signaling protein complexes. *J Cell Biol, 151*(5), F31-36. doi: 10.1083/jcb.151.5.f31

Zallen, H., & Zallen, E. M. (1976). *Ideas plus dollars : research methodology and funding*. Norman, Okla.: Academic World.

Zallen, J. A. (2007). Planar polarity and tissue morphogenesis. *Cell, 129*(6), 1051-1063. doi: 10.1016/j.cell.2007.05.050

Zallen, J. A., & Wieschaus, E. (2004). Patterned gene expression directs bipolar planar polarity in Drosophila. *Dev Cell, 6*(3), 343-355. doi: 10.1016/s1534-5807(04)00060-7

Zalokar, M. (1976). Autoradiographic study of protein and RNA formation during early development of Drosophila eggs. *Dev Biol, 49*(2), 425-437. doi: 10.1016/0012-1606(76)90185-8

Zang, J. H., & Spudich, J. A. (1998). Myosin II localization during cytokinesis occurs by a mechanism that does not require its motor domain. *Proc Natl Acad Sci U S A, 95*(23), 13652-13657. doi: 10.1073/pnas.95.23.13652

Zhao, T., Graham, O. S., Raposo, A., & St Johnston, D. (2012). Growing microtubules push the oocyte nucleus to polarize the Drosophila dorsal-ventral axis. *Science, 336*(6084), 999-1003. doi: 10.1126/science.1219147

Zihni, C., Mills, C., Matter, K., & Balda, M. S. (2016). Tight junctions: from simple barriers to multifunctional molecular gates. *Nat Rev Mol Cell Biol, 17*(9), 564-580. doi: 10.1038/nrm.2016.80

Zusman, S. B., & Wieschaus, E. F. (1985). Requirements for zygotic gene activity during gastrulation in Drosophila melanogaster. *Dev Biol, 111*(2), 359-371. doi: 10.1016/0012-1606(85)90490-7

Annex

A- Book chapter

Composite morphogenesis during embryo development

Alphy John and Matteo Rauzi

Seminars in Cell and Developmental Biology xxx (xxxx) xxx

Contents lists available at ScienceDirect

Seminars in Cell and Developmental Biology

journal homepage: www.elsevier.com/locate/semcdb

Review

Composite morphogenesis during embryo development

Alphy John, Matteo Rauzi *

Université Côte d'Azur, CNRS, Inserm, Nice, France

ARTICLE INFO

Keywords:
Concomitant tissue shape changes
Gastrulation
Neurulation
Folding
Convergence-extension
Tissue mechanics
Gene patterning synergy
Coordinated and patterned cell mechanisms
Multi-tiered cell mechanisms

ABSTRACT

Morphogenesis drives the formation of functional living shapes. Gene expression patterns and signaling pathways define the body plans of the animal and control the morphogenetic processes shaping the embryonic tissues. During embryogenesis, a tissue can undergo composite morphogenesis resulting from multiple concomitant shape changes. While previous studies have unraveled the mechanisms that drive simple morphogenetic processes, how a tissue can undergo multiple and simultaneous changes in shape is still not known and not much explored. In this chapter, we focus on the process of concomitant tissue folding and extension that is vital for the animal since it is key for embryo gastrulation and neurulation. Recent pioneering studies focus on this problem highlighting the roles of different spatially coordinated cell mechanisms or of the synergy between different patterns of gene expression to drive composite morphogenesis.

1. Introduction

During embryo development, a cluster of cells can be shaped into a plethora of different living forms. Each form is designed to provide specific features and functionalities to each animal, thus contributing to the great diversity and beauty of the animal kingdom. While the number of living shapes is innumerable, 7 is the number of fundamental epithelial transformations that are required to mold the embryo into a living form. Tissues (i) grow, (ii) shrink, (iii) thicken, (iv) thin, (v) twist, (vi) converge-extend and (vii) fold to give shape to the mature animal. Epithelial convergence-extension and folding are two fundamental tissue shape changes that often occur at the onset of embryogenesis. While extension can, for instance, elongate the animal body separating the anterior (where the head and mouth are located) from the posterior (where the anus is located), folding can translocate cells into the interior separating the outside from the inside of the animal. Over the last century, these two morphogenetic processes have been intensively studied since they are primordial for the emergence of multicellular life. Folding and extension have often been studied separately as two distinct and uncoupled processes (i.e., two 'simple' morphogenetic processes) controlled by distinct gene expression patterns and signaling pathways known to specify animal body plans [1]. Nevertheless, folding and extension often occur simultaneously (e.g., during gastrulation and neurulation) resulting in a composite morphogenetic process [2]. How *composite morphogenesis* is controlled and driven is still a question that has not been thoroughly considered and that deserves great attention.

Before addressing the problem of composite morphogenesis, in the first part of this chapter we review the common origin of the gene expression patterns responsible for different body plan specification. We then present how distinct gene expression patterns, extending along different body axes, can be uncoupled from each other to independently control simple morphogenetic processes. Finally, we present the process of composite morphogenesis resulting from multiple and concomitant changes in the shape of a tissue. More specifically, we focus on the process of concomitant tissue folding and extension that is key during embryo gastrulation and neurulation.

2. Embryonic axis specification is under the control of a common organizer

Metazoans originate from a single cell, the zygote. The zygotic cell undergoes stereotypic divisions to give rise to the embryonic blastula. Cells eventually remodel their shape, divide, die, translocate and rearrange to give shape to the mature animal. During this process, the blastoderm cells are guided by instructive signals that control body axis orientation, morphogenesis and cell specification leading to the formation of the three fundamental germ layers. For instance, Gurken-mediated EGFR signaling is necessary for anterior-posterior (AP) and dorsal-ventral (DV) axis establishment during oogenesis in *Drosophila* [3,4]. Gurken (Grk) was firstly identified in 1993 as a DV axis generator with *gurken* mRNA accumulating anterior-dorsally at a position juxtaposed to the oocyte nucleus [5] (Fig. 1 A). Gurken is a secreted ligand

* Corresponding author.
E-mail address: matteo.rauzi@univ-cotedazur.fr (M. Rauzi).

https://doi.org/10.1016/j.semcdb.2021.06.007
Received 24 March 2021; Received in revised form 23 May 2021; Accepted 13 June 2021
Available online 23 June 2021

signaling to follicle cells near the oocyte nucleus. Embryos derived from *grk* mutants were reported to exhibit ventralization [6]. In 1995 Gonzalez-Reyes et al. and Roth et al. showed that Gurken/EGFR also signals to posterior follicle cells to establish the AP axis. Therefore, mutants for *grk*, *egfr/torpedo (top)* or *cornichon* (Cni, a protein involved in Gurken secretion [7,8]) show both DV and AP defects [9,10]. *bcd* mRNA localizes to the anterior and *osk* mRNA to the posterior poles of the wild type oocyte. In *grk* mutants, *bcd* mRNA accumulates at both anterior and posterior poles and *osk* mRNA is mislocalized to the center of the oocyte [9]. Therefore, EGFR signaling between the developing oocyte and somatic follicle cells acts as a common organizer for both AP and DV gene patterning in *Drosophila*.

The planarian worm is a powerful model system for studying axes specification due to its extensive ability to regenerate: a small portion excised from any part of the worm body can regenerate to form a new and fully functional worm [11]. In planarians the midline blastema cells function as an organizer for both AP and DV gene patterning [12]. The existence of an organizer, defining the animal body axes, has also been reported during vertebrate embryogenesis [13]. It was dubbed Spemann's organizer in salamander [14] and Xenopus [15–17], Hensen's node in chick [18,19] and the 'embryonic shield' in zebrafish [20–24]. By implementing tissue grafting techniques, Spemann and Mangold discovered that a piece of dorsal lip from a donor salamander embryo generated a complete secondary axis when grafted to the recipient embryo (seemingly similar to Siamese twins, Fig. 1 B) [14]. Spemann's organizer potency for axes specification depends on the number of organizer cells [16]. The molecular identity of Spemann's organizer was later identified. One of the molecular factors participating to this organizer is, for instance, the homeobox-family protein Goosecoid (Gsc). Microinjection of *gsc* mRNA at the ventral region is sufficient to induce twinned axes [15]. Furthermore, the organizer secretes a set of BMP and Wnt antagonists (e.g., Noggin, Chordin, and Frzb under the control of Nodal and β-Catenin) to counteract the ventrally produced BMP and Wnt ligands [25,26]. Recently, an organizer with a molecular signature similar to Spemann's organizer was identified in echinoderms. Ectopic Nodal expression was sufficient to induce Siamese twin formation in the sea urchin pluteus [27]. Similarly, cells showing organizer activity and that provide positional cues to the other cells of the embryo were also identified during organ formation. Examples have been shown in the notochord during nervous system development [28], in the zone of

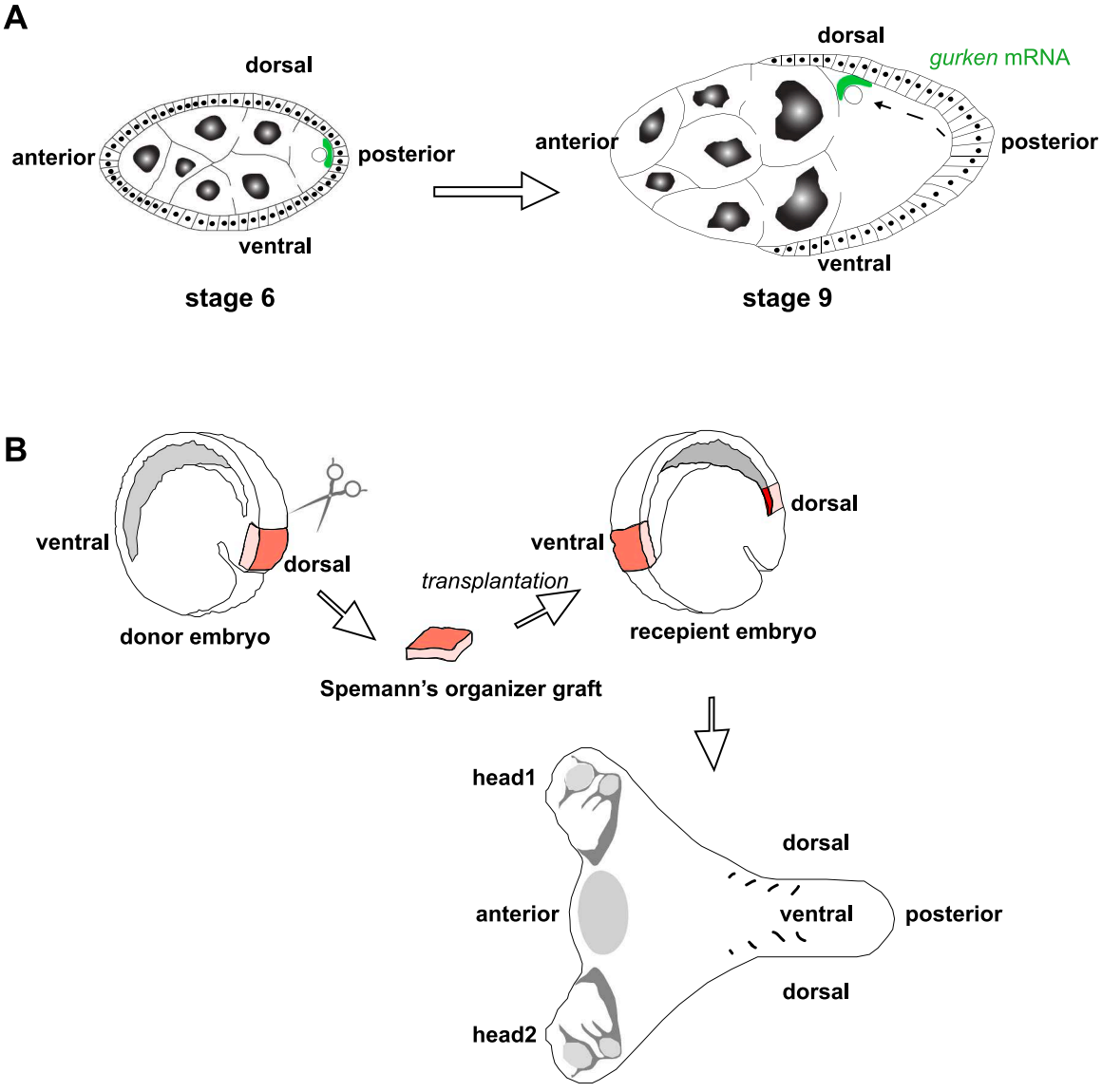

Fig. 1. Common organizers define embryonic axes. **(A)** *gurken* mRNA (green) localizes to the posterior pole during stage 6 of oogenesis (left) and translocates at a later stage (stage 9) to an anterior-dorsal position in the *Drosophila* oocyte. **(B)** Schematic representation of the grafting experiment performed by Spemann and Mangold in Newt embryos. Transplantation of the dorsal lip from a donor embryo to the ventral side of a recipient embryo leads to twinning of the embryonic axes.

polarizing activity (ZPA) of the limb bud [29], in the *zonula limitans intrathalamica* (ZLI) of the vertebrate diencephalon [30,31], and in the mid-hindbrain boundary [32]. Finally, while in insects the oocyte secretes molecules that function as organizers to determine body axes, in vertebrates the secretion of organizer molecules is performed by a specific group of cells in the embryo.

Another tier of regulation of gene expression happens during the initial phase of embryo development. At the onset of embryogenesis, when the zygotic genome is quiescent, the early developmental processes rely on the protein and RNA pool supplied by the mother. It is only during the maternal-to-zygotic transition that the zygotic genome is activated by pioneer transcription factors that boost transcription [33,34]. A well-characterized pioneer factor in *Drosophila* is Zelda [35–37]. Zelda binds to DNA sequences, enhancing gene expression [38–40]. Recent work from McDaniel and colleagues, using optogenetic tools to block Zelda activity, has shown that Zelda is required for zygotic genome activation. Blocking Zelda activity reduces the expression of gene components acting along both the AP (e.g., *eve*, *ftz*, *odd,* etc.) and the DV (e.g., *sog*, *zen*, *sna*, *twi,* etc.) body axes [41]. Transcription factors with pioneering activity have also been identified in other model systems, for instance, Oct4 in mouse [42] and Pou5f1, Nanog, and Sox1 in zebrafish [43,44].

Finally, a centralized signaling hub, working as a positional organizer, plays a pivotal role to establish gene patterning and cell specification along the different embryonic axes.

3. Gene expression patterns along different axes can be uncoupled from each other acting autonomously

While different gene expression patterns that control distinct body axes specifications originate from the same signal (provided by the organizer or from pioneer factors), the downstream signaling pathways that specify individual axes can act independently. Mutations that result in loss or gain of function in downstream components produce specific patterning defects, generating phenotypes along one body plan without altering cell specification and patterning along another body plan. One classic example is the signaling pathway responsible for the specification of body plans in *Drosophila* [45]. The AP body plan specification in the fruit fly embryo is determined by the AP spatially regulated expression of gap genes (e.g., *huckebein*, *tailless*, *giant*, *hunchback*, *Kruppel*, *knirps* [46–49]) under the control of upstream morphogens (e.g., Bicoid at anterior and Nanos at posterior sides [50–55]). DV body axis specification occurs at the same time and originates from the nuclear localization gradient of the transcription factor Dorsal that controls the transcription of *twist* and *snail* in the ventral and of *zen* and *dpp* in the dorsal region of the embryo [56–60]. Interestingly, the founding studies (identifying maternal and zygotic mutations that alter gene expression patterns along different body axes in the fly embryo) report mutations that affect either AP or DV features of the embryo and not both simultaneously [53,61–67]. This suggests that AP and DV pathways are uncoupled and act independently. This idea is also supported by the evidence that transplanting anterior plasm from wild type embryos to the anterior pole of a *bicoid* mutant embryo is sufficient to rescue AP patterning defects [68]. Similarly, it is possible to rescue a posterior gene mutated embryo by transplanting posterior pole plasm from a wild type embryo [52,69]. Siegfried Roth further tested the relationship between orthogonal gene expression patterns in 1993. Toll (a transmembrane receptor activated by the ventrally produced ligand Spatzle) induces the nuclear localization of Dorsal, thereby initiating DV axis specification. A *Toll*$^{-/-}$ embryo shows no nuclear localization of Dorsal and consequently no ventral fate specification [70]. Interestingly, the seven Even-skipped (Eve) stripes formed along the AP axis in a wild type embryo [47] are unaltered in the *Toll*$^{-/-}$ embryo [71]. Transplantation of wild type plasm induces the expression of *twi* near the injection site. Injection of wild type cytoplasm at the posterior end of a *Toll*$^{-/-}$ embryo results in the posterior expression of *twi*. Remarkably, the posterior expression of *twi* does not alter any of the seven Eve stripes (Fig. 2 A). This further supports the idea that, at this signaling level, the AP and DV signaling pathways are apparently uncoupled in the *Drosophila* embryo [63].

The planarian worm exhibits uncoupling between pathways that control the specification of different body axes. The Wnt/β-Catenin and BMP pathways have been shown to control AP and DV axis specification, respectively [72–77]. Downregulation of *β-catenin* results in hypercephalized flatworms and unaltered expression of dorsal and ventral specification genes (e.g., *septin* and *eye53,* respectively) [77]. In a similar experiment, downregulation of *admp* or *noggin* results in a dorsalized planarian (shown by the expression of *septin* on the ventral side). These experiments, using RNA interference, result in regeneration defects along the DV axis, whereas structures along the AP axis remain unaffected and regenerate normally [78,79] (Fig. 2 B). This provides further evidence for the uncoupling of AP and DV patterning and signaling in planarians.

A certain level of uncoupling between pathways that regulate AP and DV body plans is also shown in vertebrate embryos. Wnt, FGF, and retinoic acid (RA) signaling mediate vertebrate AP [80–82] while BMP signaling mediates DV [83] axis specification. Downregulation of Wnt signaling in the *Xenopus laevis* embryo, using morpholinos against *β-cat*, produces embryo ventralization, while treatment with Lithium Chloride (LiCl) induces embryo dorsalization (LiCl treatment was shown to induce radial expression of BMP antagonists such as Chordin [84]). Conversely, blocking BMP signaling by triple knockdown of *bmp2*, *bmp4* and *bmp7* results in a tail-less embryo, whereas blocking BMP and Wnt signaling together generates a head-like embryo [85]. Similarly, Varga et al. showed that accurate AP patterning of the neuroectoderm is achieved in an *ichabod* (*ich*) mutant zebrafish embryo with *bmp2* morpholino that lacks DV polarity [86]. Uncoupling between gene-patterning along different body axes is reported during vertebrate limb morphogenesis. The AP patterning defines the digit identity whereas the proximal-distal (PD) patterning defines the axis of the upper to lower arm and hand. The AP axis of vertebrate limbs is defined by Sonic hedgehog (Shh) signaling [87] while the PD axis is defined by FGF and RA signaling [88]. Chick embryos mutant for Shh signaling (as in the case of the *oligozeugodactyly* mutant) or with reduced Shh activity (by applying pharmacological inhibitors like cyclopamine) show patterning defects along the AP axis while PD pattern formation remains unaltered [89].

Finally, examples from different model systems show that the patterns of gene expression, imposing cell fate specification and defining the different body plans of the animal while stemming from the same organizing center, can be uncoupled from each other to autonomously control distinct morphogenetic processes along specific body axis. This may be the consequence of specialized signaling factors that activate ad hoc pathways devoid of cross-talk.

4. Composite morphogenesis results from multiple simultaneous changes in the shape of a tissue

The form of an organism is sculpted by the cellular and epithelial changes in shape during embryo development. Cells actively change shape and position during embryogenesis under the control of specifying signaling pathways. This process relies on the gene patterning systems established along the different body plans providing positional coordinates of gene expression. Therefore, gene expression patterns instruct cells to undergo specific shape changes and movements driving morphogenesis.

The 7 simple and fundamental epithelial transformations can take place sequentially. Nevertheless, this is not always the case. Multiple and concomitant simple morphogenetic processes can lead to the composite change in the shape of a tissue. While the mechanisms driving simple morphogenetic processes have been thoroughly studied, how composite morphogenetic processes are controlled and driven remained,

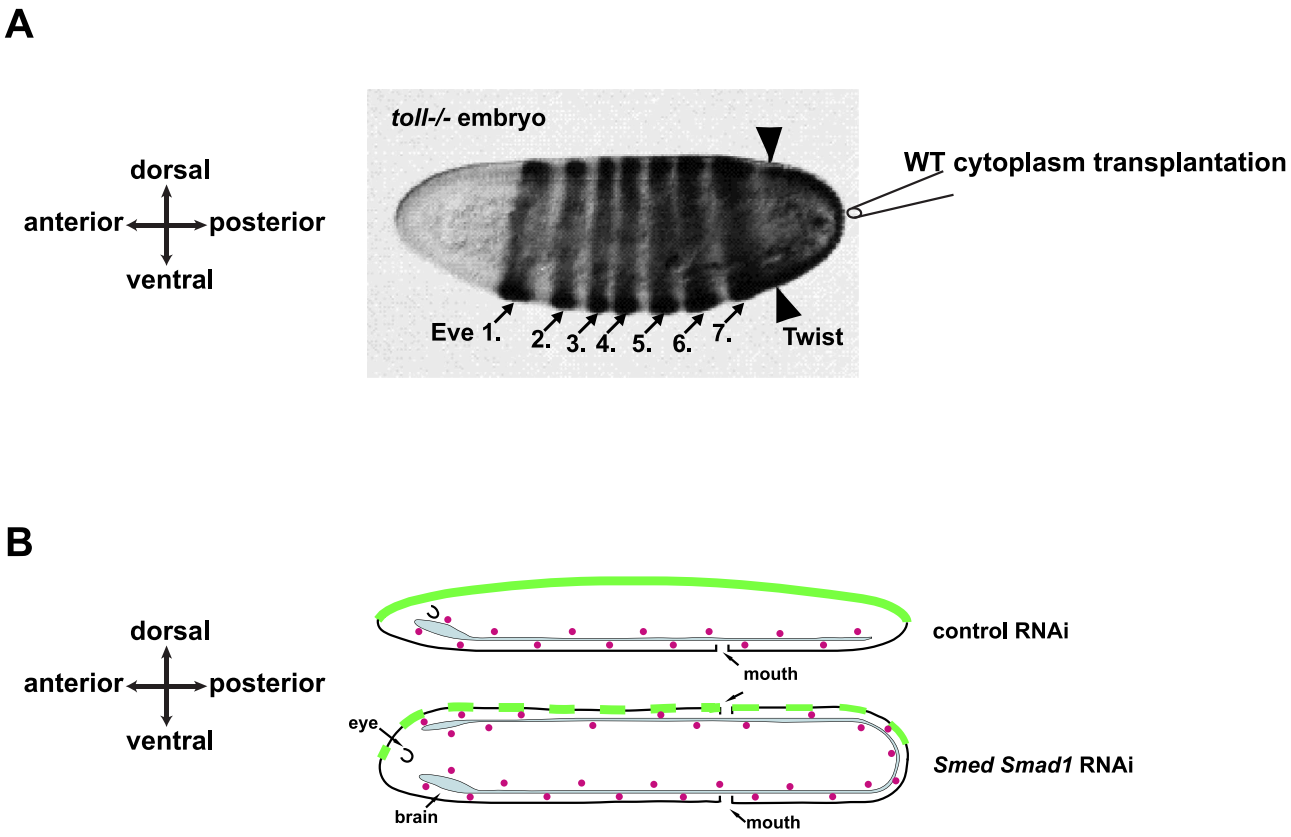

Fig. 2. Gene expression patterns are apparently uncoupled. (A) Representative image showing the seven Eve stripes (arrows) unaffected by transplantation of ventral plasm to posterior in *Toll*$^{-/-}$ embryos. Note that ventral plasm injection results in Twist expression (arrowheads) in the posterior cells. (B) Schematic representation of a ventralized regenerated planarian worm after treatment interfering with BMP signaling using *smad RNAi* (bottom). Worms display patterning defects along the DV axis, while patterning along the AP axis remain unaltered. Dorsal markers are represented as green and ventral-specific cells as magenta circles. (A) adapted from [63]. (B) Adapted from [73].

until recently, unexplored. The remainder of this chapter will focus on the process of concomitant folding and extension that is key during embryo gastrulation and neurulation. We will highlight two modes of concomitant folding-extension: (i) uniaxial and (ii) orthogonal both leading to the formation of an epithelial tube. In the former mode, folding and extension take place along the same axis synergistically driving tissue budding. This composite morphogenetic process may emerge from the coordination of multiple radially patterned cell mechanisms. In the latter mode, folding and extension take place along orthogonal axes, separately driving tissue wrapping and elongation. A recent pioneer study shows that this composite morphogenetic process is driven by a cell combo-mechanism under the synergistic control of orthogonal gene patterning signals.

5. Uniaxial tissue folding and extension

The process of simultaneous tissue folding and extension can occur along one same axis driving tissue in-pocketing (also referred to as tissue budding) and eventually the formation of an epithelial tube. Examples of this are, for instance, the processes of salivary gland [90–92], trachea [93–95], and intestine [96] formation, or endoderm/mesoderm internalization in early embryogenesis during gastrulation [97–100]. Tissue in-pocketing results from the extension of a planar epithelium into the third dimension to form a fold. During epithelial in-pocketing, tissue extension and folding cooperate to form a budding tube. As a consequence, the cell mechanisms known to drive tissue extension (e.g., polarized cell stretching, intercalation, cell division, migration) may synergize with mechanisms known to drive tissue folding (e.g., apical constriction, apical-basal shortening, basal expansion). The planar cell polarized signals and mechanisms driving out-of-plane tissue extension are patterned differently from what is usually reported for the canonical planar cell polarity (PCP) patterns driving in-plane tissue extension [101,102]. For budding tissues, the signaling factors and the cell shape and topology changes follow a circular geometry centered on the tissue budding region and develop radially from this point, resulting in out-of-plane tissue extension [91,93,94,98,103–105]. Therefore, epithelial in-pocketing is a process that results from the combination of different spatio-temporally coordinated cell mechanisms that are radially distributed and polarized in the plane of the tissue. In the remaining part of this section, we present two examples of epithelial in-pocketing (i) during salivary gland formation in the developing *Drosophila* embryo and (ii) during archenteron formation in the sea urchin gastrula.

5.1. Salivary gland placode folding and extension

A key function of the *Drosophila* salivary glands (SGs) is to produce and eventually release the secretory glue needed to affix the *de novo* formed puparium, within which the larva will undergo metamorphosis, to a substrate. During SG formation, the SG placode (an epithelial tissue formed of around 100 cells) in-pockets, forming an epithelial tube [106]. Under determined mutated conditions, the epithelial tube can evaginate. This shows that the process of tube formation in the SG placode does not require contact with internal tissues [107]. Surprisingly, cells in evaginated tubes invert their apical-basal polarity, resulting in the apical side facing the inside of the tube devoid of luminal space. This supports the idea that the process of SG tube formation takes place in a tissue-autonomous fashion and can be decoupled from the process of tube internalization. Before tissue budding, an actomyosin cable forms

around the SG placode. Katja Röper showed in 2012 that this cable is under tension and contributes to the in-pocketing of the placode. The actomyosin cable drives tissue centripetal convergence towards the budding locus, working as a contractile purse-string [108]. At the onset of tissue budding, cell shape and topology changes take place following a circular symmetry: while cells in the budding locus apically constrict, the crown of cells around the bud intercalate following a radial pattern (tangential junctions shrink while new junctions form along a radial direction) [104]. While apical constriction initiates tissue bending, extending the SG placode in the third dimension, radially polarized cell intercalation promotes centripetal tissue extension and circumferential tissue convergence (the latter reinforced by the actomyosin circumferentially contracting cable) (Fig. 3). The distribution of molecular force generators mirrors the radial cell shape and topology changes. Cells located in the center accumulate medial-apical fiber actin (F-actin) and MyoII that generate contractile forces that constrict the apical surface area of cells (seemingly similar to what is reported during mesoderm invagination [109]). The transcription factor Fork head (Fkh) is necessary for SG tube formation [91] and is required for medial-apical MyoII accumulation in apically constricting cells promoting Rho kinase (Rok) apical recruitment via Fog [107]. While cell apical constriction is necessary for the correct SG tube shape, surprisingly cell apical constriction is not necessary for tube formation per se in contrast to what is reported to occur for mesoderm fold formation [110]. In *fog*- embryos, in which apical constriction is strongly perturbed, the SG tube is intact, closed and correctly polarized with the cell apical side facing towards the inside of the tube. Nevertheless, *fog*- embryos show a great variety of tube shapes and topologies: tubes can form with normal shape, can twist or, in more than 1/3 of the cases, can evaginate and extend outside the embryonic body. These observations show that apical constriction is necessary to pre-sculpt the shape of the central budding region of the SG placode (resulting in a concave cup shape) to impose directionality during the tube extension phase providing robustness to the overall process [111]. Cells located in the crown region, surrounding the patch of cells that apically constrict, show a planar polarized distribution of MyoII with tangential junctions showing higher levels of MyoII than radial junctions. Cortical actomyosin has previously been shown to increase tension to initiate junction shortening [112]. This is the first step of cell intercalation in simple epithelia [113]. MyoII junctional accumulation is controlled by the transmembrane protein Crumbs, which is planar cell polarized and which activates the Par6/Cdc42/Pak1 pathway, modulating the dissociation rate (k_{off}) of Rok [108,114]. In *fkh*- embryos, in which apical constriction of the central SG placode is abolished, junction remodeling still takes place but is no longer polarized. Junctions with higher levels of MyoII (the motor protein is no longer planar cell polarized in an *fkh*- background) shrink to a four-way junction (i.e., a configuration in which four cells meet) but new junctions do not form, resulting in an incomplete non-polarized cell

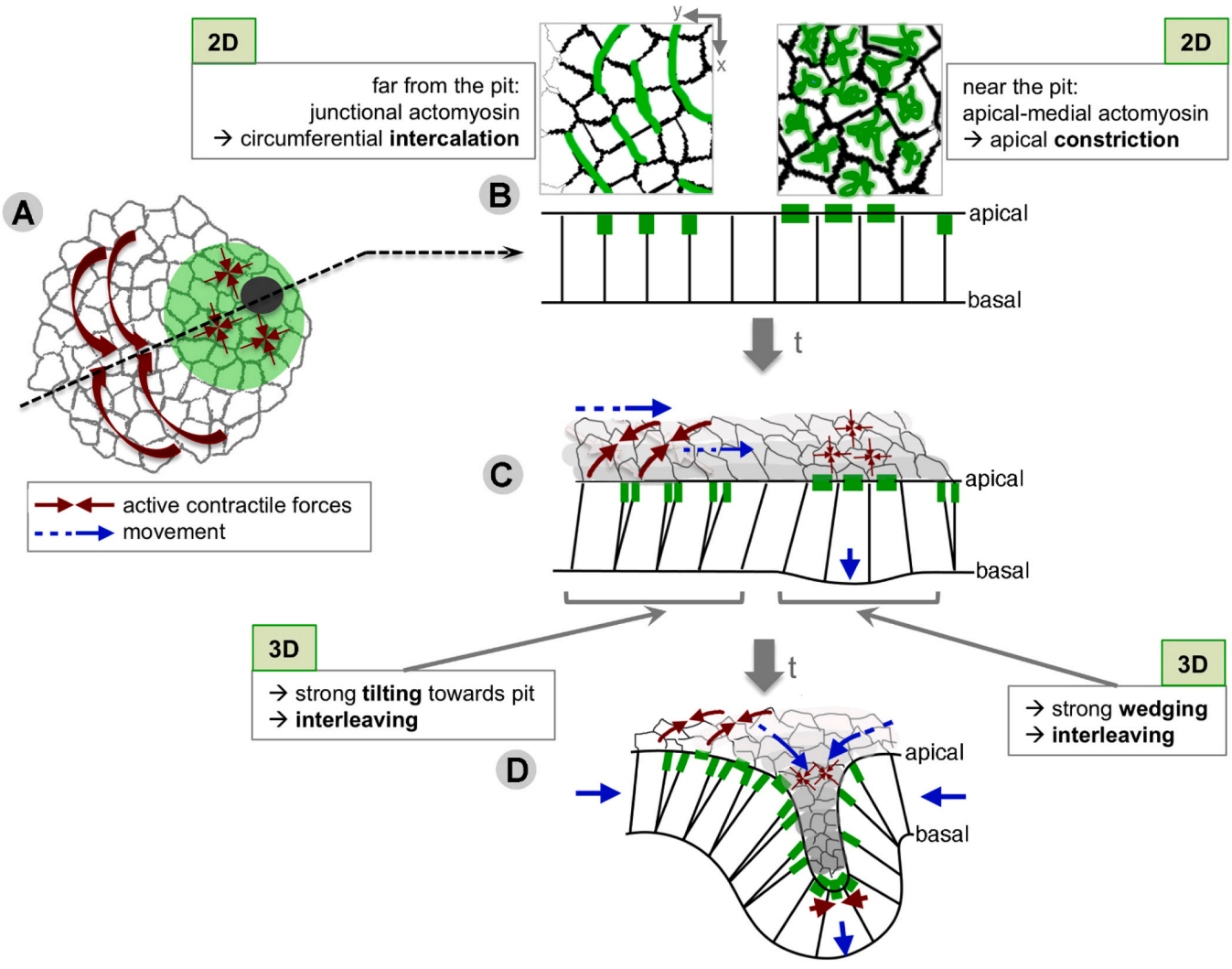

Fig. 3. Tissue in-pocketing during salivary gland formation. Schematic representation of the process of salivary gland placode folding and extension. Adapted from [104].

intercalation process. This evidence supports the idea that, while junction shrinkage is a cell-autonomous process driven by junctional actomyosin contraction, new junction formation and extension may be a passive response to the centripetal pulling force exerted by the patch of cells that apically constrict. This observation further supports the idea that the transcription factor Fkh controls MyoII radial PCP. In a circular geometry, PCP could be achieved, for instance, by a radially graded distribution of signaling factors (e.g., Fkh) from a source point outwards, following the same principle of uniaxial PCP that is controlled by a unidirectionally oriented gradient (e.g., the AP distribution of Bicoid in the early developing *Drosophila* embryo). Finally, tube formation and extension is powered by (i) cells in the central region of the SG placode that apically constrict to locally bend the tissue inward to bias the direction of bud extension and (ii) the actomyosin cable (surrounding the SG placode) accompanied by radially polarized intercalations of cells located in the crown region surrounding the central patch of apically constricting cells.

5.2. Vegetal plate folding and extension during sea urchin gastrulation

The sea urchin is historically among the first model systems used to study embryo gastrulation [115–117]. The sea urchin gastrula combines a number of outstanding features making this model system a unique opportunity to study the mechanisms and mechanics of tissue folding: (1) this embryo is a very simple thus appealing system for experimentation and mathematical modelling since it is constituted of about 1000 cells forming a hollow spherical monolayer epithelium surrounded and filled with water; (2) all 1000 cells can be imaged and 3D segmented over time since the sea urchin gastrula is transparent; (3) the signaling factors controlling sea urchin vegetal plate folding and extension are known and can be tuned to dissect their function; (4) the gastrula is a mechanically accessible tissue: it can be partitioned [118], cells can be transplanted [119], and micro-indentation and micro-pipetting techniques [120–122] can be applied to measure tissue mechanical properties. The sea urchin gastrula is thus a perfect playground for cell and developmental biologists and biophysicists. Sea urchins from different species and families are studied (e.g., *Lytechinus pictus* in the eastern Pacific Ocean, *Lytechninus variegatus* in the Caribbean Sea and in the western Atlantic Ocean, *Paracentrotus lividus* in the Mediterranean Sea and in the eastern Atlantic Ocean, *Stronglyocentrotus purpuratus* in the eastern Pacific Ocean, *Stronglyocentrotus drobachiensis* in the northern Pacific and Atlantic Oceans, *Hemicentrotus pulcherrimus* in the western Pacific Ocean, *Arbacia punctulata* in the Atlantic Ocean) providing a plethora of sea urchin model systems that can be compared.

During sea urchin gastrulation, the vegetal plate in-pockets by folding inwards and eventually by extending to form a tubular epithelium (also known as archenteron) that constitutes the primordial gut of the future sea urchin pluteus. The formation of the archenteron is divided into two phases: (i) a first phase named 'primary invagination' that results in tissue bending (forming a concave cup shape) and (ii) a second phase named 'secondary invagination', during which the folded vegetal plate extends towards the interior of the embryo crossing the inner hollow space (the blastocoel, Fig. 4). In *Lytechinus pictus*, if the vegetal pole is isolated microsurgically from the rest of the blastoderm, the vegetal plate still folds and partially extends, supporting the idea that the forces responsible for primary invagination are generated by the cells located in the vegetal 1/3 of the blastoderm [123].

During primary invagination, a ring of cells (the prospective secondary mesenchymal cells) apically constricts around a group of quiescent cells (the small micromeres) located in the center of the vegetal plate. The process of cell apical constriction is accompanied by a reorganization of the F-actin network that becomes denser in these cells. Embryos treated with a calcium channel activator or blocker show initiation or inhibition, respectively, of apical constriction and primary invagination [98]. If apically constricting cells are removed by laser ablation, the primary invagination of the vegetal plate is delayed suggesting that these cells play a role in the folding process [124].

Filopodia are formed at the basal side of cells located at the vegetal plate. Protrusion activity begins during primary invagination and it is reinforced during secondary invagination when cells extend longer and more numerous protrusions [125]. During archenteron elongation, filopodia projected from the basal side of cells located at the vegetal plate, reach the basal side of cells located at the animal pole (on the opposite side) eventually exerting traction forces. Jeff Hardin in 1988 probed the role of cell filopodia by performing filopodia laser ablation [126]. These experiments show that traction forces exerted via filopodia contribute to archenteron elongation during secondary but not primary invagination. In a filopodium ablated condition, the archenteron extension is reduced by 30%. This supports the idea that other filopodium-independent processes still account for 70% of archenteron elongation. This idea is also supported by the fact that in both *Lytechinus pictus* and *Strongylocentrotus purpuratus* exogastrulae (i.e., embryos forming an archenteron that extends outwards) the archenteron still extends by 70% [97,115,123,126]. What other mechanism could thus drive archenteron elongation? Radial cell intercalation of vegetal plate cells has been suggested to be another mechanism driving archenteron extension during secondary invagination [97,127–129]. Cells, by exchanging neighbors in a radially polarized fashion, would reduce and increase the width and length of the archenteron, respectively. A study by Jeff Hardin and Michael Weliky suggests that filopodium traction forces could also contribute to cell rearrangement in the late phase of convergence-extension of the archenteron [128]. Other mechanisms have been proposed to play a role in vegetal plate folding and extension as, for instance, cell tractoring [130], spatio-temporally coordinated swelling of the extracellular matrix [98,131] and modulation of blastocoel osmotic pressure [132]. Some of these mechanisms have been tested by implementing mathematical models [97,133–135].

Several signaling pathways driving vegetal plate folding and extension have been identified in *Lytechinus variegatus* and *Paracentrotus lividus*: (i) a non-canonical Wnt/PCP pathway transduced via the Frizzled5/8 receptor is required for primary invagination [103]. The Wnt/PCP small RhoGTPases, RhoA and Cdc42, have also been shown to

Fig. 4. Tissue in-pocketing during sea urchin embryo gastrulation. Time lapse images of vegetal plate folding and archenteron elongation during sea urchin embryo gastrulation.

be key players during primary invagination since RhoA downregulation inhibits primary invagination while RhoA overexpression induces precocious invagination [136]. (ii) The canonical Wnt/β-catenin pathway via the Frizzled1/2/7 receptor is necessary for secondary invagination [137–140] and (iii) FGF signaling is necessary to drive the invagination process in a timely fashion [141]. A renewed effort is now needed to unravel how the different signaling pathways control the mechanisms and mechanics responsible for cell shape and topology changes that drive folding and extension and result in vegetal plate in-pocketing.

6. Concomitant tissue folding and extension along orthogonal axes

Concomitant tissue folding and extension can take place along orthogonal axes. For example, during neurulation in tetrapods, the anterior-dorsal tissue folds to form the neural tube while extending (together with the rest of the animal body) to separate the head from the anus [142–145]. Another example has been recently highlighted in the study by John and Rauzi showing that the prospective mesoderm undergoes simultaneous and orthogonal tissue folding and extension on the ventral region of the *Drosophila* embryo during gastrulation [102]. Since folding and extension in these processes are orthogonal, thus a priori independent, cells may need to perform multiple independent morphological and topological transformations simultaneously. How does composite orthogonal morphogenesis take place? One hypothesis could be that simultaneous and orthogonal morphogenetic processes could result from the simple addition of independent signaling pathways or cell mechanisms driving different cell shape and topology changes. Specific changes in cell shape and topology are driven by specialized mechanisms finely tuning the cell cytoskeleton that is eventually remodeled to generate mechanical forces at the cell cortex. Even if upstream signaling pathways were instructive for distinct morphogenetic processes, downstream (at the cytoskeleton level) all pathways, that spatially and temporally superpose, are intended to cross-talk or synergize since the nature of the forces and of the force generating factors is common (Fig. 5). Therefore, the naïve hypothesis that composite orthogonal morphogenesis could result from the simple addition of independent signaling pathways driving different cellular mechanisms is to be excluded. How multiple specialized cell mechanisms coexist and act simultaneously in a coordinated fashion to remodel the same cortical cytoskeletal substrate is not clear. Signals, which are under the control of distinct gene expression patterns, may synergize at different levels of the signaling cascade (Fig. 5 – gray side bars) resulting in the emergence of novel combined mechanisms driving composite morphogenesis along orthogonal directions.

In the following, we review recent pioneering advances in the study of primary neurulation and mesoderm invagination highlighting our current understanding of how composite and orthogonal morphogenetic processes are controlled and driven.

6.1. Neural plate orthogonal folding and extension during primary neurulation

The formation of the neural tube (Fig. 6 A) is thought to rely on both extrinsic and intrinsic forces [146]. Removal of the stratified tissue (composed of the non-neural ectoderm, the mesoderm and the endoderm stacked on top of each other), located laterally to the neural-ectoderm, inhibits bending of the neural plate [147]. However, removal of the mesoderm and endoderm tissues does not impede neural plate bending [148]. This suggests that extrinsic forces generated by the non-neural ectoderm could play a key role in neural plate folding. Cells lying laterally to the neural plate could generate forces that drive bending via medially directed spreading (a process also referred to as 'tractoring') [149]. Apical surface area reduction (i.e., apical constriction) of cells located in the central-medial region of the neural plate (where the neural-groove is formed) is a process that takes place at the

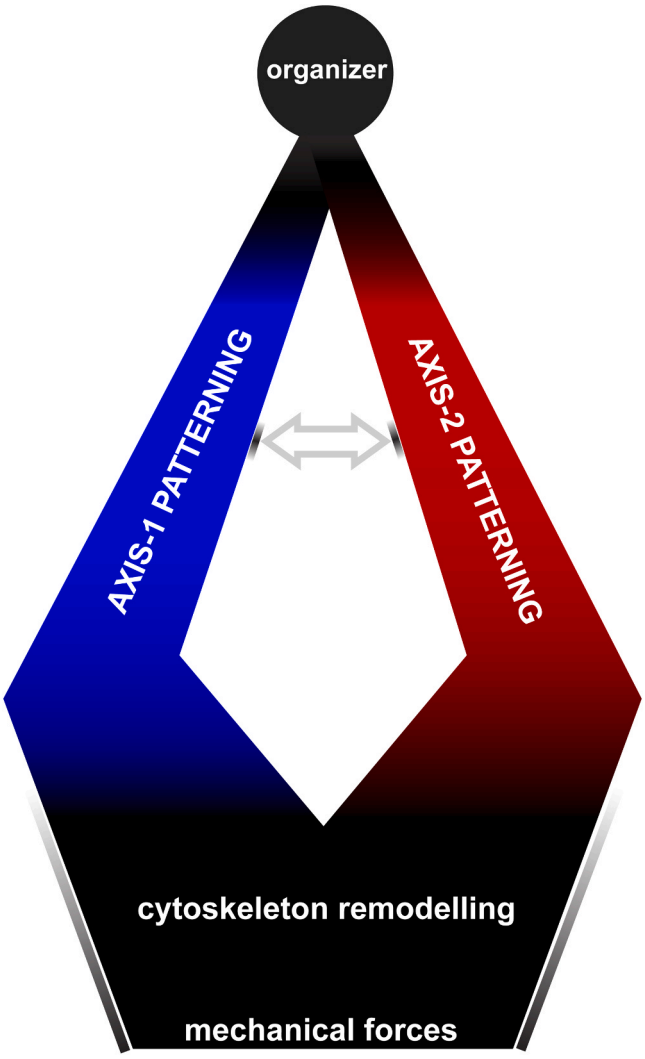

Fig. 5. Gene patterning synergy diagram. Diagram showing the signaling pathways along DV and AP axes. Gray shaded side bars indicate possible synergy between DV and AP signaling patterns. Gray double-headed arrow indicates possible upstream synergy as presented in [198] and, most remarkably, in long shaped insects (e.g., honeybee embryos) [199]. Upstream synergy can also be mediated by coordinating factors [200,201]. While upstream synergy involves ad hoc signaling factors, downstream synergy results from DV and AP signaling pathways merging towards common cellular factors/components and ultimately to physical forces of the same nature.

onset of neural plate involution (first reported in 1970 by T.E. Schroeder [150]). Apical constriction is a process that drives cell wedging and that often accompanies tissue bending [151] but which is probably not sufficient and not always necessary [107,111] for tissue folding. Quantitative studies have reported that only a small group of cells (located in the lateral and medial 'hinge' points of the neural plate) undergo apical constriction [150,152–154]. Remarkably, removal of the medial hinge region of the neural plate inhibits subsequent folding only at the forebrain level and not in the rest of the neural plate [155]. This evidence supports the idea that apical constriction in the central medial part of the neural plate is necessary for folding only in the most anterior region of the neural-ectoderm.

The neural plate, during folding, converges towards the dorsal midline and extends along the AP axis of the embryo. By using distortion diagrams, Elul and colleagues in 1997 concluded that the part of the neural ectoderm closer to the dorsal midline undergoes greater convergence-extension than the more laterally located part [156]. In addition, neural-ectoderm explants, taken from regions closer to the

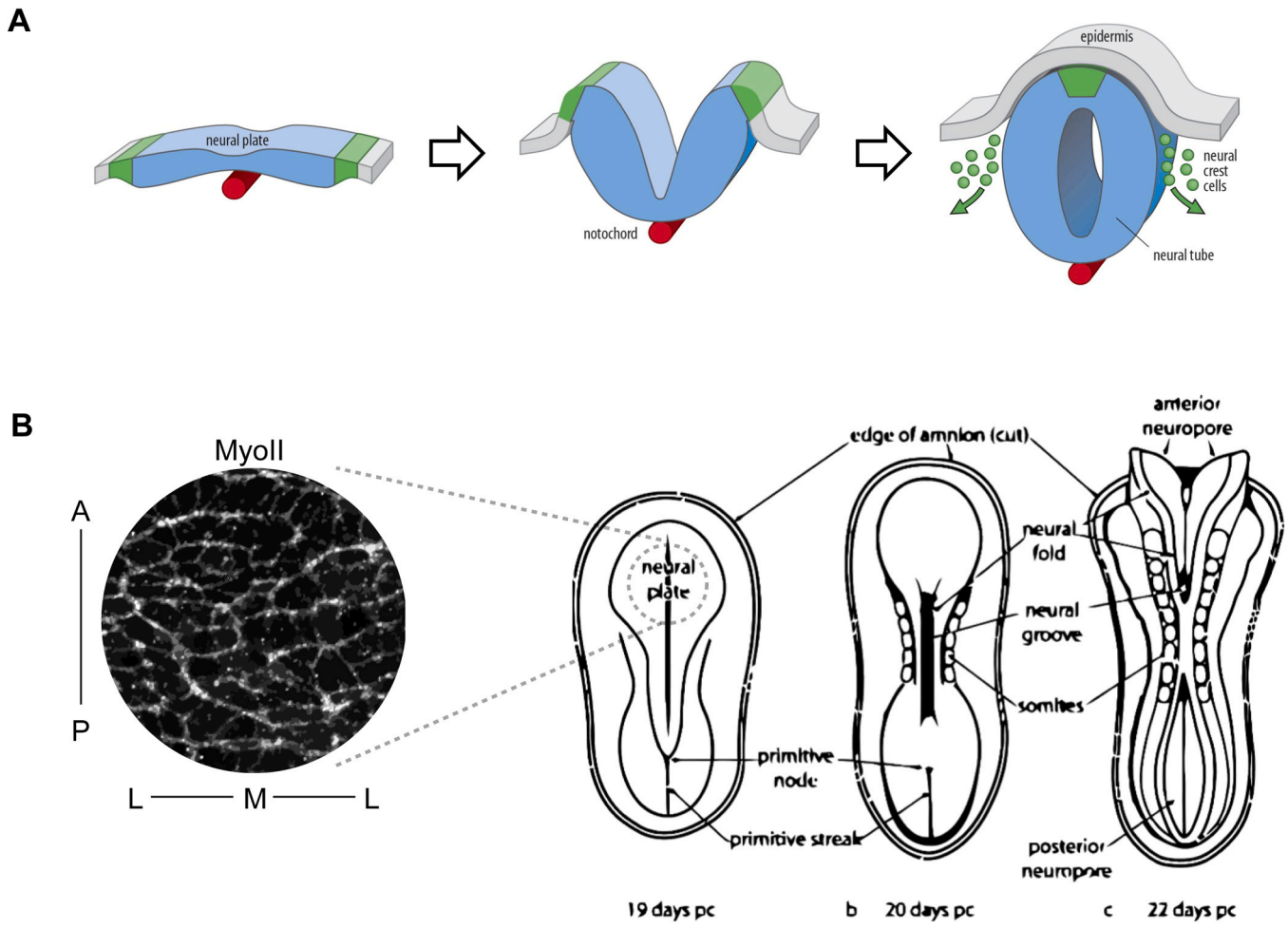

Fig. 6. Neurulation in the chick embryo. (A) Schematic representation of the process of neurulation. **(B)** MyoII distribution in the neural plate during neuroepithelium folding and extension. Anterior (A), posterior (P), medial (M) and lateral (L).
Adapted from [https://en.wikipedia.org/wiki/Neural_plate] and from [2].

dorsal midline, undergo enhanced convergence-extension. This suggests that the medial portion of the neural tissue may contribute more to convergent extension than the lateral portion that would offer resistance. A dynamic analysis at the cellular scale shows that cells located in the midline undergo planar polarized cell intercalation converging medio-laterally and separating antero-posteriorly [157]. Intercalation can take place via junction remodeling (as shown in the mouse and chick, [2,158]) or via polarized protrusive activity (for instance, as shown in the Xenopus [143,159,160]).

Changes in cell shape and topology are accompanied by cytoskeletal remodeling. For example, actomyosin accumulates along junctions and in the medio-apical cortex of neuroepithelial cells [161–164]. In the *Xenopus laevis* neural epithelium, a reduction in apical intermediate filaments and an increase in basal-to-apical microtubule arrays is also reported [165]. During neural plate folding, nuclei migrate from a more apical to a more basal position. This process was first named 'interkinetic nuclear migration' in 1978 [166] and was reported in avian [167] and amphibian [168] neurulation and in other epithelial folding processes (e.g., in *Drosophila* mesoderm invagination [58]). While the actomyosin network is known to be a key player in the generation of mechanical forces, little is known on the role of other cytoskeletal components and on the movement of intracellular organelles (e.g., the nucleus) in neural tube formation.

A great number of mutations, affecting the regulators of the actomyosin cytoskeleton, result in neural tube defects. Key actomyosin regulators are cofilin [169,170], Rac1 [171], RhoA/ROCK [2,172], ENA/WAP [173] and Shroom [174–177]. In addition, because neural plate convergence-extension relies upon planar cell polarized mechanisms, the inhibition of pathways controlling planar and apical-basal cell polarity impairs neurulation [178–180]. Nishimura and colleagues showed in 2012 that polarized short-range MyoII cables form medio-laterally at cellular junctions in the neural plate (Fig. 6 B) [2]. Since the neural plate folds anisotropically (along the medial-lateral but not the AP axis), Nishimura and colleagues proposed a model in which MyoII cables work both to initiate cell intercalation (seemingly similar to [112]) and to promote anisotropic neural plate bending. Nevertheless, the idea that cell polarized junctional cables are necessary for anisotropic folding is misleading because folding anisotropy can emerge simply from the anisotropic distribution of apically constricting cells [181]. In addition, if MyoII cables trigger cell neighbor exchange, the process of cell intercalation would reduce medial-apical tension, thus disfavoring anisotropic tissue bending. How polarized junctional actomyosin networks could simultaneously drive cell intercalation and neural plate apical constriction and thus trigger bending of the neural plate is thus not clear. Cell intercalation, driven by actomyosin planar cell polarity, is more likely to play a role in the closure of the tube rather than triggering its bending. Polarized cell neighbor exchange results in tube narrowing, which brings the neural plate lips closer to one another. This is in agreement with siRNA-mediated depletion of RhoGEF or upstream signaling factors (e.g., siRNA-mediated depletion of Celsr1) resulting in a neural plate that can bend and fold but that fails to close [2]. Finally, while important advances have been made in the recent

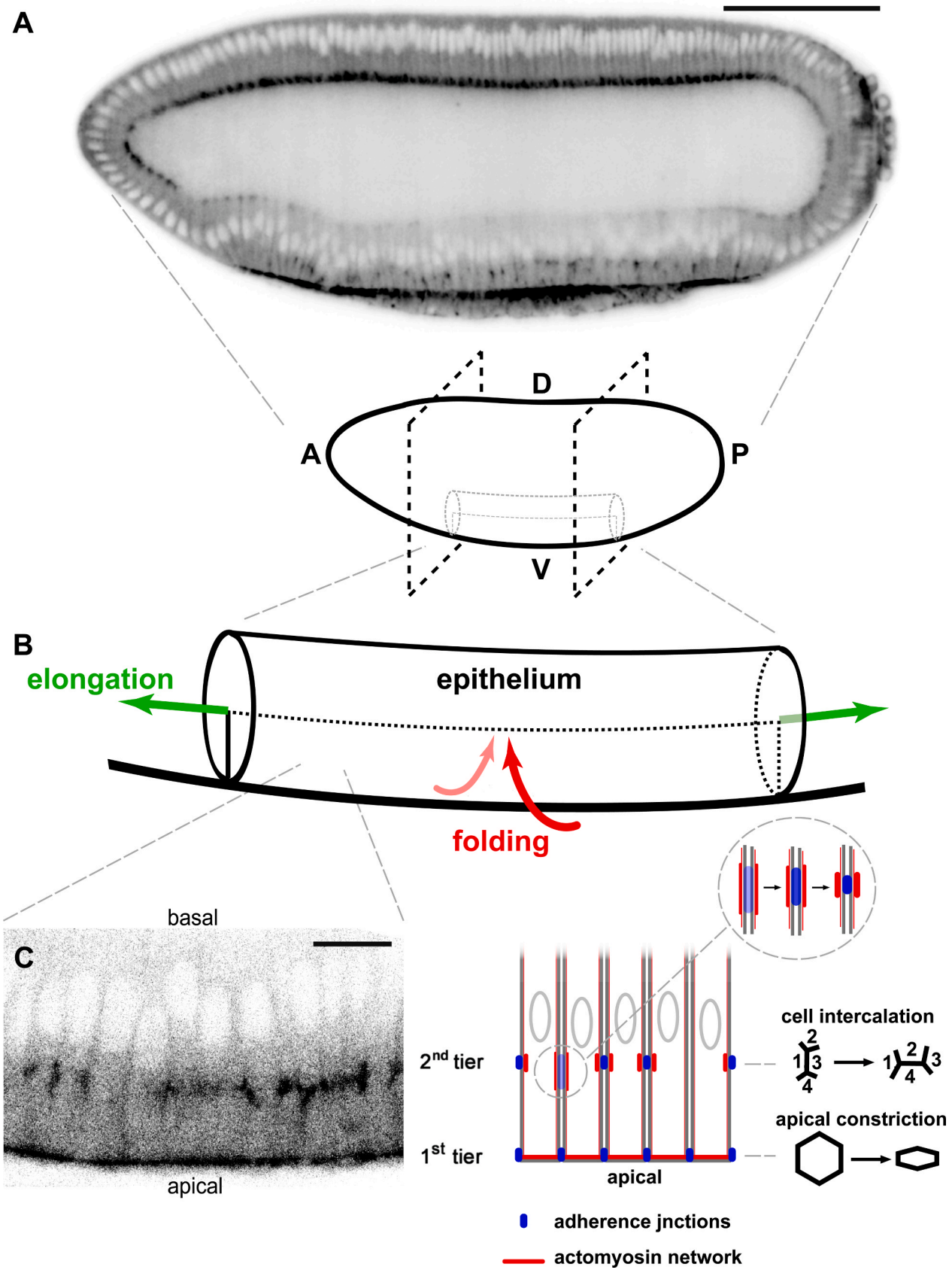

Fig. 7. A two-tier junctional mechanism drives simultaneous folding and extension. (A and B) The ventral tissue of the *Drosophila* embryo folds along the dorsal-ventral axis and extends along the anterior-posterior axis during early gastrulation. Scale bar 100 μm. **(C)** The first junctional tier mediates apical constriction while the second tier drives cell intercalation. The second tier results from cortical lateral actomyosin contractions that cluster E-cadherin and form spot adherens junctions. The two-tier junctional mechanisms promote tissue folding and extension. MyoII in black. Scale bar 10 μm.
Adapted from [102].

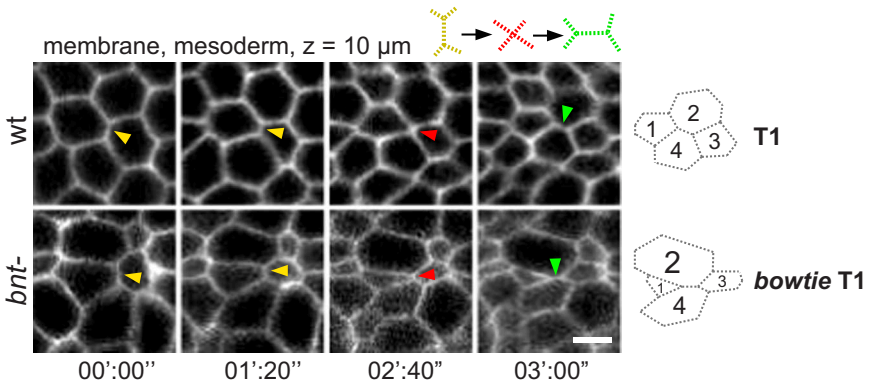

Fig. 8. Bowtie intercalation in *bnt-* embryos. Cell intercalation in the prospective mesoderm in a wild type embryo. Cell intercalation in the prospective mesoderm in a *bnt-* embryo.
Adapted from [102].

years to unravel the signaling pathways and some of the cell mechanisms playing a role in primary neurulation, further work is necessary to understand how these govern the mechanics of neural tube formation.

6.2. *Orthogonal folding and extension of the prospective mesoderm during Drosophila embryo gastrulation*

The ventral tissue of the developing *Drosophila* embryo constitutes the future mesoderm of the larva and is known to fold during early gastrulation [58,182]. Tissue folding is under the control of the Twist and Snail transcription factors that are part of the embryo DV gene patterning [58]. Apical surface area reduction of prospective mesoderm cells is a key mechanism that initiates tissue furrowing, eventually leading to epithelial folding. Cell apical surface reduction has been shown to be driven by a constricting force generated by a cell medial-apical actomyosin network coupled to adherens junctions [109]. Cellular networks are coupled with another, forming a supracellular cytoskeletal network that drives tissue-scale tension [183] and inward-directed hydrodynamic cytoplasmic flow [184]. Upregulation of cell basal MyoII blocks furrowing and eventual folding [185]. This supports the idea that cell apical and basal tension could work together to generate an active bending moment [186], backed up by cell lateral contractility [102,187], to drive tissue buckling. While apical constriction is thought to be necessary to drive tissue furrowing, it is still not clear if it is sufficient per se. Finally, embryo-scale accommodation of neighboring lateral tissues is necessary to allow the involution of the prospective mesoderm [188].

A recent study shows that the mesoderm not only furrows (and eventually folds forming an epithelial tube) but also extends along the AP axis (i.e., along a direction orthogonal to folding– Fig. 7 A and B) [102]. How are concomitant orthogonal folding and extension achieved? Cells in the prospective mesoderm undergo planar cell polarized intercalation while apically constricting. Seemingly similar to ectoderm cells [62], mesoderm cells also intercalate in such a way that AP neighbors separate while new DV neighbors come into contact. This finding, while apparently surprising, is consistent with the fact that both prospective lateral ectoderm and mesoderm express genes that control planar polarized cell intercalation and that both tissues are part of the germ band that is known to extend. Both apical constriction and cell intercalation are cell processes that result from specialized activities of the actomyosin cytoskeleton coupled to adherens junctions [109,189]. How can both cellular processes occur concomitantly in a cell? Cells located in the ventral region of the *Drosophila* embryo adopt a remarkable strategy never described before: they establish a two-tier system of adherens junctions. While the first tier is located apically and mediates apical cell constriction, the second tier is located 10 µm from the cell apical surface and initiates cell intercalation [102]. The first junctional tier originates from sub-apical adherence junctions that are established in the *Drosophila* blastoderm during cellularization under the control of the apical-basal polarity Par3/Bazooka signaling pathway [190]. In mesoderm cells, sub-apical junctions are then relocalized apically [191] under the action of tethered actomyosin networks [192]. In this way, junctions that would otherwise be dismantled by the action of Snail signaling [192,193] are rescued and reinforced to withstand tissue scale tension [183]. The second junctional tier is then established 'on the fly' during tissue furrowing: lateral actomyosin contractions, under the control of the RhoGEF2 pathway, cluster E-cadherin proteins that engage with the actomyosin network via alpha- and beta-catenins to form spot-adherence junctions (Fig. 7 C, inset). These lateral junctions, located 10 µm from the apical cell surface, are necessary to establish cell-cell contacts (a prerequisite to initiate junction remodeling and cell intercalation [113]). Similar to the process of cell intercalation in the ectoderm [189,194], mesoderm cells show a planar cell polarized distribution of the motor protein MyoII which generates cortical tension that shortens the junction and initiates AP neighboring cell separation. Therefore, the T1 transition, though initiated apically in ectoderm cells, is initiated 10 µm inside the tissue in mesoderm cells (Fig. 7 C). Cell neighbor exchange is a topological cell transformation that proceeds in two steps: (i) a junction shortens between two neighboring cells and (ii) a new junction extends bringing two new neighboring cells into contact. While the mechanism of junction shortening is similar in mesoderm and ectoderm cells, the process of new junction extension is quite different. In ectoderm cells, the pulsatile medial-apical actomyosin network plays a key role in junction extension [195]. In mesoderm cells (in absence of a medial network at 10 µm inside the tissue) a new junction extends as a result of AP tissue-scale forces that are generated by the mesoderm apical supracellular network. When AP tension is downregulated in the mesoderm (by surgically ablating the apical supracellular network using an infra-red femtosecond laser), junctions enriched in MyoII shrink but no new junction extends. This shows that junction extension is a cell autonomous process in the prospective ectoderm [195] while in the mesoderm it results from polarized tissue-scale forces (similar to those reported for salivary gland formation). In the future it will be important to investigate (for instance by entirely isolating a group of ectoderm cells using laser based cauterization [196]) whether converging forces from more dorsally located tissues may also contribute to new junction extension in the ectoderm.

How is concomitant folding and extension controlled in the prospective mesoderm? Mutations affecting the DV patterning (e.g., mutations for the *twist* and *snail* genes) result in a strong reduction of cell intercalation in the mesoderm (but not in the ectoderm where *twist* and *snail* are not expressed) and in a consequent inhibition of mesoderm extension. More specifically, in a *snail* mutant embryo, MyoII only localizes at subapical cell junctions. This shows that Snail is necessary to

establish the two-tier junctional system. AP gene patterning is key to controlling cell intercalation in the ectoderm [62]. Surprisingly, mutations affecting the AP patterning (e.g., a triple mutation for the *bicoid*, *nanos* and *torso* genes, *bnt-*) affect neither the number nor the polarity of cell intercalation in the mesoderm. Nevertheless, in *bnt-* embryos mesoderm extension is compromised. Therefore, the phenotype shown by *bnt-* embryos raises two paradoxes that underlie the following two key questions: (i) how can extension be impaired if intercalation density and polarity are not affected? And (ii) how can cell intercalation still be planar cell polarized if no instructive signal is present along the AP axis? A closer look at the dynamics of cell intercalation in *bnt-* embryos sheds light on these apparent paradoxes. In *bnt-* embryos, the T1 transition occurs in an unusual fashion: the separating and the new contacting cell duo reduces and expands in surface area, respectively, leading to a sudden exchange of cell neighbors. Given the peculiar cell conformation of the intercalating quartet, this mode of cell intercalation was dubbed *bowtie intercalation* (Fig. 8). Because of the inhomogeneity in the surface area of the intercalating cell quartet, bowtie intercalation may be ineffective in driving polarized displacement of cell center of masses (thus less tissue extension). In addition to the extension, the convergence of the mesoderm along the orthogonal axis is also compromised, resulting in a wider epithelial tube [102,197]. Remarkably in *bnt-* embryos, MyoII at the second tier is no longer planar cell polarized and forms ring patterns. This shows that AP patterning controls MyoII planar cell polarity at the second junctional tier to insure a regular T1 transition and net tissue extension. Signals emanating from the AP patterning are then not necessary to impose cell intercalation polarity which is instead oriented by tissue scale polarized forces.

Finally, AP and DV gene patterning work synergistically during *Drosophila* gastrulation, providing signals that can cross-talk to control the emergence of a combined cellular mechanism that drives and orients orthogonal folding and extension simultaneusly.

7. Outlook

Functional living shapes are built during morphogenesis. Uncovering the mechanisms driving morphogenesis is thus understanding how multicellular life emerges. Dissecting embryo morphogenesis by studying simple morphogenetic processes is pivotal to understand the fundamental cell mechanisms driving tissue shape changes. Nevertheless, during body and organ formation of an animal, tissues undergo concomitant changes in shape resulting in composite morphogenetic processes. Recent pioneer studies show that composite morphogenesis cannot be explained by the simple addition of signaling pathways and cell mechanisms responsible for simple tissue shape changes. Multiple and distinct cell mechanisms need to be spatio-temporally coordinated within different subgroups of cells or even within each cell eventually under the synergistic action of multiple gene patterning signals. A new avenue is now open to unravel the mechanisms driving composite morphogenesis and to uncover their origins.

Acknowledgments

We thank T. Lepage and S. Roth for critical reading of the manuscript. We thank B. Delorme, I. Bekri and R. Costanzo from the Rauzi lab for fruitful discussions and for sea urchin embryo images. AJ is supported by the scholarship Région SUD PACA – Enterprise (Bruker Luxendo) – UCA. This work was supported by the French government through the UCA^{JEDI} Investments for the Future project managed by the National Research Agency (ANR-15-IDEX-01), the Investments for the Future LABEX SIGNALIFE (ANR-11-LABX-0028-01), the Tramplin-ERC program of the National Research Agency (ANR-16-TERC-0018-01), the ATIP-Avenir program of the CNRS and the Human Frontier Science Program (CDA00027/2017-C), the Region SUD PACA AAP RECHERCHE and ERC BOOSTER.

References

[1] D. Gilmour, M. Rembold, M. Leptin, From morphogen to morphogenesis and back, Nature 541 (7637) (2017) 311–320.
[2] T. Nishimura, H. Honda, M. Takeichi, Planar cell polarity links axes of spatial dynamics in neural-tube closure, Cell 149 (5) (2012) 1084–1097.
[3] E.R. Gavis, Pattern formation. Gurken meets torpedo for the first time, Curr. Biol. 5 (11) (1995) 1252–1254.
[4] R.P. Ray, T. Schupbach, Intercellular signaling and the polarization of body axes during Drosophila oogenesis, Genes Dev. 10 (14) (1996) 1711–1723.
[5] F.S. Neuman-Silberberg, T. Schupbach, The Drosophila dorsoventral patterning gene gurken produces a dorsally localized RNA and encodes a TGF alpha-like protein, Cell 75 (1) (1993) 165–174.
[6] T. Schupbach, Germ line and soma cooperate during oogenesis to establish the dorsoventral pattern of egg shell and embryo in Drosophila melanogaster, Cell 49 (5) (1987) 699–707.
[7] C. Bökel, S. Dass, M. Wilsch-Bräuninger, S. Roth, Drosophila Cornichon acts as cargo receptor for ER export of the TGFalpha-like growth factor Gurken, Development 133 (3) (2006) 459–470.
[8] C.P. Castro, D. Piscopo, T. Nakagawa, R. Derynck, Cornichon regulates transport and secretion of TGFalpha-related proteins in metazoan cells, J. Cell Sci. 120 (Pt 14) (2007) 2454–2466.
[9] A. Gonzalez-Reyes, H. Elliott, D. Johnston St, Polarization of both major body axes in Drosophila by gurken-torpedo signalling, Nature 375 (6533) (1995) 654–658.
[10] S. Roth, F.S. Neuman-Silberberg, G. Barcelo, T. Schüpbach, cornichon and the EGF receptor signaling process are necessary for both anterior-posterior and dorsal-ventral pattern formation in Drosophila, Cell 81 (6) (1995) 967–978.
[11] M. Ivankovic, R. Haneckova, A. Thommen, M.A. Grohme, M. Vila-Farré, S. Werner, J.C. Rink, Model systems for regeneration: planarians, Development 146 (2019) 17.
[12] M. Sureda-Gomez, T. Adell, Planarian organizers, Semin. Cell Dev. Biol. 87 (2019) 95–104.
[13] A. Martinez Arias, B. Steventon, On the nature and function of organizers, Development 145 (2018) 5.
[14] H. Spemann, H. Mangold, Induction of embryonic primordia by implantation of organizers from a different species. 1923, Int J. Dev. Biol. 45 (1) (2001) 13–38.
[15] K.W. Cho, B. Blumberg, H. Steinbeisser, E.M. De Robertis, Molecular nature of Spemann's organizer: the role of the Xenopus homeobox gene goosecoid, Cell 67 (6) (1991) 1111–1120.
[16] R.M. Stewart, J.C. Gerhart, The anterior extent of dorsal development of the Xenopus embryonic axis depends on the quantity of organizer in the late blastula, Development 109 (2) (1990) 363–372.
[17] E.M. De Robertis, Spemann's organizer and self-regulation in amphibian embryos, Nat. Rev. Mol. Cell Biol. 7 (4) (2006) 296–302.
[18] T. Boettger, H. Knoetgen, L. Wittler, M. Kessel, The avian organizer, Int. J. Dev. Biol. 45 (1) (2001) 281–287.
[19] C.H. Waddington, G.A. Schmidt, Induction by heteroplastic grafts of the primitive streak in birds, Wilhelm. Roux Arch. Entwickl. Mech. Org. 128 (3) (1933) 522–563.
[20] B. Feldman, M.A. Gates, E.S. Egan, S.T. Dougan, G. Rennebeck, H.I. Sirotkin, A. F. Schier, W.S. Talbot, Zebrafish organizer development and germ-layer formation require nodal-related signals, Nature 395 (6698) (1998) 181–185.
[21] A.F. Schier, W.S. Talbot, The zebrafish organizer, Curr. Opin. Genet Dev. 8 (4) (1998) 464–471.
[22] J. Shih, S.E. Fraser, Characterizing the zebrafish organizer: microsurgical analysis at the early-shield stage, Development 122 (4) (1996) 1313–1322.
[23] J. Zhang, W.S. Talbot, A.F. Schier, Positional cloning identifies zebrafish one-eyed pinhead as a permissive EGF-related ligand required during gastrulation, Cell 92 (2) (1998) 241–251.
[24] L. Saúde, K. Woolley, P. Martin, W. Driever, D.L. Stemple, Axis-inducing activities and cell fates of the zebrafish organizer, Development 127 (16) (2000) 3407–3417.
[25] E.M. De Robertis, H. Kuroda, Dorsal-ventral patterning and neural induction in Xenopus embryos, Annu. Rev. Cell Dev. Biol. 20 (2004) 285–308.
[26] E.M. De Robertis, O. Wessely, M. Oelgeschläger, B. Brizuela, E. Pera, J. Larraín, J. Abreu, D. Bachiller, Molecular mechanisms of cell-cell signaling by the Spemann-Mangold organizer, Int. J. Dev. Biol. 45 (1) (2001) 189–197.
[27] F. Lapraz, E. Haillot, T. Lepage, A deuterostome origin of the Spemann organiser suggested by Nodal and ADMPs functions in Echinoderms, Nat. Commun. 6 (2015) 8927.
[28] D.L. Stemple, Structure and function of the notochord: an essential organ for chordate development, Development 132 (11) (2005) 2503–2512.
[29] C. McQueen, M. Towers, Establishing the pattern of the vertebrate limb, Development 147 (2020) 17.
[30] C. Kiecker, A. Lumsden, Hedgehog signaling from the ZLI regulates diencephalic regional identity, Nat. Neurosci. 7 (11) (2004) 1242–1249.
[31] S. Scholpp, O. Wolf, M. Brand, A. Lumsden, Hedgehog signalling from the zona limitans intrathalamica orchestrates patterning of the zebrafish diencephalon, Development 133 (5) (2006) 855–864.
[32] M. Rhinn, M. Brand, The midbrain–hindbrain boundary organizer, Curr. Opin. Neurobiol. 11 (1) (2001) 34–42.
[33] W. Tadros, H.D. Lipshitz, The maternal-to-zygotic transition: a play in two acts, Development 136 (18) (2009) 3033–3042.
[34] K.N. Schulz, M.M. Harrison, Mechanisms regulating zygotic genome activation, Nat. Rev. Genet. 20 (4) (2019) 221–234.

[35] C.A. Rushlow, S.Y. Shvartsman, Temporal dynamics, spatial range, and transcriptional interpretation of the Dorsal morphogen gradient, Curr. Opin. Genet. Dev. 22 (6) (2012) 542–546.
[36] H.L. Liang, C.Y. Nien, H.Y. Liu, M.M. Metzstein, N. Kirov, C. Rushlow, The zinc-finger protein Zelda is a key activator of the early zygotic genome in Drosophila, Nature 456 (7220) (2008) 400–403.
[37] K.N. Schulz, E.R. Bondra, A. Moshe, J.E. Villalta, J.D. Lieb, T. Kaplan, D.J. McKay, M.M. Harrison, Zelda is differentially required for chromatin accessibility, transcription factor binding, and gene expression in the early Drosophila embryo, Genome Res. 25 (11) (2015) 1715–1726.
[38] S.M. Foo, Y. Sun, B. Lim, R. Ziukaite, K. O'Brien, C.Y. Nien, N. Kirov, S. Y. Shvartsman, C.A. Rushlow, Zelda potentiates morphogen activity by increasing chromatin accessibility, Curr. Biol. 24 (12) (2014) 1341–1346.
[39] M.M. Harrison, X.Y. Li, T. Kaplan, M.R. Botchan, M.B. Eisen, Zelda binding in the early Drosophila melanogaster embryo marks regions subsequently activated at the maternal-to-zygotic transition, PLoS Genet. 7 (10) (2011), 1002266.
[40] S. Yamada, P.H. Whitney, S.K. Huang, E.C. Eck, H.G. Garcia, C.A. Rushlow, The Drosophila pioneer factor zelda modulates the nuclear microenvironment of a Dorsal target enhancer to potentiate transcriptional output, Curr. Biol. 29 (8) (2019) 1387–1393, e5.
[41] S.L. McDaniel, T.J. Gibson, K.N. Schulz, M. Fernandez Garcia, M. Nevil, S.U. Jain, P.W. Lewis, K.S. Zaret, M.M. Harrison, Continued activity of the pioneer factor zelda is required to drive zygotic genome activation, Mol. Cell 74 (1) (2019) 185–195, e4.
[42] K. Foygel, B. Choi, S. Jun, D.E. Leong, A. Lee, C.C. Wong, E. Zuo, M. Eckart, R. A. Reijo Pera, W.H. Wong, M.W. Yao, A novel and critical role for Oct4 as a regulator of the maternal-embryonic transition, PLoS One 3 (12) (2008) 4109.
[43] M.T. Lee, A.R. Bonneau, C.M. Takacs, A.A. Bazzini, K.R. DiVito, E.S. Fleming, A. J. Giraldez, Nanog, Pou5f1 and SoxB1 activate zygotic gene expression during the maternal-to-zygotic transition, Nature 503 (7476) (2013) 360–364, 360-+.
[44] M. Leichsenring, J. Maes, R. Mössner, W. Driever, D. Onichtchouk, Pou5f1 transcription factor controls zygotic gene activation in vertebrates, Science 341 (6149) (2013) 1005–1009.
[45] (St) D. Johnston, C. Nusslein-Volhard, The origin of pattern and polarity in the Drosophila embryo, Cell 68 (2) (1992) 201–219.
[46] U. Gaul, H. Jackle, Role of gap genes in early Drosophila development, Adv. Genet. 27 (1990) 239–275.
[47] M. Frasch, T. Hoey, C. Rushlow, H. Doyle, M. Levine, Characterization and localization of the even-skipped protein of Drosophila, EMBO J. 6 (3) (1987) 749–759.
[48] D.C. Knipple, E. Seifert, U.B. Rosenberg, A. Preiss, H. Jäckle, Spatial and temporal patterns of Kruppel gene expression in early Drosophila embryos, Nature 317 (6032) (1985) 40–44.
[49] D. Tautz, Regulation of the Drosophila segmentation gene hunchback by two maternal morphogenetic centres, Nature 332 (6161) (1988) 281–284.
[50] W. Driever, C. Nusslein-Volhard, The bicoid protein determines position in the Drosophila embryo in a concentration-dependent manner, Cell 54 (1) (1988) 95–104.
[51] W. Driever, C. Nusslein-Volhard, A gradient of bicoid protein in Drosophila embryos, Cell 54 (1) (1988) 83–93.
[52] R. Lehmann, C. Nusslein-Volhard, The maternal gene nanos has a central role in posterior pattern formation of the Drosophila embryo, Development 112 (3) (1991) 679–691.
[53] C. Nusslein-Volhard, H.G. Frohnhofer, R. Lehmann, Determination of anteroposterior polarity in Drosophila, Science 238 (4834) (1987) 1675–1681.
[54] G. Struhl, K. Struhl, P.M. Macdonald, The gradient morphogen bicoid is a concentration-dependent transcriptional activator, Cell 57 (7) (1989) 1259–1273.
[55] C. Wang, R. Lehmann, Nanos is the localized posterior determinant in Drosophila, Cell 66 (4) (1991) 637–647.
[56] S. Roth, D. Stein, C. Nusslein-Volhard, A gradient of nuclear localization of the dorsal protein determines dorsoventral pattern in the Drosophila embryo, Cell 59 (6) (1989) 1189–1202.
[57] D. Morisato, K.V. Anderson, Signaling pathways that establish the dorsal-ventral pattern of the Drosophila embryo, Annu. Rev. Genet. 29 (1995) 371–399.
[58] M. Leptin, B. Grunewald, Cell shape changes during gastrulation in Drosophila, Development 110 (1) (1990) 73–84.
[59] C. Rushlow, M. Frasch, H. Doyle, M. Levine, Maternal regulation of zerknullt: a homoeobox gene controlling differentiation of dorsal tissues in Drosophila, Nature 330 (6148) (1987) 583–586.
[60] B. Thisse, M. el Messal, F. Perrin-Schmitt, The twist gene: isolation of a Drosophila zygotic gene necessary for the establishment of dorsoventral pattern, Nucleic Acids Res. 15 (8) (1987) 3439–3453.
[61] M. Leptin, Twist and snail as positive and negative regulators during drosophila mesoderm development, Genes Dev. 5 (9) (1991) 1568–1576.
[62] K.D. Irvine, E. Wieschaus, Cell intercalation during Drosophila germband extension and its regulation by pair-rule segmentation genes, Development 120 (4) (1994) 827–841.
[63] S. Roth, Mechanisms of dorsal-ventral axis determination in Drosophila embryos revealed by cytoplasmic transplantations, Development 117 (4) (1993) 1385–1396.
[64] A.M. Huang, J. Rusch, M. Levine, An anteroposterior dorsal gradient in the Drosophila embryo, Genes Dev. 11 (15) (1997) 1963–1973.
[65] K.V. Anderson, G. Jurgens, C. Nusslein-Volhard, Establishment of dorsal-ventral polarity in the Drosophila embryo: genetic studies on the role of the Toll gene product, Cell 42 (3) (1985) 779–789.
[66] T. Schupbach, E. Wieschaus, Germline autonomy of maternal-effect mutations altering the embryonic body pattern of Drosophila, Dev. Biol. 113 (2) (1986) 443–448.
[67] T. Schupbach, E. Wieschaus, Female sterile mutations on the second chromosome of Drosophila melanogaster. I. Maternal effect mutations, Genetics 121 (1) (1989) 101–117.
[68] H.G. Frohnhofer, R. Lehmann, C. Nusslein-Volhard, Manipulating the anteroposterior pattern of the Drosophila embryo, J. Embryol. Exp. Morphol. 97 (Suppl) (1986) 169–179.
[69] R. Lehmann, C. Nusslein-Volhard, Abdominal segmentation, pole cell formation, and embryonic polarity require the localized activity of oskar, a maternal gene in Drosophila, Cell 47 (1) (1986) 141–152.
[70] B. Moussian, S. Roth, Dorsoventral axis formation in the Drosophila embryo–shaping and transducing a morphogen gradient, Curr. Biol. 15 (21) (2005) R887–R899.
[71] X. Hu, Y. Yagi, T. Tanji, S. Zhou, Y.T. Ip, Multimerization and interaction of Toll and Spatzle in Drosophila, Proc. Natl. Acad. Sci. USA 101 (25) (2004) 9369–9374.
[72] K.A. Gurley, J.C. Rink, A. Sanchez Alvarado, Beta-catenin defines head versus tail identity during planarian regeneration and homeostasis, Science 319 (5861) (2008) 323–327.
[73] M.D. Molina, E. Salo, F. Cebria, The BMP pathway is essential for re-specification and maintenance of the dorsoventral axis in regenerating and intact planarians, Dev. Biol. 311 (1) (2007) 79–94.
[74] M.D. Molina, E. Salo, F. Cebria, Organizing the DV axis during planarian regeneration, Commun. Integr. Biol. 4 (4) (2011) 498–500.
[75] C.P. Petersen, P.W. Reddien, Smed-betacatenin-1 is required for anteroposterior blastema polarity in planarian regeneration, Science 319 (5861) (2008) 327–330.
[76] S. Yazawa, Y. Umesono, T. Hayashi, H. Tarui, K. Agata, Planarian Hedgehog/Patched establishes anterior-posterior polarity by regulating Wnt signaling, Proc. Natl. Acad. Sci. USA 106 (52) (2009) 22329–22334.
[77] M. Iglesias, J.L. Gomez-Skarmeta, E. Saló, T. Adell, Silencing of Smed-betacatenin1 generates radial-like hypercephalized planarians, Development 135 (7) (2008) 1215–1221.
[78] M.A. Gavino, P.W. Reddien, A Bmp/Admp regulatory circuit controls maintenance and regeneration of dorsal-ventral polarity in planarians, Curr. Biol. 21 (4) (2011) 294–299.
[79] M.D. Molina, A. Neto, I. Maeso, J.L. Gómez-Skarmeta, E. Saló, F. Cebrià, Noggin and noggin-like genes control dorsoventral axis regeneration in planarians, Curr. Biol. 21 (4) (2011) 300–305.
[80] J. Gamse, H. Sive, Vertebrate anteroposterior patterning: the Xenopus neurectoderm as a paradigm, Bioessays 22 (11) (2000) 976–986.
[81] T.P. Yamaguchi, Heads or tails: Wnts and anterior-posterior patterning, Curr. Biol. 11 (17) (2001) R713–R724.
[82] H. Hikasa, S.Y. Sokol, Wnt signaling in vertebrate axis specification, Cold Spring Harb. Perspect. Biol. 5 (1) (2013), 007955.
[83] Y.G. Langdon, M.C. Mullins, Maternal and zygotic control of zebrafish dorsoventral axial patterning, Annu. Rev. Genet. 45 (2011) 357–377.
[84] M. Oelgeschläger, B. Reversade, J. Larraín, S. Little, M.C. Mullins, E.M. De Robertis, The pro-BMP activity of Twisted gastrulation is independent of BMP binding, Development 130 (17) (2003) 4047–4056.
[85] B. Reversade, H. Kuroda, H. Lee, A. Mays, E.M. De Robertis, Depletion of Bmp2, Bmp4, Bmp7 and Spemann organizer signals induces massive brain formation in Xenopus embryos, Development 132 (15) (2005) 3381–3392.
[86] M. Varga, S. Maegawa, E.S. Weinberg, Correct anteroposterior patterning of the zebrafish neurectoderm in the absence of the early dorsal organizer, BMC Dev. Biol. 11 (2011) 26.
[87] C. Tickle, M. Towers, Sonic Hedgehog signaling in limb development, Front. Cell Dev. Biol. 5 (2017) 14.
[88] I. Delgado, M. Torres, Coordination of limb development by crosstalk among axial patterning pathways, Dev. Biol. 429 (2) (2017) 382–386.
[89] M. Towers, R. Mahood, Y. Yin, C. Tickle, Integration of growth and specification in chick wing digit-patterning, Nature 452 (7189) (2008) 882–886.
[90] A.M. Cheshire, B.E. Kerman, W.R. Zipfel, A.A. Spector, D.J. Andrew, Kinetic and mechanical analysis of live tube morphogenesis, Dev. Dyn. 237 (10) (2008) 2874–2888.
[91] M.M. Myat, D.J. Andrew, Fork head prevents apoptosis and promotes cell shape change during formation of the Drosophila salivary glands, Development 127 (19) (2000) 4217–4226.
[92] M.M. Myat, D.J. Andrew, Organ shape in the Drosophila salivary gland is controlled by regulated, sequential internalization of the primordia, Development 127 (4) (2000) 679–691.
[93] V. Brodu, J. Casanova, The RhoGAP crossveinless-c links trachealess and EGFR signaling to cell shape remodeling in Drosophila tracheal invagination, Genes Dev. 20 (13) (2006) 1817–1828.
[94] M. Llimargas, J. Casanova, EGF signalling regulates cell invagination as well as cell migration during formation of tracheal system in Drosophila, Dev. Genes Evol. 209 (3) (1999) 174–179.
[95] M. Nishimura, Y. Inoue, S. Hayashi, A wave of EGFR signaling determines cell alignment and intercalation in the Drosophila tracheal placode, Development 134 (23) (2007) 4273–4282.
[96] D.D. Iwaki, K.A. Johansen, J.B. Singer, J.A. Lengyel, drumstick, bowl, and lines are required for patterning and cell rearrangement in the Drosophila embryonic hindgut, Dev. Biol. 240 (2) (2001) 611–626.
[97] J.D. Hardin, L.Y. Cheng, The mechanisms and mechanics of archenteron elongation during sea-urchin gastrulation, Dev. Biol. 115 (2) (1986) 490–501.

[98] Y. Nakajima, R.D. Burke, The initial phase of gastrulation in sea urchins is accompanied by the formation of bottle cells, Dev. Biol. 179 (2) (1996) 436–446.
[99] R.E. Keller, An experimental analysis of the role of bottle cells and the deep marginal zone in gastrulation of Xenopus laevis, J. Exp. Zool. 216 (1) (1981) 81–101.
[100] R.E. Keller, M. Danilchik, R. Gimlich, J. Shih, The function and mechanism of convergent extension during gastrulation of Xenopus laevis, J. Embryol. Exp. Morphol. 89 (Suppl) (1985) 185–209.
[101] J.R. Seifert, M. Mlodzik, Frizzled/PCP signalling: a conserved mechanism regulating cell polarity and directed motility, Nat. Rev. Genet. 8 (2) (2007) 126–138.
[102] A. John, M. Rauzi, A two-tier junctional mechanism drives imultaneus tissue folding and extension, Dev. Cell 56 (10) (2021) 1469–1483, e5.
[103] J. Croce, L. Duloquin, G. Lhomond, D.R. McClay, C. Gache, Frizzled5/8 is required in secondary mesenchyme cells to initiate archenteron invagination during sea urchin development, Development 133 (3) (2006) 547–557.
[104] Y.E. Sanchez-Corrales, G.B. Blanchard, K. Roper, Radially patterned cell behaviours during tube budding from an epithelium, eLife 7 (2018) 7.
[105] D.D. Isaac, D.J. Andrew, Tubulogenesis in Drosophila: a requirement for the trachealess gene product, Genes Dev. 10 (1) (1996) 103–117.
[106] S. Panzer, D. Weigel, S.K. Beckendorf, Organogenesis in Drosophila melanogaster: embryonic salivary gland determination is controlled by homeotic and dorsoventral patterning genes, Development 114 (1) (1992) 49–57.
[107] S. Chung, S. Kim, D.J. Andrew, Uncoupling apical constriction from tissue invagination, eLife 6 (2017) 6.
[108] K. Roper, Anisotropy of Crumbs and aPKC drives myosin cable assembly during tube formation, Dev. Cell 23 (5) (2012) 939–953.
[109] A.C. Martin, M. Kaschube, E.F. Wieschaus, Pulsed contractions of an actin-myosin network drive apical constriction, Nature 457 (7228) (2009) 495–499.
[110] G. Guglielmi, J.D. Barry, W. Huber, S. De Renzis, An optogenetic method to modulate cell contractility during tissue morphogenesis, Dev. Cell 35 (5) (2015) 646–660.
[111] B.F. Nielsen, S.B. Nissen, K. Sneppen, J. Mathiesen, A. Trusina, Model to link cell shape and polarity with organogenesis, iScience 23 (2) (2020), 100830.
[112] M. Rauzi, P. Verant, T. Lecuit, P.F. Lenne, Nature and anisotropy of cortical forces orienting Drosophila tissue morphogenesis, Nat. Cell Biol. 10 (12) (2008) 1401–1410.
[113] M. Rauzi, Cell intercalation in a simple epithelium, Philos. Trans. R. Soc. Lond. B Biol. Sci. 375 (1809) (2020), 20190552.
[114] C. Sidor, T.J. Stevens, L. Jin, J. Boulanger, K. Röper, Rho-kinase planar polarization at tissue boundaries depends on phospho-regulation of membrane residence time, Dev. Cell 52 (3) (2020) 364–378, e7.
[115] K. Dan, K. Okazaki, Cyto-embryological studies of sea Urchins.3. Role of the secondary mesenchyme cells in the formation of the primitive gut in Sea Urchin Larvae, Biol. Bull. 110 (1) (1956) 29–42.
[116] T. Gustafson, H. Kinnander, Microaquaria for time-lapse cinematographic studies of morphogenesis in swimming larvae and observations on sea urchin gastrulation, Exp. Cell Res. 11 (1) (1956) 36–51.
[117] S. Horstadius, The mechanics of sea urchin development, studied by operative methods, Biol. Rev. Camb. Philos. Soc. 14 (2) (1939) 132–179.
[118] C.A. ETTENSOHN, Primary invagination of the vegetal plate during sea urchin Gastrulation1, Integr. Comp. Biol. 24 (3) (2015) 571–588.
[119] M.L. Martik, D.R. McClay, New insights from a high-resolution look at gastrulation in the sea urchin, Lytechinus variegatus, Mech. Dev. 148 (2017) 3–10.
[120] M. Marrese, N. Antonovaité, B. Nelemans, A. Ahmadzada, D. Iannuzzi, T.H. Smit, In vivo characterization of chick embryo mesoderm by optical coherence tomography-assisted microindentation, FASEB J. 34 (9) (2020) 12269–12277.
[121] C.J. Chan, M. Costanzo, T. Ruiz-Herrero, G. Mönke, R.J. Petrie, M. Bergert, A. Diz-Muñoz, L. Mahadevan, T. Hiiragi, Hydraulic control of mammalian embryo size and cell fate, Nature 571 (7763) (2019) 112–116.
[122] J.L. Maître, R. Niwayama, H. Turlier, F. Nédélec, T. Hiiragi, Pulsatile cell-autonomous contractility drives compaction in the mouse embryo, Nat. Cell Biol. 17 (7) (2015) 849–855.
[123] C.A. Ettensohn, Primary invagination of the vegetal plate during sea-urchin gastrulation, Am. Zool. 24 (3) (1984) 571–588.
[124] E.L. Kimberly, J. Hardin, Bottle cells are required for the initiation of primary invagination in the sea urchin embryo, Dev. Biol. 204 (1) (1998) 235–250.
[125] J. Miller, S.E. Fraser, D. Mcclay, Dynamics of thin filopodia during sea-urchin gastrulation, Development 121 (8) (1995) 2501–2511.
[126] J. Hardin, The role of secondary mesenchyme cells during sea-urchin gastrulation studied by laser ablation, Development 103 (2) (1988) 317–324.
[127] C.A. Ettensohn, Gastrulation in the sea urchin embryo is accompanied by the rearrangement of invaginating epithelial cells, Dev. Biol. 112 (2) (1985) 383–390.
[128] J. Hardin, M. Weliky, Cell rearrangement induced by filopodial tension accounts for the late phase of convergent extension in the sea urchin archenteron, Mol. Biol. Cell 30 (16) (2019) 1911–1919.
[129] M.L. Martik, D.R. McClay, New insights from a high-resolution look at gastrulation in the sea urchin, Lytechinus variegatus, Mech. Dev. 148 (2017) 3–10.
[130] R.D. Burke, R.L. Myers, T.L. Sexton, C. Jackson, Cell movements during the initial phase of gastrulation in the sea urchin embryo, Dev. Biol. 146 (2) (1991) 542–557.
[131] M.C. Lane, M.A. Koehl, F. Wilt, R. Keller, A role for regulated secretion of apical extracellular matrix during epithelial invagination in the sea urchin, Development 117 (3) (1993) 1049–1060.
[132] H. Takata, T. Kominami, Shrinkage and expansion of blastocoel affect the degree of invagination in sea urchin embryos, Zool. Sci. 18 (8) (2001) 1097–1105.
[133] G.M. Odell, G. Oster, P. Alberch, B. Burnside, The mechanical basis of morphogenesis. I. Epithelial folding and invagination, Dev. Biol. 85 (2) (1981) 446–462.
[134] L.A. Davidson, M.A. Koehl, R. Keller, G.F. Oster, How do sea-urchins invaginate - using biomechanics to distinguish between mechanisms of primary invagination, Development 121 (7) (1995) 2005–2018.
[135] S.B. Nissen, S. Rønhild, A. Trusina, K. Sneppen, Theoretical tool bridging cell polarities with development of robust morphologies, eLife 7 (2018) 7.
[136] W.S. Beane, J.M. Gross, D.R. McClay, RhoA regulates initiation of invagination, but not convergent extension, during sea urchin gastrulation, Dev. Biol. 292 (1) (2006) 213–225.
[137] G. Lhomond, D.R. McClay, C. Gache, J.C. Croce, Frizzled1/2/7 signaling directs beta-catenin nuclearisation and initiates endoderm specification in macromeres during sea urchin embryogenesis, Development 139 (4) (2012) 816–825.
[138] J.C. Croce, D.R. McClay, Dynamics of Delta/Notch signaling on endomesoderm segregation in the sea urchin embryo, Development 137 (1) (2010) 83–91.
[139] J. Croce, R. Range, S.Y. Wu, E. Miranda, G. Lhomond, J.C. Peng, T. Lepage, D. R. McClay, Wnt6 activates endoderm in the sea urchin gene regulatory network, Development 138 (15) (2011) 3297–3306.
[140] I.S. Peter, E.H. Davidson, A gene regulatory network controlling the embryonic specification of endoderm, Nature 474 (7353) (2011) 635–639.
[141] E. Röttinger, A. Saudemont, V. Duboc, L. Besnardeau, D. McClay, T. Lepage, FGF signals guide migration of mesenchymal cells, control skeletal morphogenesis [corrected] and regulate gastrulation during sea urchin development, Development 135 (2) (2008) 353–365.
[142] R. Costanzo, R.L. Watterson, G.C. Schoenwolf, Evidence that secondary neurulation occurs autonomously in the chick embryo, J. Exp. Zool. 219 (2) (1982) 233–240.
[143] L.A. Davidson, R.E. Keller, Neural tube closure in Xenopus laevis involves medial migration, directed protrusive activity, cell intercalation and convergent extension, Development 126 (20) (1999) 4547–4556.
[144] G.C. Schoenwolf, Histological and ultrastructural studies of secondary neurulation in mouse embryos, Am. J. Anat. 169 (4) (1984) 361–376.
[145] G.C. Schoenwolf, J. Delongo, Ultrastructure of secondary neurulation in the chick embryo, Am. J. Anat. 158 (1) (1980) 43–63.
[146] G.C. Schoenwolf, J.L. Smith, Mechanisms of neurulation: traditional viewpoint and recent advances, Development 109 (2) (1990) 243–270.
[147] G.C. Schoenwolf, Microsurgical analyses of avian neurulation: separation of medial and lateral tissues, J. Comp. Neurol. 276 (4) (1988) 498–507.
[148] I.S. Alvarez, G.C. Schoenwolf, Expansion of surface epithelium provides the major extrinsic force for bending of the neural plate, J. Exp. Zool. 261 (3) (1992) 340–348.
[149] H. Morita, H. Kajiura-Kobayashi, C. Takagi, T.S. Yamamoto, S. Nonaka, N. Ueno, Cell movements of the deep layer of non-neural ectoderm underlie complete neural tube closure in Xenopus, Development 139 (8) (2012) 1417–1426.
[150] T.E. Schroeder, Neurulation in Xenopus-Laevis - an analysis and model based upon light and electron microscopy, J. Embryol. Exp. Morphol. 23 (1970) 427–462, 427-+.
[151] A.C. Martin, B. Goldstein, Apical constriction: themes and variations on a cellular mechanism driving morphogenesis, Development 141 (10) (2014) 1987–1998.
[152] R.B. Brun, J.A. Garson, Neurulation in the Mexican salamander (Ambystoma mexicanum): a drug study and cell shape analysis of the epidermis and the neural plate, J. Embryol. Exp. Morphol. 74 (1983) 275–295.
[153] G.C. Schoenwolf, M.E. Desmond, Descriptive studies of occlusion and reopening of the spinal canal of the early chick embryo, Anat. Rec. 209 (2) (1984) 251–263.
[154] D.C. Moore, M. Stanisstreet, G.E. Evans, Morphometric analyses of changes in cell shape in the neuroepithelium of mammalian embryos, J. Anat. 155 (1987) 87–99.
[155] J.L. Smith, G.C. Schoenwolf, Notochordal induction of cell wedging in the chick neural plate and its role in neural tube formation, J. Exp. Zool. 250 (1) (1989) 49–62.
[156] T. Elul, M.A. Koehl, R. Keller, Cellular mechanism underlying neural convergent extension in Xenopus laevis embryos, Dev. Biol. 191 (2) (1997) 243–258.
[157] T. Elul, M.A. Koehl, R.E. Keller, Patterning of morphogenetic cell behaviors in neural ectoderm of Xenopus laevis, Ann. N. Y. Acad. Sci. 857 (1998) 248–251.
[158] M. Williams, W. Yen, X. Lu, A. Sutherland, Distinct apical and basolateral mechanisms drive planar cell polarity-dependent convergent extension of the mouse neural plate, Dev. Cell 29 (1) (2014) 34–46.
[159] R. Keller, J. Shih, A. Sater, The cellular basis of the convergence and extension of the Xenopus neural plate, Dev. Dyn. 193 (3) (1992) 199–217.
[160] A.M. Ezin, P. Skoglund, R. Keller, The midline (notochord and notoplate) patterns the cell motility underlying convergence and extension of the Xenopus neural plate, Dev. Biol. 256 (1) (2003) 100–114.
[161] J.D. Hildebrand, Shroom regulates epithelial cell shape via the apical positioning of an actomyosin network, J. Cell Sci. 118 (Pt 22) (2005) 5191–5203.
[162] N. Kinoshita, N. Sasai, K. Misaki, S. Yonemura, Apical accumulation of Rho in the neural plate is important for neural plate cell shape change and neural tube formation, Mol. Biol. Cell 19 (5) (2008) 2289–2299.
[163] T. Nishimura, M. Takeichi, Shroom3-mediated recruitment of Rho kinases to the apical cell junctions regulates epithelial and neuroepithelial planar remodeling, Development 135 (8) (2008) 1493–1502.
[164] S. Nandadasa, Q. Tao, N.R. Menon, J. Heasman, C. Wylie, N- and E-cadherins in Xenopus are specifically required in the neural and non-neural ectoderm, respectively, for F-actin assembly and morphogenetic movements, Development 136 (8) (2009) 1327–1338.

[165] P.C. Baker, T.E. Schroeder, Cytoplasmic filaments and morphogenetic movement in the amphibian neural tube, Dev. Biol. 15 (5) (1967) 432–450.
[166] P.E. Messier, Microtubules, interkinetic nuclear migration and neurulation, Experientia 34 (3) (1978) 289–296.
[167] G.C. Schoenwolf, M.V. Franks, Quantitative analyses of changes in cell shapes during bending of the avian neural plate, Dev. Biol. 105 (2) (1984) 257–272.
[168] J. Lofberg, Apical surface topography of invaginating and noninvaginating cells. A scanning-transmission study of amphibian neurulae, Dev. Biol. 36 (2) (1974) 311–329.
[169] S. Escuin, B. Vernay, D. Savery, C.B. Gurniak, W. Witke, N.D. Greene, A.J. Copp, Rho-kinase-dependent actin turnover and actomyosin disassembly are necessary for mouse spinal neural tube closure, J. Cell Sci. 128 (14) (2015) 2468–2481.
[170] J. Grego-Bessa, J. Hildebrand, K.V. Anderson, Morphogenesis of the mouse neural plate depends on distinct roles of cofilin 1 in apical and basal epithelial domains, Development 142 (7) (2015) 1305–1314.
[171] A. Rolo, D. Savery, S. Escuin, S.C. de Castro, H.E. Armer, P.M. Munro, M.A. Molè, N.D. Greene, A.J. Copp, Regulation of cell protrusions by small GTPases during fusion of the neural folds, eLife 5 (2016) 13273.
[172] N. Kinoshita, N. Sasai, K. Misaki, S. Yonemura, Apical accumulation of rho in the neural plate is important for neural plate cell shape change and neural tube formation, Mol. Biol. Cell 19 (5) (2008) 2289–2299.
[173] J. Roffers-Agarwal, J.B. Xanthos, K.A. Kragtorp, J.R. Miller, Enabled (Xena) regulates neural plate morphogenesis, apical constriction, and cellular adhesion required for neural tube closure in Xenopus, Dev. Biol. 314 (2) (2008) 393–403.
[174] J.D. Hildebrand, P. Soriano, Shroom, a PDZ domain-containing actin-binding protein, is required for neural tube morphogenesis in mice, Cell 99 (5) (1999) 485–497.
[175] S.L. Haigo, J.D. Hildebrand, R.M. Harland, J.B. Wallingford, Shroom induces apical constriction and is required for hingepoint formation during neural tube closure, Curr. Biol. 13 (24) (2003) 2125–2137.
[176] C. Lee, H.M. Scherr, J.B. Wallingford, Shroom family proteins regulate gamma-tubulin distribution and microtubule architecture during epithelial cell shape change, Development 134 (7) (2007) 1431–1441.
[177] E.M. McGreevy, D. Vijayraghavan, L.A. Davidson, J.D. Hildebrand, Shroom3 functions downstream of planar cell polarity to regulate myosin II distribution and cellular organization during neural tube closure, Biol. Open 4 (2) (2015) 186–196.
[178] J.B. Wallingford, R.M. Harland, Neural tube closure requires Dishevelled-dependent convergent extension of the midline, Development 129 (24) (2002) 5815–5825.
[179] D.S. Eom, S. Amarnath, J.L. Fogel, S. Agarwala, Bone morphogenetic proteins regulate hinge point formation during neural tube closure by dynamic modulation of apicobasal polarity, Birth Defects Res. A Clin. Mol. Teratol. 94 (10) (2012) 804–816.
[180] S.Y. Sokol, Mechanotransduction during vertebrate neurulation, Curr. Top. Dev. Biol. 117 (2016) 359–376.
[181] K. Doubrovinski, J. Tchoufag, K. Mandadapu, A simplified mechanism for anisotropic constriction in Drosophila mesoderm, Development 145 (2018) 24.
[182] D. Sweeton, S. Parks, M. Costa, E. Wieschaus, Gastrulation in Drosophila: the formation of the ventral furrow and posterior midgut invaginations, Development 112 (3) (1991) 775–789.
[183] A.C. Martin, M. Gelbart, R. Fernandez-Gonzalez, M. Kaschube, E.F. Wieschaus, Integration of contractile forces during tissue invagination, J. Cell Biol. 188 (5) (2010) 735–749.
[184] B. He, K. Doubrovinski, O. Polyakov, E. Wieschaus, Apical constriction drives tissue-scale hydrodynamic flow to mediate cell elongation, Nature 508 (7496) (2014) 392–396.
[185] D. Krueger, P. Tardivo, C. Nguyen, S. De Renzis, Downregulation of basal myosin-II is required for cell shape changes and tissue invagination, EMBO J. 37 (2018) 23.
[186] O. Polyakov, B. He, M. Swan, J.W. Shaevitz, M. Kaschube, E. Wieschaus, Passive mechanical forces control cell-shape change during Drosophila ventral furrow formation, Biophys. J. 107 (4) (2014) 998–1010.
[187] M. Gracia, S. Theis, A. Proag, G. Gay, C. Benassayag, M. Suzanne, Mechanical impact of epithelial-mesenchymal transition on epithelial morphogenesis in Drosophila, Nat. Commun. 10 (1) (2019) 2951.
[188] M. Rauzi, U. Krzic, T.E. Saunders, M. Krajnc, P. Ziherl, L. Hufnagel, M. Leptin, Embryo-scale tissue mechanics during Drosophila gastrulation movements, Nat. Commun. 6 (2015) 8677.
[189] M. Rauzi, P.F. Lenne, T. Lecuit, Planar polarized actomyosin contractile flows control epithelial junction remodelling, Nature 468 (7327) (2010) 1110–1114.
[190] T.J. Harris, M. Peifer, Adherens junction-dependent and -independent steps in the establishment of epithelial cell polarity in Drosophila, J. Cell Biol. 167 (1) (2004) 135–147.
[191] V. Kölsch, T. Seher, G.J. Fernandez-Ballester, L. Serrano, M. Leptin, Control of Drosophila gastrulation by apical localization of adherens junctions and RhoGEF2, Science 315 (5810) (2007) 384–386.
[192] M. Weng, E. Wieschaus, Myosin-dependent remodeling of adherens junctions protects junctions from Snail-dependent disassembly, J. Cell Biol. 212 (2) (2016) 219–229.
[193] M. Weng, E. Wieschaus, Polarity protein Par3/Bazooka follows myosin-dependent junction repositioning, Dev. Biol. 422 (2) (2017) 125–134.
[194] C. Bertet, L. Sulak, T. Lecuit, Myosin-dependent junction remodelling controls planar cell intercalation and axis elongation, Nature 429 (6992) (2004) 667–671.
[195] C. Collinet, M. Rauzi, P.F. Lenne, T. Lecuit, Local and tissue-scale forces drive oriented junction growth during tissue extension, Nat. Cell Biol. 17 (10) (2015) 1247–1258.
[196] M. Rauzi, Probing tissue interaction with laser-based cauterization in the early developing Drosophila embryo, Methods Cell Biol. 139 (2017) 153–165.
[197] G.W. Brodland, V. Conte, P.G. Cranston, J. Veldhuis, S. Narasimhan, M.S. Hutson, A. Jacinto, F. Ulrich, B. Baum, M. Miodownik, Video force microscopy reveals the mechanics of ventral furrow invagination in Drosophila, Proc. Natl. Acad. Sci. USA 107 (51) (2010) 22111–22116.
[198] T. Koromila, A. Stathopoulos, Broadly expressed repressors integrate patterning across orthogonal axes in embryos, Proc. Natl. Acad. Sci. USA 114 (31) (2017) 8295–8300.
[199] M.J. Wilson, N.J. Kenny, P.K. Dearden, Components of the dorsal-ventral pathway also contribute to anterior-posterior patterning in honeybee embryos (Apis mellifera), Evodevo 5 (1) (2014) 11.
[200] K. Takebayashi-Suzuki, H. Konishi, T. Miyamoto, T. Nagata, M. Uchida, A. Suzuki, Coordinated regulation of the dorsal-ventral and anterior-posterior patterning of Xenopus embryos by the BTB/POZ zinc finger protein Zbtb14, Dev. Growth Differ. 60 (3) (2018) 158–173.
[201] M. Tsang, S. Maegawa, A. Kiang, R. Habas, E. Weinberg, I.B. Dawid, A role for MKP3 in axial patterning of the zebrafish embryo, Development 131 (12) (2004) 2769–2779.

B- Research article II

Embryo-scale force balance drives a furrow-shaped buckling initiating gastrulation

Julien Fierling, Alphy John, Barthelemy Delorme, Alexandre Torzynski, Guy Blanchard, Claire Lye, Gregoire Malandain, Benedicte Sanson, Jocelyn Etienne, Philippe Marmottant, Catherine Quilliet, Matteo Rauzi

Embryo-scale force balance drives a furrow-shaped buckling initiating gastrulation

Julien Fierling[1,†], Alphy John[2,†], Barthelemy Delorme[2,†], Alexandre Torzynski[1], Guy Blanchard[3], Claire Lye[3], Gregoire Malandain[4], Benedicte Sanson[3], Jocelyn Etienne[1,‡,*], Philippe Marmottant[1,‡], Catherine Quilliet[1,‡], Matteo Rauzi[2,‡,*]

1. Univ. Grenoble Alpes, CNRS, LIPhy, 38000 Grenoble, France
2. Université Côte d'Azur, CNRS, Inserm, iBV, Nice, France
3. Univ. Cambridge, Department of Physiology, Development and Neuroscience, Cambridge, Great-Britain
4. Morpheme, Université Côte d'Azur, Inria, CNRS, I3S, Nice, France

†, ‡ Contributed equally

* To whom correspondence should be sent, Jocelyn.Etienne@univ-grenoble-alpes.fr and Matteo.Rauzi@univ-cotedazur.fr

ABSTRACT

Cell apical constriction driven by actomyosin contraction forces is a conserved mechanism during tissue folding in embryo development. While much effort has been made to better understand the molecular mechanisms responsible for apical constriction, it is still not clear if apical actomyosin contraction forces are necessary or sufficient to drive tissue folding. To tackle this question, we use the *Drosophila* embryo model system that forms a furrow on the ventral side. Past computational models support the idea that cell apical contraction forces may not be sufficient and that active or passive cell apico-basal forces may be necessary to drive tissue furrowing. By using 3D computational modelling and *in toto* embryo image analysis and manipulation, we show that long range embryo scale tissue mechanics, at the surface of the curved *Drosophila* blastoderm, is necessary and sufficient to drive a buckling of the epithelial surface, forming a furrow which initiates embryo gastrulation.

Introduction

Furrow formation is a process that involves the bending of a tissue along a line. The formation of a furrow is pivotal during embryo development since it initiates tissue topology changes structuring the future animal. Understanding the mechanisms driving furrow formation is thus key to understand how vital processes such as gastrulation and neurulation are initiated. Furrow formation is a tissue shape change that emerges from a cell collective behavior. Therefore, understanding how cells mechanically interact and collectively drive furrow formation is a challenge. Ventral furrow formation (VFF) during early *Drosophila* embryo gastrulation is a quite well studied process: a fold along a line at the ventral side of the embryo (the prospective mesoderm) forms parallel to the anterior-posterior (AP) direction [1, 2]. Numerous *in vivo* studies have tackled the mechanisms driving ventral furrow formation. Cell apical constriction [3], basal expansion [4], lateral tension [5, 6] and cytoplasmic flow [7] are mechanisms that have been studied and are involved in the formation of the furrow. Cell apical constriction driven by the contraction of apical actomyosin networks is one of the most thoroughly investigated mechanisms probably because (i) it is a striking change in shape given its magnitude and rapidity and (ii) it is easier to analyze because it occurs at the surface of the tissue where microscope-based imaging technologies can be more easily applied. While numerous studies have highlighted the molecular nature and the key role of apical constriction in driving furrow formation, it is still not clear if this is necessary or sufficient to form the ventral furrow in the gastrulating *Drosophila* embryo.

Computational modelling is a powerful tool to study the mechanics and change in shape of tissues: minimal models recapitulating key features of an epithelium can be engineered and limitlessly tested to tackle the fundamental mechanisms driving a process. 3D and 2D-cross section models based on active deformation and active stress, respectively, have been developed to tackle the mechanics of ventral furrow formation [8]. Due to simplifying hypotheses, while none of the former have been informative of the stresses at work [8, 9], the latter lack the 3D geometry necessary to emulate the three dimensional boundary conditions in which the furrowing process occurs [10, 11, 12, 13, 6, 14]. 2D models, mimicking the embryo cross-section, have predicted that apical contractions may not suffice to drive furrow formation. We now

model an ellipsoidal 2D elastic sheet in the 3D space to test if apical stresses (i.e., stresses along the surface of the elastic sheet) are sufficient to drive ventral furrow formation. By implementing an experimental strategy combining computational modelling, infrared (IR) femtosecond (fs) laser manipulation coupled to multi-view light sheet microscopy and quantitative image analysis, we show that apical contraction is necessary to drive ventral furrow formation. In addition, we unveil a new emerging long range mechanism based on solely surface mechanics over a curved tissue that is sufficient to drive furrow formation.

With the intent of setting common grounds, here the definition of key terms that will be extensively used in this manuscript (Suppl. Fig.1 illustrates some of these definitions). **Furrowing**: the process by which a tissue bends forming a fold having much greater bending curvature along one direction compared to the orthogonal direction. **Invagination**: the process by which a tissue is internalized inside the embryo. **Buckling**: a sudden change in the type of mechanical equilibrium, from a state in which load is mostly balanced by forces along the plane of the tissue to a state in which load is mostly balanced by forces normal to the tissue. **Strain:** the amount of material shape change measured at a specific time and location (i.e., the current configuration) with respect to the initial shape (i.e., the rest configuration). **Pre-strain:** the strain which results from local active forces (not from changes in boundary conditions). For instance, an increase of the activity of the molecular motor myosin II (MyoII) corresponds to an increase in pre-strain. **Stress:** the internal tension within the material which is elicited by strain. **Pre-stress:** stress which is due to a change of the rest configuration (i.e., the pre-strain).

Results

Apical contraction is necessary to drive furrow formation

Apical contraction of actomyosin networks is thought to play a key role in ventral furrow formation. In order to test this, Guiglielmi and colleagues in 2015 developed a two-photon optogenetic technique that allows to indirectly perturb the actin cytoskeleton by modulating with spatial and temporal specificity the concentration of plasma membrane phosphoinositides that also plays a role in G-actin polymerization [16-20]. We now aim to test directly the role of apical contractility in tissue furrowing. To that end we implement infrared (IR) femtosecond (fs) laser dissection, a technique shown

to sever the actomyosin network with high spatio-temporal specificity without compromising cell membrane integrity. After IR fs laser dissection of the ventral actomyosin cytoskeleton, the network recoils and the cell membrane dilates. The actomyosin network eventually recovers restoring apical contraction forces and cell apical constriction (Fig. 1A). This corroborates the fact that IR fs ablation is an effective tool to sever contractile actomyosin networks while preserving cell integrity. We then performed IR fs ablation of the contractile actomyosin network during furrow formation (i.e., when the ventral tissue has a concave shape) and monitored tissue curvature changes. After ablation, the ventral tissue changes curvature from concave to convex. Eventually, after actomyosin network recovery, the ventral furrow regains its concave shape (Fig. 1B and C). This directly demonstrates that apical contraction forces, driven by apical actomyosin networks, are necessary for furrow formation. We then wonder if apical contraction forces are also necessary for tissue invagination. We thus perform sequential IR fs laser dissections of the ventral actomyosin network to periodically downregulate actomyosin contraction forces that would otherwise recover within 10 seconds. Under these conditions, ventral cells remain at the embryo surface resulting in tissue invagination failure. This demonstrates that apical contraction forces generated by actomyosin networks are necessary for furrow formation and subsequent tissue invagination.

Inferring sufficient conditions to form a furrow in an active ellipsoidal model surface

It has been demonstrated both experimentally [21, 22, 23, 24] and theoretically [25] that morphogenetic movements in the early embryo obey a global force balance, driving embryo-scale deformations. Therefore, we model the whole three dimensional shape of the *Drosophila* embryo as in [25] (Supplementary Information). During ventral furrow formation, the *Drosophila* embryo is constituted of a single epithelial cell sheet with the cell apices facing outwards, see Fig. 2A. The global shape of the embryo is ovoid, with the long axis (along anteroposterior, AP) three times the length of the short ones (along dorsoventral, DV). The embryo presents a dissymmetry with respect to the mid-coronal plane, the ventral side being more curved than the dorsal, while it is rather symmetric with respect to the mid-transverse plane and perfectly symmetric with respect to the mid-sagittal plane.

In embryos carrying mutations for the genes *slam* and *dunk (slam⁻ dunk⁻)*, the process of cellularization (prior to ventral furrow formation) is impaired: the apical membrane does not furrow to form lateral and basal side of blastoderm cells resulting in acellular embryos [7]. Remarkably, in acellular embryos a ventral furrow still forms (Fig. 2A). Therefore, we asked whether apical forces alone are sufficient to form the ventral furrow. We modelled the apical surface of the *Drosophila* blastoderm as a thin elastic surface (Fig. 2B) in order to explore whether in-plane contractility of the region corresponding to the mesoderm could lead to deformations similar to those observed *in vivo*. A more general approach would have been to consider a visco-elastic model, since the relaxation time of the *Drosophila* embryonic epithelium is estimated to be around one minute [26], which is of the same order of magnitude as the duration of the process of ventral furrow formation [24]. However, a visco-elastic model would have involved both a much higher computational complexity and a much greater difficulty of exploring the parameter space to fit the data. Since the mechanical load due to MyoII activity is constantly increasing during the process [27], we hypothesize that the effects of the viscous relaxation would be negligible in comparison to the elastic response to the increased load. Under this hypothesis, a purely elastic model is sufficient to recapitulate the main features of the process. As in previous models, the volume within this elastic surface is assumed to be constant throughout the simulations. The assumption is thus that the apical surface has sufficiently low permeability. The embryo shape is also constrained by the vitelline membrane, which is undeformable. We assumed that, before VFF, the minimal distance between cell apices and the vitelline membrane is of approximately 0.3-0.5 µm. This distance can vary locally [28, 12, 29, 30] while the global volume of perivitelline fluid was kept constant. We assume that tangential forces, such as friction or adhesion between the apical elastic surface and the vitelline membrane, are negligible at this stage, consistent with experimental and theoretical results [29, 30, 25].

Using the finite element software Surface Evolver [31], we model the mechanics of the apical surface of the embryo as a thin elastic shell of given elastic properties [32]. In this continuous model, the tissue is not partitioned into cells, nevertheless regions of space can still be assigned different properties, reflecting distinct portions of the embryo showing different gene expression patterns and mechanical properties [8, 25]. We could thus assign a local active pre-stress to finite element facets in the region corresponding to the prospective embryo mesoderm, see

Fig. 2C. We do so by assigning these facets a target area A0 which is smaller than their initial area Ai, Fig. 3D. This means that, before deformations cause relaxation, these facets experience pre-strain $\epsilon_a = (A_i - A_0)/A_0$ and thus are pre-stressed by $\sigma_a = \chi(\frac{A_i - A_0}{A_0})$, where χ is the bulk elastic modulus (see Supplementary Information and Supplementary Fig. 1A). We find that the pre-stress applied in the mesoderm region results in increased tension not only at the ventral but also at the lateral and dorsal regions of the embryo, Fig. 3A.

It has been observed that MyoII activity is not uniform across the mesodermal cells: MyoII shows a graded distribution over approximatly seven AP rows of cells on both sides of the mesoderm with highest level at the midline [27]. Experimentally, we have found that this spatial profile is well preserved during VFF, Fig. 2D. We have thus implemented a graded distribution of prestress in our computational model emulating the graded MyoII distribution. We thus applied a gradient of prestrain starting from the ventral midline where $\varepsilon_a = \varepsilon_a^m$ and decreasing according to the profile shown in Fig. 2D. The resulting stress is largest in the region where the pre-stress is applied, but decreases laterally with a profile that differs from the one of the pre-stress gradient.

Tension anisotropy emerges from tissue and embryo geometry

The increase in tension in the mesoderm during *Drosophila* VFF is known to be anisotropic [33], with a higher tension along the AP axis than along the DV axis. It has been shown that tension anisotropy is the cause of the anisotropic organization of the actomyosin network that eventually arises during VFF [34] and it has been suggested that the geometry of the embryo is responsible for the emergence of this anisotropy of tension. We thus wondered whether a mechanical model would predict anisotropic tension by imposing isotropic MyoII activity. It has been shown that in an elastic flat plate, isotropic active pre-stress in an asymmetric geometry causes stress and strain anisotropy, which are respectively larger along the long and short axis of the domain [35, 36]. Our simulations show that this effect is also at play in the embryo 3D geometry, and that mechanical tension is strongly anisotropic in the mesoderm, AP tension being twice larger than DV tension along the ventral midline (Fig. 3C and Supplementary Fig. 2A and B). What is the origin of the stress anisotropy along the AP and DV axes? By decomposing the length of the contracting ventral tissue along the AP and DV, it is noticeable that this length is two and five times less than the total

blastoderm length along the mid sagittal and mid cross sections, respectively (Supplementary Fig. 2D). Therefore, the stretch per unit tissue necessary to achieve the same contraction strain along the two orthogonal directions is about three times greater along AP than DV axis. This results in a three-times greater cell resistance to stretch along AP than DV. The shape anisotropy of the system would thus explain why the surrounding tissue appears more difficult to deform along the AP than along the DV direction even though mechanical properties of the entire tissue surrounding the mesoderm are imposed to be the same.

More specifically, the AP stress results being approximately equal to the pre-stress initially imposed on the ventral region. This is known to be consistent with the fact that little tissue deformation takes place along the AP axis (Fig. 3C), and can be related to contracting actomyosin networks anchored to stiff boundary conditions opposing resistance to deformation. [37]. On the other hand, the DV stress results being different from the pre-stress in the ventral compared to the ventro-lateral region. Consistent with the differential tissue deformation taking place in the ventral side of the embryo: in the highly contractile ventral region (for angles between 0 and π/8) the tissue contracts resulting in σ_{DV} smaller than σ_a. In the ventro-lateral region (for angles between π/8 and π/4) the tissue passively stretches resulting in σ_{DV} greater than the local value of σ_a. If the pre-stress is increased by a constant value, mimicking a homogeneous increase of MyoII activity, these features are dramatically accentuated (Fig. 3B, Supplementary Fig. 2C).

During early VFF, the anterior and posterior sides of the mesoderm tissue are under net compressive stress differently from lateral sides that are under net tensile stress (Fig. 3A and B). Eventually the stress pattern is swapped with net tensile and compressive stress acting upon pole and lateral regions of the mesoderm, respectively. The compressive stress is oriented orthogonally to directions pointing to the ventral furrow: it is thus parallel to the AP axis at lateral positions and parallel to the DV axis at anterior and posterior positions. This feature was not reported in 2D planar models [35, 36], since it is a property of the system that may emerge from the 3D curvature of the embryo. This compressive pattern can be intuitively understood by the fact that mesoderm cells located close to the poles move centripetally along different radial directions converging towards the ventral mid-line.

***In vivo* in-plane strain changes are reproduced by the mechanical model**

In order to validate our mechanical model, we compared the dynamics of area change obtained computationally to experimentally measured changes in cell surface area while imposing a localized prestress increase proportional to MyoII intensity distribution measured experimentally in both space and time (Fig. 2D and 4A). MyoII activity increases strongly in the mesoderm as ventral furrow formation engages. Quantitatively, the evolution of background-subtracted MyoII fluorescence in cells at the ventral midline is well approximated with a double exponential function:

$$I_{myo}(t) = I_0 + I_1(e^{e^{\frac{t-t_0}{T}}-1} - 1)$$

where I_0 and I_1 are coefficients in arbitrary units of fluorescence intensity, t_0 the time from which MyoII shows a progressive increase, and T the characteristic time of increase of MyoII, which we find to be T ' 20 min (Fig. 4A). The temporal dynamics of MyoII can be measured reliably only during the first phase of furrow formation. When the mesoderm tissue is strongly contracted, the MyoII intensity measurements are likely to be less accurate. We thus imposed a prestress that reliably mirrors MyoII temporal dynamics during the first part of the process of furrow formation (i.e., until minute 1 in Fig. 4A).

In our computational model, as prestress gradually increases, the ventral region reduces in area showing similar dynamics as measured *in vivo* (Fig. 4A). *In vivo*, cells located close to the ventral midline exhibits an area reduction which is proportional to MyoII intensity increase. On the contrary, cells located further away from the midline (between the 6th and the 9th cell row) increase in area (Fig. 4B) although their MyoII intensity also increases at a lesser rate (Fig. 2D). This corroborates previous experimental evidence and quantitative analysis showing that cells further away from the midline increase their surface area during furrow formation [2, 35, 24, 38]. This spatial strain pattern is reproduced by our computational model (Fig. 4B and D). These results seem now to rise a paradox: how can cells increase their surface area while simultaneously increasing the level of MyoII (i.e., the constricting prestress σ_a)? To find an answer to this question we further investigated cell shape changes by quantifying AP and DV length for cells located at different DV positions from the ventral midline. Remarkably, cells increasing surface area increase DV but not AP length (Fig. 4C) in agreement with tissue anisotropic strain shown in Fig. 3D. Consistently with our

model, we conclude that cells further away from the midline stretch along the DV axis since the MyoII based prestress exerted by these cells is inferior to the stress generated by the surrounding tissue.

The fact that cells can exhibit simultaneously an increase of apical MyoII activity and of their apical area may seem counterintuitive, since MyoII works to contract cells. Having in mind the anisotropic strain noted in Fig. 3D, we wondered whether this area increase was directly linked to the DV extension found in simulations in ventro-lateral locations. Fig. 4C, E, and Supplementary Fig. 3A show indeed that all cells more than 3 cell radii from the midline are generally stretched along the DV direction from an early time in gastrulation, in fair quantitative agreement with simulations. We conclude that, consistently with our model, cells for which neighboring cells exert an extrinsic tensile stress larger than their own MyoII-based pre-stress are being stretched towards these neighboring cells. The contraction along the AP direction, which is observed experimentally and that our simulations predict, is of smaller magnitude for cells farther from the midline, and therefore the combination of DV stretch and AP contraction results in an area increase for cells located on the ventro-lateral position.

Apical actomyosin mechanics drive AP mid-line flattening of the ventral tissue and furrow formation

Our model is now (i) tuned by imposing a pre-stress that is proportional to the experimentally measured MyoII distribution and (ii) validated since the imposed pre-stress results in surface area changes of the elastic sheet similar to cell apical surface changes measured *in vivo*. Remarkably, the 2D elastic sheet forms a buckle resulting in a furrow along the long axis of the 3D ellipsoid in the region under pre-stress (Fig. 5A and Supplementary Fig. 4B). This shows that forces applied at the surface of an ellipsoidal 3D shape can be sufficient to drive the formation of a furrow. We then tested the predictive power of our model. We analyzed the furrow at different positions from the poles: the furrow forms first and is deeper in the mid region of the ellipsoid and appears with some delay in regions further closer to the poles (Fig. 5B and C). We then measured furrow depth at different anterior-posterior positions *in vivo*. To that end, we embedded the embryo in a soft gel cylinder (preserving the embryo shape) and imaged it with multi-view light sheet microscopy to obtain isotropic resolved images (Supplementary Information). Similarly, to the computational model, the embryo shows the same feature: the furrow forms deeper in the mid region of the

embryo and eventually propagates towards the anterior and posterior poles (Fig. 5B, C and D, Supplementary movie furrow-SPIM-1.avi). The curves, representing the absolute furrow depth position at different AP locations in the embryo over time, eventually merge, highlighting a remarkable feature of VFF: while folds at distinct AP positions form at a different rate, eventually they align sequentially reaching the same absolute DV position (Fig. 5B, Supplementary Fig. 4C and Supplementary movie furrow-SPIM-2.avi). To better decipher the dynamics of ventral furrow propagation in the embryo, we digitally sectioned the 3D image of the embryo along the mid-sagittal plane (the plane separating the left from the right side of the embryo and intersecting the furrow mid-line, Supplementary Information). The mid-sagittal view of the embryo reveals a new feature: during furrow formation, the ventral tissue mid-line flattens along the embryo AP axis (Fig. 5E and Supplementary movie furrow-SPIM-3.avi). Interestingly, the acellular embryo shows similar furrow formation features (Supplementary movie acellular-furrow.avi). While ventral flattening along DV was previously characterized [1], AP flattening along the ventral tissue mid-line can only be seen in a mid-sagittal view which was not analyzed previously. To better characterize the dynamics of furrow formation in 3D, we measured and analyzed the changes of ventral tissue curvature along both the DV and AP tissue mid-lines. Ventral curvature analysis for both our computational model and the embryo show the same trend: the curvature of the AP ventral mid-line gradually decreases eventually reaching the zero value (i.e., a flat tissue), concomitantly the ventral DV curvature decreases exponentially until suddenly transiting from positive to negative values (i.e., from convex to concave). This new evidence sheds new light on the dynamics of furrow formation in 3D that can be explained by surface mechanics only on a curved tissue.

The embryo anterior and posterior polar caps function as anchoring sites for the contracting ventral tissue

The bottom region of the ellipsoidal elastic sheet contracts under pre-stress (Fig. 3) resulting in sheet deformation. While along the DV axis the ventral sheet constricts in the mid region and stretches in more lateral regions, along the AP axis the sheet shows less deformation (Fig. 3D, Supplementary Fig. 2F, Fig. 4C and D). Since AP pre-stress drives little AP strain, it results in stress within the contractile region which can only be balanced by forces acting upon neighboring tissues. We thus focused on the neighboring tissue forming the polar caps. The polar tissues are submitted to both

pressure forces exerted by the incompressible cytoplasm (Fig. 6C, gray arrow heads) and by pulling forces exerted by the contracting ventral sheet (Fig. 6C, red arrows). During sheet contraction, the polar caps are pulled inwards leading to an increase of perivitelline space at the poles (Fig. 6A and C). Remarkably, the same process occurs also *in vivo* (Fig. 6B). Therefore, the anterior and posterior polar caps may function as symmetrically positioned anchoring sites between which the ventral tissue mid-line flattens working as a contracting purse-string driving furrow formation. To test if the position of anchoring sites could bias AP tissue mid-line flattening, we implemented infrared femtosecond laser cauterization to establish ectopic anchoring sites (see [23, 39, 40, 24], and Supplementary Information). After generating two fixed sites at asymmetric positions along the AP axis of the embryo, the ventral tissue contracting in between the two ectopic fixed points and the AP midline still flattens preserving tissue furrowing (Fig. 6D and Supplementary movie cauterisation.avi). Remarkably under asymmetric boundary conditions, the ventral tissue mid-line now flattens along a direction that is no longer parallel to the AP axis and that follows a line intersecting the two ectopic anchoring sites (Fig. 6D, dashed line). This shows that the position of anchoring sites defines the boundary conditions controlling the direction of AP tissue mid-line flattening during furrow formation.

Discussion

Tissue furrowing is a fundamental process during embryo gastrulation and neurulation. The mechanism and mechanics necessary and sufficient to drive furrow formation are unclear. In this study we use as model system the *Drosophila* embryo and study furrow formation of the prospective mesoderm at the onset of gastrulation. While previous work has suggested that forces along the lateral side of cells play a key role during furrow formation [6], we now challenged this view and developed a computational model based on a 2D ellipsoidal elastic sheet in the 3D space. Our model is based on two key assumptions imposed for simplicity: i) the sheet has homogeneous linear mechanical properties, with a Poisson modulus and a ratio of Young to bending moduli which are tuned to match observed in-plane deformations, and ii) the sheet is purely elastic, therefore, viscous properties are neglected. This last assumption, while not suited for modelling mesoderm internalization (during which mesoderm cells intercalate (John et al., 2021) can be suited to model the initial rapid process of mesoderm furrowing. By imposing a ventral pre-stress proportional to MyoII

distribution measured *in vivo*, we show that our computational model can predict the magnitude and the dynamics of furrow formation and of cell shape changes at different embryo positions. The concordance between our prediction and the observed dynamics indicate that the viscous response is negligible compared to the tissue elastic response, presumably because the mechanical load generated by the pre-stress is rapidly increasing and does not allow relaxation to occur. Importantly, our model shows that stress at the apical surface of a 2D curved elastic sheet in the 3D space is sufficient to drive the formation of a furrow. After forming a furrow, the 2D elastic sheet does not invaginate. This shows that apical mechanics, while being sufficient to drive the formation of a furrow, is insufficient for tissue internalization. These computational results are in agreement with the phenotype shown by acellular embryos that succeed to form a ventral furrow which fails to internalize. Therefore, cytoplasmic compartmentalization and cell lateral or basal forces may be necessary for the second phase of mesoderm invagination in which the formed furrow is internalized.

Remarkably, the dynamics of furrow formation differ from those of MyoII and of cell shape change: while the change of MyoII intensity and cell apical area are smooth, the furrow forms abruptly (as shown by our DV curvature analysis). Such abrupt dynamics is reminiscent of the mechanical process of sheet buckling. At the onset of MyoII increase, the surface area of ventral cells is strongly reduced (from 20% at time 0 to 40% at time 2 minutes). Our model shows that during this first phase, most of the energy corresponding to the pre-stress results in DV contraction of ventral cells and in AP tension along the ventral midline. In this way, the DV curvature of the embryo surface at the ventral midline is reduced and eventually stalls at a smaller value (i.e., the tissue tends to flatten), whereas the AP curvature, which is initially smaller than the curvature along the DV axis, does not significantly change. This first phase is then followed by a second phase that results in an abrupt change of sign (i.e., from convex to concave) of the tissue curvature along the DV axis: this corresponds to the first appearance of the furrow that subsequently deepens over time. In our model, the second phase corresponds to a new mechanical balance, during which most of the energy corresponding to the pre-stress, produces work to bend the sheet. It is important to notice that, even if the formation of the furrow is abrupt, there is no discontinuity in the elastic configuration since the change in tissue shape is continuous. Since our model is free of energy dissipation, this implies that this buckling

instability is a supercritical process. Thus, the control parameter (i.e., the tissue pre-stress reflecting MyoII activity) unequivocally determines the embryo surface profile. In plants, buckling has been shown to drive tissue budding at a time scale much shorter than tissue growth (Forterre et al, 2005; Llorens et al, 2012). In this case the buckling dynamics are set by either inertial or viscous forces opposing the motion. In our model, the buckling dynamics are under control of the active molecular mechanisms generating pre-stress during VFF.

Our model makes the prediction that the ventral furrow forms by propagating from the medial towards the pole regions of the embryo. Furrow propagation emerges from the ventral tissue that folds sooner and faster in the central region of the mesoderm compared to regions closer to the poles in a way that the furrow reaches the same absolute depth at different AP positions. This results in the flattening of the mesoderm at the ventral AP midline (i.e., at the furrow apex). Our study shows that the ventral midline, subject to the highest stress, works as a contractile string (like a 'cheese cutter wire') forming the furrow. The polar caps are pulled by the contracting ventral sheet resisting the AP stress and therefore working as anchoring sites. The position of the polar caps imposes a ventral flattening that is parallel to the AP axis.

While previous 2D cross-sectional models have predicted that apical constriction may not be sufficient to drive furrow formation, our 3D model demonstrates the contrary. We show that VFF can be driven by in-plane apical forces acting at the ventral side of the *Dropsohila* embryo. We also show that the cells located on the lateral sides of the mesoderm stretch under the action of the cells located closer to the mesoderm midline. These results highlight the importance of nonlocal effects in embryo mechanics. Therefore, representing 3D systems with 2D computational models may be an oversimplification that has the potential to bias the understanding of the mechanisms driving tissue morphogenesis. Mechanical balance results from the interaction among the material units constituting the embryo. Since these physical interactions span the entire embryo and are much faster (almost instantaneous) compared to the biological molecular processes, they account for long range tissue interaction and eventual coordination. A 2D model of a 3D system, while potentially effective to provide some level of understanding with lesser computational resources and programming complexity, may miss key aspects of a process that emerges from the global mechanical balance and the intrinsic 3D physical nature of the system. While in the past, the choice of performing 2D imaging, analysis and computational

modelling was often dictated by technology limitations, we are now at an exciting time when we can study morphogenesis by bridging scales from the embryo to the cell and back. New imaging technology provide a synthetic view of the coordination of these events at the scale of the whole embryo with subcellular resolution [15, 18, 16, 17] while 3D computational modelling allows to account for the embryo complete geometry [19, 36, 37], opening new avenues to unravel the physical principles controlling morphogenesis.

References

[1] M. Leptin and B. Grunewald. “Cell shape changes during gastrulation in Drosophila”. In: Devel. 110 (1990), pp. 73–84.

[2] D. Sweeton, S. Parks, M. Costa, and E.Wieschaus. “Gastrulation in Drosophila: the formation of the ventral furrow and posterior midgut invaginations”. In: Development 112 (1991), pp. 775–789.

[3] Adam C. Martin, Matthias Kaschube, and Eric F. Wieschaus. “Pulsed contractions of an actin–myosin network drive apical constriction”. In: Nature 457 (7228 2009), pp. 495–499. DOI: 10.1038/nature07522.

[4] Daniel Krueger, Pietro Tardivo, Congtin Nguyen, and Stefano De Renzis. “Downregulation of basal myosin-II is required for cell shape changes and tissue invagination”. In: The EMBO Journal (2018). ISSN: 0261-4189. DOI: 10 . 15252 / embj . 2018100170. eprint: http : / / emboj . embopress . org / content/early/2018/11/13/embj.2018100170.full.pdf. URL: http: //emboj.embopress.org/content/early/2018/11/13/embj.2018100170.

[5] G. W. Brodland, V. Conte, P. G. Cranston, J. Veldhuis, S. Narasimhan, M. S. Hutson, A. Jacinto, F. Ulrich, B. Baum, and M. Miodownik. “Video force microscopy reveals the mechanics of ventral furrow invagination in Drosophila”. In: Proceedings of the National Academy of Sciences 107 (51 2010), pp. 22111–22116. DOI: 10.1073/pnas.1006591107.

[6] O. Polyakov, B. He, M. Swan, J. W. Shaevitz, M. Kaschube, and E. Wieschaus. “Passive Mechanical Forces Control Cell-Shape Change during Drosophila Ventral Furrow Formation”. In: Biophys. J. 107 (4 2014), pp. 998–1010.

[7] B. He, K. Doubrovinski, O. Polyakov, and E. Wieschaus. “Apical constriction drives tissue-scale hydrodynamic flow to mediate cell elongation”. In:

Nature (2014).
[8] M. Rauzi, A. H. Brezavscek, P. Ziherl, and M. Leptin. “Physical Models of Mesoderm Invagination in Drosophila Embryo”. In: Biophys. J. 105 (1 2013), pp. 3–10.
[9] R. Allena, A.-S. Mouronval, and D. Aubry. “Simulation of multiple morphogenetic movements in the Drosophila embryo by a single 3D finite element model”. In: J. Mech. Behavior Biomech. Mat. 3 (4 2010), pp. 313–323.
[10] V Conte, J Mu˜ noz, and M Miodownik. “A 3D finite element model of ventral furrow invagination in the Drosophila melanogaster embryo”. In: Journal of the Mechanical Behavior of Biomedical Materials 1 (2 2008), pp. 188–198. DOI: 10.1016/j.jmbbm.2007.10.002.
[11] V. Conte, F. Ulrich, B. Baum, J. Mu˜ noz, J. Veldhuis, W. Brodland, and M. Miodownik. “A Biomechanical Analysis of Ventral Furrow Formation in the Drosophila Melanogaster Embryo”. In: PLoS one 7 (4 2012), e34473.
[12] A Ho˘cevar Brezav˘s˘cek, M Rauzi, M Leptin, and P Ziherl. “A Model of Epithelial Invagination Driven by Collective Mechanics of Identical Cells”. In: Biophys. J. 103 (5 2012), pp. 1069–1077. DOI: 10.1016/j.bpj.2012.07.018.
[13] Jos´e J. Mu˜ noz, Kathy Barrett, and Mark Miodownik. “A deformation gradient decomposition method for the analysis of the mechanics of morphogenesis”. In: Journal of Biomechanics 40 (6 2007), pp. 1372–1380. DOI: 10 . 1016/j.jbiomech.2006.05.006.
[14] G.M. Odell, G. Oster, P. Alberch, and B. Burnside. “The mechanical basis of morphogenesis”. In: Developmental Biology 85 (2 1981), pp. 446–462. DOI: 10.1016/0012-1606(81)90276-1.
[15] P.-A. Pouille and E. Farge. “Hydrodynamic simulation of multicellular embryo invagination”. In: Phys. Biol. 5 (1 2008), p. 015005.
[16] Giorgia Guglielmi, Joseph D. Barry, Wolfgang Huber, and Stefano De Renzis. “An Optogenetic Method to Modulate Cell Contractility during Tissue Morphogenesis”. In: Developmental Cell 35 (5 2015), pp. 646–660. DOI: 10.1016/j.devcel.2015.10.020.
[17] Frank I. Comer and Carole A. Parent. “Phosphoinositides Specify Polarity during Epithelial Organ Development”. In: Cell 128 (2 2007), pp. 239–240. DOI: 10.1016/j.cell.2007.01.010.
[18] Chris Janetopoulos and Peter Devreotes. “Phosphoinositide signaling plays

a key role in cytokinesis". In: Journal of Cell Biology 174 (4 2006), pp. 485–490. DOI: 10.1083/jcb.200603156.
[19] Alessandra Reversi, Eva Loeser, Devaraj Subramanian, Carsten Schultz, and Stefano De Renzis. "Plasma membrane phosphoinositide balance regulates cell shape during Drosophila embryo morphogenesis". In: Journal of Cell Biology 205 (3 2014), pp. 395–408. DOI: 10.1083/jcb.201309079.
[20] A.L. Rozelle, L.M. Machesky, M. Yamamoto, M.H.E. Driessens, R.H. Insall, M.G. Roth, K. Luby-Phelps, G. Marriott, A. Hall, and H.L. Yin. "Phosphatidylinositol 4,5-bisphosphate induces actin-based movement of raftenriched vesicles through WASP-Arp2/3". In: Current Biology 10 (6 2000), pp. 311–320. DOI: 10.1016/S0960-9822(00)00384-5.
[21] L. C. Butler, G. B. Blanchard, A. J. Kabla, N. J. Lawrence, D. P. Welchman, L. Mahadevan, R. J. Adams, and B. Sanson. "Cell shape changes indicate a role for extrinsic tensile forces in Drosophila germ-band extension". In: Nature Cell Biol. 11 (7 2009), pp. 859–864.
[22] C. M. Lye, G. B. Blanchard, H. Naylor, L. Muresan, J. Huisken, R. Adams, and B. Sanson. "Mechanical coupling between endoderm invagination and axis extension in Drosophila". In: PLoS Biol. 13 (11 2015), e1002292.
[23] C. Collinet, M. Rauzi, P.-F. Lenne, and T. Lecuit. "Local and tissue-scale forces drive oriented junction growth during tissue extension". In: Nature Cell Biol. 17 (10 2015), pp. 1247–1258.
[24] M. Rauzi, U. Krzic, T. E. Saunders, M. Krajnc, P. Ziherl, L. Hufnagel, and M. Leptin. "Embryo-scale tissue mechanics during Drosophila gastrulation movements". In: Nature Comm. 6 (2015), p. 8677. DOI: 10.1038/ncomms9677.
[25] Mahamar Dicko, Pierre Saramito, Guy B. Blanchard, Claire M. Lye, B´en´edicte Sanson, and Jocelyn ´ Etienne. "Geometry can provide long-range mechanical guidance for embryogenesis". In: PLoS Comput Biol 13 (3 2017), e1005443. DOI: 10.1371/journal.pcbi.1005443.
[26] R. Cl´ement, B. Dehapiot, Claudio Collinet, Thomas Lecuit, and Pierre-Franc¸ois Lenne. "Viscoelastic Dissipation Stabilizes Cell Shape Changes during Tissue Morphogenesis". In: Current Biology (2017). DOI: 10.1016/j.cub.2017. 09.005.
[27] Natalie C. Heer and Adam C. Martin. "Tension, contraction and tissue morphogenesis".

In: Development 144 (23 2017), pp. 4249–4260. DOI: 10.1242/dev.151282.
[28] M. M.Witzberger, J. A. J. Fitzpatrick, J. C. Crowley, and J. S. Minden. “Endon Imaging:ANew Perspective on Dorsoventral Development in Drosophila Embryos”. In: Dev. Dyn. 237 (2008), p. 3252.
[29] Stefan M¨ unster, Akanksha Jain, Alexander Mietke, Anastasios Pavlopoulos, StephanW. Grill, and Pavel Tomancak. “Attachment of the blastoderm to the vitelline envelope affects gastrulation of insects”. In: Nature 568 (7752 2019), pp. 395–399. DOI: 10.1038/s41586-019-1044-3.
[30] A Bailles, Claudio Collinet, Jean-Marc Philippe, Pierre-Franc¸ois Lenne, Edwin Munro, and Thomas Lecuit. “Genetic induction and mechanochemical propagation of a morphogenetic wave”. In: Nature 572 (7770 2019), pp. 467–473. DOI: 10.1038/s41586-019-1492-9.
[31] Kenneth A. Brakke. “The Surface Evolver”. In: Experimental Mathematics 1 (2 1992), pp. 141–165. DOI: 10.1080/10586458.1992.10504253.
[32] C. Quilliet. “Numerical deflation of beach balls with various Poisson’s ratios: From sphere to bowl’s shape”. In: Eur. Phys. J. E 35 (6 2012), p. 1631. DOI: 10.1140/epje/i2012-12048-3.
[33] A. C. Martin, Michael Gelbart, R. Fernandez-Gonzalez, M. Kaschube, and E. F. Wieschaus. “Integration of contractile forces during tissue invagination”. In: J. Cell Biol. 188 (5 2010), pp. 735–749.
[34] Soline Chanet, Callie J. Miller, Eeshit Dhaval Vaishnav, Bard Ermentrout, Lance A. Davidson, and Adam C. Martin. “Actomyosin meshwork mechanosensing enables tissue shape to orient cell force”. In: Nat Comms 8 (2017), p. 15014. DOI: 10.1038/ncomms15014.
[35] Philipp Spahn and Rolf Reuter. “A Vertex Model of Drosophila Ventral Furrow Formation”. In: PLoS ONE 8 (9 2013), e75051. DOI: 10.1371/journal.pone.0075051.
[36] Konstantin Doubrovinski, Joel Tchoufag, and Kranthi Mandadapu. “A simplified mechanism for anisotropic constriction in”. In: Development 145 (24 2018), dev167387. DOI: 10.1242/dev.167387.
[37] Jocelyn ´ Etienne, Jonathan Fouchard,D´emosth`ene Mitrossilis, Nathalie Bufi, Pauline Durand-Smet, and Atef Asnacios. “Cells as liquid motors: Mechanosensitivity emerges from collective dynamics of actomyosin cortex”. In: Proc

Natl Acad Sci USA 112 (9 2015), pp. 2740–2745. DOI: 10.1073/pnas.1417113112.
[38] Natalie C. Heer, PearsonW. Miller, Soline Chanet, Norbert Stoop, J. Dunkel, and Adam C. Martin. “Actomyosin-based tissue folding requires a multicellular myosin gradient”. In: Development 144 (10 2017), pp. 1876–1886. DOI: 10.1242/dev.146761.
[39] Gustavo de Medeiros, Dimitri Kromm, Balint Balazs, Nils Norlin, Stefan G¨ unther, Emiliano Izquierdo, Paolo Ronchi, Shinya Komoto, Uros Krzic, Yannick Schwab, Francesca Peri, Stefano de Renzis, Maria Leptin, Matteo Rauzi, and Lars Hufnagel. “Cell and tissue manipulation with ultrashort infrared laser pulses in light-sheet microscopy”. In: Sci Rep 10 (1 2020), p. 1007. DOI: 10.1038/s41598-019-54349-x.
[40] M. Rauzi. “Probing tissue interaction with laser-based cauterization in the early developing Drosophila embryo”. In: Cell Polarity and Morphogenesis. Ed. by T. Lecuit. Vol. 139. Methods in Cell Biology. Elsevier, 2017. Chap. 8, pp. 153–165. DOI: 10.1016/bs.mcb.2016.11.003.
[41] Alphy John and Matteo Rauzi. “A two-tier junctional mechanism drives simultaneous tissue folding and extension”. In: Developmental Cell 56 (10 2021), 1469–1483.e5. DOI: 10.1016/j.devcel.2021.04.003.
[42] Yo¨el Forterre, Jan M. Skotheim, Jacques Dumais, and L. Mahadevan. “How the Venus flytrap snaps”. In: Nature 433 (7024 2005), pp. 421–425. DOI: 10.1038/nature03185.
[43] Coraline Llorens, M´ed´eric Argentina, Yann Bouret, Philippe Marmottant, and Olivier Vincent. “A dynamical model for the”. In: J. R. Soc. Interface. 9 (76 2012), pp. 3129–3139. DOI: 10.1098/rsif.2012.0512.
[44] Sebastian J Streichan, Matthew Lefebvre, Nicholas Noll, Eric F Wieschaus, and Boris I Shraiman. “Global morphogenetic flow is accurately predicted by the spatial distribution of myosin motors”. In: eLife 7 (2018). DOI: 10.7554/eLife.27454.
[45] Mehdi Saadaoui, Didier Rocancourt, Julian Roussel, Francis Corson, and Jerome Gros. “A tensile ring drives tissue flows to shape the gastrulating amniote embryo”. In: Science 367 (6476 2020), pp. 453–458. DOI: 10.1126/science.aaw1965.
[46] R. J. Tetley, G. B. Blanchard, A. G. Fletcher, R. J. Adams, and B. Sanson. “Unipolar distributions of junctional Myosin II identify cell stripe boundaries

that drive cell intercalation throughout Drosophila axis extension".
In: eLife 5 (2016), e12094.
[47] G. B. Blanchard, A.J. Kabla, N.L. Schultz, L.C. Butler, B. Sanson, N. Gorfinkiel, L. Mahadevan, and R.J. Adams. "Tissue tectonics: morphogenetic strain rates, cell shape change and intercalation". In: Nature Methods 6 (2009), pp. 458–464.

Figures

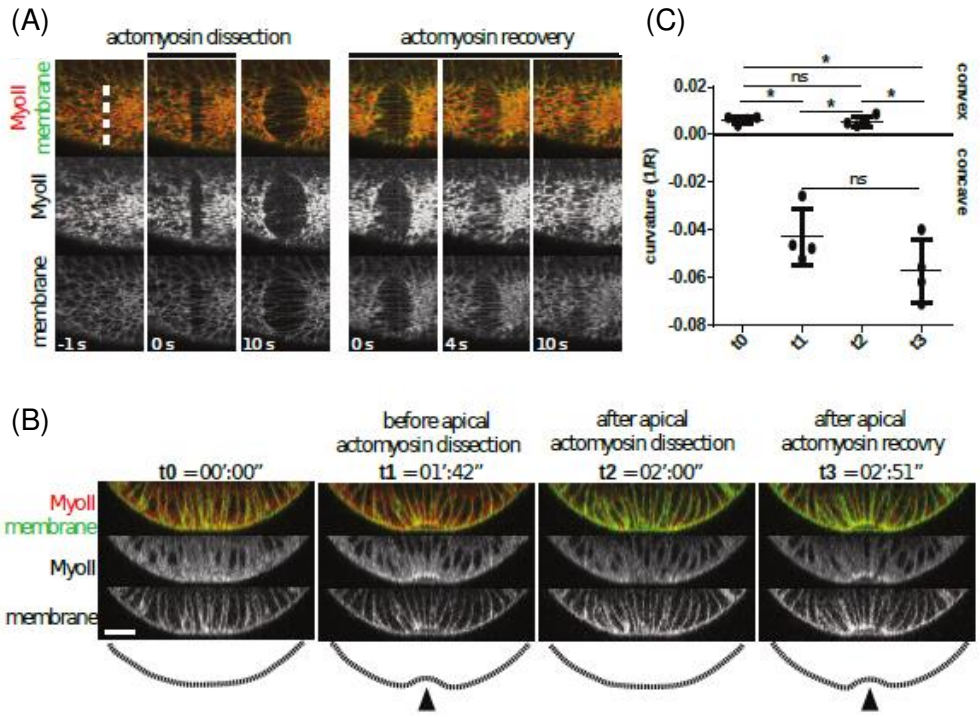

Figure 1: Apical contraction is necessary to drive furrow formation.

(A) Time-lapse showing actomyosin dissection and recovery using a pulsed IR-fs laser. (B) Time-lapse showing reversal of curvature to convex after ablation of apical actomyosin network and its subsequent recovery leading to rescue of concave curvature. (C) Plot showing curvature measurements of ablation experiment.

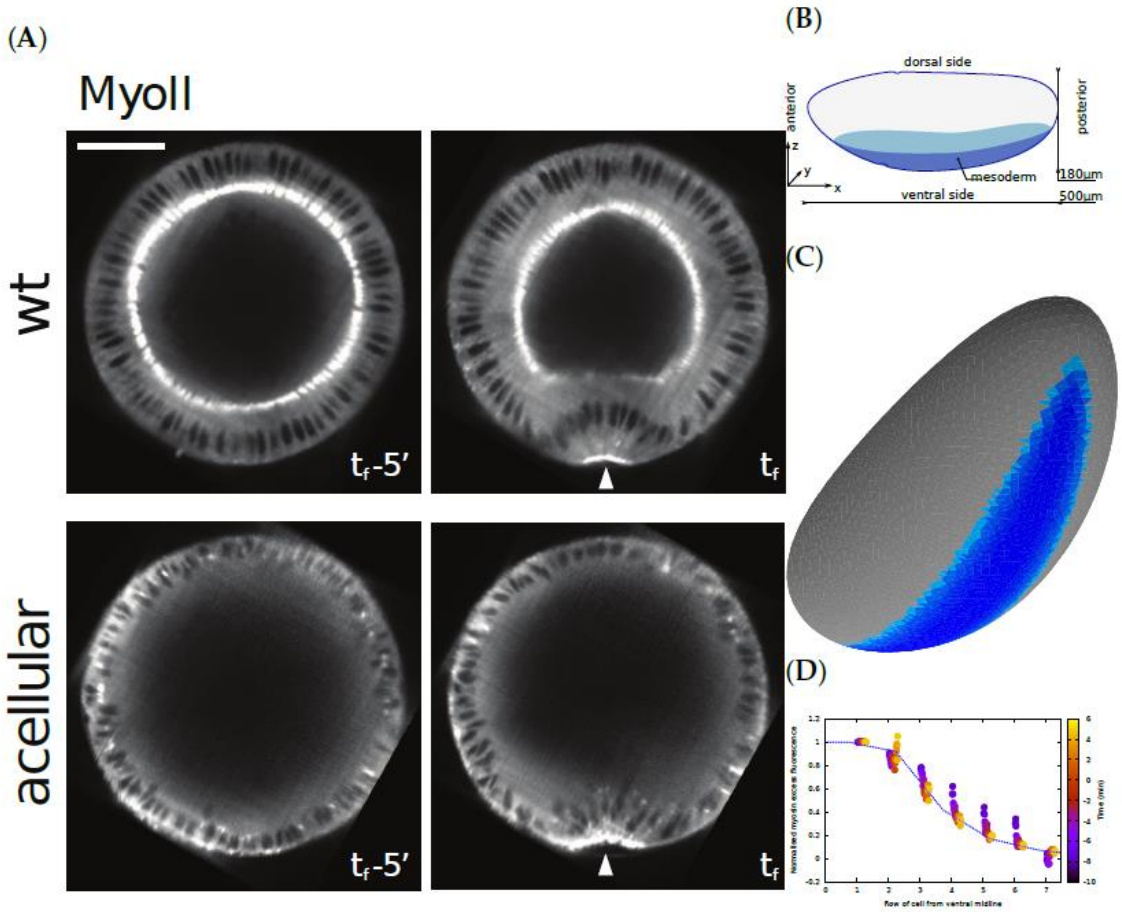

Figure 2: Using a 2D surface in the 3D space to model the Drosophila embryo.

(A) Digital mid-cross-sections before and during furrow formation in wild type and *slam-dunk*- mutant embryos. Scale bar 50 µm. (B) 3D representation of the embryo geometry. (C) A mechanical model of an embryo-shaped elastic surface where color-marked facets are pre-strained to mimic Myosin activity. (D) Circles, normalized MyoII intensity profile as a function of distance from the ventral midline at different phases of VFF (average of n = 3 embryos). Line, pre-stress profile chosen for simulations. This profile is also similar to the one reported by [38].

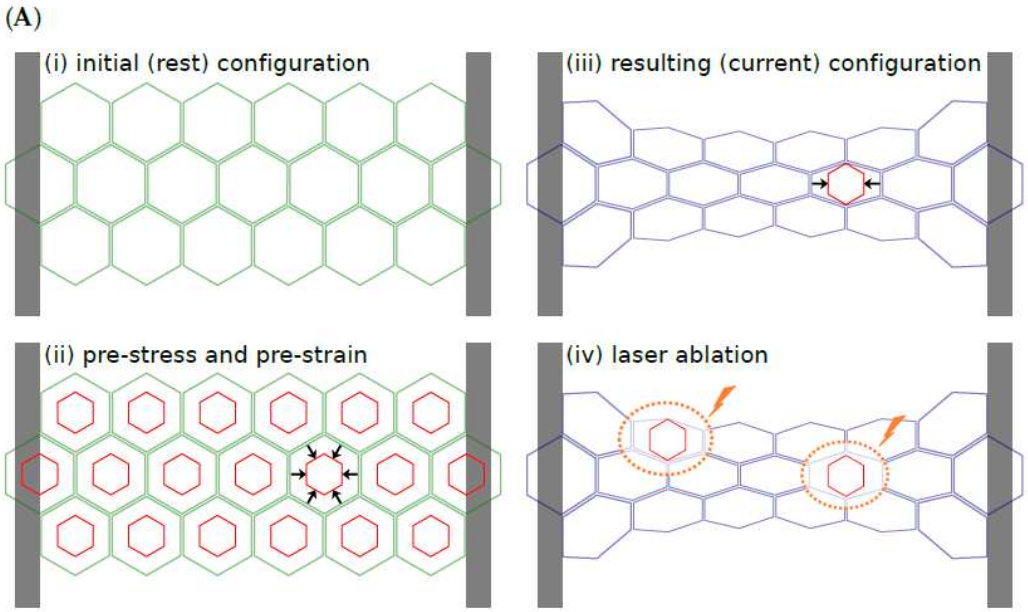

Supplementary Figure 1: (A) Deformations and stresses in a tissue with anisotropic boundary conditions and isotropic actomyosin contractile activity. (i) Initial configuration of a tissue held between two fixed points (e.g. cauterization) at its longitudinal ends, whereas it is free at along its latitudinal ends. Without any MyoII activity, this represents the equilibrium configuration. (ii) Representation of the effect of uniform isotropic MyoII activity. The initial configuration is no longer the equilibrium configuration: each cell has for equilibrium configuration the red shape and is thus pre-strained. Black arrows indicate the corresponding pre-stress (here shown for one cell). Tissue cohesion and fixed boundary conditions prevent cells from adopting their equilibrium configuration. (iii) Configuration resulting from MyoII pre-stress. Along the latitudinal direction, away from the boundaries, cells are able to contract to their equilibrium size, thus strain equals pre-strain resulting in zero stress along this direction. In the longitudinal direction, tissue cohesion and boundary conditions prevent any length change compared to the initial shape, thus strain is zero and stress (blue arrows) is equal to pre-stress along this direction. (iv) If cell-cell cohesion is inhibited, cells would relax to the equilibrium shape, revealing the anisotropy of stress in the configuration (iii).

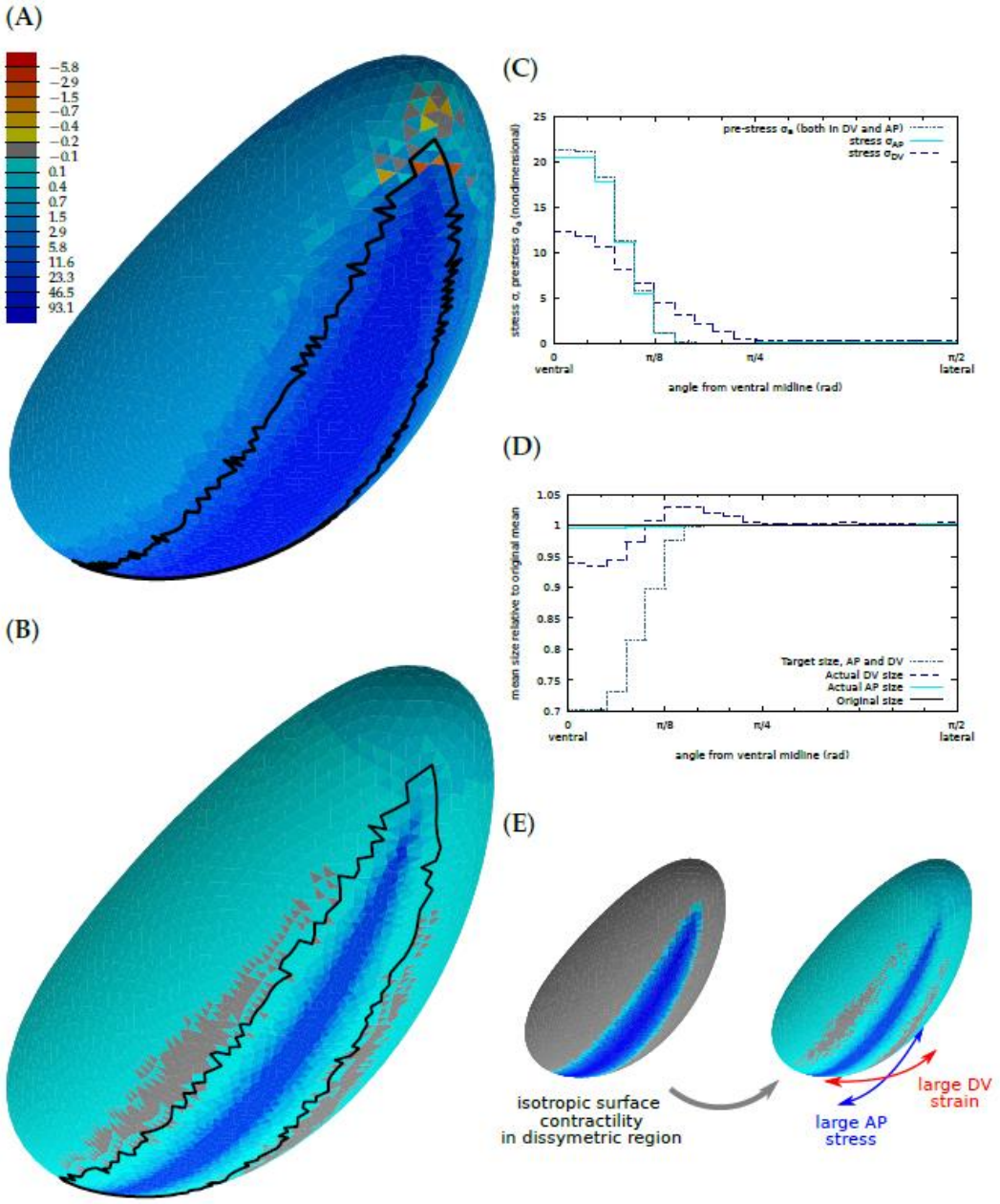

Figure 3: Actomyosin contractility drives tension anisotropy on the ventral side of the embryo.

(A and B) Mechanical stress (sum of the tensile and compressive stresses) resulting from area pre-strain at maximal values ε_a^m= 0.43 (panel A) and ε_a^m= 5.25 (panel B). (C) Angular profile of pre-stress σ_a and of the two principal stresses along AP and DV for ε_a^m= 0.43. (D) Strain angular profile (current size relative to initial size) along AP and DV for ε_a^m= 0.43. (E) Isotropic pre-strain pattern (left) yields anisotropic mechanical response, with greater stress and strain along AP and DV, respectively. All panels are for mechanical parameters γ_{2D} = 100 and ϑ_{2D} = 0.

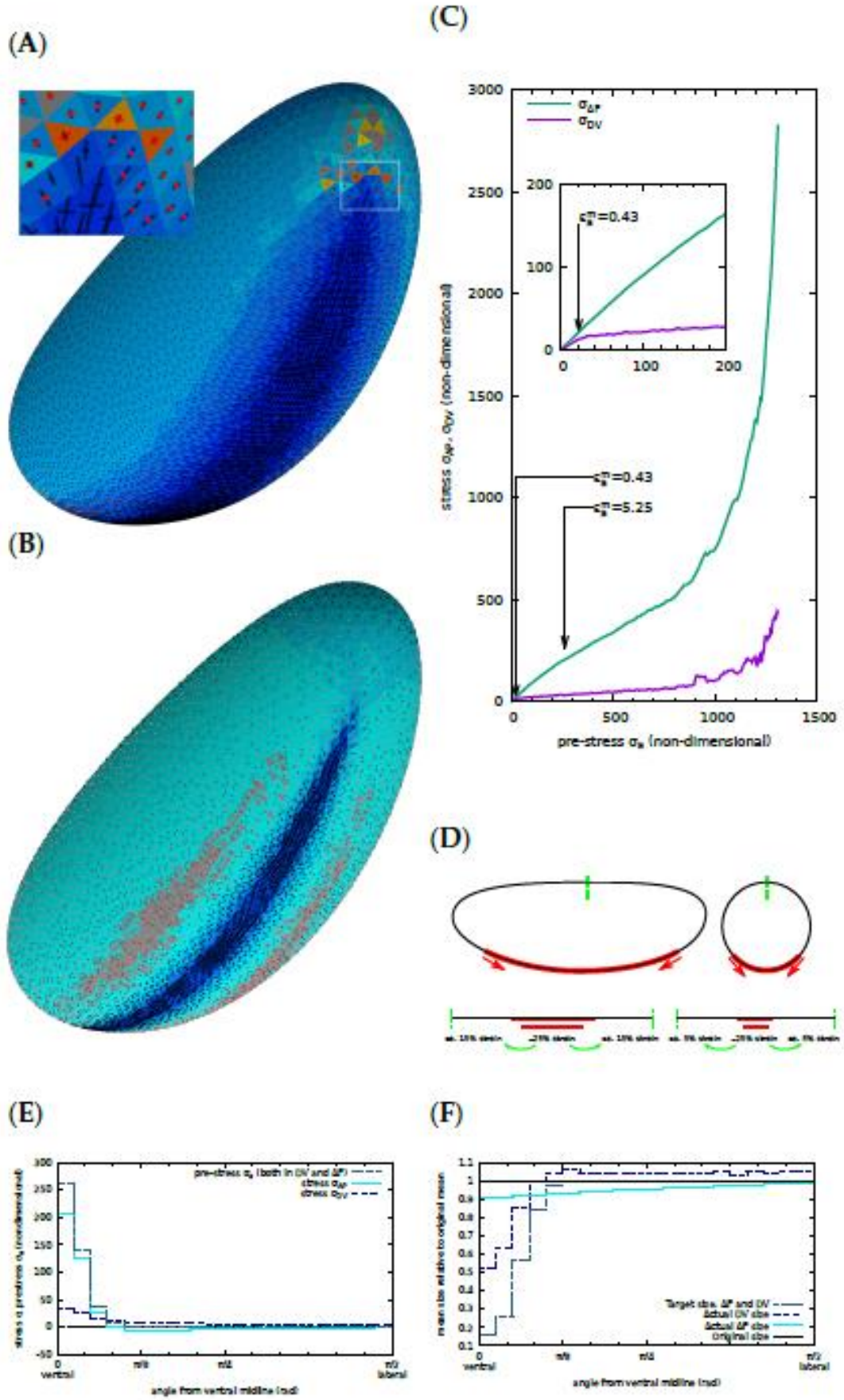
(A)
(B)
(C)
(D)
(E)
(F)
3000
2500
2000
1500
1000
500
0
0
500
1000
1500
200
100
0
0
100
200
pre-stress σ_a (non-dimensional)
stress σ_ΔP, σ_DV (non-dimensional)
ε_a^m=0.43
ε_a^m=5.25
ventral
π/4
π/2
lateral
angle from ventral midline (rad)
Target sbs, ΔP and DV
Actual DV sbs
Actual ΔP sbs
Original sbs

Supplementary Figure 2: (A) Main stresses for each facet of the elastic surface for ε_a^m= 0.43. Black segment, positive main stress (tensile); red segments, negative main stress (compressive). Insert, zoom of the region outlined in white. (B) Main stresses for each facet of simulation for ε_a^m= 5.25. (C) Evolution of AP and DV stresses along the ventral midline as a function of the pre-stress σ_a. (D) Representation of the strain in sagittal and transverse sections. (E) Same as Fig. 3C but for ϵ_a= 5.25. (F) Same as Fig. 3D but for ϵ_a = 5.25.

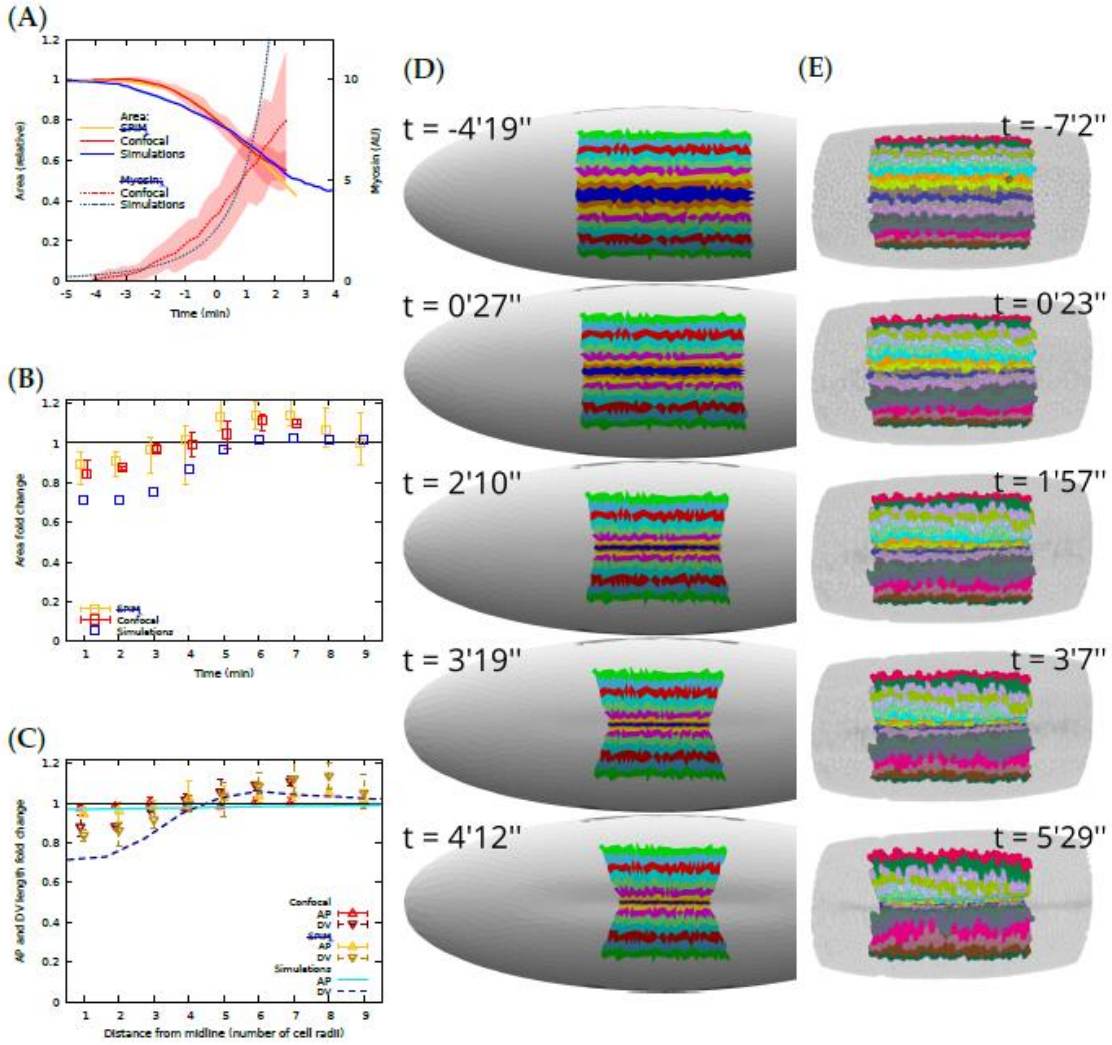

Figure 4: *In vivo* apical area changes are reproduced by the computational model.

(A) MyoII average intensity and mesoderm apical area change as a function of time, for *in vivo* analysis (3 embryos using multi-view light sheet and 3 embryos using confocal microscopy) and simulations. (B) Apical area fold change relative to the initial area of cells at different lateral distance from the midline at t = 4 min, for *in vivo* analysis (3 embryos using multi-view light sheet and 3 embryos using confocal microscopy) and simulations. (C) Apical AP and DV size fold-change relative to the initial size for cells at different lateral distance from midline at t = 4 min, for *in vivo* analysis (3 embryos using multi-view light sheet and 3 embryos using confocal microscopy) and simulations. (D and E) Time evolution of apical surface AP stripes as prestress increases in simulations and in MuVi SPIM experiments resectively.

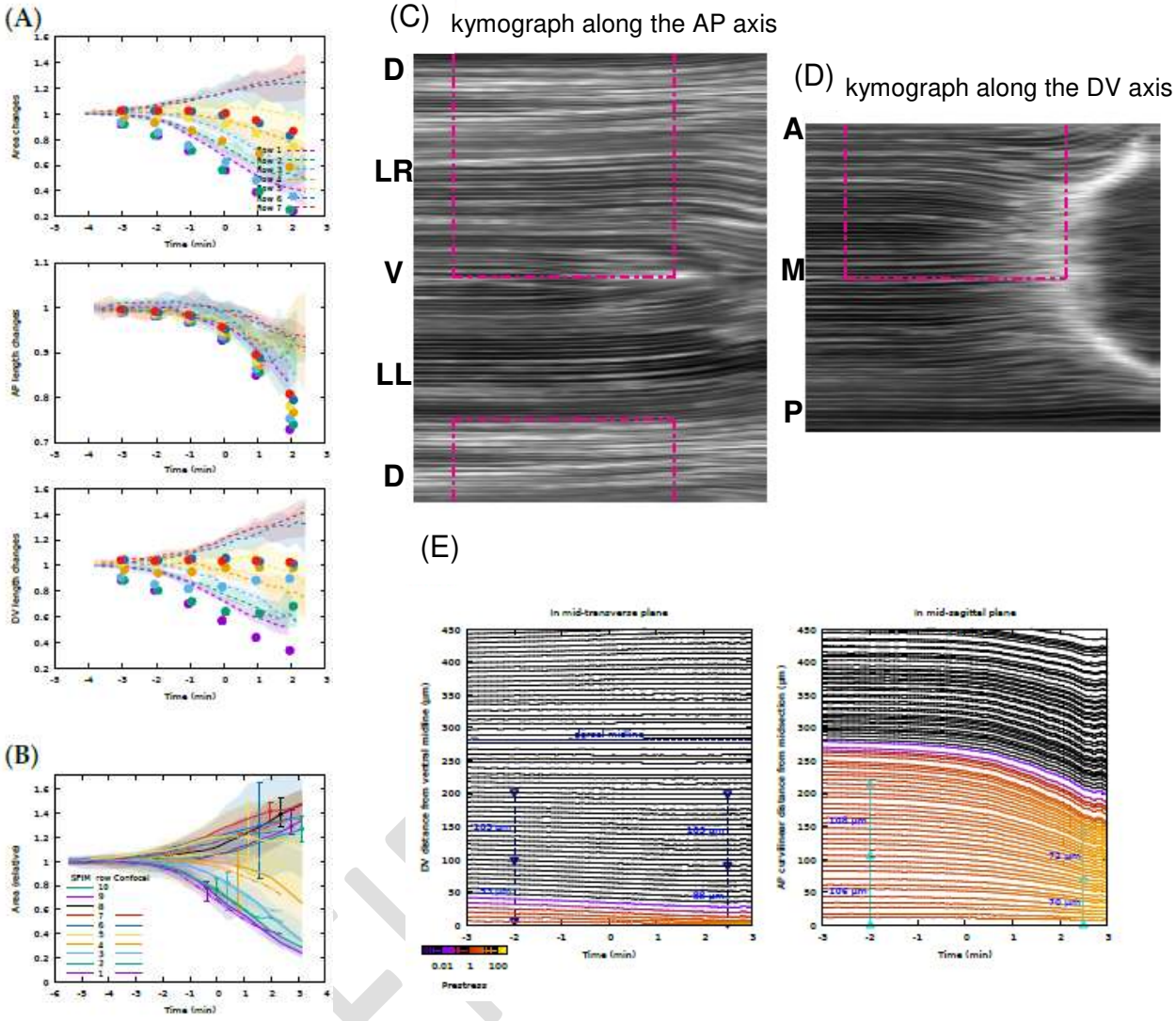

Supplementary Figure 3: (A) Time evolution of apical area, AP and DV sizes of cells at different distances from the midline, in confocal experiment. (B) Time evolution of apical area of cells in MuVi SPIM and confocal experiments. (C and D) Kymographs of membrane signal along DV (midtransverse line) and AP (midsagittal line), respectively. V, ventral; LR, lateral right; LL, Lateral left; D, dorsal; M, mid; A, anterior; P, posterior. Magenta box is from time -3' to time 3', and delineates the zone shown in panel E. (E) Kymographs in AP and DV from simulations.

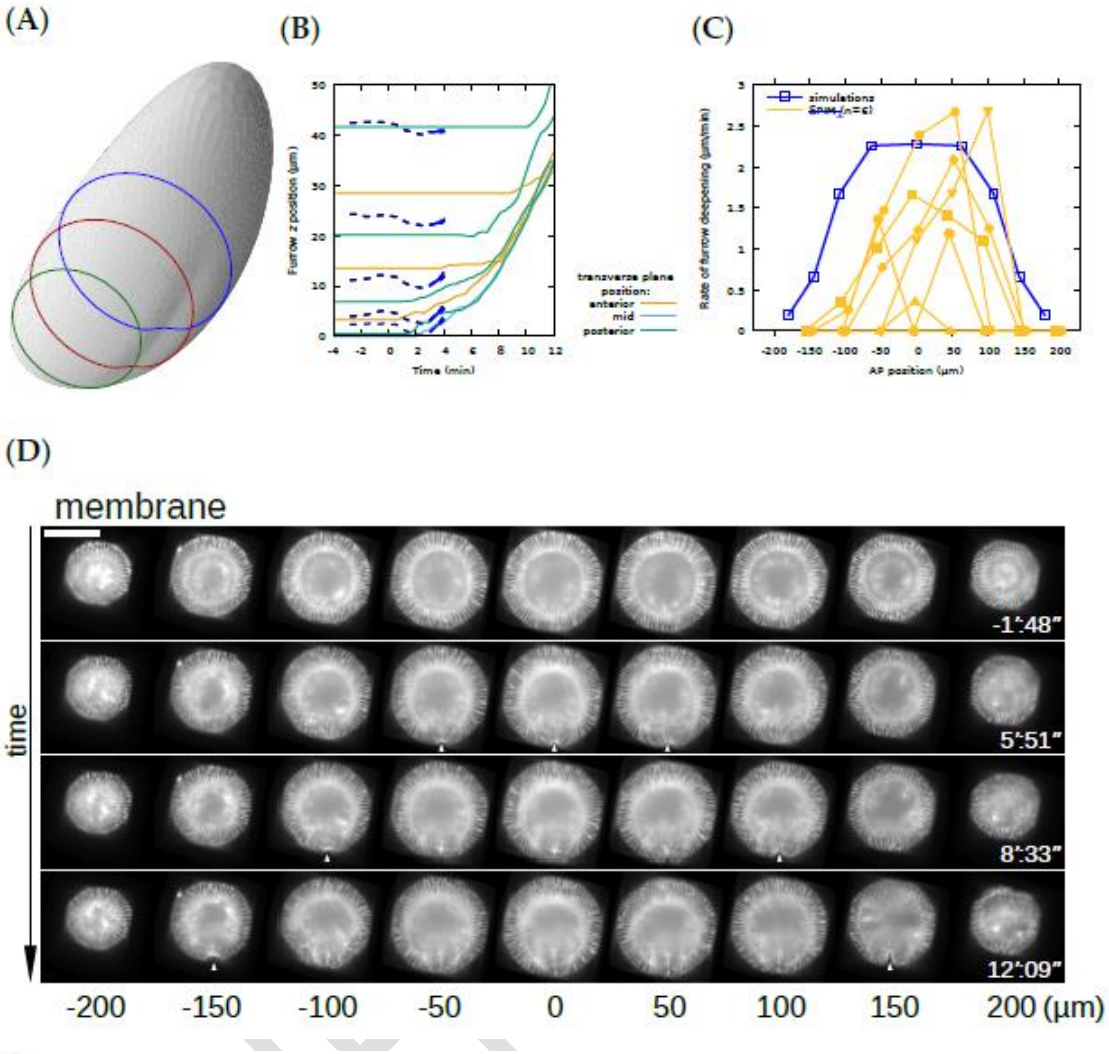
(A)
(B)
(C)
Furrow z position (µm)
Time (min)
transverse plane position:
anterior
mid
posterior
simulations
Rate of furrow deepening (µm/min)
AP position (µm)
(D)
membrane
time
-1':48"
5':51"
8':33"
12':09"
-200 -150 -100 -50 0 50 100 150 200 (µm)
(E)
membrane
-1':48"
9':27"
(F)
Curvature (µm-1)
Along AP:
simulations
SPIM
Along DV:
simulations
SPIM
Time (min)

Figure 5: VFF results in tissue curvature changes along the DV and AP axes.

(A) Embryo rendering during VFF in simulations at t = 4'12". (B) Furrow depth at different AP positions (spaced by 50 µm one from the other from the mid-point) as a function of time in MuVi SPIM experiments (solid lines, n = 6) and simulations (dashed lines and arrow showing slope at t = 30). (C) Rate of furrow formation at different AP positions at t = 3'. (D) Digital cross-sections at different AP positions. White arrow-heads indicate VFF initiation. (E) Digital mid-sagittal section of an embryo. Red line indicates ventral tissue flattening. (F) Curvature of the ventral tissue along the AP and DV axes as a function of time.

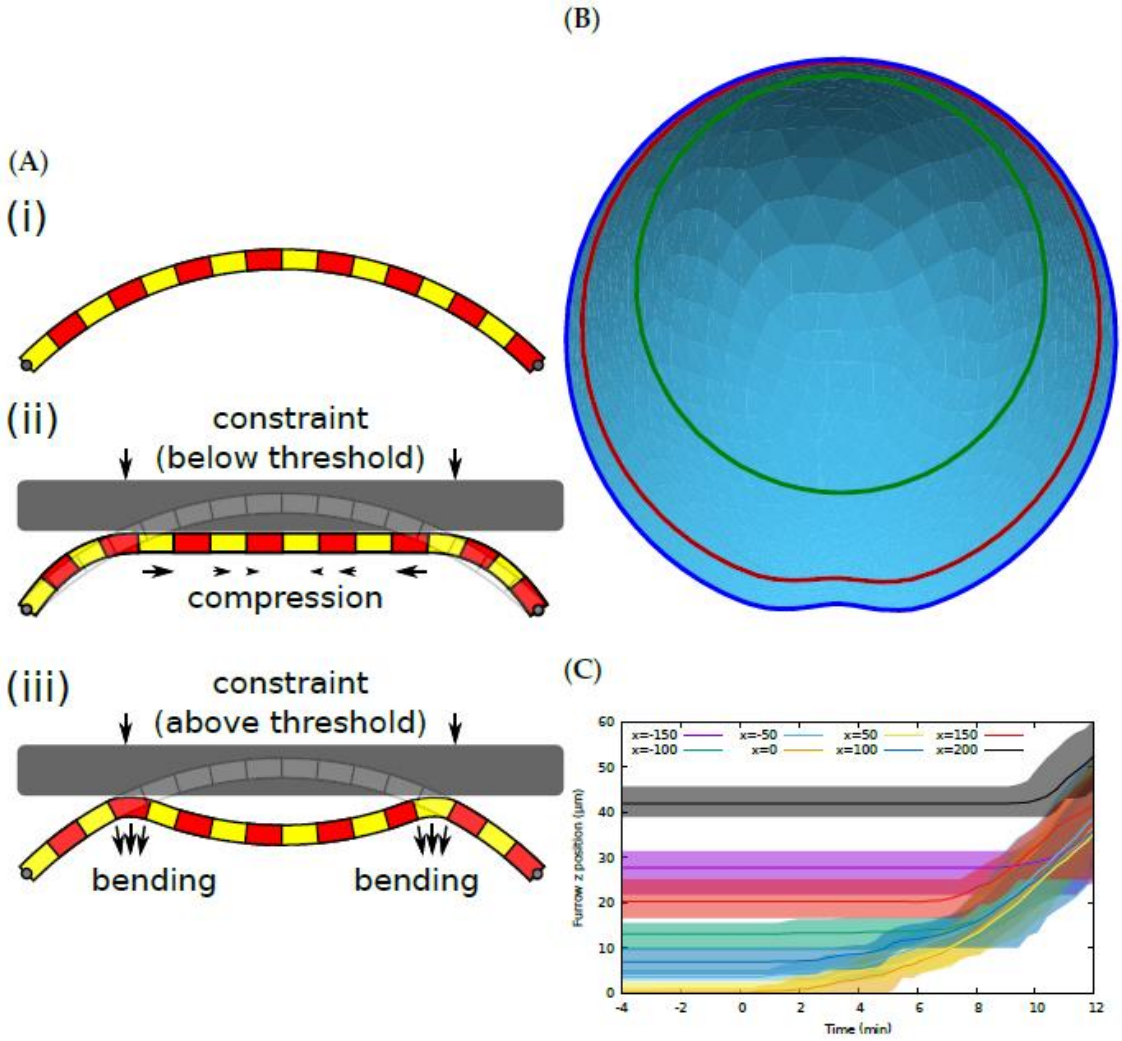

Supplementary Figure 4: (A) Schematic of the buckling process: (i) Initial configuration of a beam maintained between two fixed positions (circles). (ii) Under constrained boundary conditions (gray bar), the central part of the beam will be subject to compression and will start flattening. (iii) Buckling occurs beyond a compression threshold value: the curvature of the central part of the beam is restored (with opposite sign) and compression is relaxed, while two highly curved bends are formed. The transition phase corresponds to the configuration for which the energy in (ii) and (iii) is equal. (B) See-through view of embryo shape from the posterior end, showing that furrow has formed only in the transverse planes in the central section of the embryo. (C) Ventral furrow depth at different AP positions. Lines represent medians and shaded areas the interval between min and max values. The analysis was performed on 6 embryos.

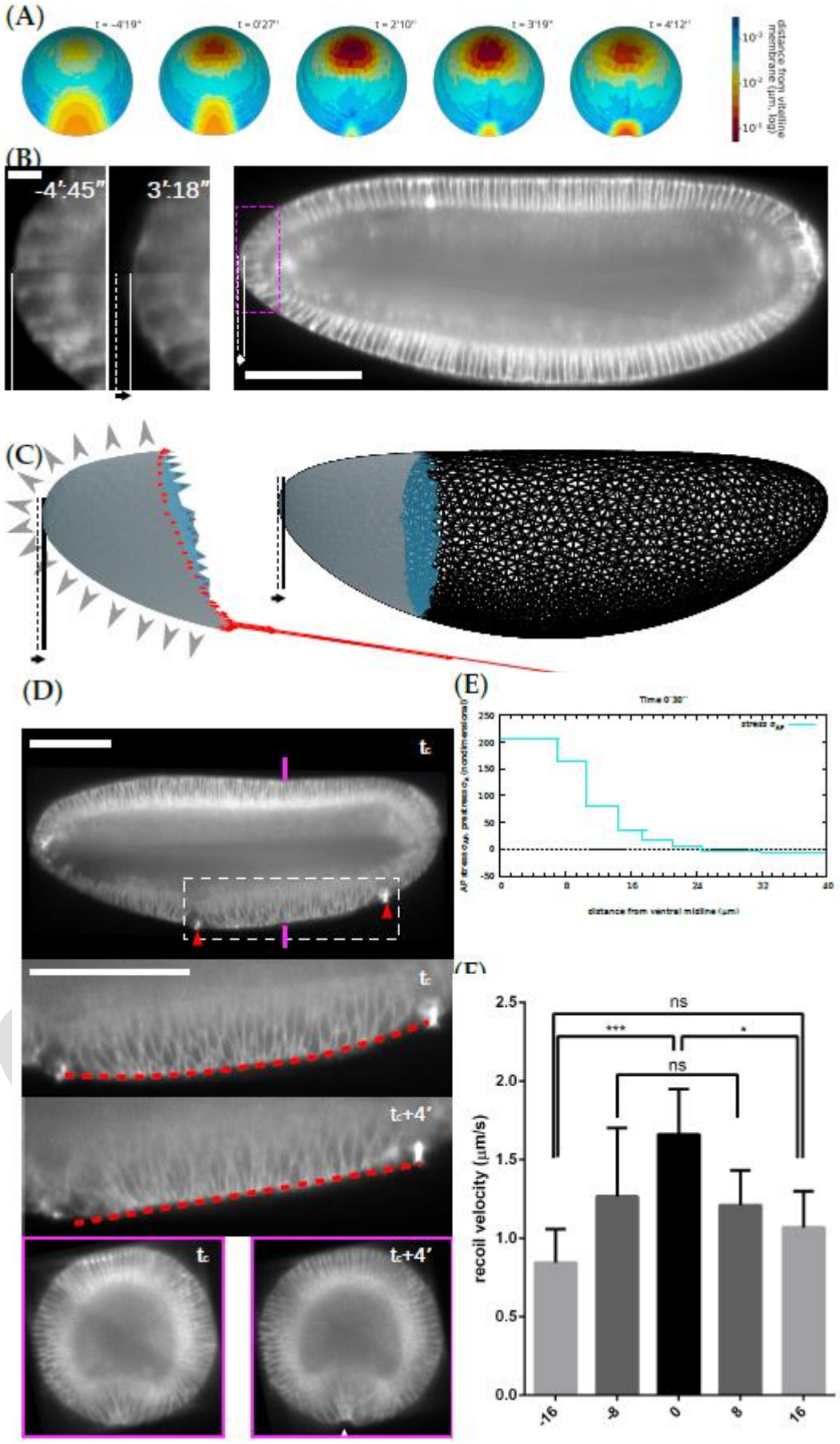
(A)
t = -4'19"
t = 0'27"
t = 2'10"
t = 3'19"
t = 4'12"
distance from vitelline membrane (µm, log)
(B)
-4':45"
3':18"
(C)
(D)
(E)
Time 0'30"
stress σ_{AP}
AP stress σ_{AP} prestress σ_A (nondimensional)
distance from ventral midline (µm)
t_c
t_c+4'
(F)
recoil velocity (µm/s)
ns
***
*
ns

Figure 6:

(A) Distance map of the apical surface to the vitelline membrane at different phases of VFF. (B) Digital mid-sagittal section showing inward displacement of the pole tissue during VFF. (C) Forces exerted on the poles by the rest of the tissue (red arrows), and pressure forces from the incompressible cytoplasm (black arrow heads). (D) Digital mid-sagittal section of an embryo on which two cauterizations (red arrow-heads), acting as fixed points, have been performed at the ventral side (tc indicates time of cauterization). The red line indicates tissue straightening along the embryo mid-sagittal section in between the two cauterized regions. Magenta shows a cross-section view of the embryo during tissue straightening. Scale bar 100 µm. (E) Plot showing tension distribution at different DV positions from the furrow mid-line in simulations. (F) Plot showing recoil velocity distribution after IR fs ablation at different DV positions from the furrow mid-line.

Author contributions

MR and JE conceived the project. MR planned the *in vivo* experiments. AJ, BD and MR performed the laser-based manipulations and light sheet experiments and analysis. JE and MR wrote the manuscript. All authors commented on the manuscript.

Acknowledgments

We thank the company Luxendo Bruker and SPARK LASERS for fruitful collaborations. We thank PRISM imaging facility for technical support. This work was supported by the French government through the UCA^{JEDI} Investments for the Future project managed by the National Research Agency (ANR-15-IDEX-01), the Investments for the Future LABEX SIGNALIFE (ANR-11-LABX-0028-01), the ATIP-Avenir program of the CNRS, the Human Frontier Science Program (CDA00027/2017-C) and the Region SUD PACA Research and ERC Booster programs.

Supplementary video captions

Video actomyosin_dissection+recovery: Time-lapse showing actomyosin network recoil after IR fs laser dissection and eventual actomysin network recovery. Scale bar 10 µm.

Video sequential_ablation: Time-lapse showing mesoderm internalization failure as a consequence of periodic ventral tension inhibition. The ventral actomyosin network is periodically dissected using a IR fs laser over a grid patterned ROI. Scale bar 10 µm.

Video 3D_stripes: 3D rendering of segmented apical surfaces of ventral cells. Scale bar 50 µm.

Video wt: Time-lapse showing digital sections along the sagittal plane (top) and along different cross-section planes at different AP positions in a wild type embryo. Scale bar 100 µm.

Video furrow_propagation:

Video acellular: Time-lapse showing digital sections along the sagittal plane (top) and along different cross-section planes at different AP positions in a *slam*$^{-}$*dunk*$^{-}$ embryo. Scale bar 100 µm.

Video cauterization: Time-lapse showing ventral tissue flattening along a line connecting cauterized loci. Scale bar 100 µm.

Methods

Mutants and fly stocks

All fly stocks were reared on standard corn meal in the 25ºC incubator. For collecting embryos for live imaging, flies were kept in cages and were allowed to deposit eggs on agar plates. *ubi*:Gap43::mCherry; ; *klar* flies (John and Rauzi, 2021) that express a plasma-membrane targeted protein fused to mCherry fluorophore were used to 3D segmentation of mesoderm cells during folding. In all other experiments to monitor membrane in live, embryos were collected from *ubi*:Gap43::mCherry (I) fly stock. For laser ablation experiments, embryos were collected from Sqh::mCherry; Spider::GFP fly stock, in which the Myosin II regulatory light chain (MRLC) (Spaghetti Squash, Sqh, in *Drosophila*) is labelled by mCherry and membrane by Spider (Gilgamesh) fused to GFP. For wild-type embryo cross section depicting MyoII localization, embryos were collected from fly stock expressing Sqh::mCherry. For cross section of acellular mutant embryos showing MyoII localization, embryos were collected from *Δhalo slam dunk*^{1}/ CyO, SqhGFP fly stock.

Actomyosin meshwork ablation

Apical actomyosin meshwork was ablated using a tunable femtosecond-pulsed infrared laser (IR fs, MaiTai) mounted on Zeiss LSM 780 NLO confocal microscope tuned at 950 nm. Experiment were performed using a 40x 1.2 NA objective, the bleach mode on the Zeiss Zen software (140 mW laser power at the focal plane, single iteration, 1 µs pixel dwell, 1 s frame rate). For segmented ablations and experiments to probe the necessity of apical actomyosin contractility for furrowing, only single ablations were performed. For experiments to block furrow invagination, a grid pattern of iterative ablations of the apical actomyosin network were performed every time the network was recovering.

Measuring furrow propagation along the AP axis

We used *in toto* 4D time-lapses (acquired with MuVi SPIM) of developing *Drosophila* embryos expressing a fluorescent protein targeted to the plasma membrane. Cross-sections were digitally made 50 µm apart along the AP axis. Furrow depth at different AP positions was measured using a developed point-picker ImageJ macro.

Measuring anterior pole distance

Mid-sagittal sections were digitally extracted from the time-lapses and the position of the vitelline membrane at the anterior pole and the apical position of the anterior-most blastoderm cell were recorded using the point-picker plugin. Relative position of apical position of anterior-most blastoderm cell was calculated with respect to the position of the vitelline membrane at the anterior pole and this was plotted over time.

Measuring tissue shortening

Digital mid-cross and sagittal sections were obtained using ImageJ to measure tissue shortening along DV and AP axes, respectively. Different embryos were aligned in time by keeping t0 as the frame at which cell apical area reduces to 20%. To measure tissue shortening along the AP axis, an identity cell was fixed at the half-length along the mid-sagittal section. Cells located 100 µm anteriorly and posteriorly from this point were marked and their distance from the identity cell was measured over time along the embryo surface. To measure tissue shortening along the DV axis, an identity cell was fixed at the midline of cross sections images at the ventral side. The distance along the embryo surface of the two cells located on opposite sides four cells away from the identity cell was then measured over time.

Recoil velocity

To measure actomyosin network recoil after ablation, the point-picker plugin was used to follow the cut end. Distance moved by the network after ablation was plotted against time and the maximum recoil velocity was measured by calculating the first derivative.

Curvature analysis

An ImageJ macro was developed to measure the radius (R) of a circle generated from three consecutive points. The curvature was calculated as 1/R and was plotted against time. Curvature of the mesoderm tissue was measured both along the AP and DV axes. A convex curvature is given by a positive and a concave curvature is given by a negative value.

3D image segmentation and analysis

Mesodermal cells are segmented and tracked by inter-registration based on iterative projections of segmentations from one-time point to another using the ASTEC algorithm [L. Guignard et al., Science 2010]. Morphological data are extracted and analyzed using Python. ImageJ dedicated macros are used for image treatment and the 3D Viewer plugin for rendering [*Schmid et al.BMC Bioinformatics 2010*].

In toto embryo imaging and laser cauterizatin

Embryos were staged dechorionated in bleach before mounting. Embryos were mounted in a glass capillary filled with 0.5% gelrite, with their long axis parallel to the capillary. A small portion of gelrite containing the embryo was then pushed out from the capillary. The embryo was imaged on a MuVi SPIM (Luxendo, Bruker) equipped with Olympus 20x 1.0 NA objectives, 488 nm and 594 nm lasers. Z-stacks were

acquired with a step-size of 1 µm and during each acquisition, embryos were imaged in two opposing orthogonal views (0˚-dorsal-ventral view, 90˚-lateral view). Thus, for every single time point, four 3-D stacks were recorded. Fusion of four stacks was obtained by using Matlab [*Rauzi, M. et al.*, 2015] resulting in a final isotropic pixel resolution of 0.29 µm. Laser cauterization was performed by coupling a femtosecond 920 nm laser (Alcor2, SPARK LASERS) to MuVi SPIM and by following a similar protocol as presented in [*De Medeiros et al. Scientific Reports 2020*].